

An Investigation Into The Surface Finish of Laterally Face Milled
Cobalt-Chromium-Molybdenum Alloys

Sam Lees

ME

2016

An Investigation Into The Surface Finish of Laterally Face Milled Cobalt-Chromium-Molybdenum Alloys

A thesis

Submitted to Auckland University of Technology in
partial fulfilment of the requirements for the degree

of

Master of Engineering

at

**School of Engineering, Computer, and Mathematical Sciences,
Auckland University of Technology**

by

Sam Lees



2016

Abstract

The surface finish of multiple machined dental alloy specimens has been analysed, evaluated and compared. The dental alloy used in this investigation was cobalt-chromium-molybdenum (CoCrMo). CoCrMo is a popular biomedical material commonly found in artificial joints and dental implants. Lateral side milling was used to machine the specimens while four different cemented tungsten carbide (WC) mills were used at varying rotational spindle speeds to provide a comprehensive look into how different configurations would affect the surface quality of this alloy. In dental applications a high quality surface finish of the implant is crucial to minimize plaque and food build up and therefore an in-depth investigation into the link between machining specifications and surface finish was needed. Cutting forces of each experiment were supplied with the milled specimens. Scanning electron microscopy of each specimen and mill in this study was then undertaken. Furthermore, micro hardness testing, and roughness testing were undertaken on the dental alloys to create a comprehensive results profile. It was observed that in general, roughness increased with increasing spindle speed, though multiple data sets were incomplete. Obtained cutting forces were shown to vary for each mill and spindle speed. The primary observation from this study was that surfaces that appeared to be smooth were microscopically rough with chip rewelding, mill vibrations, mill wear, and the minimum chip thickness mechanism dictating the extent of the surface roughness. Finally, a DLC mill coating was found to be not suitable for milling CoCrMo.

Key Words: Cobalt-chromium alloys; Dental alloy; CoCrMo alloy; Dental Mills; Side Milling; Scanning electron microscopy; Tool Wear; Surface Finish; Dental Application; Micro-milling.

Table of Contents

Abstract.....	i
List of Figures	v
List of Tables	ix
Attestation of Authorship	x
Acknowledgements.....	xi
1.0. Introduction	1
2.0. Problem Statement and Aim.....	4
3.0. Literature Review.....	5
3.1. Implants and Prosthetics	5
3.2. Defining Surface Finish.....	7
3.3. CoCr Alloys	9
3.4. CoCrMo Alloys.....	10
3.5. Machining CoCrMo	13
3.6. Micro-Machining.....	19
3.7. Summary of Literature	25
4.0. Methodology.....	27
4.1. Material.....	28
4.1.1. Heat Treatments	29
4.2. Milling Tools.....	30
4.3. Scanning Electron Microscopy (SEM)	32
4.4. Metallography.....	32
4.4.1. Etching.....	32
4.5. Micro-Hardness Testing	34
4.6. Roughness Testing	34
4.7. Experimental Layout	36
4.7.1. Milled Specimen Parameters	37
5.0. Results.....	39
5.1. Scanning Electron Microscopy (SEM) Image Analysis.....	39
5.1.1. 10,000 RPM.....	43
5.1.2. 15,000 RPM.....	49
5.1.3. 20,000 RPM.....	55
5.1.4. 25,000 RPM.....	61

5.1.5. 30,000 RPM.....	67
5.1.6. 35,000 RPM.....	73
5.1.7. Mill A: Meisinger HM23LR. Used, Milling As-received (AR) CoCrMo.....	79
5.1.8. Mill B: Shofu 21N. Used, Milling As-received (AR) CoCrMo.....	81
5.1.9. Mill B: Shofu 21N. Used, Milling Annealed (HT4H) CoCrMo.....	83
5.1.10. Mill C: Meisinger HM23GX. Used, Milling As-received (AR) CoCrMo.....	85
5.1.11. Mill D: Meisinger HMB23G. Used, Milling As-received (AR) CoCrMo.....	88
5.1.12. Chip Analysis	93
5.2. Micro Hardness	96
5.3. Metallography and Microstructure	97
5.3.1 EDS Analysis of CoCrMo Specimen	97
5.4. Roughness Testing	99
5.4.1. Annealed (HT4H) CoCrMo, Mill B: Shofu 21N.....	100
5.4.2. As-received (AR) CoCrMo, Mill A: Meisinger HM23LR.....	101
5.4.3. As-received (AR) CoCrMo, Mill B: Shofu 21N.....	102
5.4.4. As-received (AR) CoCrMo, Mill C: Meisinger HM23GX.....	103
5.4.5. As-received (AR) CoCrMo, Mill D, Meisinger HMB23G.....	104
5.5. Cutting Forces	105
5.6. Minimum Chip Thickness Evaluation	111
5.6.1. Sample Calculation – Mill B: Shofu 21N.....	111
5.6.2. Mill A: Meisinger HM23LR	112
5.6.3. Mill B: Shofu 21N	113
5.6.4. Mill C: Meisinger HM23GX.....	114
5.6.5. Mill D: Meisinger HMB23G	115
5.6.6. Theoretical h/r Values for Mills A, B, C, D vs. Spindle Speed (RPM).....	116
6.0. Discussion.....	117
6.1. Scanning Electron Microscopy (SEM) Images	117
6.1.1. Mill A: Meisinger HM23LR	117
6.1.2. Mill B: Shofu 21N	118
6.1.3. Mill C: Meisinger HM23GX.....	121
6.1.4. Mill D: Meisinger HMB23G	122
6.1.5. Overall Evaluation	124
6.2. Micro-Hardness Testing	126
6.3. Roughness Testing	127

6.4. Cutting Forces	131
6.5. Minimum Chip Thickness Effect.....	134
6.6. Mill Gyration and Run-out	137
6.7. Implications and Limitations of Study.....	140
6.8. Further Thoughts	142
7.0. Conclusion.....	144
8.0. Further Work.....	146
References	147
Glossary.....	152
Appendices.....	153

List of Figures

Figure 1 Classification of geometrical properties according to DIN 4760 (45).	8
Figure 2 SEM micrographs of the as-cast (AC) CoCrMo sample (grain boundary etched and carbide stained). J. Cawley et al. (8).	12
Figure 3 SEM micrographs of the heat-treated (HT) CoCrMo sample (grain boundary etched and carbide stained) J. Cawley et al. (8).	12
Figure 4 SEM images of surface defects found in dry turning of ASTM F1537 CoCrMo (7).	14
Figure 5 Experimental setup for investigating milling operations. M. Takahashi et al. (29).	16
Figure 6 Fishbone diagram listing parameters that affect surface roughness. P G Benardos (43).	18
Figure 7 Chip formation process. (a) $h = 0.1R$ (0.2mm); (b) $h = 0.2R$ (0.4mm); (c) $h = 0.3R$ (0.6mm). X. Lai et al. (35).	20
Figure 8 Experimental matrix for micro-scale and macro-scale milling tests. F. Brandao et al. (32). ..	21
Figure 9 Theoretical surface profile, assuming the minimum cutting depth (h_{min}) determines the achievable surface roughness. V. Huntrupl et al. (53).	23
Figure 10 Schematic representation of the minimum chip thickness in orthogonal cutting; r : edge radius of cutting tool, h : depth of cut, hm : minimum chip thickness. F. Ducobu et al. (34).	23
Figure 11 Chip morphologies for h/r values ranging from 0.5 to 0.05. F. Ducobu et al. (34).	24
Figure 12 Experimental milling setup. M. Takahashi et al. (29).	27
Figure 13 Lateral face milling diagram. T. Pasang et al. (28).	28
Figure 14 Cobaltan ingot from above.	29
Figure 15 Cobaltan ingot showing milled surfaces.	29
Figure 16 Dental Mills; A, B, C and D respectively in unused condition.	31
Figure 17 Dental Mill Shapes.	31
Figure 18 Examples of rewelded material on the milled surface.	39
Figure 19 Left: SEM image of surface waviness. Right: A 3D scan of surface waviness. www.mdpi.com (56).	40
Figure 20 Examples of ridges/ripples on the milled surface.	40
Figure 21 Tearing and craters on the milled surfaces.	41
Figure 22 Gouge marks on the milled surface.	41
Figure 23 Visible differences in surface finish. (A) Showing a relatively good surface finish milled with mill C at 20,000 RPM. (B) Showing a relatively poor surface finish milled with mill A at 20,000 RPM. 42	
Figure 24 Low magnification SEM images of specimens laterally face milled at 10,000 RPM showing; (a) as-received CoCrMo milled with Mill A, (b) as-received CoCrMo milled with Mill B, (c) as-received CoCrMo milled with Mill C, (d) as-received CoCrMo milled with Mill D, (e) HT4H CoCrMo milled with Mill B.	44
Figure 25 200x magnification SEM images of specimens laterally face milled at 10,000 RPM showing; (a) as-received CoCrMo milled with Mill A, (b) as-received CoCrMo milled with Mill B, (c) as-received CoCrMo milled with Mill C, (d) as-received CoCrMo milled with Mill D and (e) HT4H CoCrMo milled with Mill B.	46
Figure 26 1000x magnification SEM images of specimens laterally face milled at 10,000 RPM showing; (a) as-received CoCrMo milled with Mill A, (b) as-received CoCrMo milled with Mill B, (c) as-received CoCrMo milled with Mill C, (d) as-received CoCrMo milled with Mill D and (e) HT4H CoCrMo milled with Mill B.	48

Figure 38 1000x magnification SEM images of specimens laterally face milled at 30,000 RPM showing; (a) as-received CoCrMo milled with Mill A, (b) as-received CoCrMo milled with Mill B, (c) as-received CoCrMo milled with Mill C and (d) HT4H CoCrMo milled with Mill B.	72
Figure 39 Low magnification SEM images of specimens laterally face milled at 35,000 RPM showing; (a) as-received CoCrMo milled with Mill B, (b) as-received CoCrMo milled with Mill C, (c) as-received CoCrMo milled with Mill D and (d) HT4H CoCrMo milled with Mill B.	74
Figure 40 200x magnification SEM images of specimens laterally face milled at 35,000 RPM showing; (a) as-received CoCrMo milled with Mill B, (b) as-received CoCrMo milled with Mill C and (c) HT4H CoCrMo milled with Mill B.	76
Figure 41 1000x magnification SEM images of specimens laterally face milled at 35,000 RPM showing; (a) as-received CoCrMo milled with Mill B, (b) as-received CoCrMo milled with Mill C and (c) HT4H CoCrMo milled with Mill B.	78
Figure 42 SEM images of Mill A: Meisinger HM23LR after milling As-received CoCrMo.	79
Figure 43 SEM images of Mill B: Shofu 21N after milling As-received CoCrMo.	81
Figure 44 SEM images of Mill B: Shofu 21N after milling HT4H CoCrMo.	83
Figure 45 SEM images of Mill C: Meisinger HM23GX after milling As-received CoCrMo.	85
Figure 46 Mill C BUE verification using EDS scanning.	86
Figure 47 Mill C BUE EDS scan.	87
Figure 48 SEM images of Mill D: Meisinger HMB23G after milling As-received CoCrMo.	88
Figure 49 Mill D, DLC layer two point EDS test.	90
Figure 50 Mill D, DLC layer two point EDS test counts.	90
Figure 51 Mill D, DLC layer EDS window scan properties.	91
Figure 52 Mill D, DLC layer EDS window scan maps.	92
Figure 53 SEM images of chips obtained from AR CoCrMo milled at 25,000 RPM. (a, and b) chips from Mill A, (c, and d) chips from Mill B.	93
Figure 54 SEM images of chips obtained from milling; AR CoCrMo milled with Mill C (a, b), AR CoCrMo milled with Mill D (c, d) and HT4H CoCrMo milled with Mill B (e, f). All milling was undertaken at a spindle speed of 25,000 RPM.	94
Figure 55 Chips vs corresponding surface finish for AR CoCrMo milled with Mills C, and D at 25,000 RPM.	95
Figure 56 EDS composition scan of AR CoCrMo specimen.	98
Figure 57 Ra and Rq roughness values for HT4H CoCrMo laterally milled with Mill B: Shofu 21N. ...	100
Figure 58 Ra and Rq roughness values for AR CoCrMo laterally milled with Mill A: Meisinger HM23LR.	101
Figure 59 Ra and Rq roughness values for AR CoCrMo laterally milled with Mill B: Shofu 21N.	102
Figure 60 Ra and Rq roughness values for AR CoCrMo laterally milled with Mill C: HM23GX.	103
Figure 61 Ra and Rq roughness values for AR CoCrMo laterally milled with Mill D: Meisinger HMB23G.	104
Figure 62 Milling diagram with force directions. M. Takahashi et al. (29)	105
Figure 63 Mill A: Meisinger HM23LR cutting edge radius (r).	112
Figure 64 Mill B: Shofu 21N cutting edge radius (r).	113
Figure 65 Mill C: HM23GX cutting edge radius (r).	114
Figure 66 Mill D: HMB23G cutting edge radius (r).	115
Figure 67 Theoretical h/r Values vs spindle speed (RPM) for all mills.	116
Figure 68 Micro-hardness of CoCrMo vs annealing time.	126

Figure 69 Complete Ra data for lateral milling of CoCrMo with all mills.....	127
Figure 70 Average Ra and Rq values (μm) vs Spindle Speed (RPM) for all mills.....	130
Figure 71 Cutting forces of laterally milled CoCrMo displaying Cutting Force (N) vs Spindle Speed (RPM) for all mills.....	131
Figure 72 Saw tooth profile typical of the minimum chip thickness effect. V. Huntrupl et al. (53) ...	134
Figure 73 Minimum chip thickness analysis of the surface milled by Mill A at 10,000 RPM.....	135
Figure 74 Run-out deviation diagram. P. Connor et al (57)	137
Figure 75 Mill gyration diagram. P. Connor et al. (57).....	138

List of Tables

Table 1 Chemical composition of CoCrMo (Cobaltan) alloy.	28
Table 2 Milling tool details.	30
Table 3 Chemical etchants tested.	33
Table 4 SEM + roughness testing experiment list.	36
Table 5 Micro-hardness + metallography experiment list.	36
Table 6 AR CoCrMo – Mill A parameters.	37
Table 7 AR CoCrMo – Mill B parameters.	37
Table 8 AR CoCrMo – Mill C parameters.	37
Table 9 AR CoCrMo – Mill D parameters.	38
Table 10 HT4H CoCrMo – Mill B parameters.	38
Table 11 Mill C BUE EDS results showing weight percentage.	87
Table 12 Mill D, DLC layer two point EDS weight percentage.	91
Table 13 Micro hardness results.	96
Table 14 EDS composition of AR CoCrMo specimen.	98
Table 15 Manufacturers composition specifications of AR CoCrMo.	98
Table 16 Roughness testing values for HT4H CoCrMo laterally milled with Mill B: Shofu 21N.	100
Table 17 Roughness testing values for AR CoCrMo laterally milled with Mill A: Meisinger HM23LR.	101
Table 18 Roughness testing values for As Received CoCrMo laterally milled with Mill B: Shofu 21N.	102
Table 19 Roughness testing values for AR CoCrMo laterally milled with Mill C: Meisinger HM23GX.	103
Table 20 Roughness testing values for AR CoCrMo laterally milled with Mill D: Meisinger HMB23G.	104
Table 21 Cutting forces of HT4H CoCrMo laterally milled with Mill B: Shofu 21N.	106
Table 22 Cutting forces of AR CoCrMo laterally milled with Mill A: Meisinger HM23LR.	107
Table 23 Cutting forces of AR CoCrMo laterally milled with Mill B: Shofu 21N.	108
Table 24 Cutting forces of AR CoCrMo laterally milled with Mill C: Meisinger HM23GX.	109
Table 25 Cutting forces of AR CoCrMo laterally milled with Mill D: Meisinger HMB23G.	110
Table 26 Sample minimum chip thickness calculations.	111
Table 27 Mill A: Meisinger HM23LR h/r ratio calculations.	112
Table 28 Mill B: Shofu 21N h/r ratio calculations.	113
Table 29 Mill C: Meisinger HM23GX h/r ratio calculations.	114
Table 30 Mill D: Meisinger HMB23G h/r ratio calculations.	115

Attestation of Authorship

I hereby declare that this submission is my own work and that, to the best of my knowledge and belief, it contains no material previously published or written by another person (except where explicitly defined in the acknowledgements), nor material which to a substantial extent has been submitted for the award of any other degree or diploma of a university or other institution of higher learning.

A handwritten signature in black ink, appearing to read 'Sam Lees', written in a cursive style.

Sam Lees

Acknowledgements

Firstly I would like to thank my supervisor, Associate Professor Tim Pasang of the School of Engineering at Auckland University of Technology. I am extremely grateful for the opportunity to be a part of this research and for the constant support and feedback given during the course of the research and writing period. He allowed this paper to be my own work, but provided strong guidance when it was needed.

I thank Associate Professor Mamoru Takahashi and Tatsuya Fujita for conducting the milling experiments at their labs at Akita University, Japan. I would also further like to thank some of the staff at Auckland University of Technology who made this work possible. Mr Patrick Connor at the SEM lab not only provided strong guidance and help with the operation and usage of the scanning electron microscope, but he also helped me with many insights into the research and I feel these conclusions could not have been achieved without him. Mark Masterton and Jim Crossen; lab technicians at the Auckland University of Technology also helped me many times with sample preparation and testing. Without their guidance I would not have been able to acquire the needed data.

Finally, I would like to express my gratitude to my friends and family, specifically to my parents for providing me with unfailing support and continuous encouragement throughout my years of study and through the process of researching and writing this thesis. A special mention is due for Avinash for his support and feedback during the writing of this thesis. Lastly, I would like to thank my amazingly wonderful girlfriend York for all her love and support during the final stages of this research, not limited to, but inclusive of all the times she paid for our dates while I was a typical broke student. This accomplishment would not have been possible without them.

Thank you.

Sam Lees

1.0. Introduction

Due to their excellent mechanical properties such as wear resistance, corrosion resistance, biocompatibility, high melting points and being non-magnetic (1–16), cobalt-chromium (CoCr) based alloys such as cobalt-chromium-molybdenum (CoCrMo) alloys, are widely used in orthopaedic and dental applications. CoCrMo is specifically used in the area of prosthetics and implants (1,3,5–11,13–23).

In dental applications a high quality surface finish is crucial to minimize plaque and food build-up which can lead to poor oral health and potential disease. These claims are backed with multiple studies showing an increased presence of dental caries, gingivitis and periodontal disease due to high surface roughness of the materials present in the oral cavity (24–27). Therefore an in-depth investigation into the surface finish of machined dental alloys used in the fabrication of prosthetics and implants is crucial. One way to achieve this is by experimentally evaluating the surface finish of machined alloy specimens. Furthermore, by machining these specimens with differing machining parameters, the conditions in which these common defects occur, and any trends present, can be identified.

An overall lack of literature exists discussing the machinability of as-cast (AC) cobalt-chromium-molybdenum (CoCrMo). A. Bordin et al. (1) looked at the machinability of EBM CoCrMo compared with wrought CoCrMo in semi-finishing turning operations. They found that surface roughness was heavily dependent on the feed rate with the main issues being the formation of craters, laps and cracks between feed marks (1). Further research undertaken by A. Bordin et al. (7) investigated the surface integrity of CoCrMo subjected to dry turning. Surface roughness was once again attributed to the feed rate, with smeared material, burrs, tears, adhered chip particles and adhered material fragments being the main surface defects found on the ASTM F1357 CoCrMo surface (7). Recent research was undertaken investigating the cutting (milling) forces for CoCrMo and TiAlNb by T. Pasang et al. (28). This study focused primarily on cutting forces; however there was an observation of surface quality. Surface quality was shown to be affected heavily by the mill flutes and how they retained the chips. Significant “surface variations were present related to the extent to which metal chips retained in the mill flutes had frictionally re-welded onto the surfaces behind the mill” (28). Further research by M. Takahashi et al. (29) investigating cutting forces during milling of cobalt based dental alloys, concluded that frictionally rewelded chips were a

leading cause of poor surface quality. A. Deshpande et al. (30) used cryogenic cooling during machining of CoCrMo to lower workpiece and mill temperatures and showed an improved surface quality. R. Polini et al. (31) investigated the use of CVD diamond dental tools on CoCrMo. Key observations taken from the study were: feed rates need to be extremely low when machining CoCrMo and are recommended to be even lower than 0.01 m/min, the CVD coated tools experienced significantly longer tool life and a much lower cutting force, and chip breakers on the milling tool are crucial to reducing force and improving tool life (31).

Micro-scale machining is becoming increasingly popular as the need for the production of miniaturized components rises (32–34). Biomedical instruments, electronic products, the aerospace industry and the defence industry are major areas where micro-scale machining will be vastly important (33–37). Size effect and the minimum chip thickness are two components in micro-machining that are said to heavily affect surface finish and tool wear (32,35,36,38). The minimum chip thickness theory states that a chip will not be formed if the uncut chip thickness is less than the minimum thickness of cut h_{min} , due to the highly negative tool rake angle occurring owing to the comparable cutting thickness (h) and tool edge radius (R) (32,34,35,38). When cutting thickness is below h_{min} a phenomena will occur known as ploughing, this is an elastic-plastic deformation without effective material removal (32,35,38). X. Lai et al. (35) studied the “Modelling and analysis of micro scale milling considering size effect, micro cutter edge radius and minimum chip thickness”. X. Lai et al. (35) found the minimum chip thickness to be approximately 0.25R (25% of cutting edge radius). Work undertaken by H. Autenrieth et al. (38) evaluated both the size effect and minimum chip thickness occurring in micro-machining. They showed that a transition period occurs from ploughing being the dominant mechanism, to chip formation being the dominant mechanism. Work undertaken by F. Brandao et al. (32) proposed an experimental method to “determine the size effect, specific cutting force and minimum uncut chip thickness in micro-milling of dual phase carbon steel”. The authors concluded by stating the research showed that the minimum uncut chip thickness varies from 1/4 to 1/3 of the tool cutting edge radius (0.25R and 0.33R respectively), regardless of the workpiece material, tool geometry, mechanical machining process or techniques used for measuring or estimating h_{min} . The theory was validated by comparing their results with significant literature on the subject (32). An in-depth literature review led F. Ducobu et al. (34) to conclude that the down-sizing of

milling induces significant changes in the cutting phenomena with minimum chip thickness being a major factor. The authors predicted a minimum chip thickness value in the order of 25% of R, with a lower limit around 12.5% of R and an upper limit of 50% of R, with R representing the cutting edge radius of the tool (34). K. Aslantas et al. (36) studied the “Cutting performance of nano-crystalline diamond (NCD) coating in micro-milling of Ti 6 Al 4 V alloy” and found a minimum chip thickness value of roughly 0.3R. Finally, relating to micro-machining, J. Pathak (33) investigated the design, assembly and testing of an ultra-high speed micro-milling spindle. One of the most notable motivations for design was the tool run-out. The author claimed that “Typical milling spindles used for these small tools employ either rolling element bearings or air bearings to support the spindle shaft and the combination of asynchronous spindle bearing error motions and clamping errors often results in tool run-out 3 to 20 times the nominal chip thickness” (33). This tool run-out deviation means that it is possible for some cutting edges to not contact the surface at all while others are forced to cut chips several times larger than the desired depth of cut (33). While tool run-out of similar proportions in macro-machining is not an issue, the significant differences in the ratio of tool cutting edge radius to depth of cut, means tool run-out can be extremely detrimental in micro-machining.

This thesis involves examination of the surface finishes of machined/milled dental alloy specimens. The dental alloy used was cobalt-chromium-molybdenum (CoCrMo), supplied as ‘as-cast ingots’ in an as-received state. Lateral face milling was undertaken along the ingot face. Four different cemented tungsten carbide (WC) mills were used in the milling of these specimens with each mill having a varied geometry. Furthermore, three of the mills were uncoated, with the fourth coated in a diamond-like carbon (DLC) coating. The mills’ spindle speed was varied from 10,000 RPM to 35,000 RPM in increments of 5000 RPM with the tool forward speed held constant at 0.15 mm/second. The machined surfaces were analysed using scanning electron microscopy (SEM) primarily, with EDS, micro-hardness testing and roughness testing further undertaken on selected specimens. Furthermore, cutting forces were supplied with the milled specimens to allow a deeper analysis. The study can be classified as an experimental approach which can be thought of as the most ‘obvious’ approach. Factors that were thought to be most likely to contribute to the obtained surface finishes such as mill geometry, tool coatings and spindle speeds, were tested at differing

conditions. The obtained results then allowed for an investigation into how each factor affected the obtained surface finish, and to what extent. In experimental studies the researcher's intuition and insight play a great role in the obtained conclusions and hypothesis; however a solid understanding of the examined and expected phenomenon is necessary for the conclusions to have any scientific weight leading to the need for an in-depth literature review to be undertaken.

2.0. Problem Statement and Aim

Cobalt-chromium-molybdenum (CoCrMo) alloys are widely used in the dentistry industry and offer an adequate surface finish if machined correctly. However, due to the lack of knowledge surrounding the milling of these alloys with complex conical dental mills, the optimal milling parameters are not definitively known for dental applications. Furthermore, a lack of knowledge surrounding how machining affects the surface of dental alloys on a microscopic scale exists. This lack of knowledge leads to the machining used by dentists to shape dental implants and structures being imprecise. In dental applications a high quality surface finish of the implant is crucial to minimizing plaque and food build up and therefore an in-depth investigation into the link between machining and microscopic surface finish is needed.

This research aims to investigate laterally milled CoCrMo specimens by using SEM imaging, roughness testing and measured cutting forces to link obtainable surface finish qualities to mill geometry and spindle speeds, and, furthermore, identifying the common defects and their causations. This knowledge gained will fill the gap in the literature and help lead to the achievement of optimised milling parameters for CoCrMo.

3.0. Literature Review

The following chapter examines existing literature surrounding dental implants, defining surface finish, cobalt chromium alloys, the machining of cobalt-chromium-molybdenum and micro-machining.

3.1. Implants and Prosthetics

Medical implants are devices that are either inserted into the human body, or attached to the surface of the body. They are most commonly employed to replace a broken or missing biological structure but may also be used to enhance an existing structure or support the biological structure during recovery (39). Implants differ from transplants as they are man-made devices and most commonly constructed from biomaterials. Implants can be roughly distinguished into groups based on their intended application. Some common groups are: cardiovascular implants, contraceptive implants, neurological implants, orthopaedic implants and dental implants. Biomedical implants have been in use for many decades and are well established as a viable technology. Although biomedical implants are now constructed from a range of materials including composites, metallic implants and metal alloys used for fixed dental prosthesis are still widely used in the industry (2,3,14,40). Furthermore, work undertaken by M. Niinomi et al. (18) claims that between 70 and 80% of all medical implants are constructed from metallic biomaterials, and that the demand for metallic implants is increasing rapidly due to the world's increasingly aging population and the fact that elderly people have a much higher chance of hard tissue failure.

Prosthodontics is the area of dentistry that focuses on dental prostheses and implants. Missing teeth, damaged teeth, missing bone structures and even missing soft tissue can be replaced using combinations of prostheses and/or implants. Because of the nature of the oral environment, corrosion resistant materials are critical. Saliva, bacterial plaque and changes in PH and temperature related to food or beverage intake all lead to a highly corrosive environment (40). Historically, precious metals such as gold based alloys were used extensively and quite successfully for many years due to their biocompatibility and ease of use (12). Approximately 40 years ago the industry started to move away from precious metals. Three major factors influenced the move: the first being pricing stability and availability of these metals, the second being the growing need for better physical properties of the alloys such as a high elastic moduli, and the third being the growing public and professional concern

about corrosion and biocompatibility (20). Owing to gold's rapid price increase during the seventies there was a need for new precious metal alloys for use in dentistry and gold–silver–palladium and palladium–silver alloys were two favourites. Despite their popularity they still were highly expensive, and base metal alloys such as nickel chromium (NiCr) and cobalt chromium (CoCr) alloys started to be alternatively used in dental prosthetics (12). The demand for better physical properties of materials used in dental implants also led to a shift away from precious alloys in search of materials with a better modulus of elasticity. A high modulus of elasticity is important in multiple-material implants. For example, in metal-ceramic dentures any flexure of the metal structure can lead to the brittle failure of the bonded porcelain structure. Furthermore the higher elastic modulus will lead to less bending when loaded in flexure leading to a more efficient transmission of the forces to the contacted teeth or tissue (20). The final reason for the shift away from precious metals was a growing public concern about corrosion resistance and biocompatibility. The increasing public awareness of the release of metals from alloys into the body led to the development of many new dental alloys and furthered the move away from precious metals. Due to the cost of these precious metals, the need for better physical properties and issues surrounding corrosion and biocompatibility, the use of non-precious alloys in the dentistry industry has increased significantly (2,3,20).

The most commonly used metallic biomaterials can be broken up into three groups; stainless steels, cobalt chromium (CoCr) alloys, and titanium (Ti), and its alloys. Titanium (Ti) alloys exhibit the highest biocompatibility, corrosion resistance and specific strength compared with stainless steels and cobalt chromium (CoCr) alloys. Cobalt chromium (CoCr) alloys exhibit the highest wear resistance and relatively higher strength compared with stainless steels and titanium (Ti) alloys. Stainless steels generally exhibit higher ductility and cyclic twist strength compared with cobalt chromium (CoCr) and titanium (Ti) alloys (18).

CoCr alloys are the most commonly used base material in metal-ceramic prostheses which are extensively used in dentistry and have been for many decades. These metal-ceramic prostheses have a proven record of good clinical performance, aesthetics and durability (12). The structure is composed of a metallic framework providing solid mechanical properties, and by a ceramic veneer for aesthetic features. Four major manufacturing techniques are used in the creation of the metal frameworks; CAD/CAM manufacturing, milling, casting or direct laser sintering (LS) (3,11,40,41). Typical casting techniques face porosity defects occurring

from the casting process, and owing to this the industry is slowly shifting away from traditional casting techniques, while CAD/CAM, laser sintering and other techniques are being researched and implemented; though for the fabrication of implants such as femoral knee joints and complex dental prostheses, the traditional casting technique is unavoidable (11). Aside from obvious economic reasons, these cobalt chromium alloys are favourable due to increased rigidity (CoCrMo is 40-50% more rigid than precious alloys), and being significantly lighter than precious alloys (2,20). This allows prostheses to be fabricated much thinner while still providing comparable mechanical properties. Furthermore, the presence of chromium, molybdenum and tungsten in these non-precious alloys leads to greater corrosion resistance and biocompatibility (2,3,6,8,9,14,22). Understanding the metallurgy of these dental alloys is a complex and demanding task for both the laboratory and the dentist, however the proper selection and manipulation of these alloys and their microstructures is critical to the ability of the dental prostheses to perform adequately. Poor material selection and/or manipulation during fabrication by the laboratory or the dentist could lead to failure of expensive restorations, possibly leading to health and wellbeing issues which could result in legal action by the patient.

3.2. Defining Surface Finish

In manufacturing processes, machinability is the term used to describe how easily a material can be machined to a desired shape and quality, with respect to the tooling and machining processes involved. One of the most important goals in manufacturing is the achievement of a predefined product quality. Product quality can generally be defined as the product's surface finish, machined tolerances and material defects. Surface finish is the nature of a surface as defined by two major characteristics: surface roughness and waviness (42). Surface roughness is generally what most people would consider as surface finish, "Surface roughness is a widely used index of product quality and in most cases a technical requirement for mechanical products" (43). Waviness is the measure of surface irregularities that are spaced further apart than the roughness irregularities and are generally cyclic in nature. A well respected standard in the surface metrology field is the DIN 4760 standard, DIN 4760: Form deviations; Concepts; Classification system. (1982) Deutsches Institut für Normung e. V. The DIN 4760 standard is related to the influence of manufacturing parameters on the product's surface finish. These parameters include things such as tool vibration, tool wear,

misalignment, etc. (44). The DIN 4760 standard was influential in the way it proposed to separate the different orders of deviation in the surface's overall wavelength, as illustrated in Figure 1.

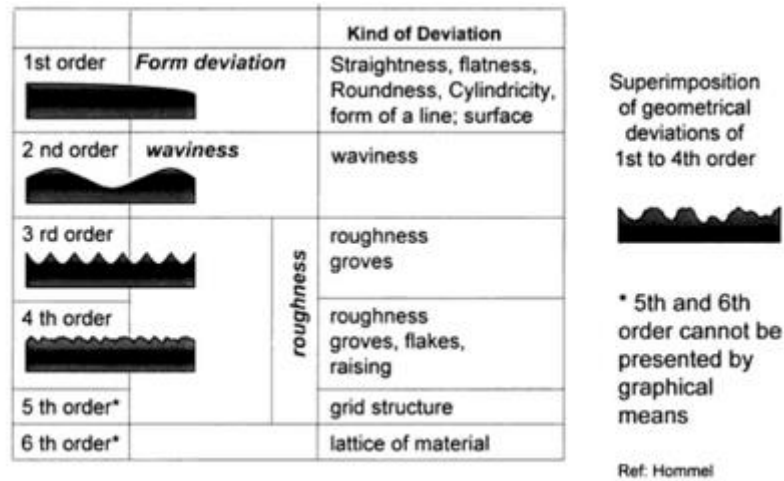


Figure 1 Classification of geometrical properties according to DIN 4760 (45).

As shown in Figure 1, roughness is defined as the third, fourth and fifth order of deviation from the nominal surface wavelength. The first order of deviation refers to form: straightness, flatness, roundness, etc. The second order of deviation refers to waviness. The most common causes of waviness are vibrations, machining chatter, residual stress, work deflections or heat treatment (42). First and second order deviations are due to set-up or machine errors such as poor alignment, material being not properly clamped/restrained, tool and/or machine vibrations, material deflection, material inhomogeneity and tool errors. Third and fourth order deviations are due to irregularities such as grooves, flaking, raising and cracks. Such irregularities are directly related to the tool cutting surface, tool shape, tool condition, the chip formation mechanism and kinematics during machining (43–45). The fifth and sixth order of deviation cannot be represented graphically but are due to the material structure of the workpiece. The material structure is heavily connected to physical-chemical mechanisms acting on a grain and lattice scale (slip, diffusion, oxidation, residual stress, etc.) (43). Figure 1 also shows the first to fourth order superimposed to allow an insight into a sample surface wavelength.

The surface wavelength can be measured to find surface roughness values using a form of surface profile measurement over a sampling length. These can be either contact based; such as a stylus dragged across the surface, or non-contact based; such as an optical measurement.

The most common one-dimensional measurement for surface roughness is R_a , or arithmetic average of the roughness profile. Though many different roughness measurements exist such as R_{RMS} root mean square average, R_V maximum valley depth, R_p maximum peak height, R_{sk} skewness, etc., these roughness tests can be helpful for quality control checks or experimental machining where multiple surfaces are machined using set parameters then measured and compared to find the best performing parameters. The issue arising from this is that the actions occurring that lead to surface roughness are so complex and interacting that explanations cannot be derived from a simple single-dimensioned representation of roughness; nor can they be easily predicted.

Mechanical properties of implant materials are extremely important; however a CoCrMo hip implant for example, is easily adequate to support the weight of a patient. A bigger concern with implants is more focused on how materials behave at the contacting surface (19). This is why the surface quality in dental implants and structures is extremely important. The surface quality of the machined structure (roughness and morphology) determines the area of the contact surface. This contact surface, and its size, are critical to the biocompatibility behaviour, corrosion behaviour and the microorganism and/or human cell interactions with the alloy in the oral cavity (46,47). These claims are backed with multiple studies showing an increased presence of dental caries, gingivitis and periodontal disease due to the high surface roughness of materials present in the oral cavity (24–27). Furthermore A. Aydin (48) showed that by improved finishing and polishing of CoCr castings, oral health and alloy resistance to corrosion may be increased while plaque retention is decreased.

3.3. CoCr Alloys

Cobalt-chromium (CoCr) is a group of non-ferrous metal alloys composed primarily of cobalt and chromium. CoCr alloys are well known to exhibit desirable mechanical properties such as wear resistance, corrosion resistance, biocompatibility and high melting points, and they are non-magnetic (1–16). Although as-cast alloys are commonly used, they do suffer from a relatively low ductility which is a concern when used in implants and prosthetics. As well as medical use such as knee implants, hip implants and dental prosthetics, CoCr alloys are also widely found in gas turbine applications due to their extreme strength under high temperatures and great wear resistance. It is possible for pure cobalt to exhibit two possible crystal microstructures: hexagonal close packed (HCP) at temperatures below 417°C, and face

centred cubic (FCC) at temperatures above 417°C (6). CoCr alloys on the other hand, act differently. The equilibrium phase diagram for CoCr alloys shows that at temperatures above 900°C a face centred cubic (FCC) microstructure is expected, and at temperatures below 900°C a hexagonal close packed (HCP) structure is expected (49). As-cast CoCr alloys are known to exhibit large grains with dendritic-like structures, these dendritic and interdendritic regions forming into FCC and HCP phases respectively (3,11,50). Although CoCr alloys should exhibit a HCP structure at room temperature they tend to exhibit a Co-FCC metastable matrix with the presence of a secondary phase with carbides precipitated at grain boundaries and interdendritic zones (3,41). This is due to the sluggish FCC → HCP transformation that occurs under normal cooling conditions (3,11,19,41,51). Owing to this sluggish transformation, a majority of the FCC structure is retained in the as-cast state, some studies even showing that as little as 4% of HCP remain in as-cast ASTM F75 CoCrMo alloy samples (51). The FCC → HCP transformation can however be isothermally induced, therefore it is possible to have CoCrMo alloys with various volume fractions of the HCP phase (15). Furthermore the stability of these phases can be altered with minor alloying elements added. Elements such as Ni, Fe and N are known to stabilize the FCC structure, whereas Cr, Mo and W tend to stabilize the HCP structure (3).

3.4. CoCrMo Alloys

Cobalt-chromium-molybdenum (CoCrMo) alloys are widely used in orthopaedic and dental applications, specifically in prosthetics and implants (1,3,5–23). CoCrMo is the most popular cobalt based implant material; however two configurations exist and can be distinguished by the carbon content. Low carbon (LC) CoCrMo has a carbon content of less than 0.06%, while high carbon (HC) CoCrMo has a carbon content between 0.15-0.25% (6,8,11,19,22). Both HC CoCrMo and LC CoCrMo contain approximately 28% chromium and 5% molybdenum (13–15,22,41). CoCrMo is used in either cast or wrought forms in dentistry applications and hip/knee implants. Casting provides the ability to manufacture complex shapes that cannot be machined; however un-equal cooling rates, shrinkage porosity and the development of inhomogeneous microstructures limit the abilities of castings (6,8,11,40,41). Because of these limitations, wrought CoCrMo alloys are favourable at times. Wrought CoCrMo alloys are obtained through large castings being hot forged or thermo-mechanically processed, which can then be reworked into smaller sizes (6,8). Furthermore, this process provides the alloy

with superior mechanical and fatigue properties due the closure of existing shrinkage voids and the altered microstructure (8,11,40). Various heat treatments exist for CoCrMo alloys. These heat treatments used for biomedical CoCrMo alloys vary from company to company. Shofu Inc., Japan, supplied the CoCrMo specimens as 'as-cast' (referred to as the as-received (AR) condition), where some companies provide the material in pre-existent heat treated states. Heat treatment of CoCrMo alloys generally serves to alter the microstructure of the material and also strongly affects the carbide phases present. In general CoCrMo heat treatment leads to an altered microstructural phase and/or some of the carbides dissolving into the matrix (6,8,11,41). Variations in the microstructure due to the manufacturing processes, solution treatment and solidification processes have a strong effect on the material's mechanical properties such as strength, corrosion resistance and wear resistance. Therefore it is not uncommon to see samples with the same chemistry exhibiting different microstructures and mechanical properties depending on their thermal history (4,6,8). As-cast CoCrMo alloys, such as the one used in this study, contain a coarse Co-FCC dendritic matrix with the presence of interdendritic and grain boundary carbides in the matrix (1,5,8,9,11,12,15,23,52). This is characteristic of investment casting (6,9,11,15,41), and a major strengthening mechanism in the as-cast condition (11,20). In the case of CoCrMo, it is the chromium and molybdenum elements that migrate to interdendritic areas to form, together with carbon, carbide precipitations (5,23). Chromium is what is responsible for the corrosion resistance properties of CoCrMo, chromium levels above 25% providing great biocompatibility and wear resistance (40). The relatively high levels of chromium present lead to the formation of a chromium rich oxide film (Cr_2O_3) on the surface of the metal (6,11,12,14,22,23,40,52). This spontaneous film and its resulting corrosion resistance is what leads to CoCrMo exhibiting such high biocompatibility. The extreme wear resistance that makes CoCrMo so favourable in implants and prosthetics is due to the carbides present in the microstructure of the material. Carbides have a higher hardness than the surrounding material and therefore create a higher overall abrasion resistance for the material. The wear rate of these alloys is directly related to the size, distribution and amount of carbides present in the microstructure. It is well known that thermal processing affects carbide size and distribution, and as such as-cast CoCrMo alloys have been found to have greater wear resistance than heat treated specimens due to having a higher volume fraction of carbides present (6,8). As-cast CoCrMo alloys contain a large, irregular and blocky carbide morphology

within the grains and at the grain boundaries, with the carbides being rich in chromium and molybdenum. Heat treated CoCrMo alloys tend to display an agglomeration of particulate carbides which are finely dispersed at grain boundaries with the carbides being richer in chromium than molybdenum (3,5,6,8,23,41). Pictures of these microstructures showing the large, irregular, blocky carbide morphology of as-cast CoCrMo alloys and the finely dispersed agglomeration of particulate carbides in heat treated CoCrMo alloys are shown in Figures 2 and 3. Note the AC sample was supplied 'as-cast' and complied with ASTM F-75, with the heat treated sample being "An as-cast sample having a solution annealed heat treatment of $(1200\pm 10)^{\circ}\text{C}$ in a soft vacuum $< 5\times 10^{-1}$ mbar, for 4 h, then quenched in nitrogen gas from 1200 to 800°C at a cooling rate of $50^{\circ}\text{C}/\text{min}$ (minimum)" Images were taken from work done by J. Cawley et al. (8).

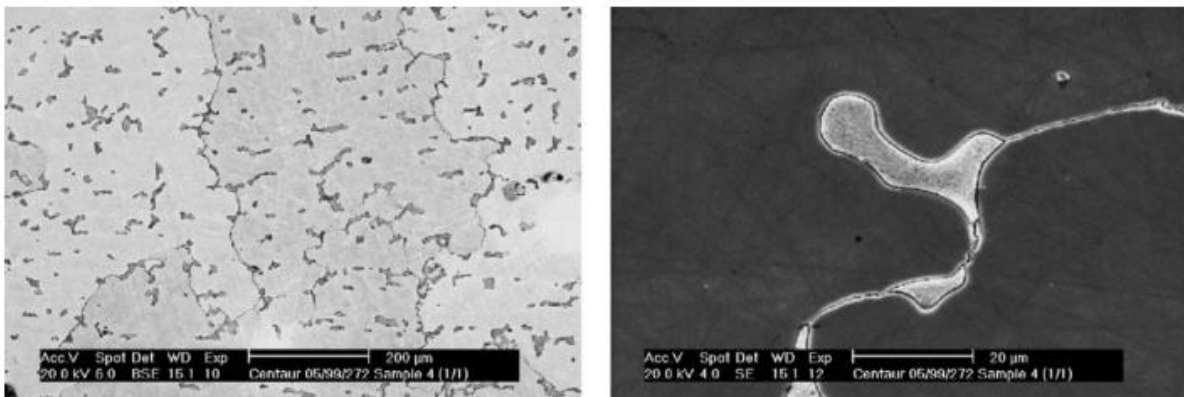


Figure 2 SEM micrographs of the as-cast (AC) CoCrMo sample (grain boundary etched and carbide stained). J. Cawley et al. (8).

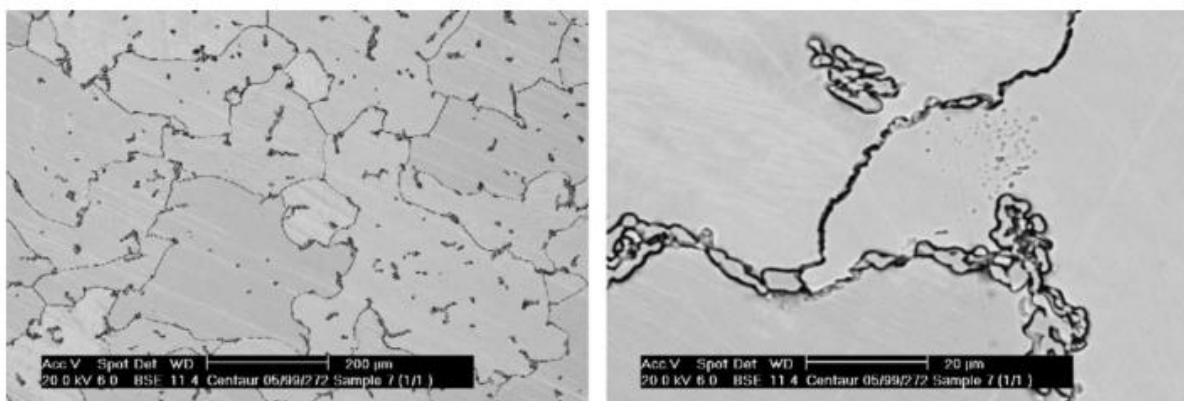


Figure 3 SEM micrographs of the heat-treated (HT) CoCrMo sample (grain boundary etched and carbide stained) J. Cawley et al. (8).

Shown in Figures 2 and 3 are the comparative microstructures of as-cast (AC) and heat-treated (HT) CoCrMo samples with the grain boundaries etched and the carbides stained. Figure 2 shows the AC sample with its large, irregular, and blocky carbide morphology, and Figure 3 shows the HT sample with the finely dispersed agglomeration of particulate carbides.

Although the microstructure of as-cast CoCrMo is well documented, there has been research into this lately to confirm these predictions. B. Henriques et al. (12) analysed the microstructure of an cast CoCrMo sample. The specimen was found to contain a Co-FCC rich dendritic matrix with interdendritic HCP regions. Due to the alloy used by B. Henriques et al. (12) containing very little or no carbon content there were no carbides seen. This work undertaken by B. Henriques et al. (12) agrees with work undertaken by Y S Al Jabbari (41), which showed that the cast CoCrMo specimens exhibited a typical cast structure of a CoCr dental alloy. This typical cast structure was defined as being composed of a dendritic Co-FCC matrix, and a heavier dispersed second phase that occupies the interdendritic spaces and grain boundaries (11,40,41). This was reiterated by B. Karpuschewski (14). However, contrary to claims by B. Henriques (12), Y. S. Al Jabbari (41) found that it was possible for low carbon content raw material to form carbides during the manufacturing process which will affect the nominal properties. The most commonly observed carbides in these alloys consist of carbon and chromium and/or molybdenum and include M₆C, M₇C₃, M₁₂C, and M₂₃C₆ (11,19,21).

3.5. Machining CoCrMo

Little scientific literature exists relating to the machining of CoCrMo, specifically the milling of as-cast alloys. A. Bordin et al. (1) looked at the machinability of electron beam melted (EBM) CoCrMo compared with wrought CoCrMo in semi-finishing turning operations, the work focusing on machinability; specifically tool wear and surface integrity. A wrought alloy; ASTM F1537, and an EBM alloy; F75EBM, were machined with a TiAlN PVD tungsten carbide (WC) tool (1). Adhesion, notching and chipping of the tool cutting edge were the most significant wear mechanisms for the wrought alloy, though “none of the tested cutting conditions resulted in reaching the tool wear criteria” (1). In the case of the EBM alloy, extreme abrasion was the most significant wear mechanism. In all cases the tool’s coating was worn after just 3 minutes of turning; furthermore the tool life criteria for three of the four cutting conditions was reached (1). The increased tool wear was associated with the large amount of hard

carbide particles that characterize the EBM microstructure. It was observed that the surface roughness was mainly affected by the feed rate, “for all the turning times the average (roughness) values are incremented of more than 50% by increasing the feed rate from 0.1 to 0.15 mm/rev” (1). In the case of turning it was shown that the main surface defects were material side flow and plastic deformation for both alloys, though for the EBM alloy these kinds of defects could be considered secondary issues with the main issues being the formation of craters, laps and cracks between feed marks (1). Further research undertaken by A. Bordin et al. (7) showed that under certain conditions, the surface integrity of CoCrMo alloys subjected to dry turning was not altered by the dry conditions and showed comparable results to typical wet turning. A CoCrMo bar was machined using a semi-finishing turning test with a PVD TiAlN tungsten carbide tool (7). The variations in surface finish were attributed mainly to the change in feed rate, “The smoothest surface resulted from a feed rate of 0.1mm/rev, while for a feed rate of 0.15 mm/rev, the surface roughness resulted was not useful for biomedical applications.” (7). The predominant tool wear mechanism was adhesion, with large of amounts of material adhering to the tool rake face. Smearred material, burrs, tears, adhered chip particles and adhered material fragments were the major surface defects found on the CoCrMo surface. These defects were linked to the feed rate, “At the highest level of feed rate, a sensible increment of burrs and adhered chip fragments were noted on the machined surfaces” (7). Examples of these defects are shown in Figure 4 taken from work done by A. Bordin et al. (7).

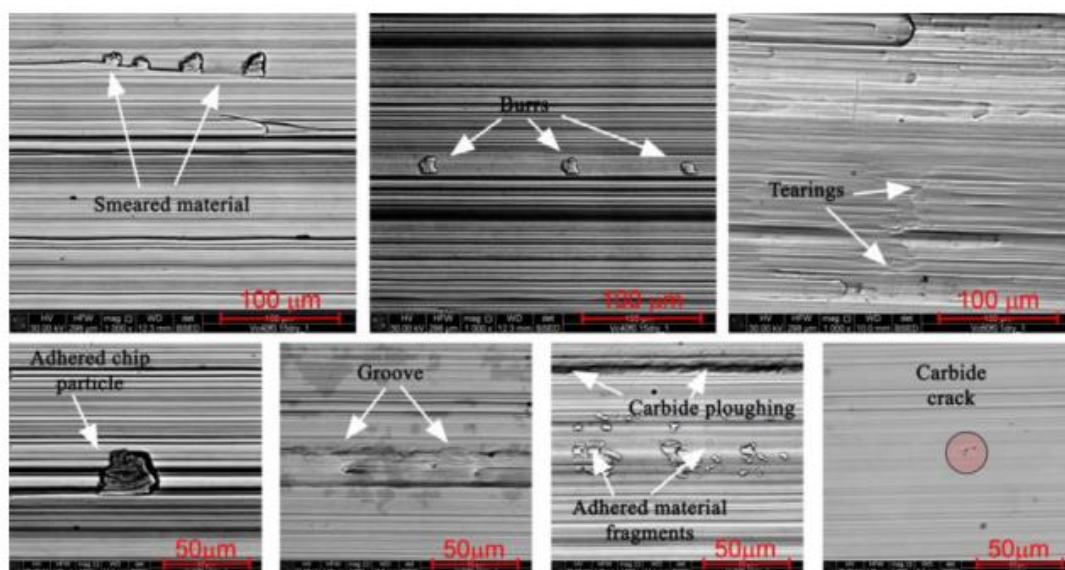


Figure 4 SEM images of surface defects found in dry turning of ASTM F1537 CoCrMo (7).

T. Pasang et al. (28) researched the machining of two biomedical alloys: cobalt-chromium-molybdenum (CoCrMo), and titanium-aluminium-niobium (TiAlNb). CoCrMo is well known for applications in the dental industry, while TiAlNb is extensively used in joint prostheses (28). The study aimed to examine the performance of each alloy while undergoing lateral face milling, the performance being measured with respect to the cutting (milling) forces, and the obtained surface finish. Four different cemented tungsten carbide (WC) mills were used, three of them uncoated, and the fourth coated in a diamond-like carbide (DLC) layer. Milling spindle speed was adjusted from 10,000 RPM to 35,000 RPM in 5000 RPM increments (28). Milling was undertaken at room temperature with no lubrication or cooling, with a load cell measuring cutting forces, then SEM analysis was used to look at the surface finish and tool wear (28). TiAlNb showed fairly consistent cutting forces for all speeds between 10,000 RPM and 35,000 RPM, mill geometry and speed having little effect on the cutting forces which ranged from 0.5N to 2N (28). CoCrMo was more sensitive to cutting speed and showed generally higher forces at speeds of 10,000 RPM, with one mill not experiencing this trend. Between 15,000 RPM to 35,000 RPM the mills experienced comparable forces of approximately 1N (28), though one mill required much less force. The surfaces were examined using scanning electron microscopy (SEM), the SEM images of both alloys showing surface finishes with “significant variations related to the extent to which metal chips retained in the mill flutes had frictionally re-welded onto the surfaces behind the mill” (28). This was associated with a combination of high machining temperature and tool wear. ‘Machining Cobalt-Based Dental Alloys with Tungsten Carbide Mills’ by M. Takahashi et al. (12) looked at the cutting forces experienced during lateral milling of CoCrTi and CoCr with cemented tungsten carbide (WC) mills. Two types of milling were undertaken: side milling and central slot milling. The study emphasised the need for a reliable and repeatable test to evaluate tool performance. The secondary priority was to investigate the milling characteristics of cobalt chromium (CoCr) and cobalt chromium titanium (CoCrTi) (29). As in the aforementioned study by T. Pasang et al. (28), four different cemented tungsten carbide (WC) mills were used, three of them uncoated with the fourth being coated in a diamond-like carbon (DLC) layer. The specimens were machined by means of a modified bench milling machine with the normal spindle replaced by a high speed dental spindle held securely in place as shown in Figure 5 taken from work done by M. Takahashi et al. (29).

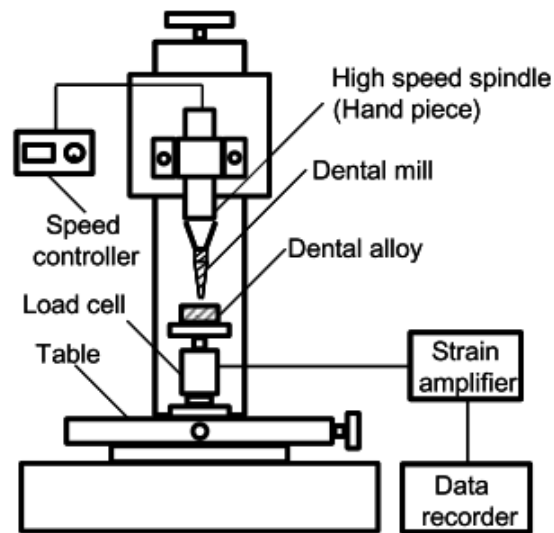


Figure 5 Experimental setup for investigating milling operations. M. Takahashi et al. (29).

The setup used allowed repeatability and removed many factors that could influence the results. Spindle speeds were varied from 10,000 RPM to 35,000 RPM, in increments of 5000 RPM, with the feed rate held constant at 0.15mm/second (29). During central slot milling of CoCr it was found that lower speeds had generally higher cutting forces with speeds of 12,000 RPM to 20,000 RPM experiencing greater forces than speeds of 24,000 RPM to 30,000 RPM. Some instability occurred at lower speeds, but forces were relatively stable at speeds ranging between 25,000 RPM to 30,000 RPM (29). The DLC coated mill did not show significantly lower forces during milling; though it was believed, and later shown under SEM, that the coating was rapidly worn off. There is a lack of data regarding the central milling experiments with CoCrTi. Two of the mills were not used at any speeds, while two more were used for low speed passes only. Extreme mill wear, failure and machining heat led to the abandonment of these experiments, however they did show that CoCrTi had a much lower machinability than CoCr (29). Lateral milling cutting forces were lower than those of central slot milling for both alloys, cutting forces being generally relatively high at low speeds of 10,000 RPM but decreased at higher speeds and stabilised (29). At higher speeds, multiple mills were having slipping issues where the spindle would loosen on the mill during milling. The DLC coated drill did not have this issue, possibly due to its lowered coefficient of friction (29). SEM analysis of the milled surfaces in both central slot milling and side milling showed that re-welded chips were a leading cause of poor surface quality. It is recommended that the use of cooling fluid during machining is likely to reduce the problem of chip re-welding and abrasion issues (29).

R. Polini et al. (31) investigated the use of chemical vapour deposition (CVD) diamond coated dental tools to see whether adding a HFCVD (Hot Filament Chemical Vapour Deposition) diamond coating was feasible. CoCrMo specimens were milled by three different WC-Co mills with different geometries in both coated and uncoated conditions (31). According to the authors this was the first time anyone had “studied and compared the cutting behaviour of both virgin and diamond-coated dental tools by measuring both wear and cutting force time evolution under milling a very hard Co–Cr–Mo dental alloy” (31). A modified bench milling setup was used to ensure consistent cutting speeds and feed rates of 20,000 RPM and 0.01 m/min respectively (31). One of the primary focuses of this study was to constantly measure cutting forces throughout the entire milling experiment, as opposed to peak measurements or average measurements. This constant force measurement combined with consistent cutting conditions was used in order to allow a deeper characterization of the dental mills, “In this way, it is possible to separate several effects than can be present during milling (such as tool loading, built-up edge formation, tool–material friction reduction)” (31). It was noted that although various cutting force measurement experiments have been undertaken in the past they all used simple inserts and never complex mill geometry with a conical multi-cutting surface, such as those found in small dental mills. Lateral down milling was used in this study. The milling machine had no issues with force and maintained its rotational speed throughout the milling, the feed rate also staying constant with no resistance issues (31). Two of the mills; one uncoated and one coated, were successfully used to complete a milling pass. They were then examined under SEM imaging, which clearly showed a CoCr built up edge on the cutting surface (31). The same two mills were then used for a second milling pass, the CVD coated mill completing the pass, whereas the uncoated mill suffered a catastrophic failure. It was shown under SEM analysis that the uncoated mill failed due to high temperature that provoked a sudden degradation (31). A similar test was run using two new mills; one uncoated and one coated, with the hope of running two milling passes to compare. However both mills suffered catastrophic failure. The failure was linked to the lack of chip breaker geometry in these mills, chip breakers being necessary to reduce mill loading. The forces observed before failure were similar to the two mills tested earlier “thus confirming that the main factor which led to inadequate performance of both mills was the cutting edge geometry and the lack of the chip-breaker” (31). Key observations taken from this study were that: feed rates need to be extremely low when machining CoCrMo and are recommended to be even lower than 0.01

m/min; the CVD coated tools experienced significant longer tool life and a significantly lower cutting force; chip breakers are crucial to reducing cutting forces and improving tool life (31). Further work discussing CoCrMo showed that CoCrMo components formed using casting exhibit excellent creep strength and toughness. These characteristics can be desirable for certain applications but also lead to poor machinability, this being due to poor chip segmentation and their high hardness (10,12). Though casting does exhibit some machining benefits due to CoCrMo alloys' poor machinability, by casting complex implants with dimensions close to final tolerances, the reduction of high cost machining operations can be achieved (11).

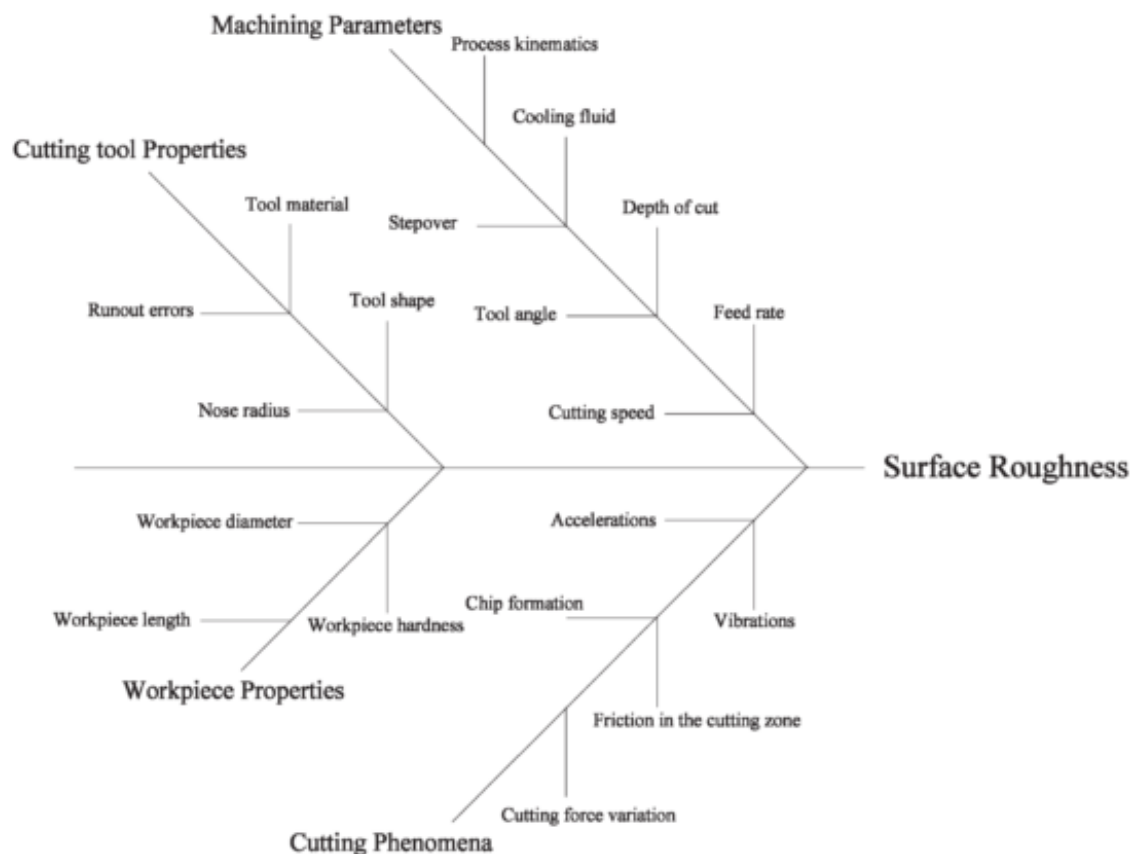


Figure 6 Fishbone diagram listing parameters that affect surface roughness. P G Benardos (43).

Finally, Figure 6 from work done by P G Benardos et al. (43), shows factors that affect surface roughness. Cutting speed and tool shape will be the adjustable factors in this study, while the remaining workpiece properties, cutting tool properties and machining properties will be maintained as consistently as possible throughout all experiments.

3.6. Micro-Machining

In macro-machining it is generally assumed that the cutting thickness per tool edge (h) is larger than the cutting tool edge radius (R) and this ratio leads to complete surface removal and generation of chips. However in micro-machining the ratios of the cutting thickness per tool edge (h) compared to cutting tool edge radius (R) are significantly smaller and this often leads to ploughing, rubbing and compression occurring. The difference occurring due to the significant scaling of the macro-machining process is known as the “size effect” in literature, and results in the nonlinear change of the surface quality and cutting forces for processes with small cutting thickness (32,34,38).

Micro-scale machining is becoming increasingly popular as the need for the production of miniaturized components rises (32–34). Biomedical instruments, electronic products, the aerospace industry and the defence industry are major areas where micro-machining will be vastly important (33–37). Micro-milling is considered as one of the most successful micro-machining techniques currently in use, allowing for the fabrication of minute components with complex micro features in a variety of metallic and non-metallic materials (32–35). However, it has become apparent that micro-machining is much more complicated than simply scaling down macro-machining tools and parameters and as such, investigations into these micro-machining techniques are becoming increasingly popular and desired. Size effect and the minimum chip thickness are said to heavily effect surface finish and tool wear in micro-machining (32,35,36,38). The minimum chip thickness theory states that a chip will not be formed if the cutting thickness is less than the minimum thickness of cut h_{min} , this being due to the highly negative tool rake angle occurring owing to the comparable cutting thickness (h) and tool edge radius (R) (32,34,35,38). When cutting thickness is below h_{min} a phenomena will occur known as ploughing, which is an elastic-plastic deformation without effective material removal (32,35,38). X. Lai et al. (35) studied the “Modelling and analysis of micro scale milling considering size effect, micro cutter edge radius and minimum chip thickness”. X. Lai et al. (35) undertook this research to provide a deeper understanding of the micro scale milling process. The study started by modifying a Johnson-Cook (JC) constitutive equation using SG plasticity. Next a finite element (FE) model for micro scale orthogonal machining was developed. From there a milling force model could be developed from the FE simulation results, this allowing the chip formation and size effect of micro scale milling to be investigated by applying the model (35). It was found that for OFHC copper the minimum chip

thickness is $0.25R$ (25% of cutting edge radius) when the cutter radius is $2\mu\text{m}$ and rake angle is 10° , this agreed well with previous predictions seen in their literature review (35). Shown in Figure 7 is part of the FE simulation showing the chip formation process under different ratios of h (cutting thickness per edge) and R (cutting edge radius). It is shown that, at $h = 0.2R$ Fig. 8 (b), no chip formation occurs, whereas, at $h = 0.3R$ Fig. 8 (C), there is chip formation and this led to the hypothesis of minimum chip thickness being $0.25R$.

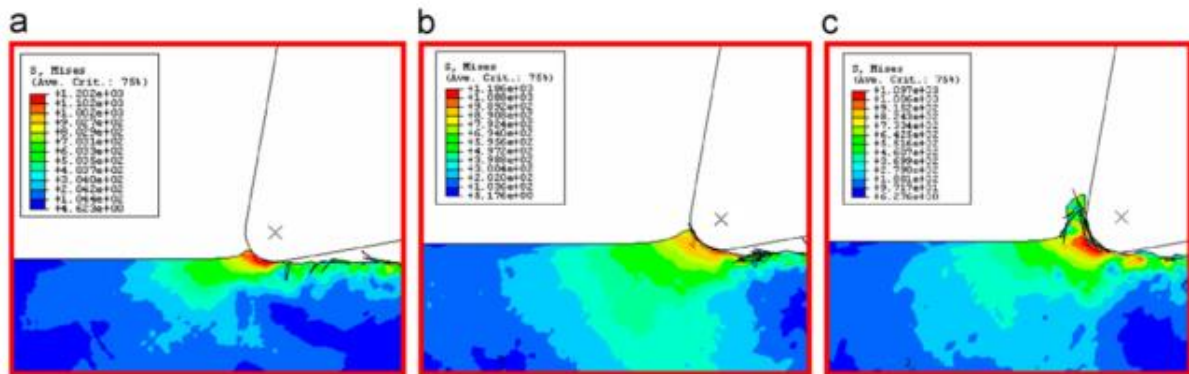


Figure 7 Chip formation process. (a) $h = 0.1R$ (0.2mm); (b) $h = 0.2R$ (0.4mm); (c) $h = 0.3R$ (0.6mm). X. Lai et al. (35).

The ploughing phenomenon was also noted in this work and occurred when the cutting thickness per edge (h) was less than the minimum chip thickness (h_{min}). When cutting thickness per edge (h) was less than the minimum chip thickness (h_{min}), the chip was not formed after the first tool pass, resulting in the chip thickness doubling for the second tool pass. It was concluded that “the chip thickness would be accumulated until the actual chip thickness is larger than (h_{min}), which will in turn cause the increase in the milling force and the SSE ” (35,38). Furthermore, the research undertaken by X. Lai et al. (35) stated that “the size effect of micro scale milling process is caused by the material strengthening behaviours at the micron level” (35) meaning this ploughing effect is causing severe work hardening to occur.

Further work undertaken by H. Autenrieth et al. (38) into “the transition from ploughing to cutting in micro machining and evaluation of the minimum thickness of cut” evaluated both the size effect and minimum chip thickness occurring in micro-machining, specifically micro-milling. H. Autenrich et al. (38) heavily stated that the micro milling process is determined by both the ploughing and chip formation mechanism (38). Therefore in order to obtain the best surface finish and avoid the ploughing mechanism a better understanding of the minimum chip thickness was needed. A major point of discussion in this work was the effect of the built

up edge (BUE) and how it needs to be taken into account when determining h_{min} . In metal cutting a BUE will occur on the tool face often when a continuous chip is being formed due to the accumulation of workpiece material on the rake face of the cutting tool (38). These BUEs are created under high pressure and temperature and often occur while machining materials with a high work hardening characteristic. The rewelded layers can be torn down by the effluent chip and rewelded to the workpiece surface (38). Conclusions drawn from this work show that a definite transition period occurs from ploughing being the dominant mechanism, to chip formation being the dominant mechanism. Furthermore the values required for the minimum cutting thickness per edge required for chip formation significantly increase with lower cutting velocities and higher cutting edge radii (BUE) and this is believed to be due to the suppressed chip formation under these conditions (38).

Research undertaken by F. Brandao et al. (32), proposed an experimental method to “determine the size effect, specific cutting force and minimum uncut chip thickness in micro-milling of dual phase carbon steel”. Validation for this study was achieved by correlating their results with high factoring machining variables such as cutting force, chip formation and workpiece roughness (32). Further validation was achieved through comparisons to macro-milling and literature results (32). Milling tests were undertaken using a CNC machining centre Hermle C800U. Figure 8 shows the experimental matrix. Carbide endmill tools with TiNAl coatings and two flutes were used (32).

Experimental matrix for micro- and macroscale milling.

Cutting parameters	Micromilling/microscale ($w = d_t = 0.8 \text{ mm}$)				Macromilling/macroscale ($w = d_t = 2.0 \text{ mm}$)			
	f [$\mu\text{m}/\text{tooth}$]	5	10	5	10	10	20	10
d [μm]	80	80	160	160	160	160	320	320
Nomenclature	$f5-$ $d80$	$f10-$ $d80$	$f5-$ $d160$	$f10-$ $d160^a$	$f10-$ $d160^a$	$f20-$ $d160$	$f10-$ $d320$	$f20-$ $d320$

^a Feed per tooth (f) and depth of cut (d) adopted as maximum for micromilling and minimum for macromilling.

Figure 8 Experimental matrix for micro-scale and macro-scale milling tests. F. Brandao et al. (32).

Once all tests were completed the obtained data were statistically analysed using Analysis of Variance (ANOVA). Results showed that the size effect is present in both micro- and macro-scale milling; however it is generally ignored in macro-scale milling owing to the fact that the

“ratio between uncut chip thickness and tool edge is always greater than unity. Otherwise, the size effect can be significant for micro-milling because the aforementioned ratio can reach values lower than unit” (32). The authors concluded by stating that the minimum uncut chip thickness varies from 1/4 to 1/3 of tool cutting edge (0.25R and 0.33R respectively), regardless of workpiece material, tool geometry, mechanical machining process or techniques used for measuring or estimating h_{min} . This was validated by comparing their results with significant literature on the subject (32). Furthermore, the authors stated that despite the h_{min} guaranteeing complete chip formation, it does not guarantee a good surface finish and “another thickness above the minimum uncut chip thickness which minimizes the ploughing effect must exist and be pursued” (32). This agrees with work done by V. Huntrupl et al. (53). Research into micro-milling steel by V. Huntrupl et al. (53) noted the significance BUE can have in the surface finish of micro-milled materials. It is stated that the increase of surface roughness at low cutting velocities and/or soft workpiece states is caused by the BUE (53). It is further recommended that the use of high cutting velocities and hard homogeneous materials is the best way to obtain acceptable surface finishes, also stating that cutting edge radius is a major factor in surface finish of micro-milling (53). The research goes on to state that originally it was difficult to definitively link the minimum cutting depth h_{min} , to the achievable surface roughness. It was said that the obtainable surface roughness was given by the following equation in Equation 1, with h_{min} being minimum depth of cut, r the tool edge radius, f_z the feed per tooth, and R_{th} the theoretically achievable surface finish.

Equation 1 Theoretically Achievable Surface Finish.

$$R_{th} = \frac{f_z^2}{8r} + \frac{h_{min}}{2} \left(1 + \frac{r \cdot h_{min}}{f_z^2} \right) \quad (1)$$

The fault with this lay in the fact that the minimum cutting depth can only be obtained using estimation or experimental results. Therefore a new way to prove the importance of h_{min} was needed. By analysing the equation, it was concluded that the cross section of the machined surface should present a saw tooth-like profile if the minimum chip thickness effect is occurring, as illustrated in Figure 9 (53).

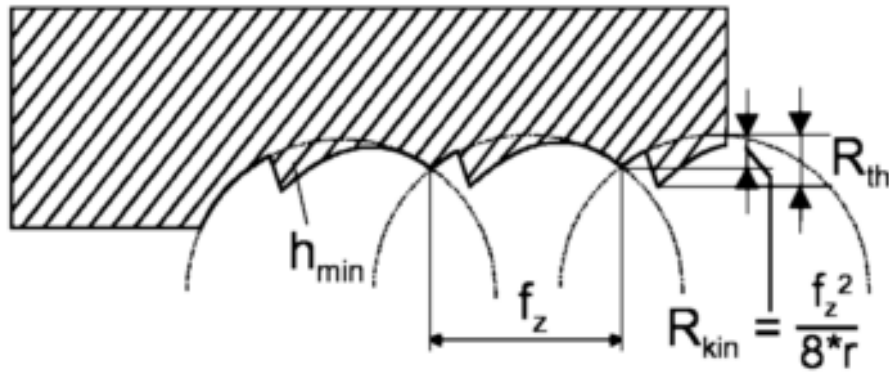


Figure 9 Theoretical surface profile, assuming the minimum cutting depth (h_{min}) determines the achievable surface roughness. V. Huntrupl et al. (53).

V. Huntrupl et al. (53) then measured the topography of a micro-milled surface using a laser based topography device, and confirmed the presence of a saw tooth-like profile and therefore validated that h_{min} is highly probably responsible for the acquired surface quality (53). This research was concluded with the following statement “In order to improve the achievable surface quality a deeper understanding of the influence of the material properties on the minimum cutting depth is needed” (53).

F. Ducobu et al. (34) looked to further clarify the chip formation process in micro-cutting and investigated the approximate value of the minimum chip thickness h_{min} related to the tool edge radius (R). It was stated that three main conditions occur with $h < h_{min}$ leading to ploughing, $h \approx h_{min}$ leading to ploughing and chip formation, and $h > h_{min}$ leading to complete chip removal. This is illustrated in Figure 10 showing the transition from pure ploughing to complete material removal and agrees with work done by H. Autenrieth et al. (38).

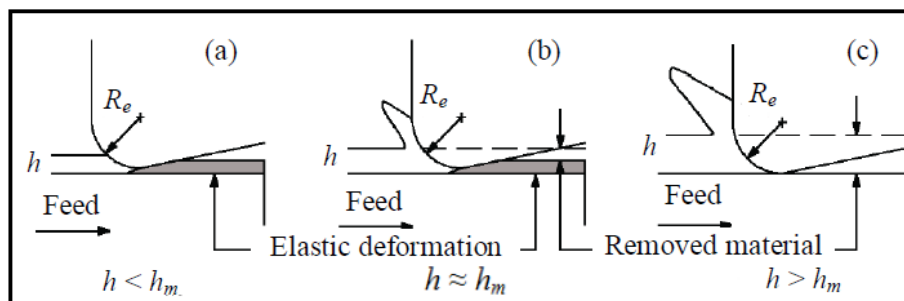


Figure 10 Schematic representation of the minimum chip thickness in orthogonal cutting; r : edge radius of cutting tool, h : depth of cut, h_m : minimum chip thickness. F. Ducobu et al. (34).

The study tested eight ratios of h/r ranging from 14 to 0.05. It was found that for values where $h/r < 0.25$ no chip was formed. In this region the material seemed not to be sheared but

instead pushed and deformed under the tool, this material then accumulating in front of the tool until it reaches a thickness greater than h_{min} when it is sheared off (34). Chip morphologies for h/r from 0.5 to 0.05 are shown in Figure 11.

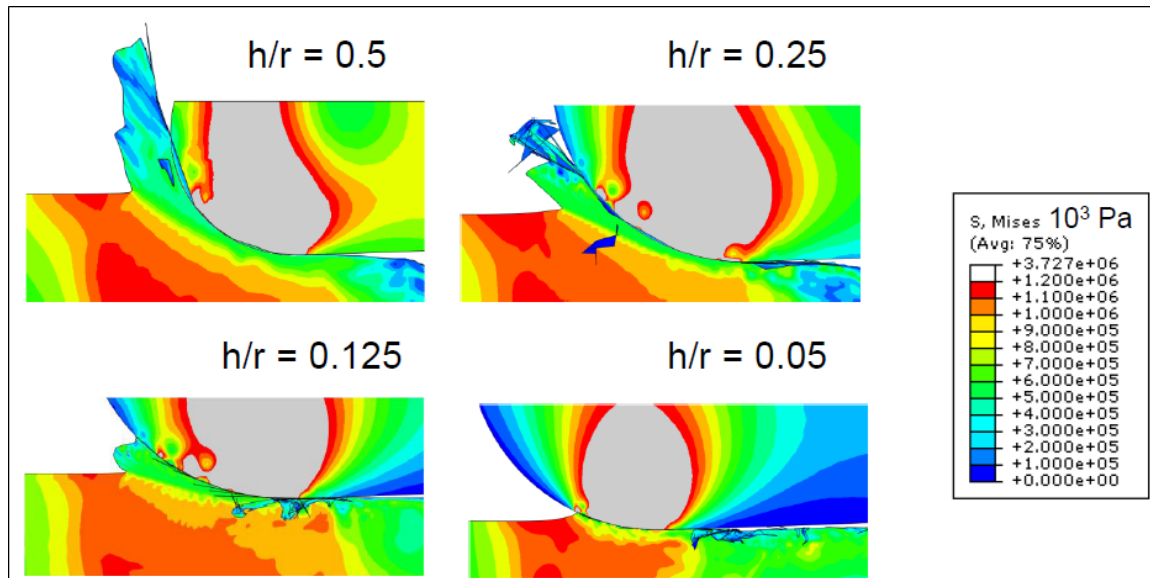


Figure 11 Chip morphologies for h/r values ranging from 0.5 to 0.05. F. Ducobu et al. (34).

F. Ducobu et al. (34) concluded that the down-sizing of milling does induce significant changes in the cutting phenomena with minimum chip thickness being a major factor. The authors predict a minimum chip thickness value in the order of 25% of R , with a lower limit around 12.5% of R and an upper limit of 50% of R with R representing the cutting edge radius (34).

K. Aslantas et al. (36) studied the “Cutting performance of nano-crystalline diamond (NCD) coating in micro-milling of Ti 6 Al 4 V alloy”, an experimental study involved the milling of Ti-6Al-4V with multiple mill coating conditions. They found the critical value of feed per tooth to be $f_z = 0.5 \mu m$ regardless of tool coating, this being with an average tool cutting edge radius of $1.65 \mu m$ (36). Calculating this leads to an h/r ratio of roughly 0.3.

M. Malekian et al. (54) investigated the modelling of the minimum cutting thickness per edge in micro machining of aluminium, the model being based on the minimum energy principle and the infinite shear strain method. After analysis the average minimum cutting thickness per edge was determined experimentally to be approximately 0.23 of the edge radius, this agreed well with the model predictions (54).

J. Pathak investigated the design, assembly and testing of an ultra-high speed micro-milling spindle (33). One of the most notable motivations for design was the tool run-out. The author claimed that “Typical milling spindles used for these small tools employ either rolling element

bearings or air bearings to support the spindle shaft and the combination of asynchronous spindle bearing error motions and clamping errors often result in tool run-out 3 to 20 times the nominal chip thickness". This means that it is possible for some tool edges to not contact the surface at all while others are forced to cut chips several times larger than the desired depth of cut (33). This tool run-out is much larger than comparative figures occurring in macro-milling and therefore runs a very large risk of overloading the tool due to extreme cutting force variations. G. Beruvides et al. (37) also stated that chatter and run-out have an extremely strong influence on obtainable surface finish in micro-milling processes.

3.7. Summary of Literature

Despite modern biomedical implants being constructed from a range of materials including composites; metallic implants and metal alloys used for fixed dental prostheses are still widely used in the industry (2,3,14,40).

Cobalt-chromium (CoCr) alloys are well known to exhibit desirable mechanical properties such as wear resistance, corrosion resistance, biocompatibility and high melting points, and are non-magnetic (1–16). As-cast CoCr alloys are known to exhibit large grains with dendrite-like structures, these dendritic and interdendritic regions form into FCC and HCP phases respectively (3,11,50). CoCr alloys exhibit a Co-FCC metastable matrix with the presence of a secondary phase and carbides precipitated at grain boundaries and interdendritic zones (3,41). This is due to the sluggish FCC → HCP transformation that occurs under normal cooling conditions (3,11,19,41,51). Cobalt-chromium-molybdenum (CoCrMo) alloys are widely used in orthopaedic and dental applications, specifically in prosthetics and implants (1,3,5–23). Little scientific literature exists relating to the machining of CoCrMo. A. Bordin et al. (1) looked at the machinability of CoCrMo. The predominant tool wear mechanism found was adhesion with large amounts of material adhering to the rake face. Smear material, burrs, tears, adhered chip particles and adhered material fragments were the main surface defects found on the CoCrMo surface (1). T. Pasang et al. (28) researched machining work performed on two biomedical alloys: cobalt-chromium-molybdenum (CoCrMo), and Titanium-aluminium-niobium (TiAlNb). SEM images of both alloys showed surface finishes with "significant variations related to the extent to which metal chips retained in the mill flutes had frictionally re-welded onto the surfaces behind the mill" (28). M. Takahashi et al. (29) looked at the cutting forces experienced during lateral milling of CoCrTi and CoCr with cemented tungsten

carbide (WC) mills. SEM analysis of the milled surfaces showed that rewelded chips were a leading cause of poor surface quality. Further issues were extreme tool wear (29). R. Polini et al. (31) investigated the use of CVD diamond coated dental tools. Key observations taken from this study were: feed rates need to be extremely low when machining CoCrMo, the CVD coated tools experienced significant longer tool life and a much lower cutting force, and chip breakers on the mill are crucial to reducing force and improving tool life (31).

In micro-scale machining the size effect and the minimum chip thickness are said to heavily effect surface finish and tool wear and there is also said to be a distinct transition from ploughing to chip formation when a minimum chip thickness is reached (32,35,36,38). X. Lai et al. (35) found that for OFHC copper, the minimum chip thickness is 0.25R (25% of cutting edge radius) and this agreed well with previous predictions seen in their literature review (35). Work undertaken by H. Autenrieth et al. (38) showed that a transition period occurs from ploughing being the dominant mechanism, to chip formation being the dominant mechanism. Work undertaken by F. Brandao et al. (32) concluded by stating that the minimum uncut chip thickness varies from 0.25R to 0.33R regardless of workpiece material, tool geometry, mechanical machining process or techniques used for measuring or estimating h_{min} . Research into micro-milling steel by V. Hunrupl et al. (53) stated that if h_{min} does exist a saw tooth-like profile should be present. V. Hunrupl et al. (53) then measured the topography of a micro-milled surface using a laser based topography device. It confirmed the presence of a saw tooth-like profile and therefore validated that h_{min} is highly probably responsible for the acquired surface quality (53). F. Ducobu et al. (34) predicted a minimum chip thickness value in the order of 0.25R (34). K. Aslantas et al. (36) calculated a minimum chip thickness of roughly 0.3R. M. Malekian et al. (54) investigated the modelling of minimum chip thickness in micro machining of aluminium calculating a minimum chip thickness of approximately 0.23R. J. Pathak (33) claimed that "Typical milling spindles used for these small tools employ either rolling element bearings or air bearings to support the spindle shaft and the combination of asynchronous spindle bearing error motions and clamping errors often resulted in tool run-out 3 to 20 times the nominal chip thickness". Therefore it is possible for some tool edges to not contact the surface while others are forced to cut chips several times larger than the desired depth of cut (33). Finally it was noted through literature that cutting conditions including maximum cutting speed, minimum feed rate and low depth of cut resulted in minimum surface roughness and the best obtained surface qualities (33,53,55).

4.0. Methodology

The CoCrMo specimens used in this study were machined/milled at Akita University, Japan. The force measurements were recorded during milling. A short description of the milling undertaken is provided by M. Takahashi et al. (29), "A bench milling machine was modified by the addition of a vertical spindle milling device. The standard spindle of the milling machine was replaced with a high speed spindle (hand piece) fitted by a dental technician and held in a securely fixed position. The high speed spindle (Push-BL50) was supplied by Shofu Inc., Japan. The cutting tool rotation speed of the spindle was able to be varied in the range of 1000~50000 RPM". This set-up is shown in Figure 12 taken from work done by M. Takahashi et al. (29).

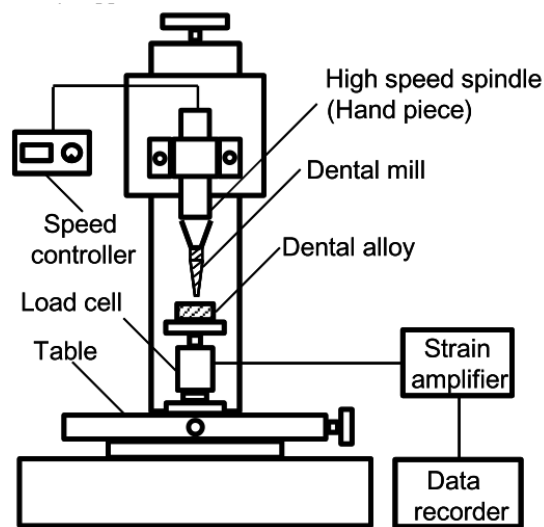


Figure 12 Experimental milling setup. M. Takahashi et al. (29).

The specimens were machined using lateral face milling with varying rotational spindle speeds. The spindle speed ranged from 10,000 RPM to 35,000 RPM, in increments of 5000 RPM. The forward feed rate was fixed at 0.15 mm/sec for all experiments. The experimental milling was undertaken at room temperature with a milling and drilling oil, Fras und Bohrol, supplied by Bredent GmbH & Co., Germany. The milling and drilling oil was used for lubrication and cooling and was manually sprayed onto the surface as milling was undertaken. A schematic of the milling is shown in Figure 13 showing the depth of cut and thickness of cut. This image was obtained from prior work done by T. Pasang et al. (28) using similar materials and identical milling tools as in this study.

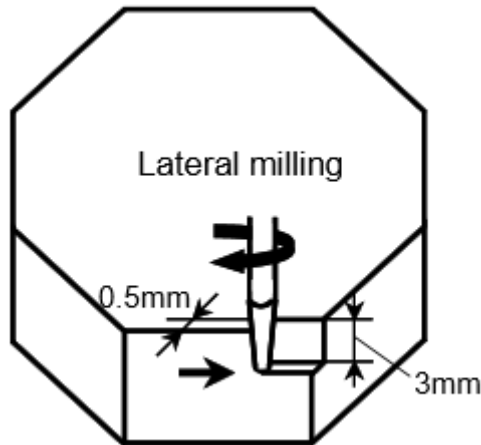


Figure 13 Lateral face milling diagram. T. Pasang et al. (28).

The supplied specimens were labelled with the material name and milling parameters, and were packaged with chips from the milling, the used milling tool and an unused milling tool for comparison. Once these specimens were supplied they underwent a series of testing including: scanning electron microscopy (SEM), micro hardness testing, energy dispersive X-ray spectroscopy (EDS) and roughness testing. Furthermore, the supplied cutting forces were analysed. The technique/equipment was used in order to better understand the cutting process and how the rotational spindle speeds, use of coolant, material hardness and mill geometry selection affected the surface finish.

4.1. Material

The material used in this study was a CoCrMo alloy; specifically a high carbon Co-29Cr-6Mo alloy (Cobaltan) supplied by Shofu Inc., Kyoto, Japan. 20g ingots of 'Cobaltan' from Shofu Inc. were used. The specimens were supplied in an octagonal prism shape. The octagonal prism shape offered the perfect design for this experiment. Each ingot was assigned a milling tool, then 6 of the eight flat faces were milled at various speeds to obtain a single specimen that contained six milling passes ranging from 10,000 RPM to 35,000 RPM from the same mill. This setup offered great comparability. Examples are shown in Figures 14 and 15. The chemical composition of the CoCrMo alloy (Cobaltan) is shown in Table 1.

Table 1 Chemical composition of CoCrMo (Cobaltan) alloy.

Chemical Composition of CoCrMo (Cobaltan) Weight %								
Co	Cr	Mo	Ni	Fe	C	N	Mn	Si
Bal.	28.9	5.91	0.01	0.04	0.18	0.23	0.26	0.49



Figure 14 Cobaltan ingot from above.

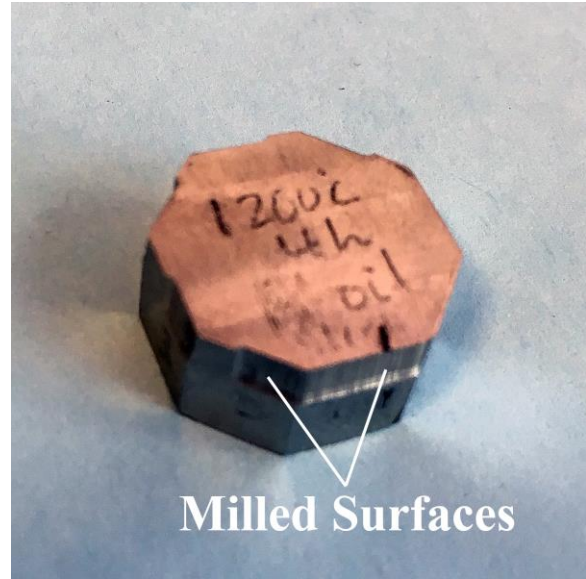


Figure 15 Cobaltan ingot showing milled surfaces.

4.1.1. Heat Treatments

In this study three separate states of CoCrMo existed relating to thermal treatments: an as-received specimen, a heat treated specimen annealed at 1200°C for 2 hours then water quenched, and a heat treated specimen annealed at 1200°C for 4 hours then water quenched. These are further reinforced and explained below.

As-received (AR): as-cast cobalt-chromium-molybdenum (CoCrMo) alloy supplied by Shofu Inc., Japan with no post manufacture thermal treatments, complying with the listed chemical properties.

Heat-treated 2 hours (HT2H): as-cast cobalt-chromium-molybdenum (CoCrMo) alloy supplied by Shofu Inc., Japan which was then subjected to post manufacturing annealing at 1200°C for two hours and then water quenched.

Heat-treated 4 hours (HT4H): as-cast cobalt-chromium-molybdenum (CoCrMo) alloy supplied by Shofu Inc., Japan which was then subjected to post manufacturing annealing at 1200°C for four hours and then water quenched.

It is believed that heat treating these samples in the aforementioned method and then water quenching the specimens will result in a single phase microstructure with an almost complete FCC structure and a reduction in carbides (15,16).

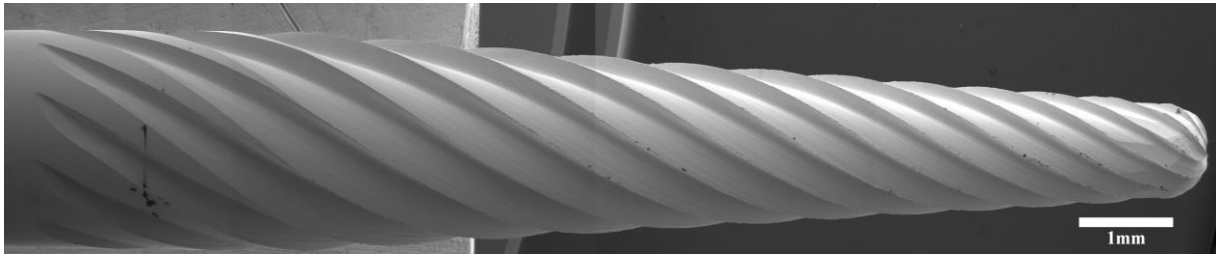
4.2. Milling Tools

Four different cemented tungsten carbide (WC) milling tools were used in this study. Cemented tungsten carbide (WC) tools are currently used in dental applications for prosthesis fabrication (31). The tools were referred to as mills A, B, C and D. In this section the individual milling tools are discussed in depth.

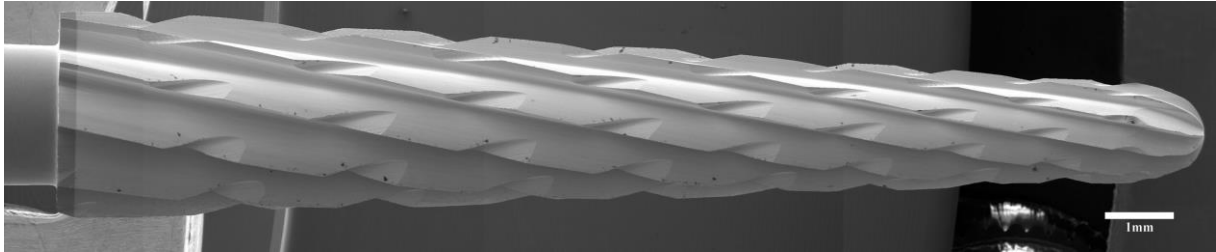
Table 2 Milling tool details.

	Milling Tool	Material	Shape	Chip Breaker	DLC Coating
Mill A	HM23LR (Hager & Meisinger)	Cemented Tungsten Carbide (WC)	Spiral	No	No
Mill B	S21N (Shofu)	Cemented Tungsten Carbide (WC)	Cross (Large)	Yes	No
Mill C	HM23GX (Hager & Meisinger)	Cemented Tungsten Carbide (WC)	Cross (Small)	Yes	No
Mill D	HMB23G (Hager & Meisinger)	Cemented Tungsten Carbide (WC)	Spiral	Yes	Yes

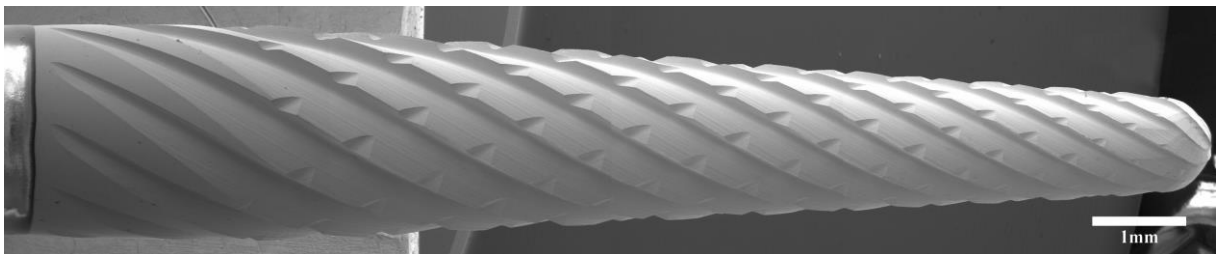
Two companies supplied the mills: Shofu Inc., Japan provided the S21N mill (B), while Hager & Meisinger Inc., Germany provided the HM23LR (A), HM23GX (C), and HMB23G (D) mills. All four mills were constructed of cemented tungsten carbide (WC). The HM23LR, S21N, and HM23GX mills were uncoated. The HMB23G mill was coated in a diamond-like carbon coating (DLC), the DLC coating showing better performance in work undertaken by K. Aslantis et al. (36) so validation of the coatings performance was attempted in this study. Furthermore, the four mills were different also in their geometry, with the HM23LR and HMB23G having a spiral shape, and the S21N and HM23GX having a cross shape. The HM23LR was the only mill without chip breakers. The properties of each mill are summarised in Table 2. SEM images of each mill in the unused condition is also shown in Figure 16. All four mills had a 44mm total length with Mills A, C and D having a 12mm long conical cutting surface and Mill B a 15.5mm long conical cutting surface. Figure 17 shows the mill shapes.



HM23LR: Type A Mill



S21N: Type B Mill



HM23GX: Type C Mill



HMB23G: Type D Mill

Figure 16 Dental Mills; A, B, C and D respectively in unused condition.

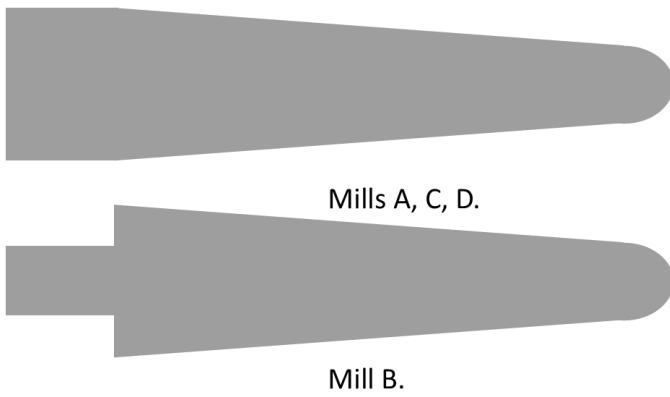


Figure 17 Dental Mill Shapes.

4.3. Scanning Electron Microscopy (SEM)

Prior to SEM observation, the specimens were cleaned using an S-10h ultrasonic cleaner, where the material was submerged in a beaker of ethanol which was placed inside the ultrasonic water bath for approximately 30 seconds. All milled surfaces were analysed at a low magnification (30x to 50x), a 200x magnification and a 1000x magnification.

In cases where chip samples had been collected from the millings and were to be observed, the chip samples were lightly rinsed in ethanol to try and remove as much excess cutting fluid as possible, and laid out under a Leica EZ4 stereo microscope. Small toothpicks were used to transplant chips onto double sided carbon conductive tape. Six sections of this tape were prepared at one time which allowed for milling chips from all six spindle speeds to be analysed at once. The six chip specimens were then placed on a purpose designed mounting holder.

4.4. Metallography

Metallography was to be undertaken on both the as-received and heat treated CoCrMo alloy specimens. Optical microscopic analysis of prepared specimens allows for the observation of the materials' microstructure.

Small samples of each specimen were cut from the larger ingots, these samples were then mounted with a hot mounting method using 'Polyfast' resin and a LaboPress-3 metallurgical mounting press. Once the samples were mounted in resin the grinding and polishing process could begin. The surfaces were first wet ground with a rough abrasive pad using a rotary grinder and slowly progressed towards finer and finer abrasive pads. The order of this progression was as follows; 180 grit, 500 grit, 1200 grit and 2400 grit. Once the material surface had been sufficiently polished using 2400 grit paper leaving all surface blemishes and marks removed, it was subjected to an auto-polishing machine for the final polish.

4.4.1. Etching

Once the specimens had been polished to a suitable standard the next stage was to chemically etch the specimens. The aim was to etch the three specimens prepared in the previous section and then view and compare the microstructure of these specimens. A number of proposed etchants were available throughout literature for similar CoCrMo alloys with slightly different compositions, but no definitive etchant for the composition used in this study was mentioned. This caused issues choosing an etchant as they seemed to be very dependent on the precise

chemical composition of the CoCrMo alloy used. The five most likely etchants selected to be tested are listed in Table 3.

Table 3 Chemical etchants tested.

Chemical Etchants	
1	50 mL H ₂ O + 50 mL HCL + 4g K ₂ S ₂ O ₅ as a reagent
2	100 mL HCL + 100 mL Ethanol + 5g CuCl ₂
3	120 mL HCL + 20 mL H ₂ O ₂
4	33 ml H ₂ O + 33 ml HCL + 33 ml Ethanol + 1.5 g CuCl ₂
5	50 ml H ₂ O + 50 ml HCL + 10 g CuSO ₄ and 15 drops of H ₂ SO ₄ to activate

Etchants number 1, 2 and 3 were chosen as the most likely etchants. They were then prepared by the chemistry department for use in this study. The recommended times for etching to take affect were 2-5 minutes, 15-30 seconds and an unknown time, respectively. However when they were tested neither of the three etchants showed any successful results. The specimens were left in the etchant for a much longer time period – 10-13 minutes – and still no reaction was seen to occur.

Following the failure of the first three etchants, etchants 4, and 5 were prepared by the chemistry lab for use in this study. The recommended times for these etchants were not well documented, however they were generally in the area of less than 10 minutes. The first etchant tested was etchant number 4 with the specimen being submerged in it for 30 minutes, but still no reaction was observed. Following this etchant number 5 was tested with the specimens being submerged in this solution overnight, still no reaction was observed. At this point time constraints limited the workload and the etching of these CoCrMo specimens was deemed a failure.

4.5. Micro-Hardness Testing

A secondary objective of this study was an investigation into annealed CoCrMo specimens. Three specimens with different thermal histories were tested in order to offer insight into how annealing CoCrMo would affect its micro-hardness. The first specimen was an as-received CoCrMo alloy (AR CoCrMo), the second specimen was heated to 1200°C, held at this temperature for 2 hours and then water quenched (HT2H CoCrMo), and the third specimen was heated to 1200°C, held at this temperature for 4 hours and then water quenched (HT4H CoCrMo). These three specimens were micro-hardness tested, with the HT4H specimen also milled with Mill B for comparison to AR CoCrMo milled with Mill B.

The CoCrMo specimens were first wet ground and polished. Once the surfaces needed for testing had been polished to a single grit finish the specimens were ready for micro-hardness testing. A Leco LM800AT micro hardness tester was used. The measurement used was Vickers hardness with a 300 gram load held for 10 seconds. Three measurements were taken of each specimen spaced out along the longest face. Indentations were marked as similarly as possible between each specimen to offer a more comparable data set.

4.6. Roughness Testing

Roughness testing was undertaken to allow for a more extensive experimental profile. Roughness values on their own allow for little conclusions to be drawn due to the complex interacting nature of factors leading to surface roughness; however when combined with other recorded data in this study such as SEM images, hardness testing and cutting force data, the roughness values allow for a deeper insight and also serve to confirm hypotheses made from the observations of other results. The roughness testing was undertaken using a Taylor Hobson Precision Formtalysurf 50 roughness tester.

The specimens were clamped in position and the stylus was lined up as close to the vertical middle of the pass as possible. Care was taken to ensure the specimen was square to the tester and as flat as possible, although the roughness tester can measure Ra and Rq regardless of slope. The sample pass was set to 6mm, this being the roughly the length of a full face of the ingot and therefore only specimens that had been completely milled were examined. Partial milling and incomplete passes were not measured as the roughness tester disregarded the first and last 1.2mm of each surface, making partial pass readings unreliable. The data was exported to Taylor Hobson 'ultra' Software which allowed a look at the raw and adjusted

surface profile as well as the slope, arithmetic average of roughness (Ra), root mean squared average of roughness (Rq) and peak height (Rt) parameters. Once the data was obtained it could be inserted into tables for each specimen and this allowed multiple graphs to be generated and trends to be evaluated.

4.7. Experimental Layout

Owing to the nature of this research project, with multiple studies involved in a larger overall research topic, there are some irregular patterns of samples being analysed. With specimens and data supplied from research partners in Japan there is also an existence of multiple data sets, some incomplete. To better summarise and understand the various specimens that have been examined, two tables are shown below. Table 4 lists the machined specimens that further underwent roughness testing and SEM examination. All machined specimens were supplied with cutting force data. Table 5 lists the heat treated specimens that underwent micro-hardness and attempted metallography testing.

Table 4 SEM + roughness testing experiment list.

SEM + Roughness Testing				
Material	Heat Treatment	Milling Tool	Lubrication (Fras und Bohrol)	Mill Analysed
CoCrMo	As Received	A	Yes	Yes
CoCrMo	As Received	B	Yes	Yes
CoCrMo	As Received	C	Yes	Yes
CoCrMo	As Received	D	Yes	Yes
CoCrMo	1200°C 4H Water Quenched	B	Yes	Yes

Table 5 Micro-hardness + metallography experiment list.

Micro-Hardness + Metallography Testing			
Material	Heat Treatment	Micro-Hardness Tested	Metallography Tested
CoCrMo	As Received	Yes	Attempted
CoCrMo	1200°C 2H Water Quenched	Yes	Attempted
CoCrMo	1200°C 4H Water Quenched	Yes	Attempted

4.7.1. Milled Specimen Parameters

Table 6 AR CoCrMo – Mill A parameters.

CoCrMo – As Received – Mill A	
- As received state	
- Fras und Bohrol Milling Oil	
- Meisinger HM23LR Mill	
- 10K – 35K RPM	

Table 7 AR CoCrMo – Mill B parameters.

CoCrMo – As Received – Mill B	
- As received state	
- Fras und Bohrol Milling Oil	
- Shofu 21N Mill	
- 10K – 35K RPM	

Table 8 AR CoCrMo – Mill C parameters.

CoCrMo – As Received – Mill C	
- As received state	
- Fras und Bohrol Milling Oil	
- Meisinger HM23GX Mill	
- 10K – 35K RPM	

Table 9 AR CoCrMo – Mill D parameters.

CoCrMo – As Received – Mill D	
<ul style="list-style-type: none"> - As received state 	
<ul style="list-style-type: none"> - Fras und Bohrol Milling Oil 	
<ul style="list-style-type: none"> - Meisinger HMB23G Mill 	
<ul style="list-style-type: none"> - 10K – 35K RPM 	

Table 10 HT4H CoCrMo – Mill B parameters.

CoCrMo – HT4H – Mill B	
<ul style="list-style-type: none"> - Annealed at 1200°C for 4H, then Water Quenched 	
<ul style="list-style-type: none"> - Fras und Bohrol Milling Oil 	
<ul style="list-style-type: none"> - Shofu 21N Mill 	
<ul style="list-style-type: none"> - 10K – 35K RPM 	

5.0. Results

5.1. Scanning Electron Microscopy (SEM) Image Analysis

SEM images of the milled surfaces are organised and discussed in groups of spindle speeds in the following section. All five specimens are discussed side by side for given spindle speeds ranging from 10,000 RPM to 35,000 RPM in increments of 5000 RPM. Occasionally some milled surfaces were excluded due to mill instability leading to unreliable results. 1000x magnification, 200x magnification and low magnification (30x to 50x) images are shown for each milling pass with larger images of each available in Appendix A. Furthermore, SEM images of the used mills and machined chips are also analysed separately.

These images were evaluated on the occurrence of common defects and overall surface quality with common points of interest including waviness, tearing, craters, gouging (due to ploughing) and rewelded chips/material on the milled surface. As the literature review suggested, frictionally rewelded chips/material are expected to be one of the most detrimental phenomena to the surface finish. The rewelding occurs as chips and severed BUE chunks are frictionally rewelded to the material behind the milling tool, examples of which are shown in Figure 18.

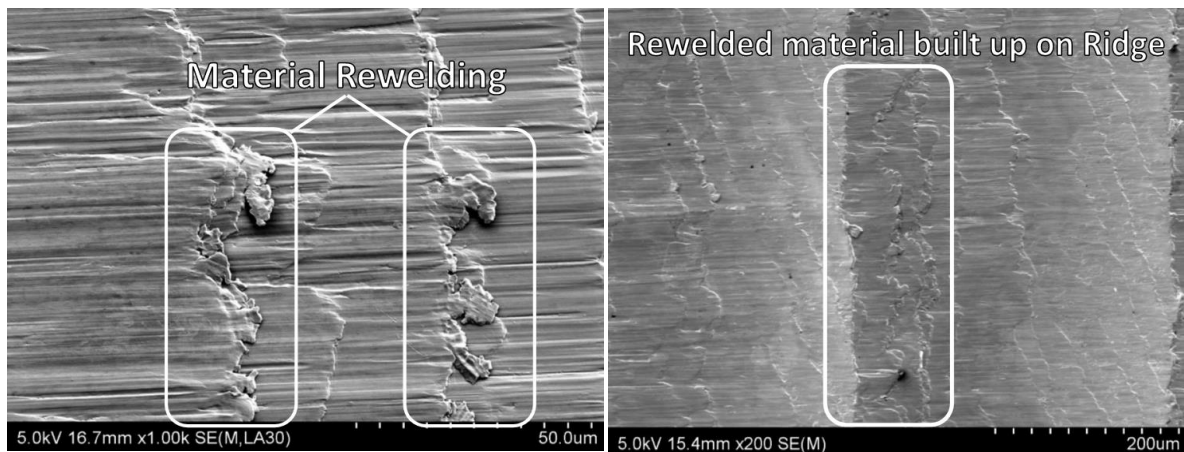


Figure 18 Examples of rewelded material on the milled surface.

The occurrence of waviness is another expected detrimental phenomenon. Waviness occurs due to machining errors such as mill instability (chatter), and excess vibrations affecting the milling tool. It is crucial to identify waviness and not confuse it (and related causations) with other mechanisms and phenomena occurring during machining. Waviness appears as widely spaced cyclic peak and valley formations occurring on a much larger scale than the roughness

formations. Examples of waviness are shown in Figure 19, showing both an SEM image and a 3D representation of waviness.

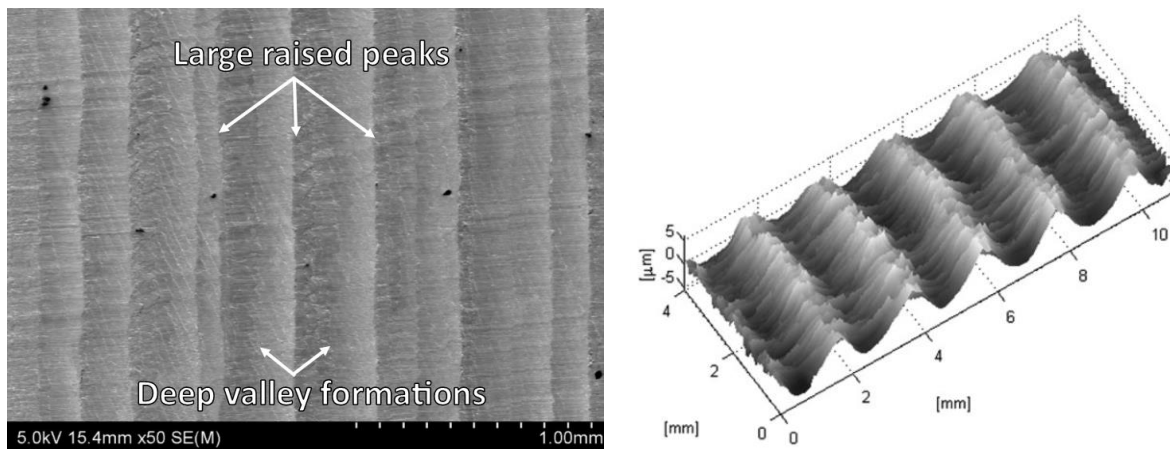


Figure 19 Left: SEM image of surface waviness. Right: A 3D scan of surface waviness. www.mdpi.com (56).

As well as the large ridges occurring due to the waviness formations, there are also smaller ridge/ripple formations shown on the surface of these milled specimens. The height and nature of these ridges (clean edge vs fractured edge) plays a significant role in the surface finish quality of the specimens. These ridges are generated due to the chip forming mechanism and often attract large amounts of rewelded material, further offering a place for bacteria to breed if used in dental implants. As such these ridges/ripples are detrimental to surface finish. Examples of these are shown in Figure 20.

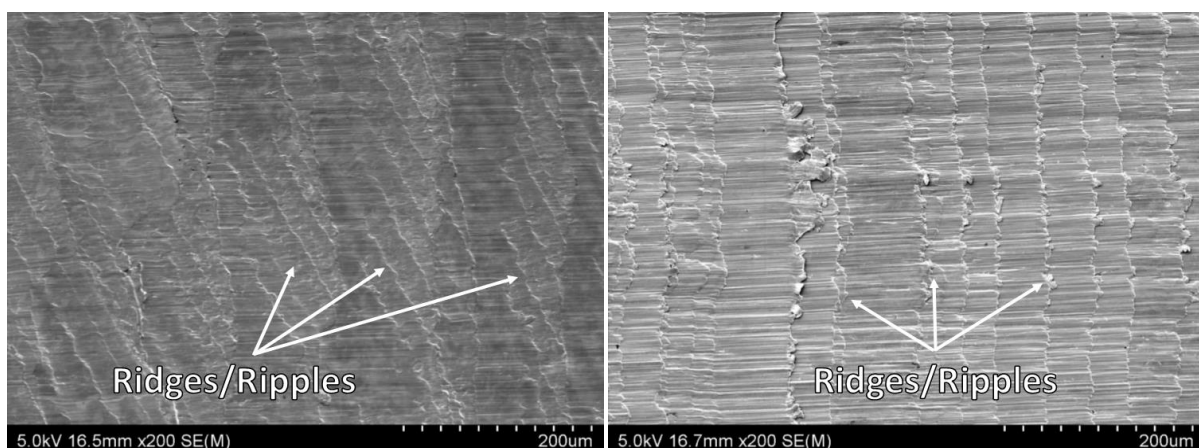


Figure 20 Examples of ridges/ripples on the milled surface.

Surface tearing and crater formations are further detrimental characteristics of a milled surface. Tearing occurs when the material is torn from the workpiece rather than sheared cleanly from the surface and can occur due to a variety of reasons, however BUE on the tool cutting edge and lack of lubrication are common causes. It is not known what caused the

horizontal bands of crater formations seen to occur in this study, though worn cutting edges, BUE on the tool and mill vibrations are thought to be likely causations. Examples are shown in Figure 21.

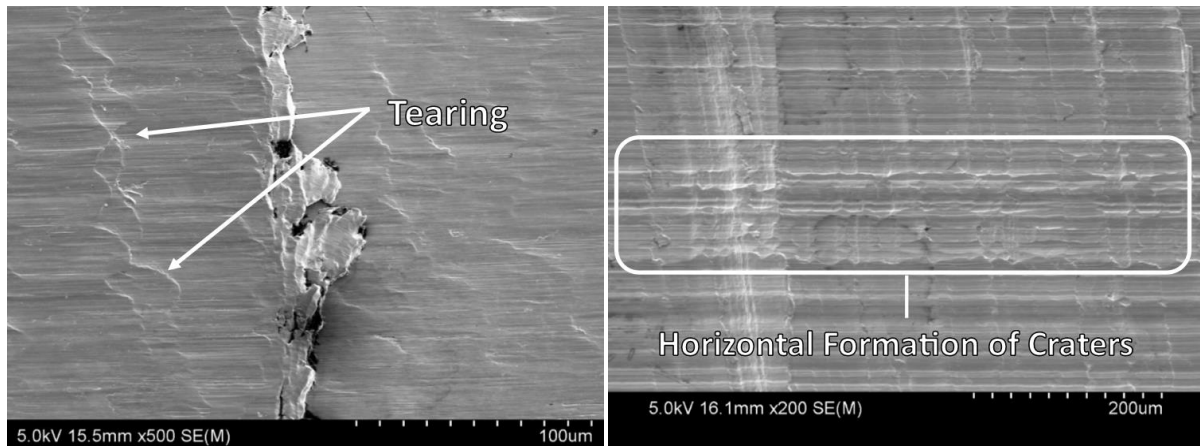


Figure 21 Tearing and craters on the milled surfaces.

The final major surface defect is gouging, these defects appearing as horizontal grooves gouged into the material. Gouges can be caused by a number of factors, however BUE on the mill cutting edge that is then dragged across the surface owing to the ploughing mechanism is strongly suspected as the main cause in this study. It can be summarised that ploughing is therefore the cause of the defect, with the defect being the gouge marks. An example of gouge marks on the milled surface is shown in Figure 22.

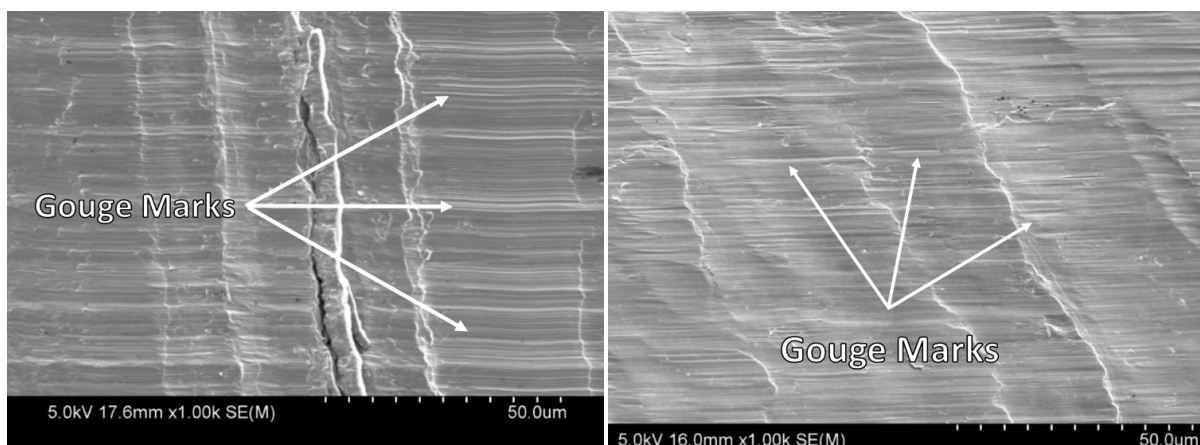
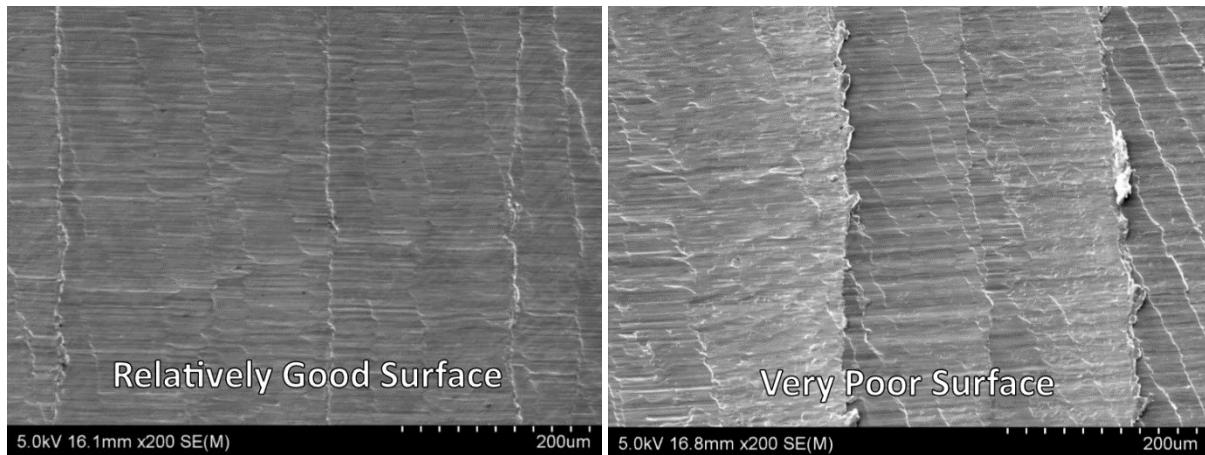


Figure 22 Gouge marks on the milled surface.

Surface roughness data were obtained via the surface roughness testing explained in previous sections. Although this allows a numerical value to be assigned to the roughness, there can also be clear observations made by viewing the SEM images and spotting defects that occur

on a microscopic level that cannot be reflected in a numerical value. Research knowledge can then be combined with the recorded values to obtain more solid conclusions. An example of a relatively good surface finish vs a poor surface finish is shown in Figure 23. Both images are at 200x magnification showing surfaces milled at 20,000 RPM. Large differences in the surface quality can be seen relating to waviness, chip rewelding, gouging and ridge/ripple formations.



(A)

(B)

Figure 23 Visible differences in surface finish. (A) Showing a relatively good surface finish milled with mill C at 20,000 RPM. (B) Showing a relatively poor surface finish milled with mill A at 20,000 RPM.

5.1.1. 10,000 RPM

At 10,000 RPM all five specimens were milled to an adequate level that allowed the capture of SEM images of the surface quality.

Mill A, Figure 24 (a). The surface milled by Mill A at 30x magnification is shown in Figure 24 (a). Finely spaced vertical ridges can be seen occurring along the length of the milled surface. These do not appear to be waviness owing to the flat appearance of the surface though; furthermore, some distinct horizontal gouging occurs across the entire surface.

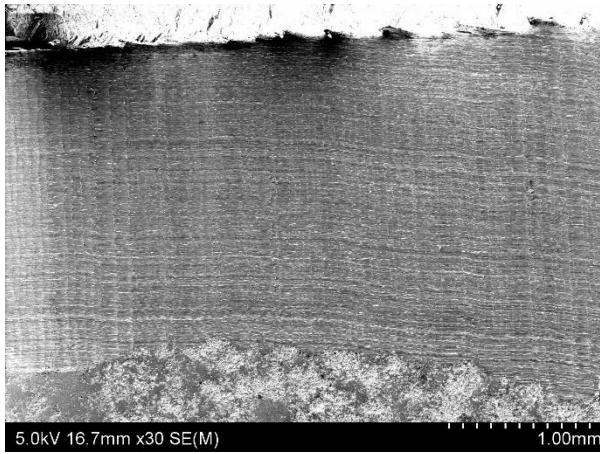
Mill B, Figure 24 (b). The surface milled by Mill B is shown in Figure 24 (b). The surface shows high amounts of defects. The surface shown has a relatively poor quality with large amounts of horizontal gouging, large craters, vertical ridges and horizontal bands of differing surface finish occurring across the entire surface leading to a poor overall quality.

Mill C, Figure 24 (c). The SEM image shows the surface obtained by Mill C. Small waviness peaks and spaces are seen with minor angled ridges occurring within these wider spaced waviness ridges. The waviness peaks appear small though the presence of waviness does indicate drill instability occurred.

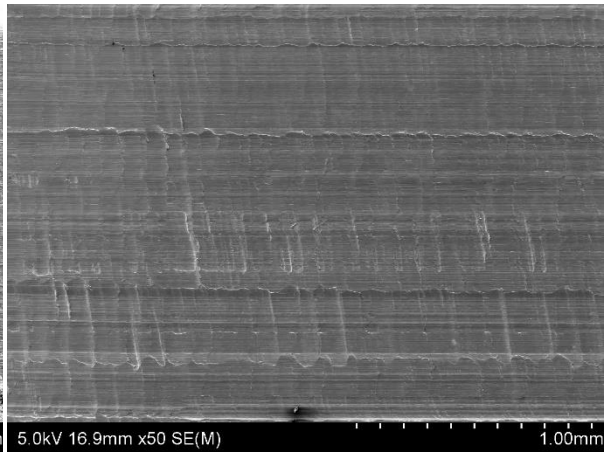
Mill D, Figure 24 (d). The surface milled by Mill D is shown in Figure 24 (d). Mill D appears to have produced the best surface finish at this magnification with shallow vertical ridges and minimal gouging being the only defects occurring. The surface finish is shown to exhibit some form of oil contamination as large black spots on the surface, though this would not affect surface finish quality.

Mill B, HT4H CoCrMo, Figure 24 (e). The surface shown in the SEM image exhibits a very different surface finish than the AR CoCrMo specimen milled with Mill B. In this surface finish, deep vertical ridges are shown combined with horizontal gouging and deep craters in the lower regions. Overall, a much lower quality finish is shown with the milled HT4H CoCrMo than the milled AR CoCrMo.

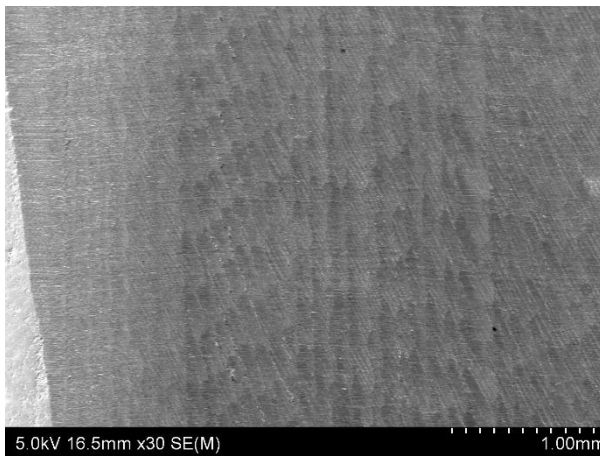
Low magnification images of all passes are shown in Figure 24 (a-e).



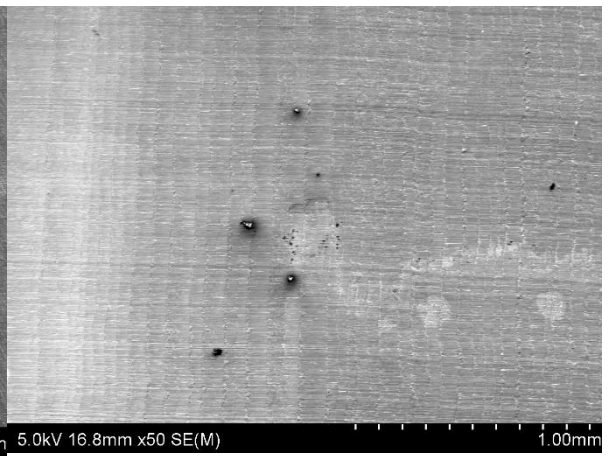
(a)



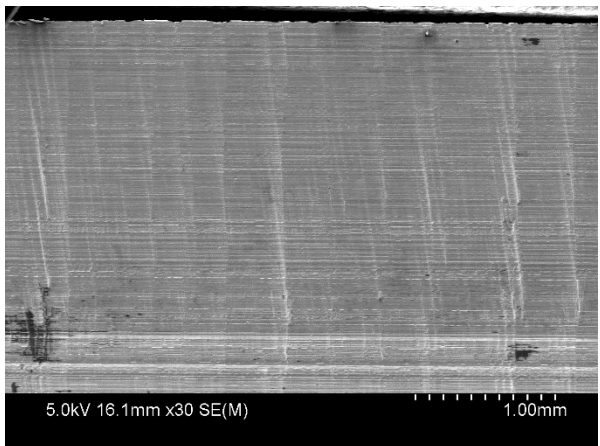
(b)



(c)



(d)



(e)

Figure 24 Low magnification SEM images of specimens laterally face milled at 10,000 RPM showing; (a) as-received CoCrMo milled with Mill A, (b) as-received CoCrMo milled with Mill B, (c) as-received CoCrMo milled with Mill C, (d) as-received CoCrMo milled with Mill D, (e) HT4H CoCrMo milled with Mill B.

The SEM images captured at 200x magnification show the extent at which the surface defects are occurring, and at this magnification the severity of these defects is more apparent.

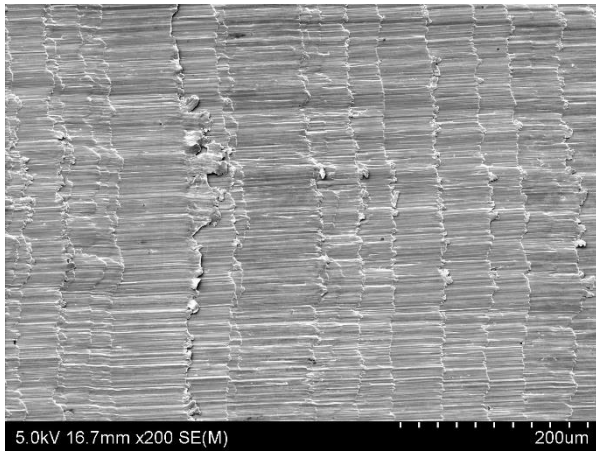
Mill A, Figure 25 (a). Heavy amounts of chip rewelding are shown in the image, combined with strong horizontal gouging across the entire surface. Finely spaced deep vertical ridges are present and this is where the chip rewelding is occurring. It is unknown if these ridges are due to waviness or the chip formation mechanism (potentially minimum chip thickness theory). Mill A was the only mill without chip breaker geometry used in this study, which could be a major factor in the low quality surface finish obtained.

Mill B, Figure 25 (b). The surface milled by Mill B is shown with crater formation being the most detrimental phenomenon to the surface finish. Moderate amounts of gouging are also present, as are some vertical ridges. Chip rewelding is shown occurring on the rough fractured edges of the crater formations.

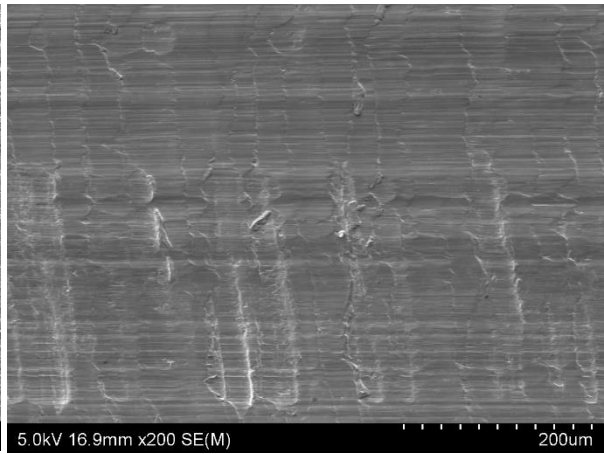
Mill C, Figure 25 (c). The surface milled by Mill C exhibits a combination of horizontal waviness, likely due to mill vibration and angled ridges within these wider spaced waviness ridges. A combination of moderate rewelding, tearing and gouging is also apparent leading to a relatively poor surface finish. These defects were not apparent at low magnifications and highlight the importance for microscopic analysis.

Mill D, Figure 25 (d). The surface milled by Mill D provided the best surface finish quality shown at 10,000 RPM. The main detriment was the minimal to moderate amounts of chip rewelding present on the shallow vertical ridges. There is also some gouging and tearing present though the severity is relatively low. Though this surface is far from ideal, comparative to other surfaces at this speed it is easily the best performing. Some oil contamination can be seen indicated by the dark spots on the surface but these would not affect surface quality.

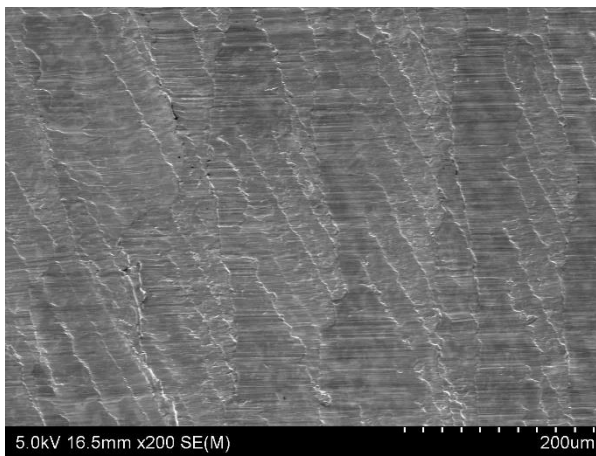
Mill B, HT4H CoCrMo, Figure 25 (e). The surface finish of HT4H CoCrMo milled with Mill B is shown and despite the extremely poor surface finish, material rewelding is basically non-existent. The major detriments are large, deep craters present in horizontal belt formations, with deep ploughing/gouging also occurring. Furthermore deep fractured ridges are shown occurring occasionally along the milled surface, most likely due to mill vibration. The 200x magnification images of the surfaces are shown in Figure 25 (a-e)



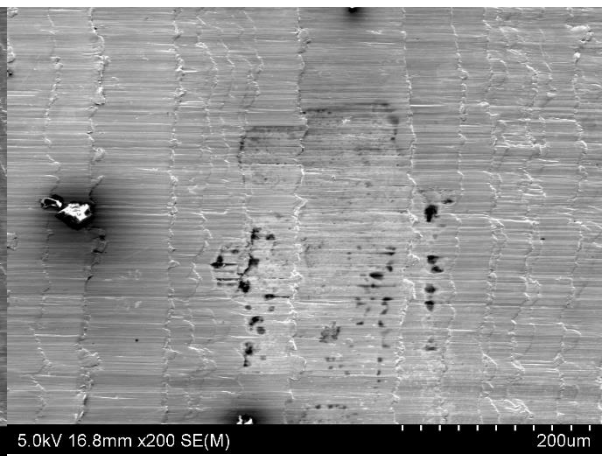
(a)



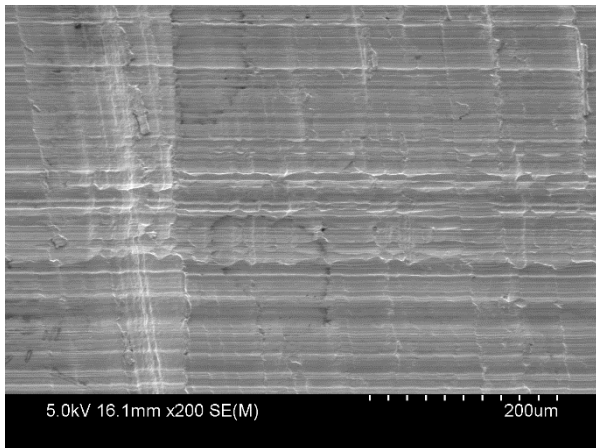
(b)



(c)



(d)



(e)

Figure 25 200x magnification SEM images of specimens laterally face milled at 10,000 RPM showing; (a) as-received CoCrMo milled with Mill A, (b) as-received CoCrMo milled with Mill B, (c) as-received CoCrMo milled with Mill C, (d) as-received CoCrMo milled with Mill D and (e) HT4H CoCrMo milled with Mill B.

Images captured at 1000x magnification allow for a deeper insight into particularly interesting regions of the surface finish.

Mill A, Figure 26 (a). A magnified look at the surface milled with Mill A is shown, particularly the chip rewelding occurring. A deep ridge formation can be seen with varying degrees of material rewelded along it vertically. The aforementioned ridge edge also shows a layered nature indicating high amounts of rewelded material have adhered. Furthermore, the heavy gouging shown indicates that high amounts of ploughing was occurring.

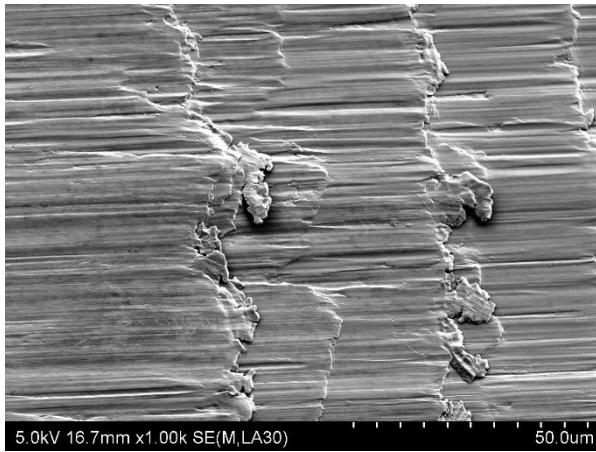
Mill B, Figure 26 (b). The surface milled with Mill B shows heavily fractured edges with high amounts of tearing, gouging, crater formations and chip rewelding occurring. The severity of chip rewelding shown is far worse than all other surfaces seen at this spindle speed and chip rewelding can be stated to be the primary defect in this surface.

Mill C, Figure 26 (c). The SEM image shows a transition from a very smooth surface on the right hand side, to a rougher surface on the left, with tearing, rewelding and ridges formed on the surface. It is unknown what caused this transition, however it is believed that the central area where the surface finishes are divided is a raised peak caused by waviness. Differing cutting forces and mill vibrations are therefore expected to be occurring on either side of the peak, leading to different cutting conditions and chip forming mechanisms occurring on either side of the ridge and therefore differing surface finishes.

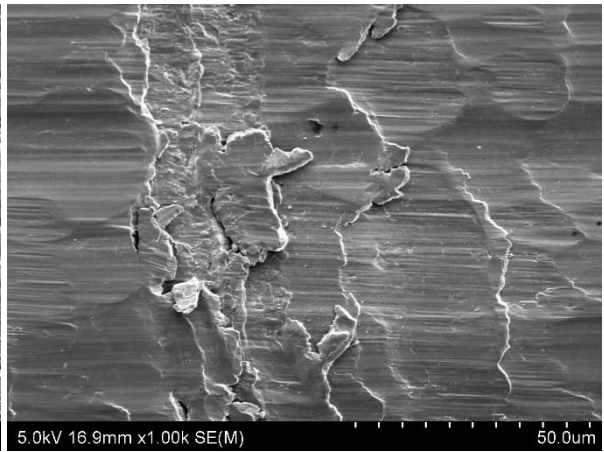
Mill D, Figure 26 (d). An almost ideal surface is shown in this SEM image, which was milled with Mill D. Minor gouging is shown occurring, however no visible craters or fractures are shown. There is a slight vertical ridge present in the centre of the image, though a noticeable lack of rewelded material is present on or near the ridge. This is significantly different from the similar ridge formation shown in Figure 26 (a), where the amount of rewelded material adhered to the ridge was high.

Mill B, HT4H CoCrMo, Figure 26 (e). The obtained surface at 1000x magnification shows very minor amounts of rewelding occurring, with gouging and crater formations somewhat typical of Mill B, however the severity is exponentially worse. Deep gouging is shown covering almost the entire surface with fractured surfaces and small cracks also shown. The main detriment is the depth and frequency of the craters shown. The extensive ploughing/gouging is believed to be due to the softened material creating larger BUE formations on the milling tool, and therefore leading to significantly more detrimental ploughing occurring.

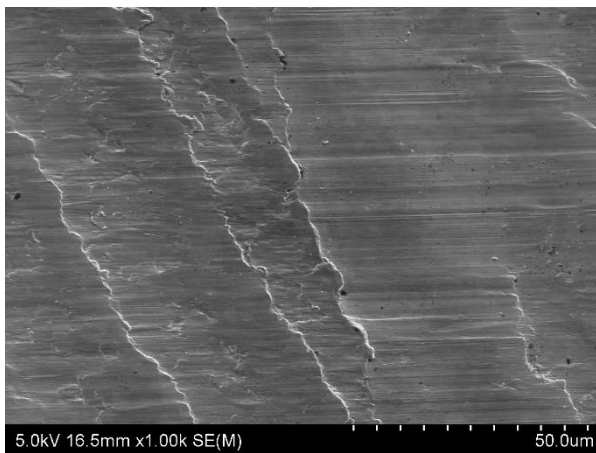
These 1000x magnification images are shown in Figure 26 (a-e).



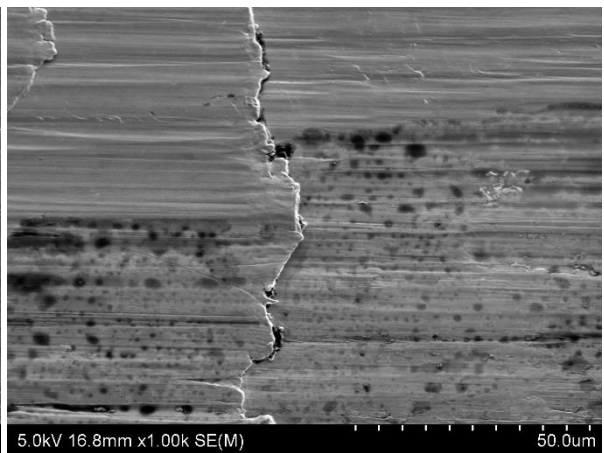
(a)



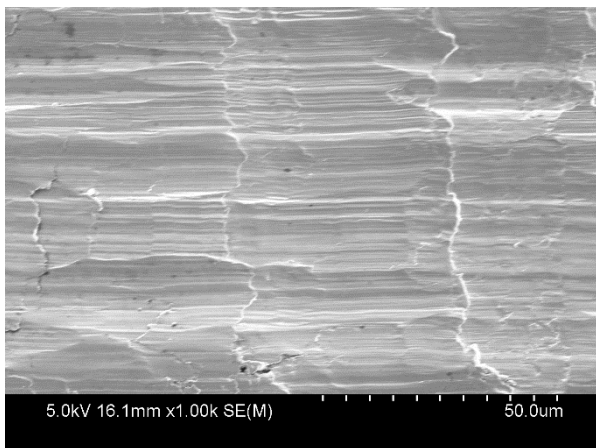
(b)



(c)



(d)



(e)

Figure 26 1000x magnification SEM images of specimens laterally face milled at 10,000 RPM showing; (a) as-received CoCrMo milled with Mill A, (b) as-received CoCrMo milled with Mill B, (c) as-received CoCrMo milled with Mill C, (d) as-received CoCrMo milled with Mill D and (e) HT4H CoCrMo milled with Mill B.

5.1.2. 15,000 RPM

Once again at 15,000 RPM all specimens were able to be milled to an adequate level to allow SEM analysis.

Mill A, Figure 27 (a). Waviness in the surfaces milled by Mill A is shown to have escalated rapidly from the severity shown at 10,000 RPM. Deep valley formations have formed with large waviness spacing, indicating high amounts of mill vibration and chatter has occurred. Rewelding is also shown on these waviness ridges, particularly towards the end of the pass.

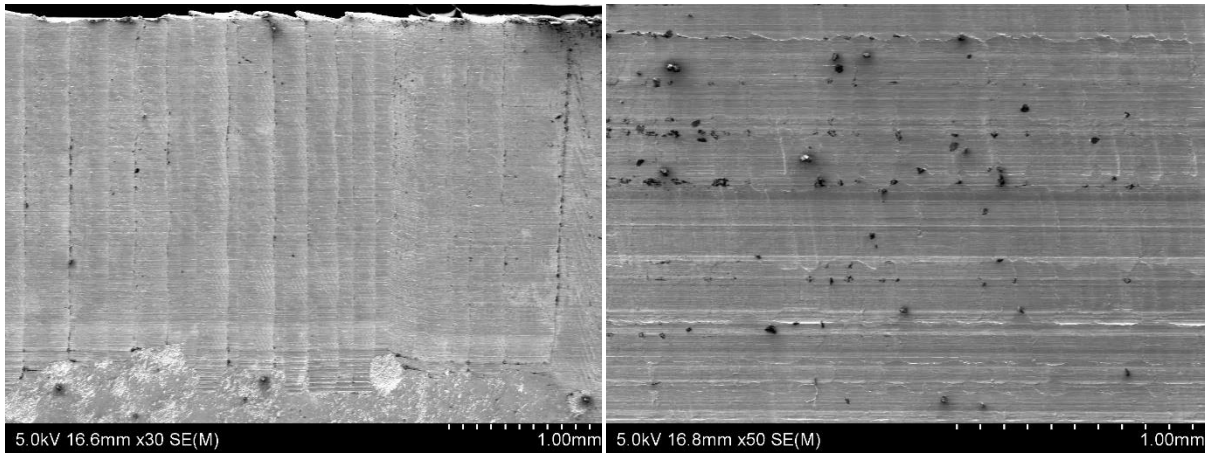
Mill B, Figure 27 (b). The surface finish obtained at 15,000 RPM by Mill B appears very similar to the surface finish obtained while milling at 10,000 RPM. Gouging, cratering and horizontal bands of varying surface finishes are shown to be the main detriments. The extent of the horizontal gouging and cratering occurring at 15,000 RPM is less severe than at 10,000 RPM though. Note that Figure 27 (b) exhibits high amounts of oil staining and contamination but this will not affect surface finish quality.

Mill C, Figure 27 (c). The surface milled with Mill C appears visibly smooth at a magnification of 30x, though there is a notable waviness briefly occurring on the left hand side of the image towards the end of the milling pass. The right hand side shows very faint waviness suggesting the peak height is small. The waviness appearing towards the end of the pass could be an anomaly, or due to complex mill loading leading to excess vibrations towards the end of the milling path.

Mill D, Figure 27 (d). The surface finish obtained by Mill D at 15,000 RPM shows a significantly lower quality than achieved at 10,000 RPM with Mill D. High amounts of waviness are present with high waviness peak heights and large waviness spacing. Rewelded material is shown adhered to these ridges, and gouging and vertical ridges are shown inside these large peaks.

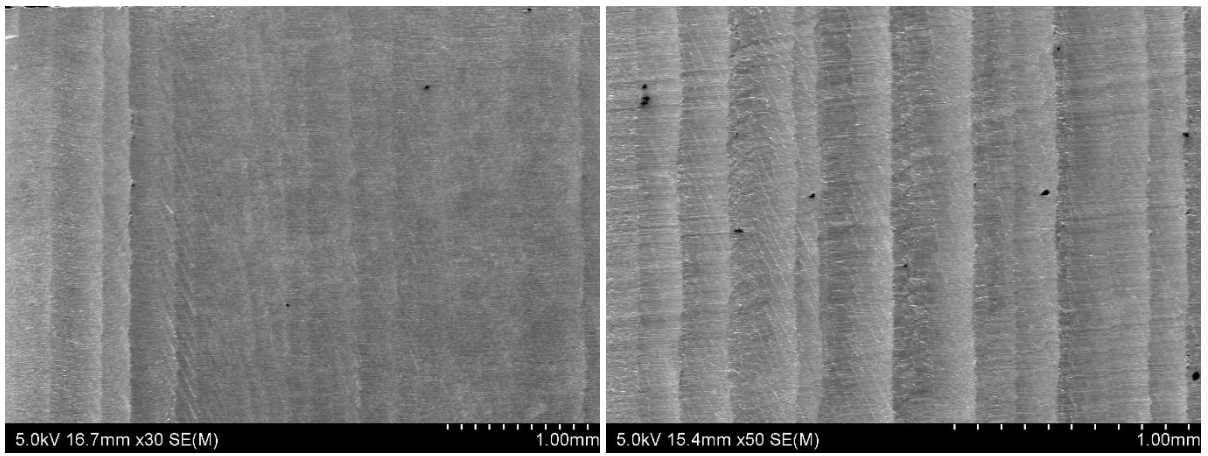
Mill B, HT4H CoCrMo, Figure 27 (e). The surface obtained from milling HT4H CoCrMo with Mill B shows a surface finish that is significantly different to any AR CoCrMo specimens milled with Mill B. The surface has both deep horizontal gouging and a pattern of deep and rugged vertical ridges. Rewelding and large, semi-detached chips can be seen hanging off the deeper vertical ridges and more excessive craters and fracturing occurring in the lower region suggests the mill tip was highly unstable.

Low magnification images of these surfaces are shown in Figure 27 (a-e).



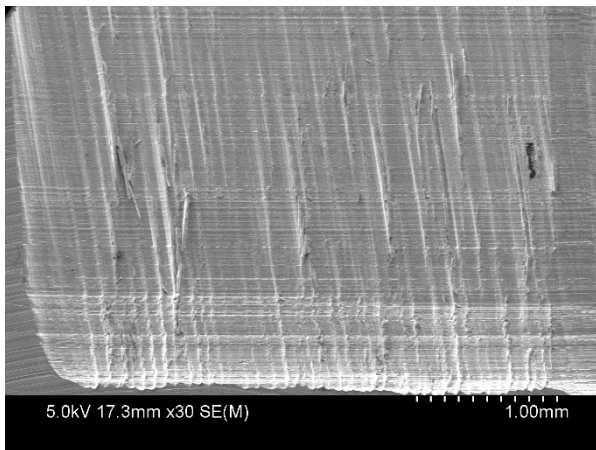
(a)

(b)



(c)

(d)



(e)

Figure 27 Low magnification SEM images of specimens laterally face milled at 15,000 RPM showing; (a) as-received CoCrMo milled with Mill A, (b) as-received CoCrMo milled with Mill B, (c) as-received CoCrMo milled with Mill C, (d) as-received CoCrMo milled with Mill D and (e) HT4H CoCrMo milled with Mill B.

Mill A, Figure 28 (a). Large valley and peak formations can be seen on the surface milled with Mill A exhibiting a typical waviness profile. High amounts of rewelded material are shown present on the ridges of these waviness peaks, though rewelding has also occurred between these peaks to a lesser extent. Once again, gouging and tearing is present, however the implications of this are overshadowed by the severity of the waviness occurring. It appears that larger amounts of rewelded material are present on the upward climb of the waviness peak than on the downwards descent of these peaks. This is occurring for an unknown reason but can be observed in the images, possibly due to the change in forces/vibrations as the mill moves over the peak.

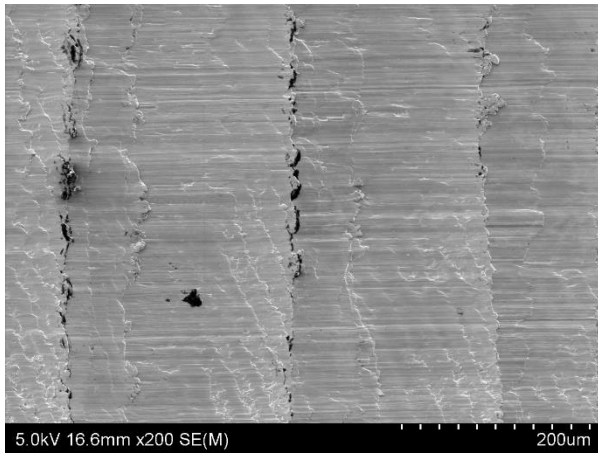
Mill B, Figure 28 (b). The amount of rewelding seen in this image is relatively low, and moderate gouging is shown occurring. Minor tearing and horizontal ridges are shown occurring on the surface. The overall quality of the surface shown in this image is relatively high though it is known from Figure 27 (b) that significant horizontal gouging and craters occurred on the surface.

Mill C, Figure 28 (c). The SEM image captured shows a relatively smooth surface with occasional vertical ridges occurring, potentially caused by very small waviness and therefore low mill vibration. High amounts of small gouges do exist however and minor material tearing. Owing to the scale of these defects, the surface can be considered relatively smooth overall compared to other surfaces obtained in this study.

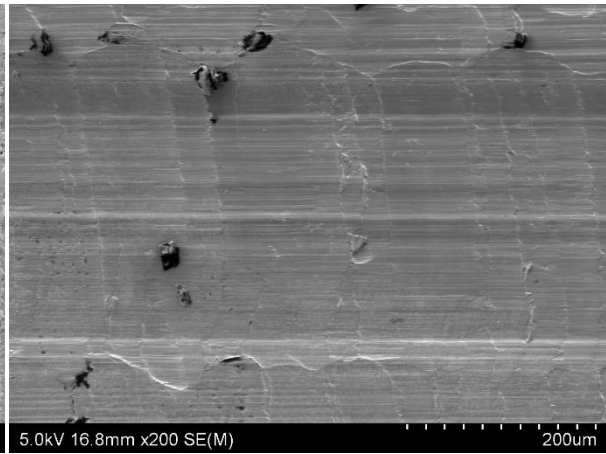
Mill D, Figure 28 (d). The surface milled by Mill D shows severe waviness, with large waviness peak heights and waviness spacing. There is a high amount of rewelded material present on the upward climb of the peaks, much higher than on the descent of the peaks. As stated previously, it is possible that this has to do with the change in cutting forces and/or vibrations as the mill moves over the peak. Other typical defects occur such as gouging, tearing, small angled ridges etc; however due to the extreme severity of the waviness formations these can be thought of as secondary issues.

Mill B, HT4H CoCrMo, Figure 28 (e). The surface finish obtained with HT4H milled with Mill B is very poor with large ridges shown with partially detached chips. Furthermore, chip rewelding on the vertical ridges and huge amounts of ploughing/gouging indicate a large BUE on the milling tool.

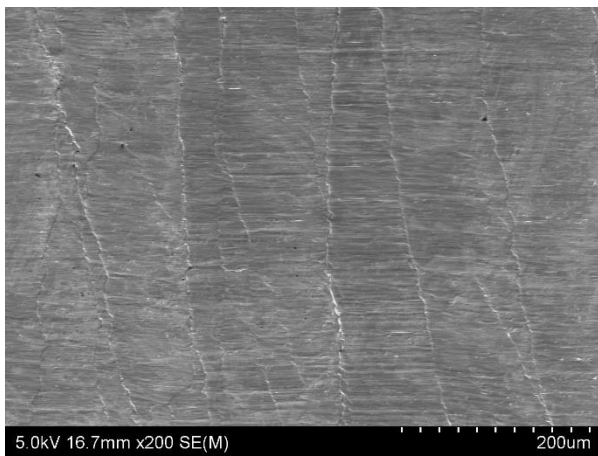
Images of these magnifications are shown in Figure 28 (a-e).



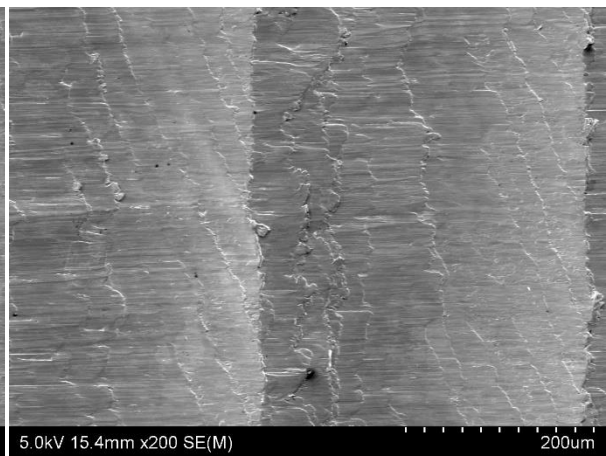
(a)



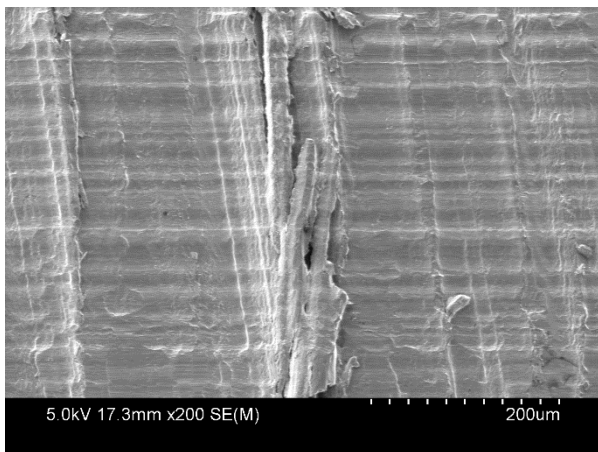
(b)



(c)



(d)



(e)

Figure 28 200x magnification SEM images of specimens laterally face milled at 15,000 RPM showing; (a) as-received CoCrMo milled with Mill A, (b) as-received CoCrMo milled with Mill B, (c) as-received CoCrMo milled with Mill C, (d) as-received CoCrMo milled with Mill D and (e) HT4H CoCrMo milled with Mill B.

Mill A, Figure 29 (a). 1000x magnification of the surface milled by Mill A, shows the extent to which material has been frictionally rewelded. Material can be seen rewelded to both the vertical ridge and the surface directly before and after it. Large amounts of gouging indicating ploughing are also shown and it is known from lower magnifications that waviness is occurring.

Mill B, Figure 29 (b). The surface milled by Mill B shows a good surface finish between ridges, however the rewelded chips in the centre of the image and vertical ridges are detrimental to the overall quality. It is also known from lower magnifications that the surface outside of this sample area is relatively poor. The lack of waviness shown in surfaces milled with Mill B is of interest.

Mill C, Figure 29 (c). An almost ideal surface finish is shown achieved with Mill C. The only detriment shown is the slight vertical ridge occurring. The surface either side of this ridge is excellent and very little gouging, no visible tearing and extremely minimal rewelding are seen. If the phenomena leading to the formation of this vertical ridge, which is believed to be due to either waviness or the minimum chip thickness effect, could be removed and/or further minimized, in future tests this surface would be above adequate.

Mill D, Figure 29 (d). The SEM image is taken directly on top of a large waviness ridge on the surface milled by Mill D. The waviness peak is seen running through the centre of the image with the uphill climb on the right and the downward descent on the left. Chips have been minimally rewelded to both the waviness peak ridge and the minor ridges formed on each side. Gouging is present but is not hugely significant. The surface finish seen in this image is of a much higher quality than other areas, though regardless, the extremity of the waviness seen at low magnification in this pass creates a very poor surface finish.

Mill B, HT4H CoCrMo, Figure 29 (e). The surface is shown to exhibit huge chip rewelding. The size of the rewelded chips and semi-detached chunks of material seen in this specimen are far larger than anywhere else. The right hand side of the image shows a rugged surface filled with high amounts of craters, gouging and tearing. The left hand side of the image shows a large ridge with a huge chunk of material either partially rewelded or not completely sheared off, though it is believed to be frictionally rewelded. This large ridge is part of a wider spaced linear pattern of ridges typical of HT4H CoCrMo milled with Mill B. Whether it is related to waviness and machine errors or some material property is unknown at this point; however it

certainly has not been shown to occur with the AR CoCrMo specimen milled using Mill B. Images of these magnifications are shown in Figure 29 (a-e).

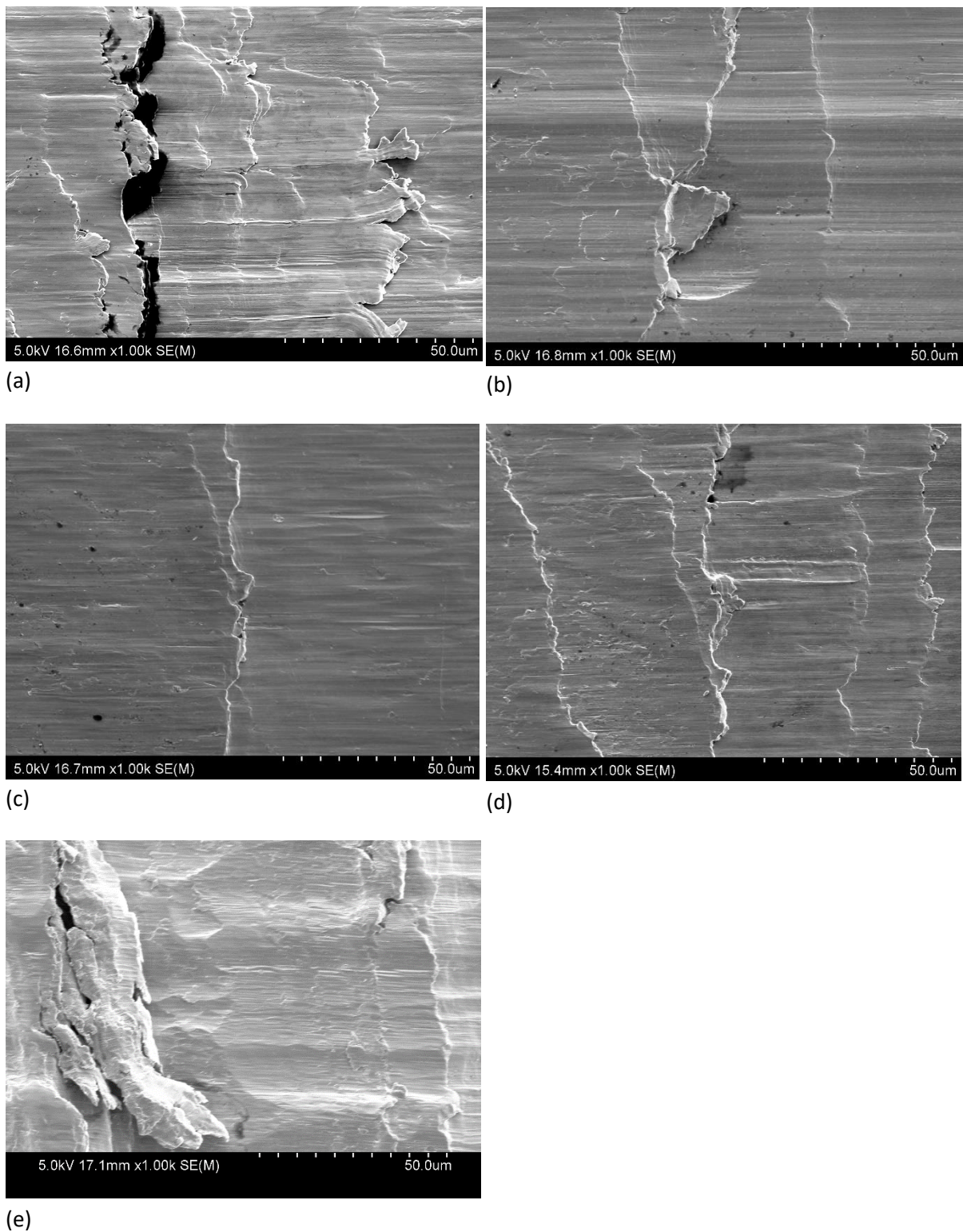


Figure 29 1000x magnification SEM images of specimens laterally face milled at 15,000 RPM showing; (a) as-received CoCrMo milled with Mill A, (b) as-received CoCrMo milled with Mill B, (c) as-received CoCrMo milled with Mill C, (d) as-received CoCrMo milled with Mill D and (e) HT4H CoCrMo milled with Mill B.

5.1.3. 20,000 RPM

At 20,000 RPM all five surfaces were successfully milled to an extent that allowed SEM images to be captured for analysis.

Mill A, Figure 30 (a). The SEM image at 40x magnification of the surface obtained at 20,000 RPM continues the trend of increasing waviness as spindle speeds increased for Mill A, this being likely due to increasing vibrations. Large waviness peak heights are shown with moderate spacing creating a very poor surface and rewelding is shown on the waviness peak ridges. Horizontal gouging and smaller ridges inside the waviness peaks are also shown.

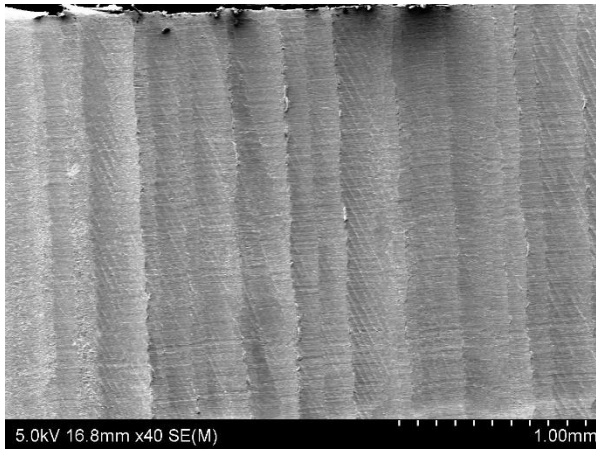
Mill B, Figure 30 (b). The surface obtained at 20,000 RPM by Mill B at 50x magnification initially shows deeper craters, more severe horizontal ridges and more material tearing than was present at 15,000 RPM. Though low magnifications can be deceiving, it is shown that a relatively poor surface has been achieved.

Mill C, Figure 30 (c). The surface obtained with Mill C at 20,000 RPM shows an improvement over its 15,000 RPM pass. Waviness appears to be very slight with little depth, no obvious chip rewelding is seen, and furthermore no large horizontal or vertical ridges can be seen. At low magnification this appears to be a very good surface.

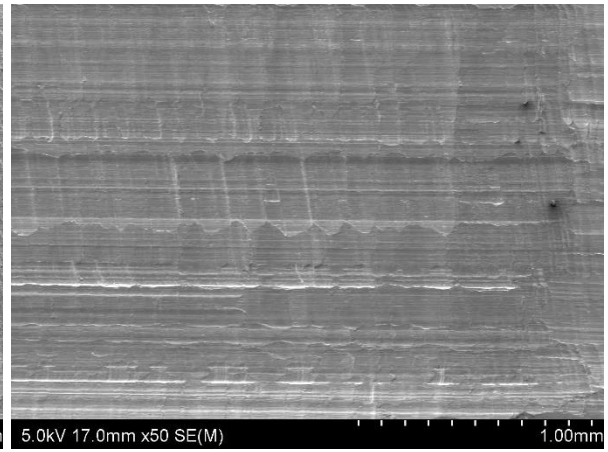
Mill D, Figure 30 (d). The SEM image shows the surface milled with Mill D. Waviness appears only slightly worse than what occurred at 15,000 RPM. It should be noted however that at 20,000 RPM the milling pass undertaken by Mill D was only partially completed due to excessive chatter and vibrations. This further enforces the increase in chatter/waviness as spindle speed increases and highlights the dangers of drawing conclusions from only partially completed experiments.

Mill B, HT4H CoCrMo, Figure 30 (e). The SEM image shows the surface obtained is typical of this material. The surface is filled with deep vertical ridges and large amounts of chip rewelding on these ridges. The vertical ridges appear to reduce in occurrence as the milling pass moves towards the end, suggesting mill stability might increase as it settles. Strong horizontal gouging due to ploughing and/or tool wear is shown. Furthermore, cavities and craters occurring along the bottom area of the milled surface are present indicating high mill vibration and/or tool wear towards the tip of the mill.

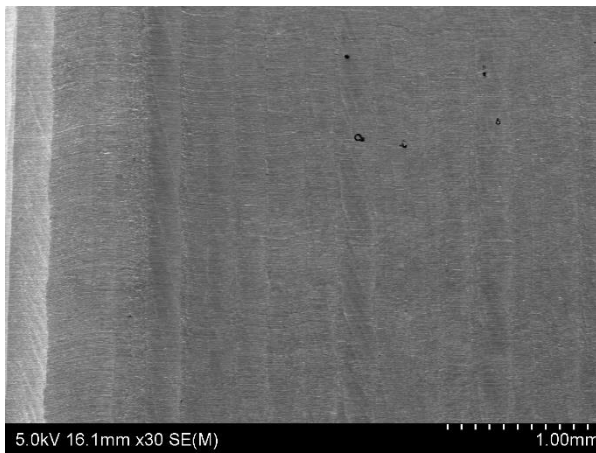
These images are shown below in Figure 30 (a-e).



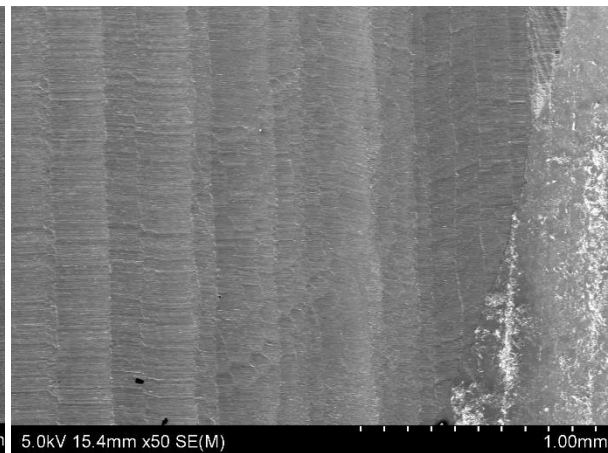
(a)



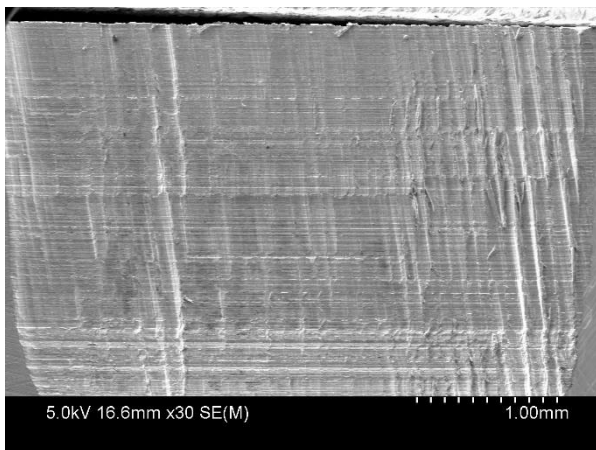
(b)



(c)



(d)



(e)

Figure 30 Low magnification SEM images of specimens laterally face milled at 20,000 RPM showing; (a) as-received CoCrMo milled with Mill A, (b) as-received CoCrMo milled with Mill B, (c) as-received CoCrMo milled with Mill C, (d) as-received CoCrMo milled with Mill D and (e) HT4H CoCrMo milled with Mill B.

Mill A, Figure 31 (a). At 200x magnification the size of the waviness peak in the surface milled by Mill A becomes apparent. Not only is the peak height considerably larger than other passes, there is also a significant amount of rewelded material on each peak. This combination of high waviness peaks and rewelded material on the ridges is exactly the opposite of what is needed in dental implants. Moderate amounts of horizontal gouging, tearing and rewelded material are also seen between these large cyclic peaks; however, they can be considered secondary defects as the sheer size of the waviness peak height and amount of rewelded material is of primary concern.

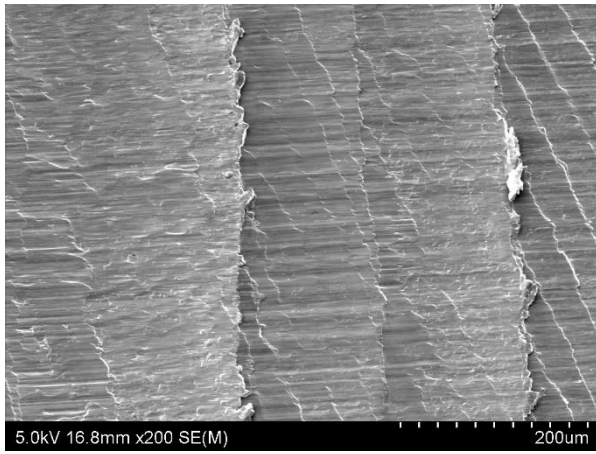
Mill B, Figure 31 (b). The captured SEM image shows the types of crater and ridge formations typically occurring with surfaces milled by Mill B, a noticeably low amount of rewelded material is seen relative to the amount of exposed ridges and fractured edges. However the amount and frequency of these craters leads to an unsuitable surface for biomedical use.

Mill C, Figure 31 (c). The surface milled by Mill C at 20,000 RPM is the best surface finish shown so far. The vertical ridges are shallow and exhibit very little rewelded material. Furthermore the surface between these shallow ridges has almost no rewelded material present. Craters and cavities are also non-existent and only very minimal gouging occurred.

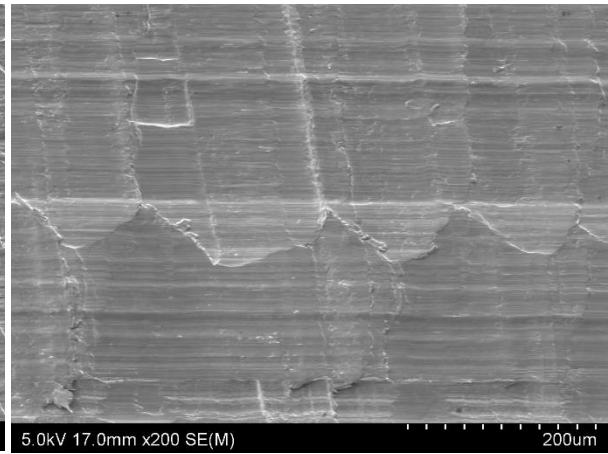
Mill D, Figure 31 (d). The defects present on the surface milled with Mill D are the rewelded chips present on the ridge edges, some small gouging and a few small crater formations. The surface finish is not extremely poor in this area, however the amount of ridges present and the large waviness peak heights mean it is not suitable for use in dentistry. If the issues leading to mill vibrations were resolved then the surface obtained may perform significantly better.

Mill B, HT4H CoCrMo, Figure 31 (e). HT4H CoCrMo milled with Mill B is shown in the SEM image. Deep valleys and ridges are seen with rewelded chips primarily adhered to these edges. Deep horizontal gouging occurs across the whole image indicating extensive BUE induced ploughing was taking place. Long semi-attached fragments of material are adhered to the deep ridges. It is unknown if these are rewelded chips, plastically deformed material, or semi-detached material.

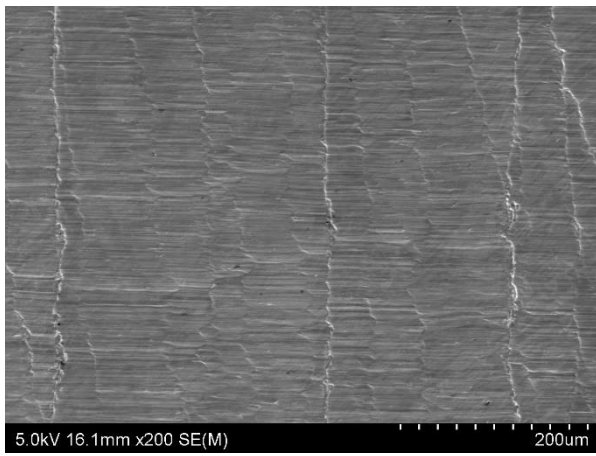
The images of the 200x magnifications are shown in Figure 31 (a-e).



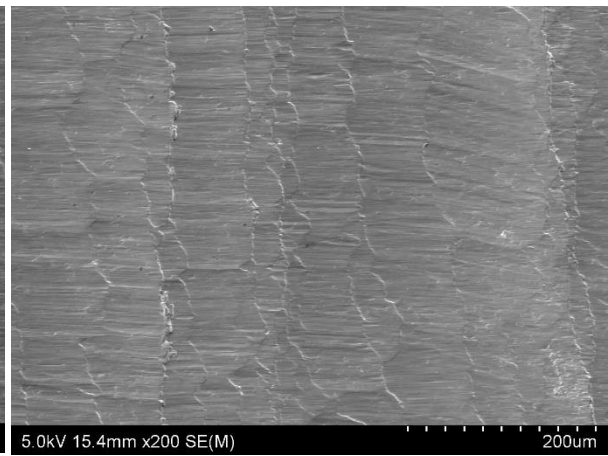
(a)



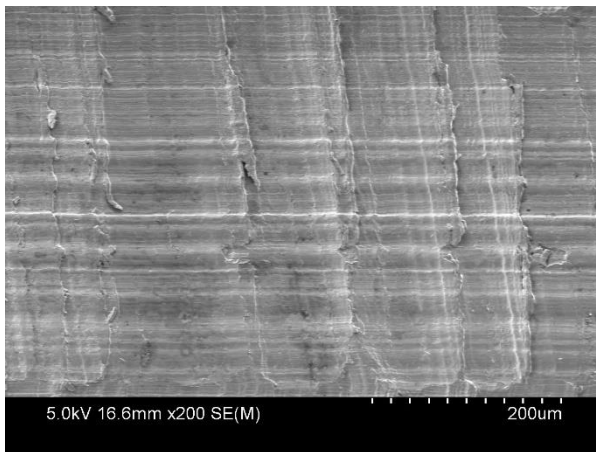
(b)



(c)



(d)



(e)

Figure 31 200x magnification SEM images of specimens laterally face milled at 20,000 RPM showing; (a) as-received CoCrMo milled with Mill A, (b) as-received CoCrMo milled with Mill B, (c) as-received CoCrMo milled with Mill C, (d) as-received CoCrMo milled with Mill D and (e) HT4H CoCrMo milled with Mill B.

Mill A, Figure 32 (a). The SEM image shows the 1000x magnification of the surface milled with Mill A, an uneven surface filled with cracking, cavitation and rewelded chips on the surface. These properties, combined with the appearance of a layered ridge suggests that large amounts of material have been frictionally rewelded at this ridge and smeared across the surface preceding it. This material was likely resulting from a combination of severed BUE, and material ejected from the mill flutes and body.

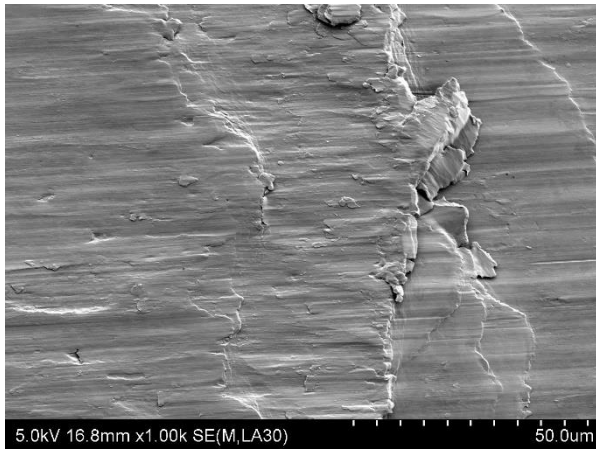
Mill B, Figure 32 (b). Looking at the surface milled with Mill B, a deep multi-layered ridge on the edge of a crater formation is shown. High amounts of chip rewelding can be seen occurring on this ridge. To the right of the edge a small amount of rewelding does occur, however the chips are relatively small. Light gouging appears fairly consistently across the entire surface with small patches of cavitation appearing either side of the ridge.

Mill C, Figure 32 (c). On the surface milled with Mill C a single ridge is shown running through the centre of the image with a small section of rewelded material in the middle. Aside from this small rewelded chip, the surface is in great condition, with very minor gouging and tearing being the only defects. Mill C has provided the smoothest surfaces shown so far, with this pass at 20,000 RPM providing the best overall.

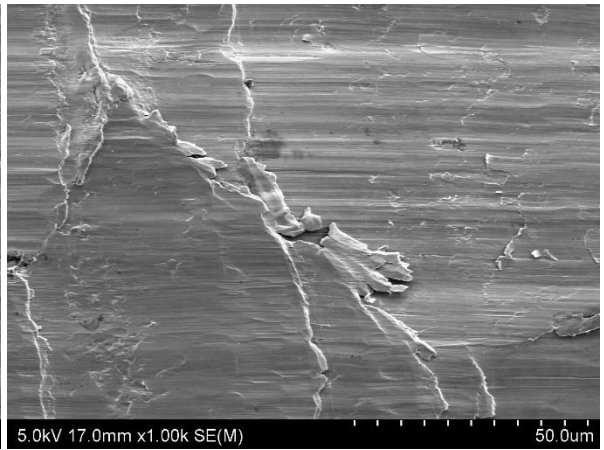
Mill D, Figure 32 (d). The surface finish of the specimen milled with Mill D shows 2 to 3 moderate depth ridges appearing through the centre of the photo with minor chip rewelding occurring on each ridge. Moderate gouging and tearing is also occurring, most likely due to ploughing. The section of the surface shown presents a reasonable surface finish quality; however the large waviness peak height is largely detrimental to the overall surface finish.

Mill B, HT4H CoCrMo, Figure 32 (e). The obtained surface from HT4H CoCrMo milled with Mill B shows huge amounts of chip rewelding at this magnification and cavitation, large gouges and very deep ridges are present. This surface quality obtained by Mill B with HT4H CoCrMo is unusable despite showing improvements from the surface obtained at 15,000 RPM.

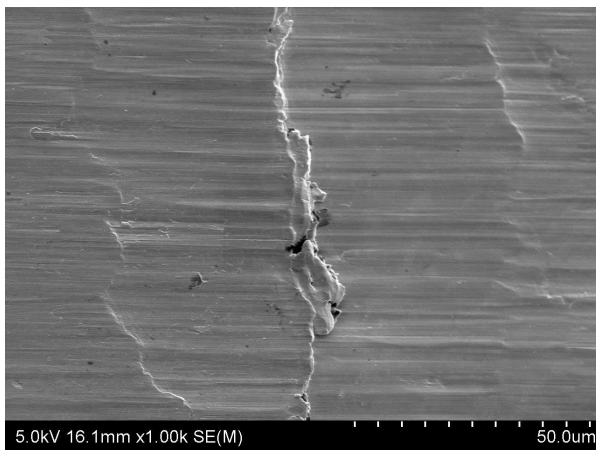
The images for these 1000x magnifications are shown below in Figure 32 (a-e).



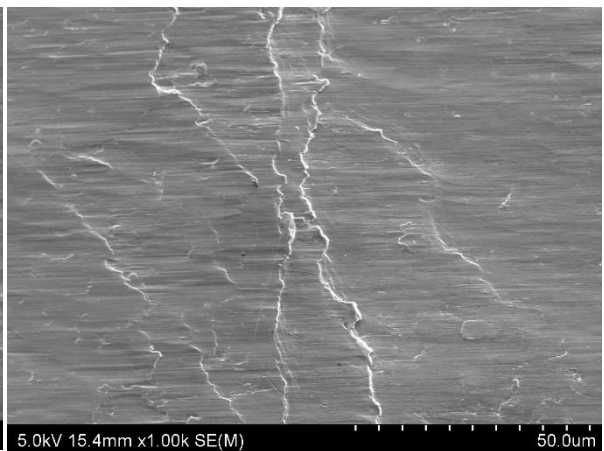
(a)



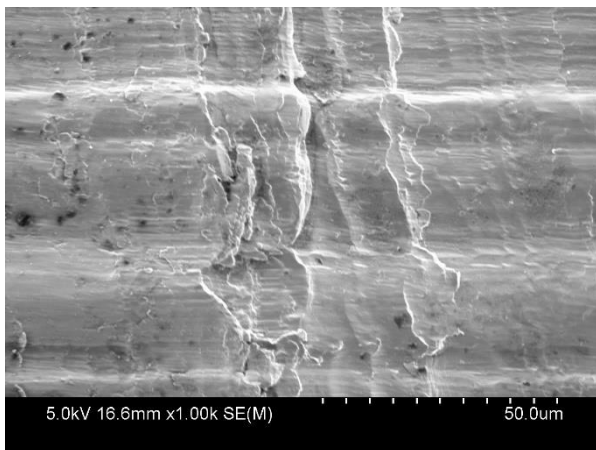
(b)



(c)



(d)



(e)

Figure 32 1000x magnification SEM images of specimens laterally face milled at 20,000 RPM showing; (a) as-received CoCrMo milled with Mill A, (b) as-received CoCrMo milled with Mill B, (c) as-received CoCrMo milled with Mill C, (d) as-received CoCrMo milled with Mill D and (e) HT4H CoCrMo milled with Mill B.

5.1.4. 25,000 RPM

At 25,000 RPM all five specimens were milled to an adequate level to capture SEM images of the surface, though it should be noted that passes on specimen A, Figure 33 (a), and D, Figure 33 (e) were only partially completed. It is believed this is owing to a manual stoppage of the milling pass due to excess vibrations and mill instability which if continued could lead to mill fracture. The excessive peak size and spacing of waviness shown conforms to this hypothesis.

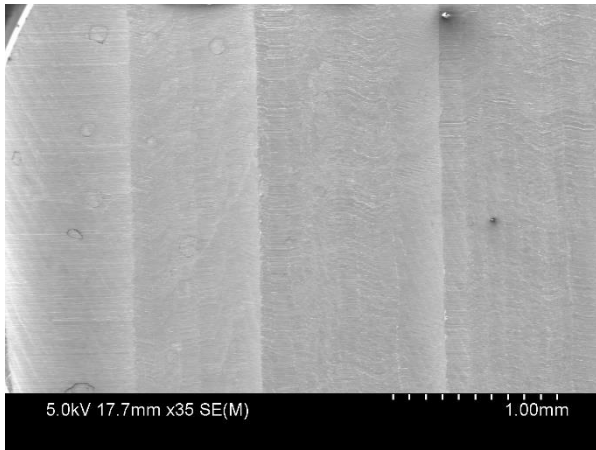
Mill A, Figure 33 (a). The surface milled with Mill A shows that both waviness peak heights and waviness spacing are noticeably increased from the 20,000 RPM pass. Interestingly the surface between these peaks appears to be relatively smooth though, with only minor gouging seen as a detriment.

Mill B, Figure 33 (b). As was noted at previous spindle speeds, Mill B seems to not be affected by waviness and mill vibrations in the same way the other mills are. However large gouging, crater formations and rough fractured ridges typical of Mill B led to a relatively poor surface in Figure 33 (b). There are also high amounts of oil contamination seen as the black spots, though this would not affect surface quality.

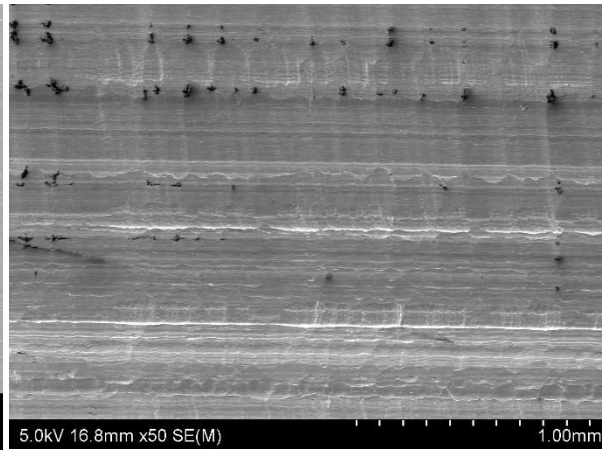
Mill C, Figure 33 (c). At lower speeds Mill C provided very good surface finishes; however increasing from 20,000 RPM to 25,000 RPM led to a noticeable increase in waviness peak height and a slight increase in visible horizontal gouging. The ideal spindle speed seems to have been exceeded for Mill C.

Mill D, Figure 33 (d). A partial milling pass is shown signified by the un-milled section on the bottom right hand side of the image. Furthermore, uneven waviness spacing, combined with a large peak height, confirms that drill instability was a serious issue here. Rewelded material is also notably significant. Finally, the horizontal gouging and ridges can be seen to angle downwards as the milling pass moves forward indicating that drill drop off was occurring. Cutting forces for Mill D at 25,000 RPM confirm this.

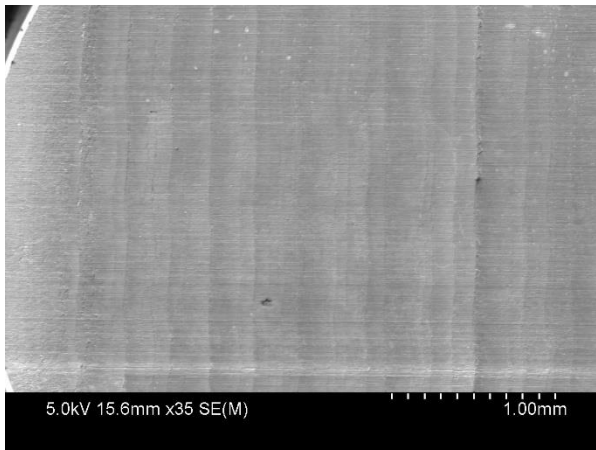
Mill B, HT4H CoCrMo, Figure 33 (e). The deep vertical ridges formed at lower speeds are less of an issue at 25,000 RPM although deep gouging and horizontal belts of crater formations typical of Mill B can be seen to be present and are the main detriments in this surface finish. There also seems to be horizontal bands of differing surface finish quality. It is unknown whether this is due to complex mill vibration, uneven tool wear or different edge quality of the mill itself. Images of these passes are shown in Figure 33 (a-e).



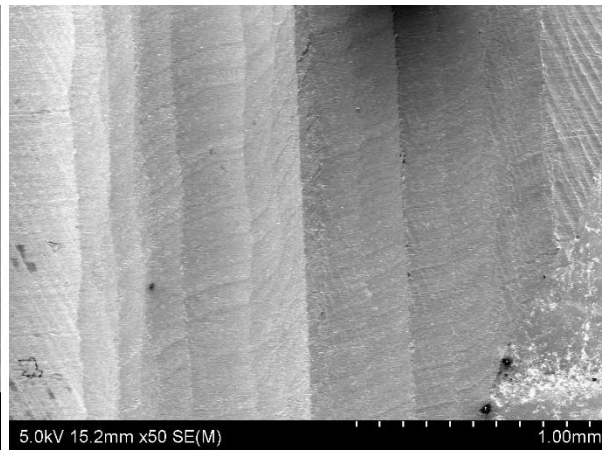
(a)



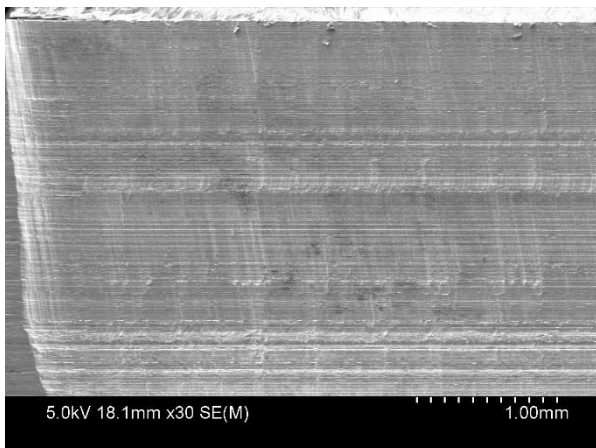
(b)



(c)



(d)



(e)

Figure 33 Low magnification SEM images of specimens laterally face milled at 25,000 RPM showing; (a) as-received CoCrMo milled with Mill A, (b) as-received CoCrMo milled with Mill B, (c) as-received CoCrMo milled with Mill C, (d) as-received CoCrMo milled with Mill D and (e) HT4H CoCrMo milled with Mill B.

Mill A, Figure 33 (a). Surface quality has increased significantly from 20,000 RPM despite the increase in waviness, peak height and spacing. The minor ridges are relatively shallow and smooth as opposed to deep fractured ridges. Significantly less gouging and tearing is also present. Most interesting is the seemingly large decline in rewelded material, specifically on the waviness peak ridges. However the SEM image shown is relatively bright with low contrast which may be hiding some of the defects.

Mill B, Figure 34 (b). The surface seen milled by Mill B is relatively poor. The edge of a crater formation can be seen running through the centre of the image. It is shown that large fractured craters, chip rewelding on ridges, horizontal ridges and gouging are the defects for the surface obtained with Mill B.

Mill C, Figure 34 (c). The surface finish shown is of a very high quality, gouging is shallow and in-between the waviness peaks there is very little chip rewelding or tearing shown. However the increase in waviness peak height has led to the formation of large ridges where chip rewelding and material rewelding is taking place. This was not seen at 20,000 RPM and shows that an optimal spindle speed has been passed.

Mill D, Figure 34 (d). Huge amounts of rewelding can be seen on the uphill face of the waviness peak with large amounts of chip rewelding also present on the waviness peak ridge. As seen previously, the uphill face is showing a worse surface finish than the downhill face. Moderate gouging is shown, though this can be considered as a secondary issue in this case as waviness, drill instability and severe rewelding all outweigh the other issues.

Mill B, HT4H, Figure 34 (e). HT4H CoCrMo milled with Mill B is shown, higher magnifications allowing for the appearance of vertical ridges to be identified, though far less extensive than those seen at lower speeds. Deep horizontal gouging is seen indicating ploughing occurred and strongly suggesting a large BUE on the tool face was present. Moderate chip rewelding is shown occurring on the vertical ridges, the chips themselves being very large and seeming to be half detached. As stated previously, it is unknown if these are rewelded chips or partially removed material. The identifying features seen in the milling of this HT4H material is the fractured and rugged state of the surface finish. Deep ridges occur with heavily fractured edges, and even the surface between these ridges exhibit a fractured and rough nature. Mill B with AR CoCrMo also experienced horizontal gouging and large fractures as the major detriments; however it was not so much affected by vertical ridges as is seen here, and

exhibited a much less rugged and fractured nature. These images are shown in Figure 34 (a-e).

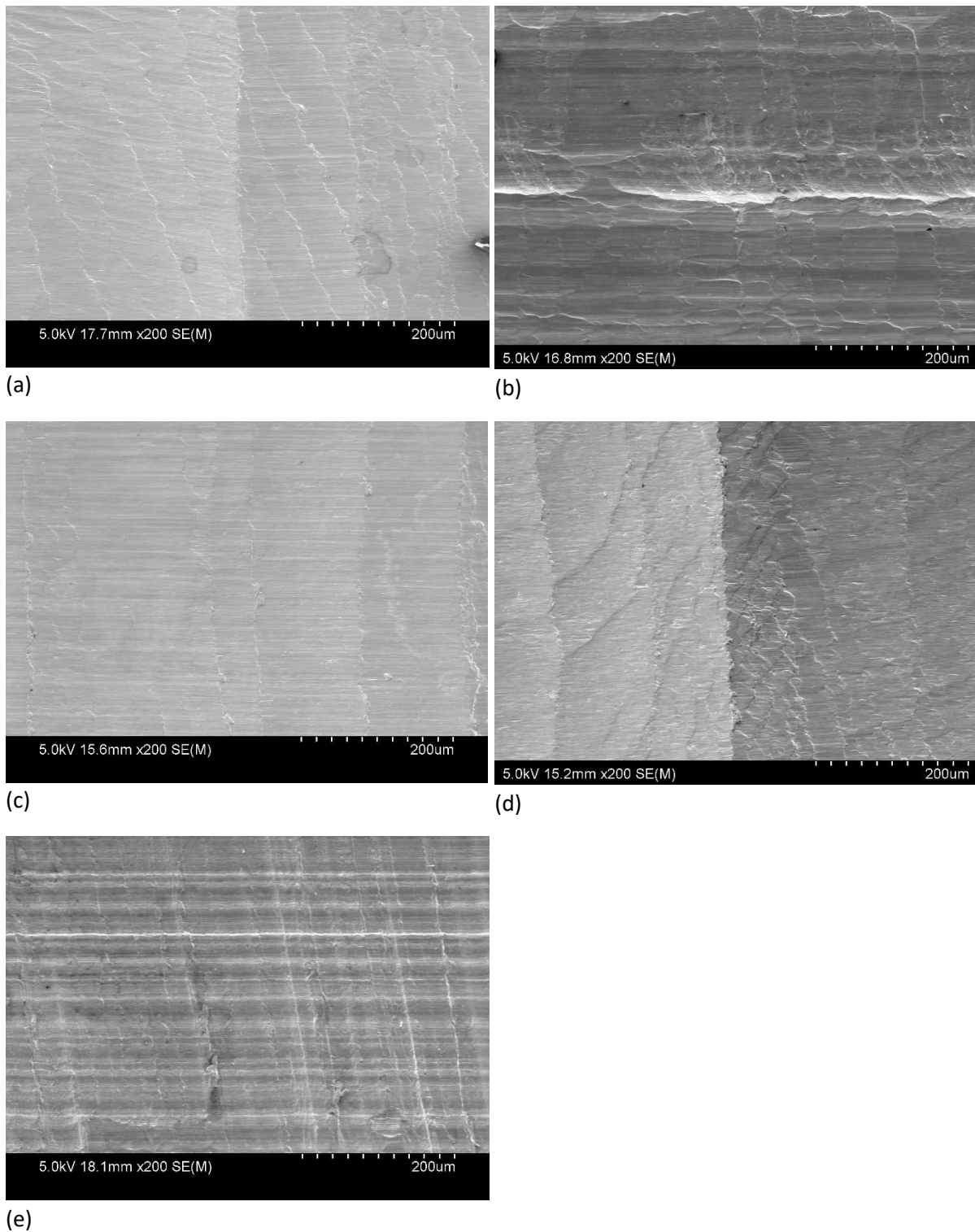


Figure 34 200x magnification SEM images of specimens laterally face milled at 25,000 RPM showing; (a) as-received CoCrMo milled with Mill A, (b) as-received CoCrMo milled with Mill B, (c) as-received CoCrMo milled with Mill C, (d) as-received CoCrMo milled with Mill D and (e) HT4H CoCrMo milled with Mill B.

Mill A, Figure 35 (a). The 1000x magnification of AR CoCrMo milled with Mill A shows the potential for a good surface finish. Despite the lack of chip breaker geometry this area of milled surface is in great condition. The only significant detriment is the waviness peak height and spacing. There are however a small amount of chips rewelded to the peak ridge, though the overall amount of rewelding is significantly low considering the extent shown with the same mill at 20,000 RPM. Small cavities can be seen on the left hand side, and minor gouging all around. Despite the aforementioned faults, the surface is near ideal with exception of waviness.

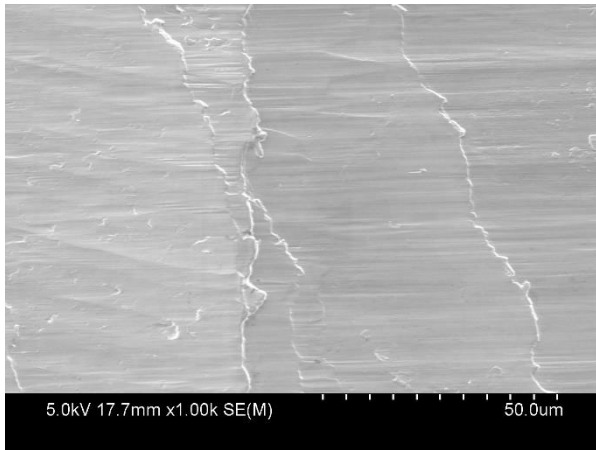
Mill B, Figure 35 (b). The surface milled with Mill B shows the full extent of the fractured craters typical of Mill B. Steep, rough, jagged edges are seen. High amounts of rewelding inside these craters are now visible that was not apparent at lower magnifications. Although typical cyclic waviness is not seen with Mill B and AR CoCrMo, the extent of these fractures are significant and could be caused by mill vibration potentially, with BUE and tool wear being two other possibilities.

Mill C, Figure 35 (c). AR CoCrMo milled with Mill C is shown. As stated earlier, the surface is near immaculate between ridges. Gouging is minimal, few cavities exist and the overall roughness is minimal. The waviness is the only detriment with the peaks forming areas of rewelded chips and leaving a wavy surface.

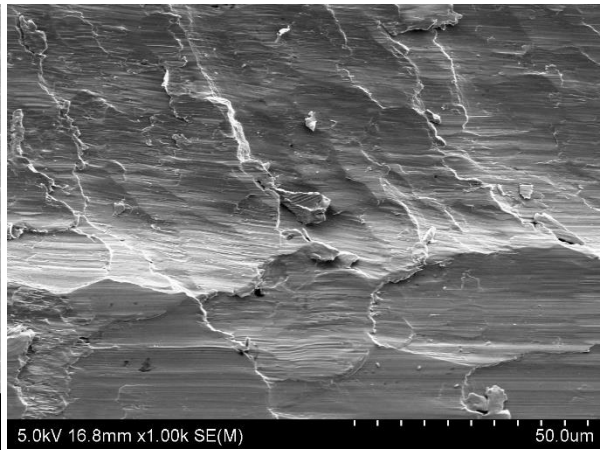
Mill D, Figure 35 (d). A large ridge formed on top of the waviness peak is shown in the image. Chip rewelding is heavy on this ridge, gouging is also seen either side of the ridge. Minor cavities are also visible, though anything aside from waviness and rewelding can be called secondary issues in this case as the two were shown to be very severe in the lower magnification SEM images.

Mill B, HT4H, Figure 35 (e). The layered and fractured nature of the vertical ridges is shown in this image with large chips also rewelded to the ridges. Gouging is shown in the image with it being more severe on the right hand side of the large ridge. The layered nature of these ridges is notable as this has not been seen so extensively in any other example. The way Mill B is interacting with this HT4H material has completely changed the obtainable surface features and defects. Whether this can be attributed to machining error or strictly to the change in material structure is undetermined at this point.

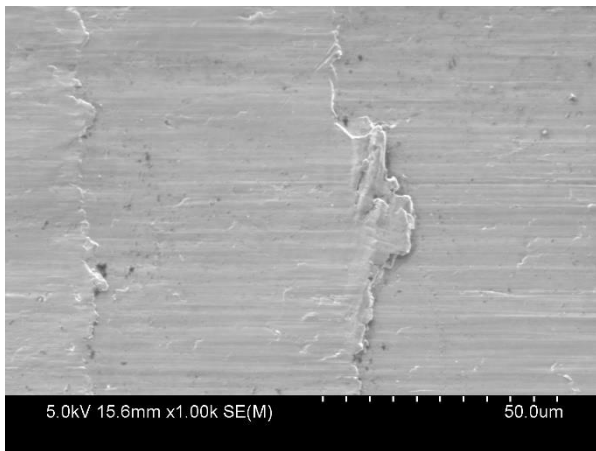
SEM images of these 1000x magnifications are shown in Figure 35 (a-e).



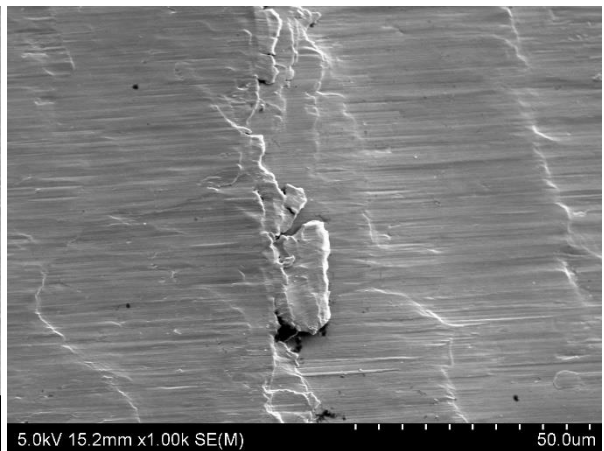
(a)



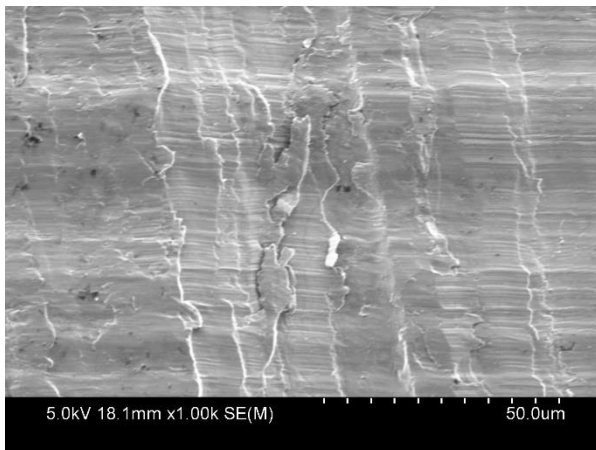
(b)



(c)



(d)



(e)

Figure 35 1000x magnification SEM images of specimens laterally face milled at 25,000 RPM showing; (a) as-received CoCrMo milled with Mill A, (b) as-received CoCrMo milled with Mill B, (c) as-received CoCrMo milled with Mill C, (d) as-received CoCrMo milled with Mill D and (e) HT4H CoCrMo milled with Mill B.

5.1.5. 30,000 RPM

Low magnification images are shown in Figure 36 for all five milled specimens, though Mill D failed the milling pass completely. Mill A was also only partially completed due to excess tool vibrations occurring leading to an unstable experiment.

Mill A, Figure 36 (a). The appearance of un-milled material on the bottom right and left of the image shows this is a partially completed milling pass. However, due to the length that was successfully milled, it is believed to be reliable enough to be discussed. The appearance of drop off, mill instability and severe waviness is apparent in the surface milled by Mill A. Chip rewelding on the waviness peak ridge and material rewelding on the uphill climb of the peak can also be seen. Also noted is the shift in surface texture at various points showing a very unstable milling process was occurring.

Mill B, Figure 36 (b). The SEM image shows a very similar surface to the surface shown at 25,000 RPM. Deep gouging, moderate horizontal ridges and deep vertical ridges can be seen. The lower section of the image shows severe roughness indicating the mill tip has significantly degraded. Horizontal bands of varying surface finish are also seen occurring which is typical of surfaces milled with Mill B.

Mill C, Figure 36 (c). The trend that showed a decrease in surface finish for Mill C after 20,000 RPM continues. A large waviness peak height is shown with chip rewelding on the peak ridges. Noticeable horizontal gouging is present indicating ploughing. Smaller ridges inside the waviness peaks are also seen, believed to be due to the chip forming mechanism.

Mill D, Figure 36 (d). Most notable about this image is the very partial pass shown, believed to be due to extreme mill instability and drop-off leading to the manual cancellation of the milling pass. This was also validated with the force measurements noting that complete mill drop-off occurred. The 30x magnification is shown for the surface milled with Mill D, however no further magnification or analysis is shown owing to the complete failure of the pass creating unreliable data. Drill drop off, severe waviness and vibrations, and high cutting forces led to the abandonment of this pass.

Mill B, HT4H, Figure 36 (e). The surface finish shown is typical of Mill B with HT3H CoCrMo and is similar to the surface at 25,000 RPM. Deep horizontal gouging, crater formations, vertical ridges and chip rewelding are the defects. Crater depth and severity has slightly increased from the surface at 25,000 RPM, with a slight increase of rewelding also occurring.

Images of all five milled surfaces at low magnification are shown in Figure 36 (a-e).

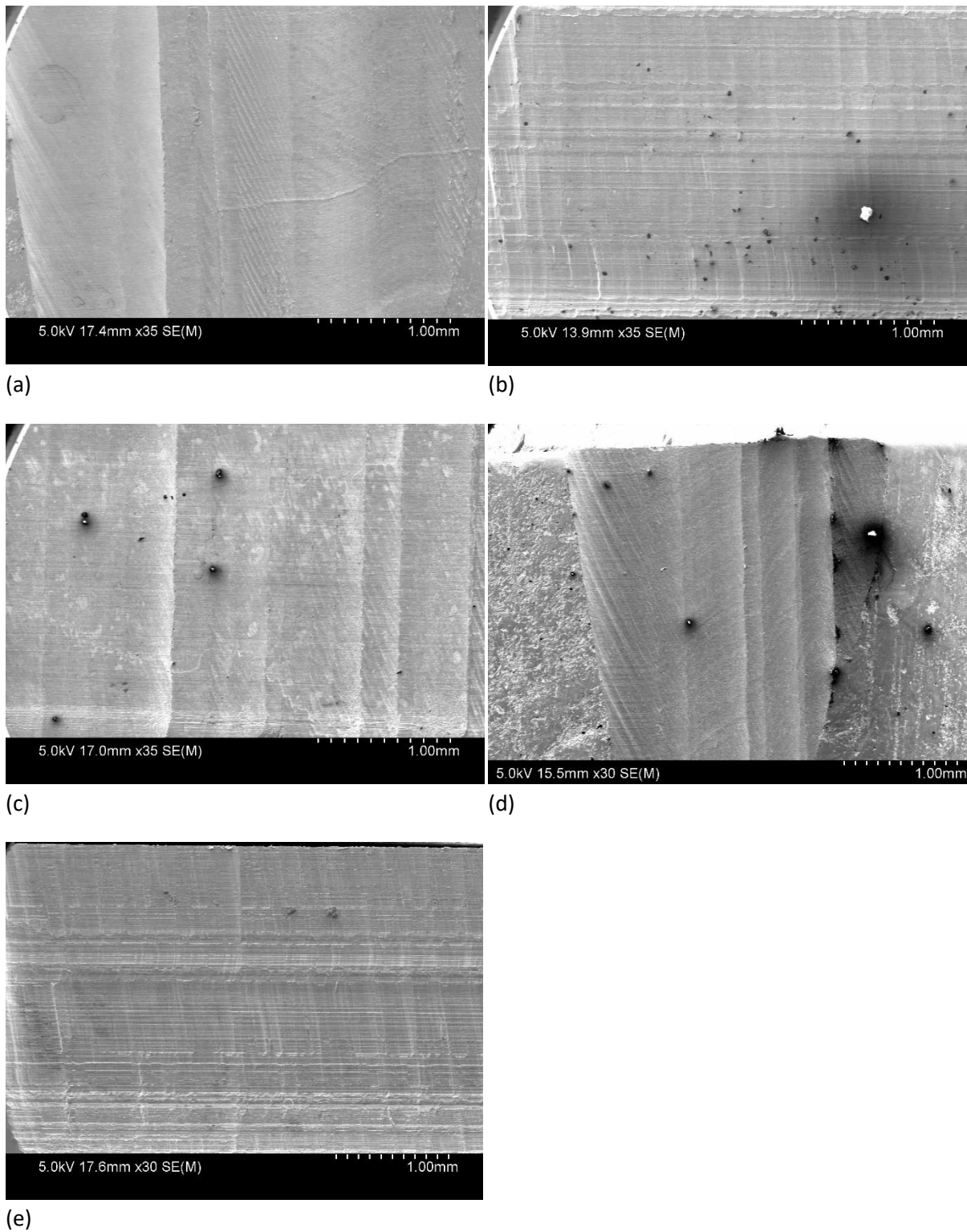


Figure 36 Low magnification SEM images of specimens laterally face milled at 30,000 RPM showing; (a) as-received CoCrMo milled with Mill A, (b) as-received CoCrMo milled with Mill B, (c) as-received CoCrMo milled with Mill C, (d) as-received CoCrMo milled with Mill D and (e) HT4H CoCrMo milled with Mill B.

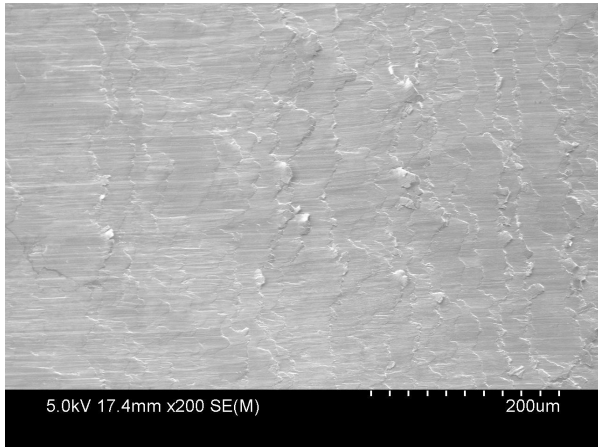
Mill A, Figure 37 (a). The SEM image shows with AR CoCrMo milled with Mill A, a large amount of ridges can be seen combined with flaky rewelded material on and near these ridges. Moderate amounts of gouging is also visible. The main defect in this pass was waviness peak height and spacing, which cannot be shown at this magnification and implies high amounts of mill vibration and instability was present at this speed.

Mill B, Figure 37 (b). The area observed shows the typical defects of Mill B with craters, vertical and horizontal ridges and gouging leading to a poor surface finish. Some minimal chip rewelding can be seen on the crater edges and ridges. Overall the surface finish seems superior to 25,000 RPM, however, as mentioned below, image contrast can heavily affect how a surface is viewed and the extent of these craters is unknown.

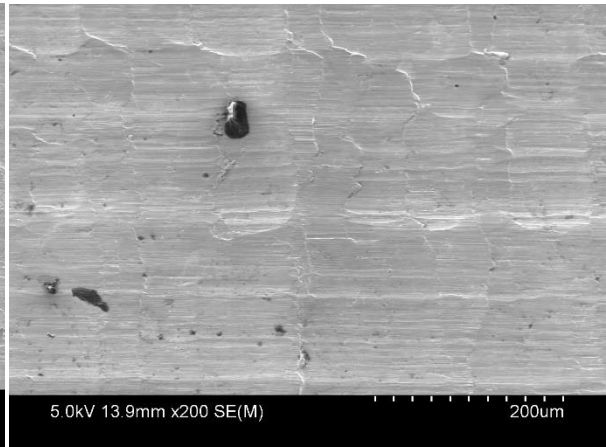
Mill C, Figure 37 (c). Large waviness peaks can be seen with chip rewelding occurring on these peak ridges, also angled ridge formations between peaks are present showing minor rewelding occurring. Furthermore horizontal gouging is shown as well as various deposits of rewelded material appearing sporadically. This is considered a very poor surface finish and very different to the relatively good surface finishes achieved at 15,000 RPM and 20,000 RPM.

Mill B, HT4H, Figure 37 (d). The SEM image shows HT4H CoCrMo milled with Mill B, this image offering a good example of the horizontal belts of differing surface finishes that are typical of Mill B. The top half of the image shows a belt of fractured crater-like surfaces with rugged ridges and moderate chip rewelding, while the bottom half shows a completely different surface with heavy horizontal gouging and vertical ridges formed. The larger cyclic spacing of vertical ridges contain a lot of large needle-like rewelded chips. These horizontal belts of differing finish are so repeatable throughout experiments that either complex mill vibrations, or irregular drill wear must be occurring as BUE edge formation should not lead to such repeatable results.

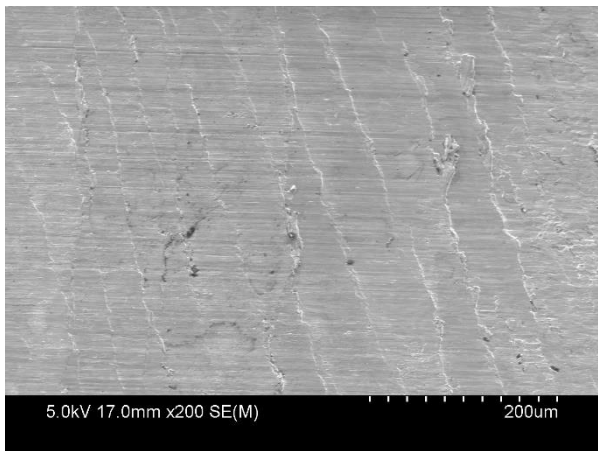
The SEM images at 200x magnification are shown in Figure 37 (a-d).



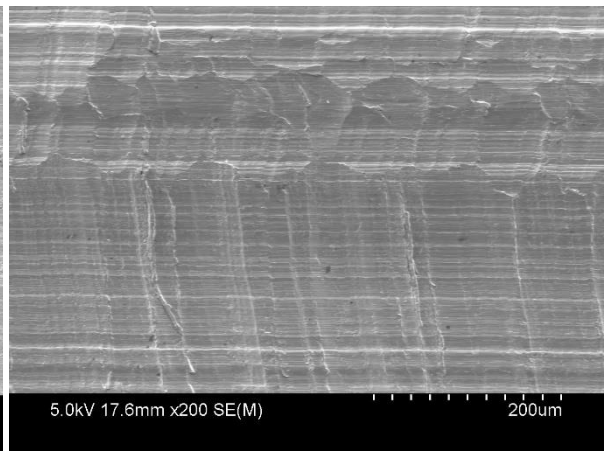
(a)



(b)



(c)



(d)

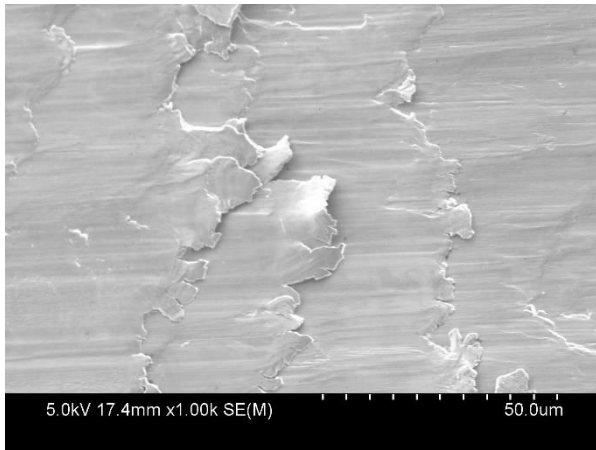
Figure 37 200x magnification SEM images of specimens laterally face milled at 30,000 RPM showing; (a) as-received CoCrMo milled with Mill A, (b) as-received CoCrMo milled with Mill B, (c) as-received CoCrMo milled with Mill C and (d) HT4H CoCrMo milled with Mill B.

Mill A, Figure 38 (a). The SEM image gives a good look at the flaky rewelding occurring. This type of rewelding has not been observed in other passes in this study and it is uncertain why it would occur at 30,000 RPM, though perhaps it is due to the additional frictional heat, or mill vibrations or a combination of both. Minor gouging is also shown on the surface.

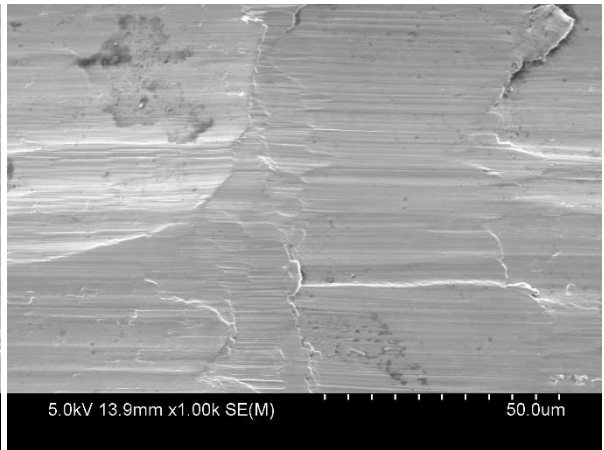
Mill B, Figure 38 (b). The top left hand corner of the SEM image shows the edge of a crater formation, though this one is particularly smooth with flowing edges as opposed to the deep fractured edges which are usually seen. High amounts of gouging and tearing indicative of ploughing is shown, as well as a large chip rewelded to a ridge in the top right hand corner. Despite the small section shown here exhibiting a relatively smooth surface, the rest of the surface finish of this pass was of a significantly lower quality.

Mill C, Figure 38 (c). In the captured SEM image a large cluster of rewelded chips is shown attached to the waviness peak ridge, note the dark residue present between the rewelded chips. This residue is cutting oil that could not be cleaned off, giving a perfect example of how negatively these rough surfaces will be for dental implants when plaque and bacteria build up in these crevices. Aside from the cluster of chip rewelding occurring on the ridge, minor gouging and a second minor ridge to the right are the other detriments.

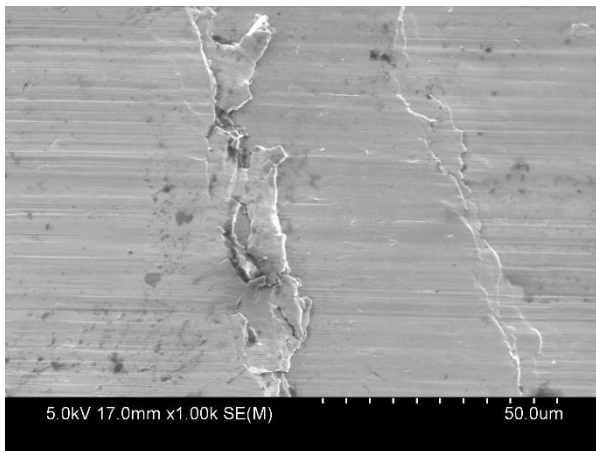
Mill B, HT4H, Figure 38 (d). A clear example of long rewelded needle-like chips typical of this material can be seen attached to the ridge in the centre of the image. Heavy gouging is also present across the entire surface indicating high amounts of ploughing were taking place. The SEM images of the 1000x magnifications are shown in Figure 38 (a-d).



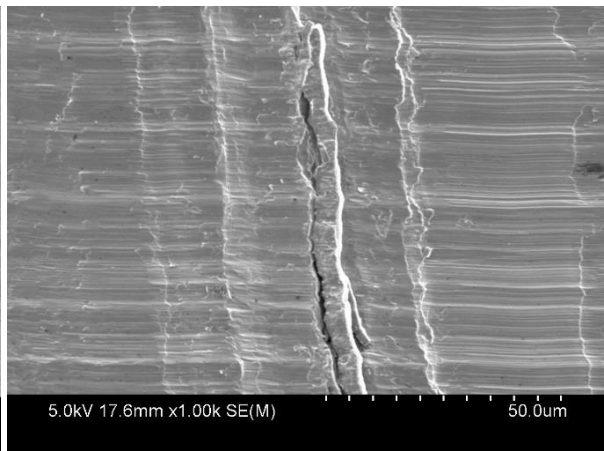
(a)



(b)



(c)



(d)

Figure 38 1000x magnification SEM images of specimens laterally face milled at 30,000 RPM showing; (a) as-received CoCrMo milled with Mill A, (b) as-received CoCrMo milled with Mill B, (c) as-received CoCrMo milled with Mill C and (d) HT4H CoCrMo milled with Mill B.

5.1.6. 35,000 RPM

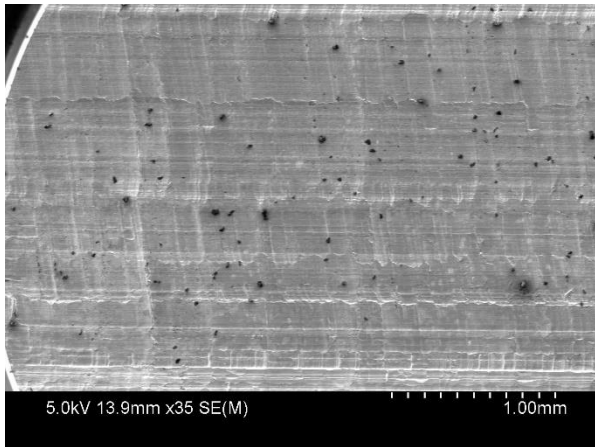
Figure 39 shows the four milling passes attempted at 35,000 RPM. Mill A was only partially milled and images were not obtained, while Mill D was attempted but was only very partially milled also. This leaves three completed passes with AR CoCrMo milled with mill B, Figure 39 (a), AR CoCrMo milled with mill C, Figure 39 (b) and HT4H CoCrMo milled with Mill B, Figure 39 (d). Figure 39 (c) shows the attempted milling pass with Mill D, note the mill silhouette and angled ridges mimicking the flutes suggesting the mill either dropped off completely, and/or jammed. Owing to the failed milling pass, Mill D is not discussed any further.

Mill B, Figure 39 (a). Visually at low magnifications AR CoCrMo milled with Mill B appears similar to previous passes at 30,000 RPM and 25,000 RPM. Horizontal gouging and ridges, vertical ridges and large crater formations led to a rough, fractured and rugged surface with varying horizontal bands of surface quality. The surface shown appears to have a much lower quality surface finish than that shown at 30,000 RPM or 25,000 RPM, however it is believed the high contrast of the image is exaggerating some features.

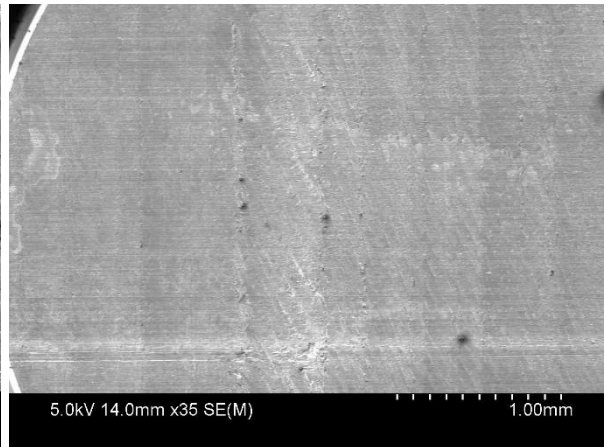
Mill C, Figure 39 (b). Waviness peak height and spacing shown in the SEM image appears similar to that of 30,000 RPM, however the amount of ridges inside these peaks and rewelded material has exponentially increased. A scaly rough surface with huge amounts of rewelded material is the result. This continues the trend of decreasing surface quality for Mill C after a spindle speed of 20,000 RPM.

Mill B, HT4H, Figure 39 (d). The SEM image shows HT4H CoCrMo milled with Mill B. Surface finish has degraded from the pass at 30,000 RPM significantly and once again deep vertical ridges are a major detriment. Furthermore horizontal bands of deep and fractured craters can be seen in combination with deep horizontal gouging. High amounts of material rewelding is also seen, specifically occurring on the horizontal bands of craters and deep vertical ridges formed.

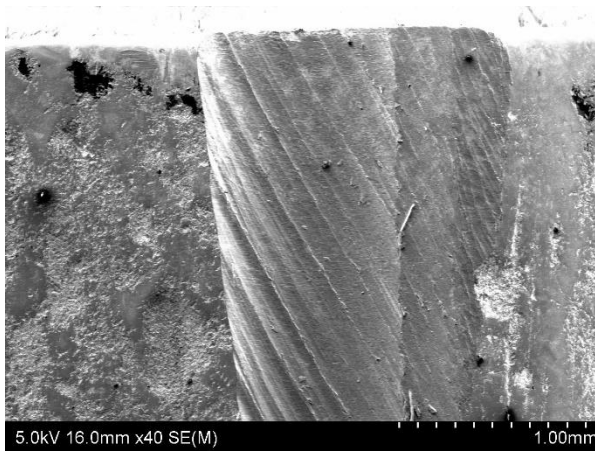
Images of these low magnification passes are shown in Figure 39 (a-d).



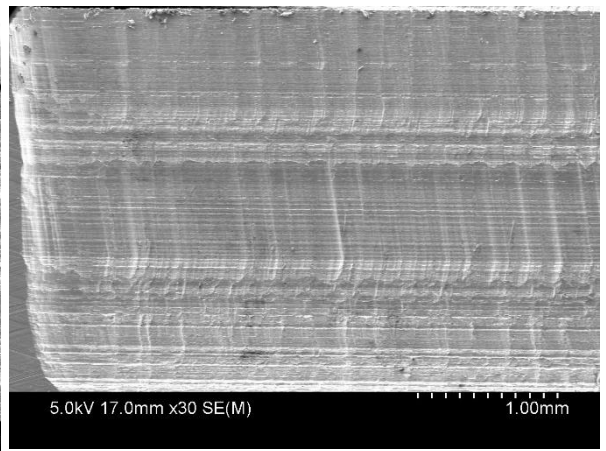
(a)



(b)



(c)



(d)

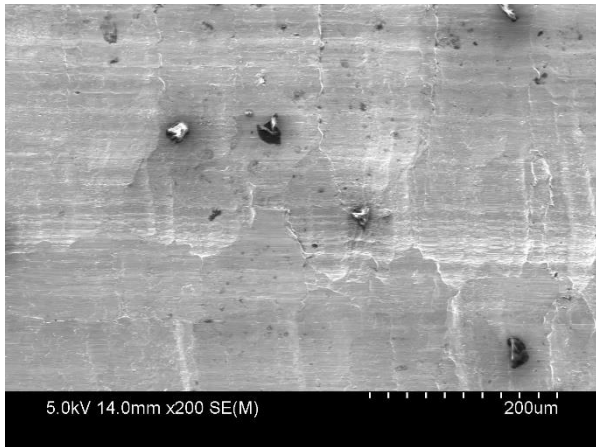
Figure 39 Low magnification SEM images of specimens laterally face milled at 35,000 RPM showing; (a) as-received CoCrMo milled with Mill B, (b) as-received CoCrMo milled with Mill C, (c) as-received CoCrMo milled with Mill D and (d) HT4H CoCrMo milled with Mill B.

Mill B, Figure 40 (a). A good view of the horizontal bands of differing surface finish can be seen in this image. This is shown roughly through the middle of the image with typical crater formations and generally a more rugged surface dominating the top half of the image, and a smoother less rugged surface shown in the bottom half. Some chip rewelding is shown on the crater ridges and throughout various other ridges formed in both the upper and lower half of the image, though notably the surface is worse in the 'crater belt' in the top half.

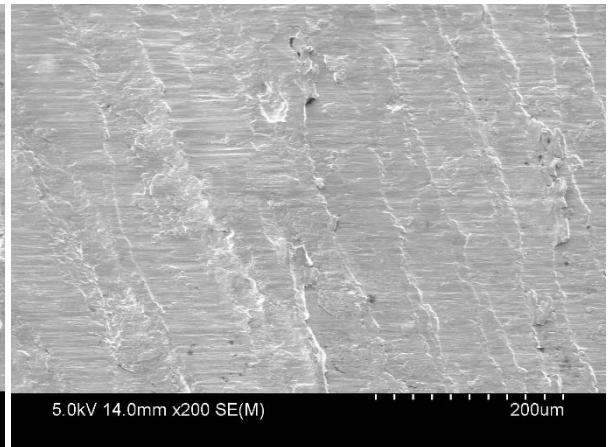
Mill C, Figure 40 (b). The extent to which material rewelding is occurring is shown in this image, huge amounts of ridges having been formed with massive amounts of material rewelded to them. Large chips are also rewelded on some of the larger waviness peak ridges. Furthermore horizontal gouging is present on some flat regions between ridges. A huge drop in quality has occurred from previous surfaces at lower spindle speeds by Mill C.

Mill B, HT4H, Figure 40 (c). The deep vertical ridges discussed earlier are shown in greater detail here, exhibiting a very layered and rugged progression of vertical ridges with shallow ridges continually occurring and large deep ridges periodically occurring. This occurrence of periodically larger ridges suggests that waviness and drill instability is occurring despite having quite a different profile to other specimens exhibiting waviness. Where waviness most commonly appears as a round cyclic appearance, this is more of a saw tooth-like profile with quick rises and falls that are very linear. Huge amounts of chip rewelding is occurring along these larger ridges with further material rewelding occurring sporadically also. Furthermore large horizontal gouging typical of Mill B is present once more.

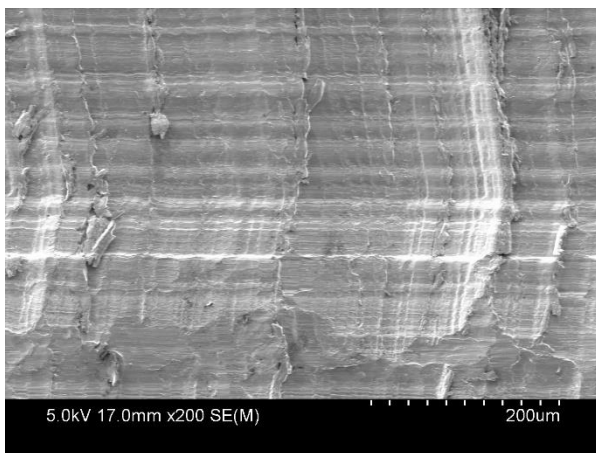
These images are shown in Figure 40 (a-c).



(a)



(b)



(c)

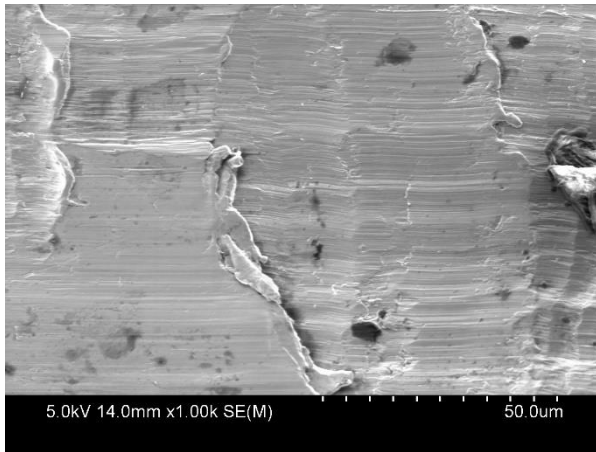
Figure 40 200x magnification SEM images of specimens laterally face milled at 35,000 RPM showing; (a) as-received CoCrMo milled with Mill B, (b) as-received CoCrMo milled with Mill C and (c) HT4H CoCrMo milled with Mill B.

Mill B, Figure 41 (a). In this SEM image a magnified look at the edge of the crater is shown, with chip rewelding occurring on this edge. Horizontal gouging is also seen with a few cavities occurring inside the crater. Some smaller ridges can be seen inside the crater with minimal rewelding occurring on these, but not to the extent in which it is occurring on the larger ridges.

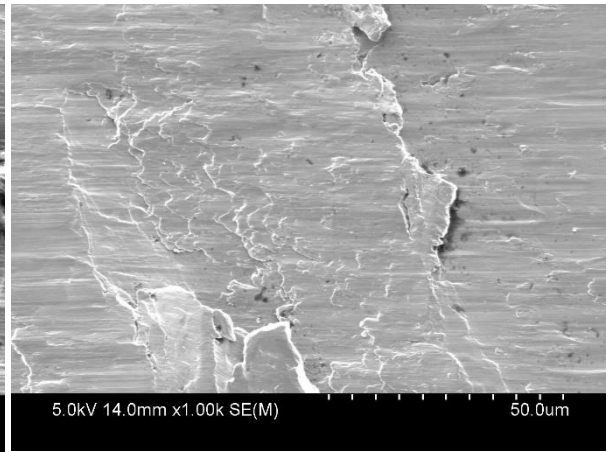
Mill C, Figure 41 (b). This SEM image shows AR CoCrMo milled with Mill C, the high amount of rewelding previously mentioned being shown in this image. Notably there is a large ridge to the right with chip rewelding occurring, and another ridge just coming into the image that is also showing large amounts of chip rewelding present. Furthermore a large amount of layered ridge-like edges through the centre are shown in an almost liquid looking phase. This appearance shows that a significantly large amount of material must have been frictionally rewelded onto this area in an almost molten state. Although some gouging, tearing and cavities occurred, it is far overshadowed by the amount of material rewelding occurring.

Mill B, HT4H, Figure 41 (c). The high magnification allows for a better look into the patterns of the vertical ridge formations. In the centre of the image, slightly to the right, there is a large deep ridge with heavy chip rewelding occurring. This ridge appears to rise up quickly then drops down in steps of shallower ridges before the formation of another large ridge is seen on the far left. This large ridge is also experiencing heavy chip rewelding occurring where the minor ridges between are not. Furthermore deep horizontal gouging can be seen running across the image horizontally indicating the ploughing mechanism was a strong factor in the obtained surface finish. Overall a very rough and rugged surface is shown here with deep ridges, craters and chip rewelding occurring, and although gouging and cavities do exist these can be thought of as secondary issues.

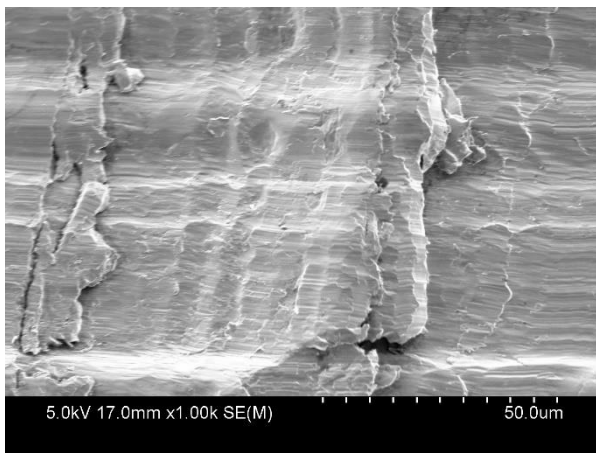
These images are shown in Figure 41 (a-c).



(a)



(b)



(c)

Figure 41 1000x magnification SEM images of specimens laterally face milled at 35,000 RPM showing; (a) as-received CoCrMo milled with Mill B, (b) as-received CoCrMo milled with Mill C and (c) HT4H CoCrMo milled with Mill B.

5.1.7. Mill A: Meisinger HM23LR. Used, Milling As-received (AR) CoCrMo.

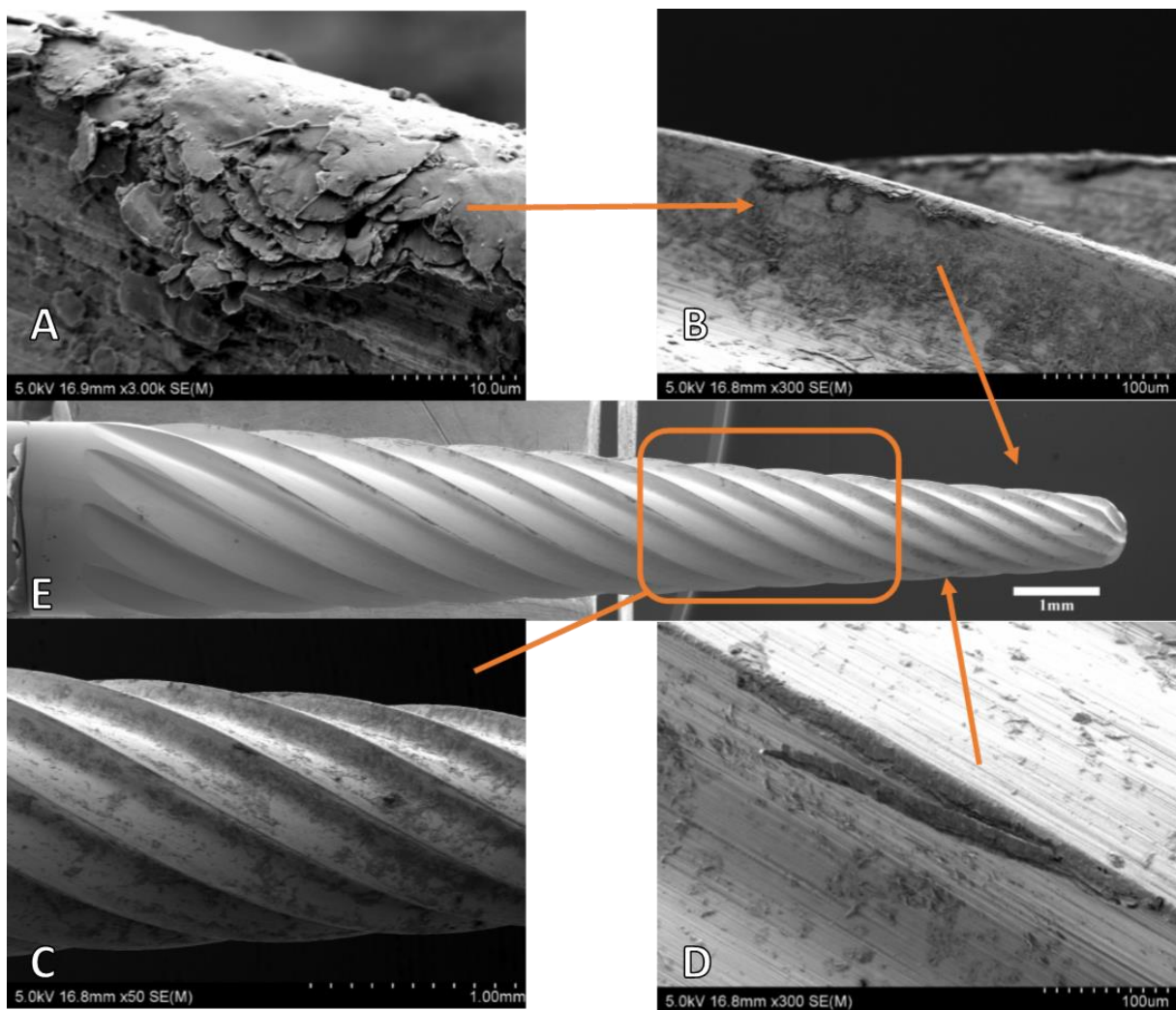


Figure 42 SEM images of Mill A: Meisinger HM23LR after milling As-received CoCrMo.

Mill A: Meisinger HM23LR, is a spiral shaped cemented tungsten carbide (WC) mill. Mill A was the only mill used in this study without chip breaker geometry. SEM images were captured of the mill after it had completed all milling passes on the AR CoCrMo specimen. Despite severe mill gyration and instability occurring during milling, the mill is relatively undamaged, though there is a severe amount of built up edge BUE and adhered material present on the mill. Unfortunately the brightness/contrast of Figure 42 (E) fails to highlight the true extent of it. Figure 42 (C) shows an enlarged view illustrating just how much material is adhered to the mill. Figures 42 (A and B), show an example of a BUE on the mill, with 3000x and 300x magnifications respectively. In Figure 42 (A), a highly layered BUE is shown indicating that it built up over a period of cycles. Figure 42 (B) shows the 300x magnification view of the

discussed BUE, however it should also be noted that the flute seen in the background of the image also contains a similar BUE along the whole visible length. The frequency of BUEs occurring in a small area indicates the severity of this phenomena. Figure 42 (D) shows a BUE on the tool edge that is half sheared off, leading to BUE induced edge fractures which exposed the cemented tungsten carbide (WC) matrix and accelerated edge wear. Minor edge wear is seen across this mill with chipped edges and BUEs occurring, however no complete failure is shown.

5.1.8. Mill B: Shofu 21N. Used, Milling As-received (AR) CoCrMo.

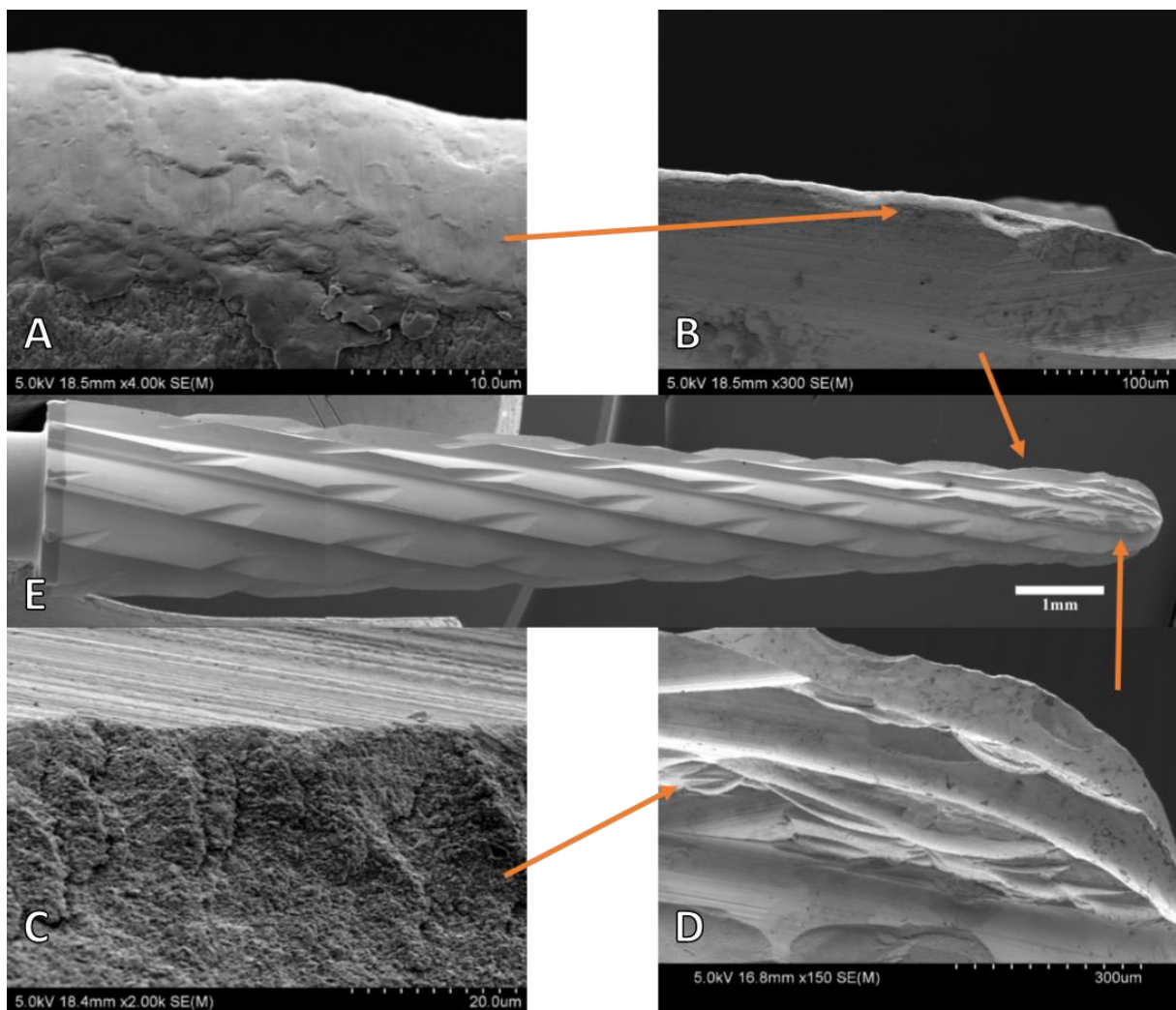


Figure 43 SEM images of Mill B: Shofu 21N after milling As-received CoCrMo.

Mill B: Shofu 21N, is a cross (large) shaped cemented tungsten carbide (WC) mill with chip breaker geometry. SEM images have been captured after the mill was used to mill AR CoCrMo. Mill B suffered significantly higher amounts of damage than Mill A, with huge amounts of edge chipping occurring. Figure 43 (C) shows a 2000x magnification of the exposed tungsten carbide matrix while Figure 43 (D) shows a 150x magnification of this same area. The 150x magnification in Figure 43 (D) clearly shows the heavily chipped flutes. The nature of these fractures suggests brittle failure. Figure 43 (A) shows 4000x magnification of a BUE on Mill C. The appearance of the BUE is smoother and less layered than in Mill A, with an almost molten look to it, potentially suggesting significantly higher frictional heats were experienced although the cutting forces for Mill B were significantly less than Mill A. Figure 43 (B) shows a 300x magnification of the area in which the BUE in Figure 43 (A) occurred, to the right and left

of the aforementioned BUE, a chipped tool edge is seen. This suggests that a lot of the edge chipping that occurred could be due to BUE induced fracturing. Despite the severe edge chipping, the mill has less debris and adhered chips than shown on Mill A. Finally, it is noted that the majority of damage occurred in the tip of the mill. The first 1.5 to 2 mm of the mill sustained most of the damage while there was a depth of cut of 3mm.

5.1.9. Mill B: Shofu 21N. Used, Milling Annealed (HT4H) CoCrMo.

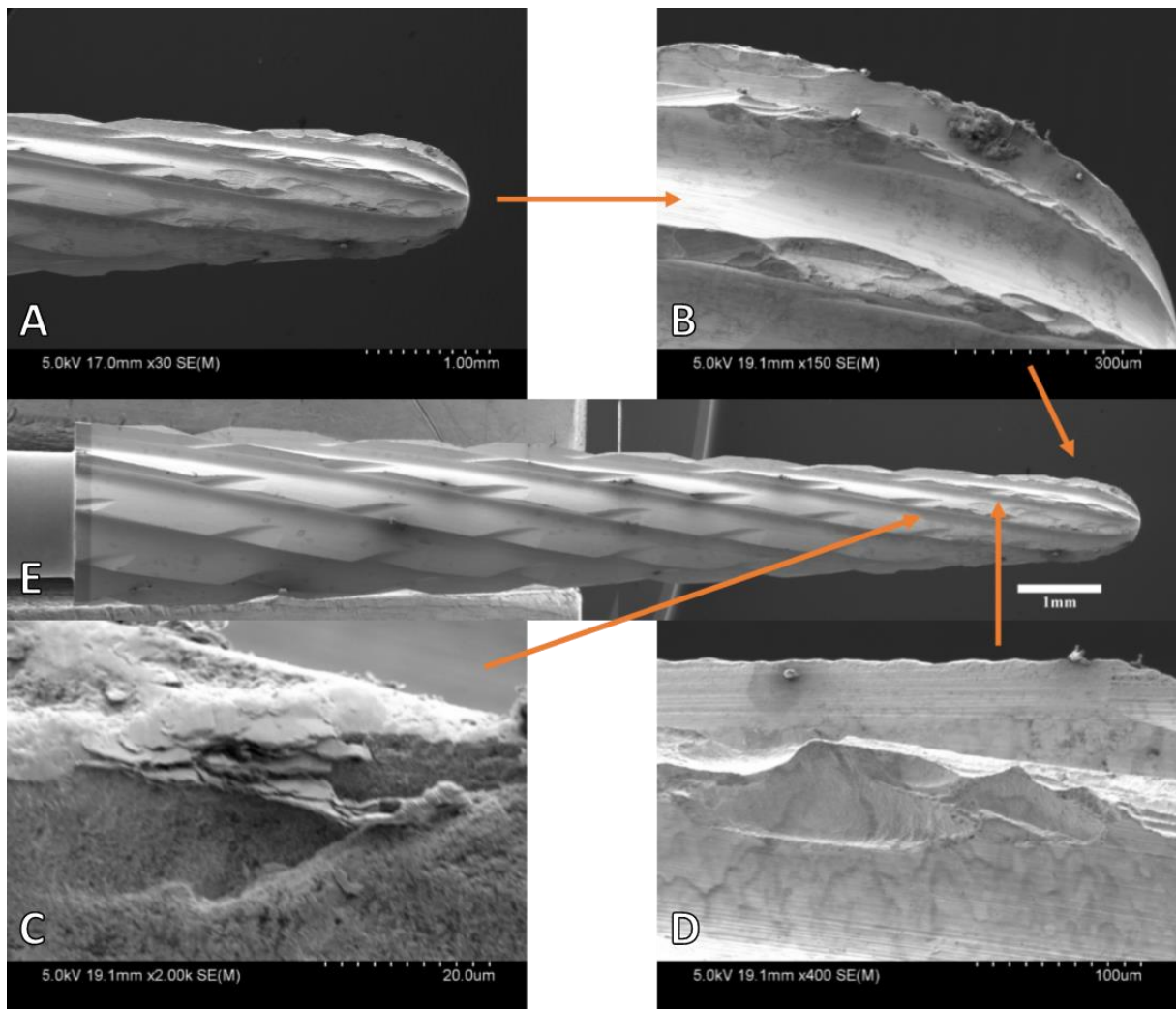


Figure 44 SEM images of Mill B: Shofu 21N after milling HT4H CoCrMo.

Mill B, HT4H, Shofu 21N. Shofu 21N mills were used to mill both AR CoCrMo, and HT4H CoCrMo in this study and in this section SEM images of the mill used to mill HT4H CoCrMo for all speeds is shown. Figure 44 makes it blatantly apparent that Mill B suffered significantly more tool wear while milling HT4H CoCrMo than it did milling AR CoCrMo. This increased tool wear occurred despite HT4H CoCrMo exhibiting a lower hardness value than AR CoCrMo. In Figure 44 (A), the tip of the used mill can be seen showing the extensive flute wear that occurred. It can be seen that similarly to Mill B used to mill AR CoCrMo, the majority of this tool wear occurs in the first 2mm of the mill, where the cutting depth was 3mm. It is unknown why this occurs, though one possibility is the thinner diameter of the mill towards the tip could be leading to an increase in tool vibration near the tip of the mill. Figure 44 (B) shows a magnified look at the tip wear, the presence of oil stains on the surface of the mill indicating

that high frictional temperatures were reached during milling. Entangled chips are shown on the flute edges in this image as well. As with the mill used to mill AR CoCrMo, the chipped edges exhibit a rather clean fracture appearance, suggesting brittle failure was occurring. Figure 44 (C) shows a BUE formed on the tool cutting edge with edge chipping occurring on the same edge just below the BUE. This further reinforces the idea that BUE induced edge fractures are a leading cause of edge chipping. In Figure 44 (D) a better look at the flute damage is shown, the way the material has fractured off the tip of the tool edge and down the face of the flute is highly suggestive that BUE induced edge fracturing has occurred. Overall the mill is relatively chip and debris free with little adhered material visible, as was seen with the AR CoCrMo Mill B. The major detriment is the heavily chipped tool edges and flutes and in this case the damage to the mill is considered catastrophic.

5.1.10. Mill C: Meisinger HM23GX. Used, Milling As-received (AR) CoCrMo.

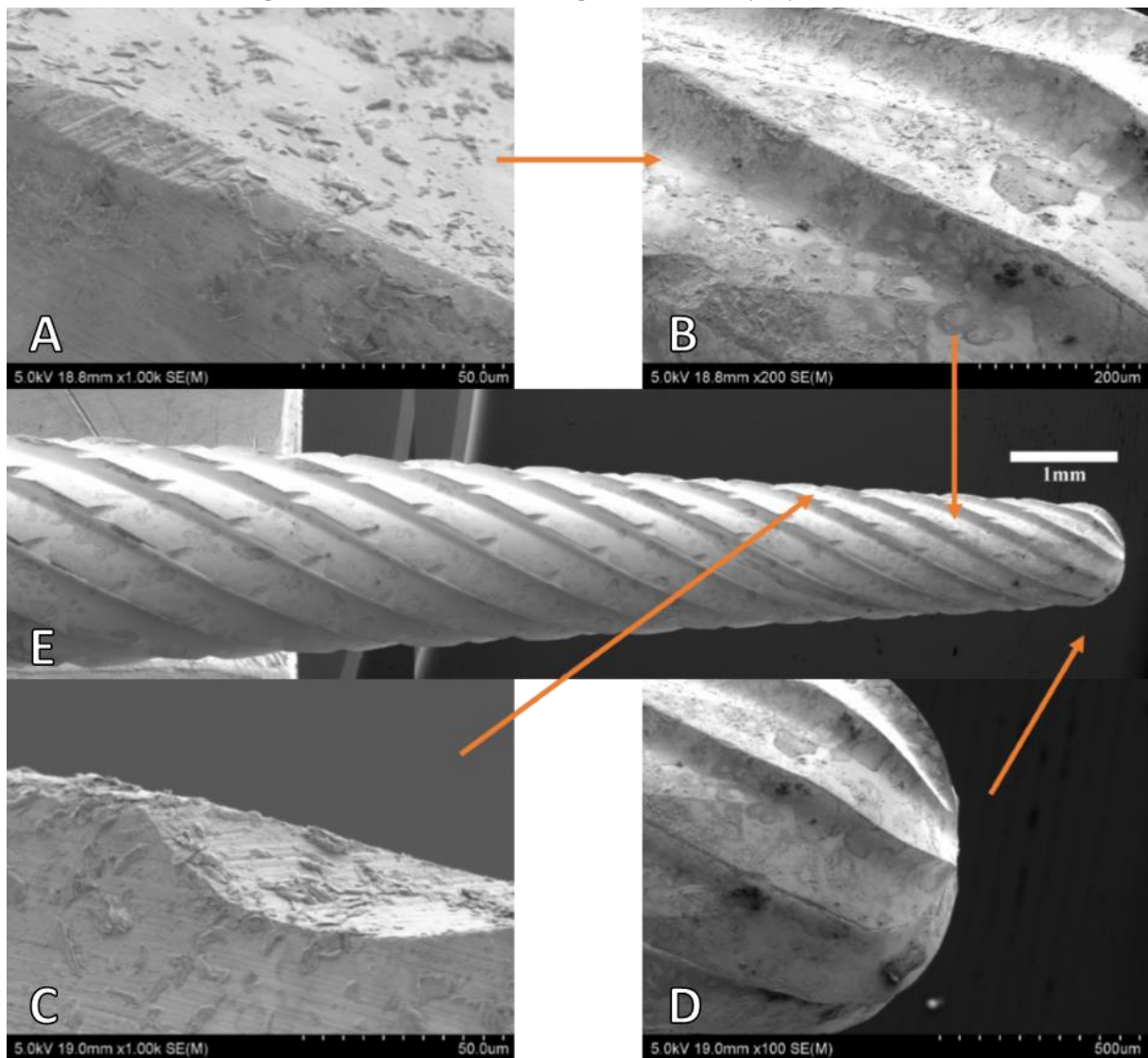


Figure 45 SEM images of Mill C: Meisinger HM23GX after milling As-received CoCrMo.

Mill C: Meisinger HM23GX, is a cross (small) shaped cemented tungsten carbide (WC) mill that was used to mill AR CoCrMo at all speeds. SEM images of the mill are shown in Figure 45. First impressions are that the mill's surface is littered with adhered chips, entangled chips and oil staining and this is seen in all images. However, despite the amount of adhered material the mill is shown to be in reasonable condition, certainly better than the condition of both Mill Bs though there are large amounts of BUE formations and some edge wear has occurred. Figures 45 (A and B) both show cutting edges with chip breakers visible. A moderate amount of BUE is shown on the tool edges in these images forming a smoothed round edge. Huge amounts of adhered chips all over the mill body can be seen in these magnified views of Figures 45 (A and B). Figure 44 (B) shows a view that suitably illustrates the extent of the

adhered chips, oil stains, BUE and edge wear occurring on Mill C. BUE induced edge fractures are strongly believed to have occurred. Figure 45 (D) shows the tool tip with moderate edge wear, BUE and debris, seemingly to no more extent than the rest of the mill. In Figure 45 (E), oil burn marks are shown covering the entire mill shaft, while only the lower area of the mill would have come in contact with the milled surface. This suggests that very high milling temperatures occurred.

5.1.10.1. Mill C: Meisinger HM23GX BUE Verification

In order to verify the BUE on Mill C consisted of the milled CoCrMo material, an EDS scan was undertaken on the tool edge. The scan consisted of a simple single point, standard less test with the point centred on what is believed to be a BUE formation as shown in Figure 46.

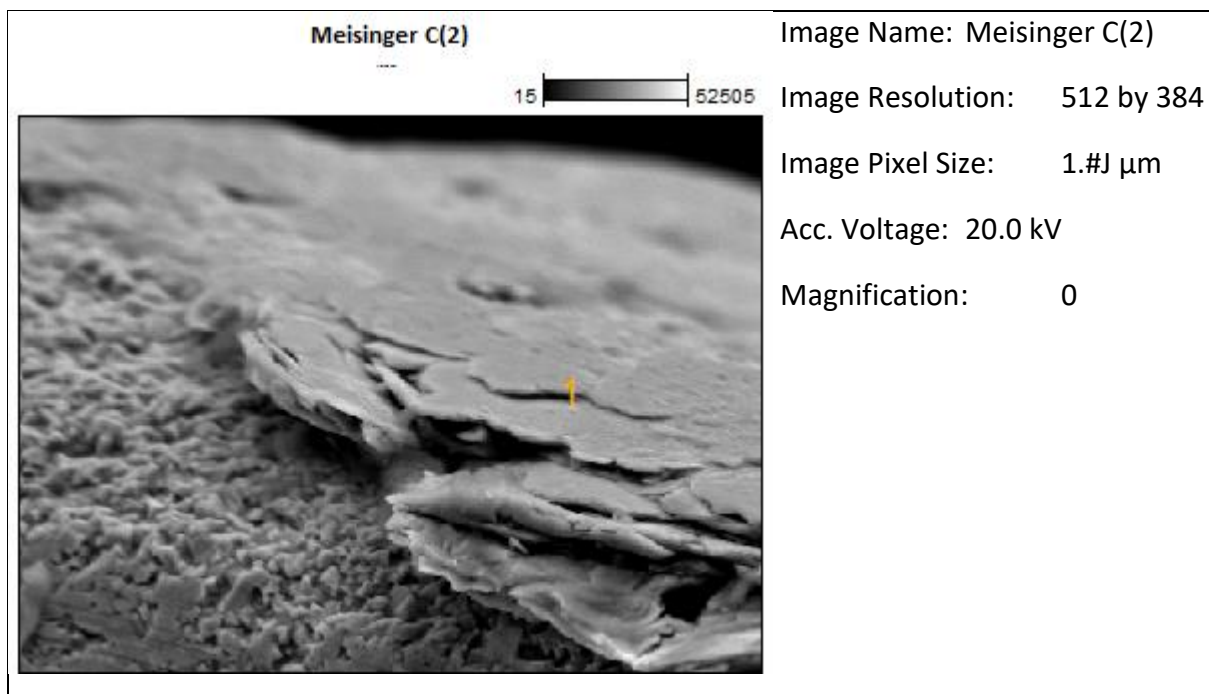


Figure 46 Mill C BUE verification using EDS scanning.

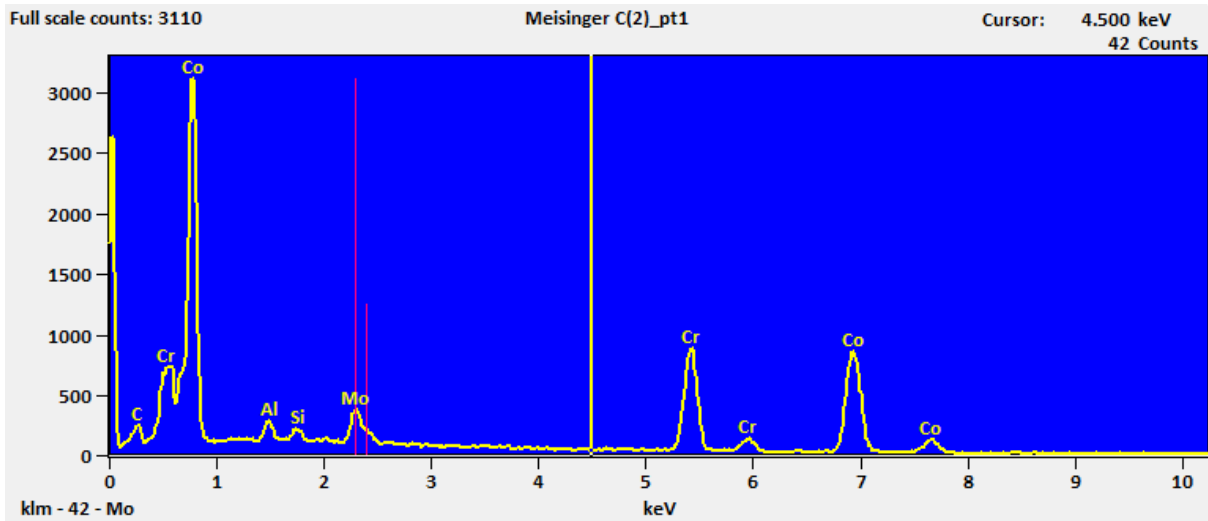


Figure 47 Mill C BUE EDS scan.

Table 11 Mill C BUE EDS results showing weight percentage.

	C-K	Al-K	Si-K	Cr-K	Co-K	Mo-L
Meisinger C(2)_pt1	3.53	1.40	0.79	30.46	55.68	8.14

The EDS results for the single point standard less test are shown in Table 11 and Figure 47. The composition consists mostly of Co, Cr, and Mo with low concentrations of C and Al and minor traces of Si. The amount of Co, Cr, and Mo present in the BUE strongly reflects the composition of the base material that was milled (55.68%, 30.46%, 8.14% and 63.98%, 28.9%, 5.91% respectively). The results obtained from the EDS scan show the BUE material on Mill C is strongly consistent with the specifications of the AR CoCrMo material that was milled by Mill C. This is conclusive enough to state that the formation believed to be a BUE of the material being milled is confirmed to be a BUE of the milled CoCrMo material.

5.1.11. Mill D: Meisinger HMB23G. Used, Milling As-received (AR) CoCrMo.

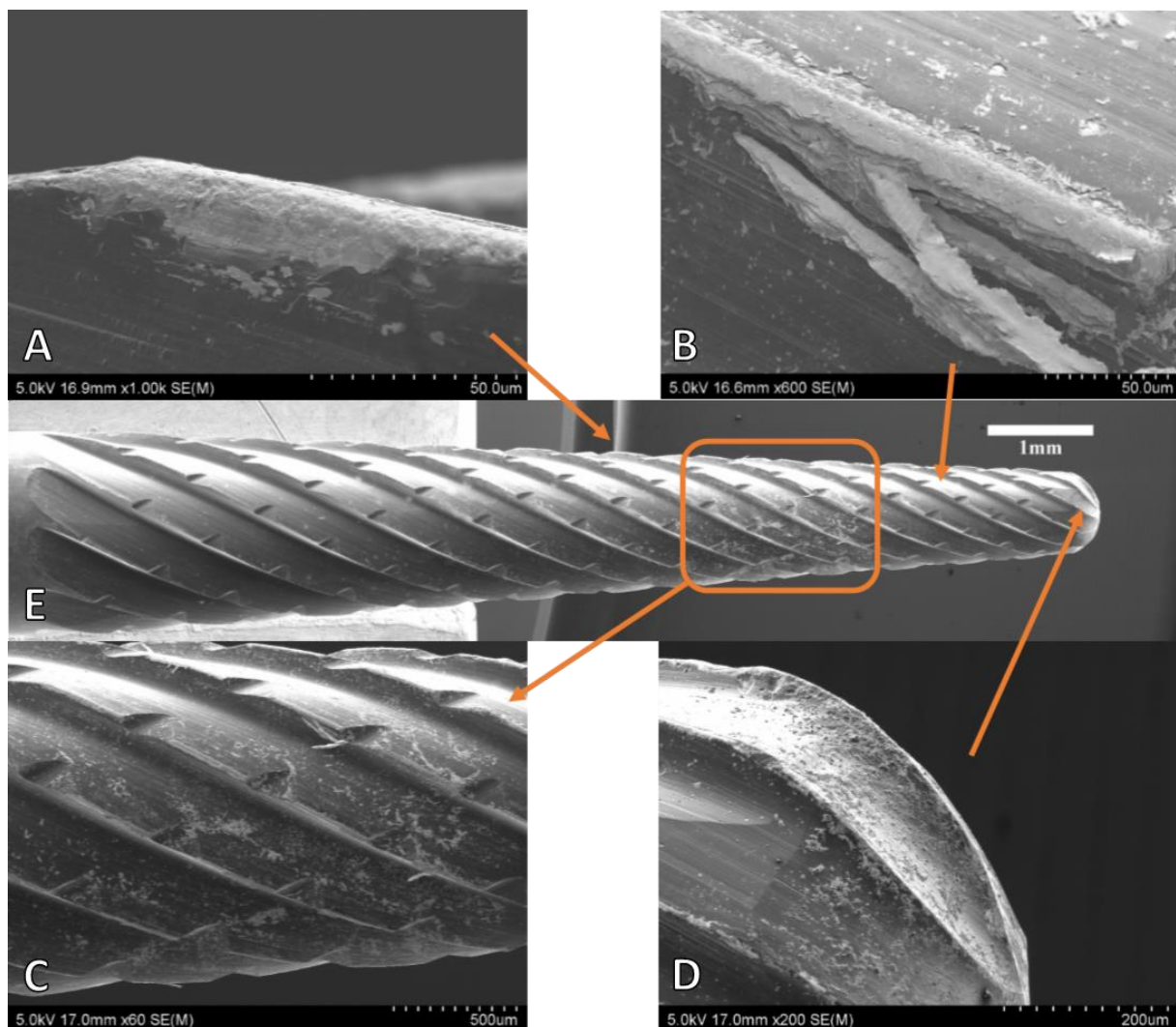


Figure 48 SEM images of Mill D: Meisinger HMB23G after milling As-received CoCrMo.

Mill D: Meisinger HMB23G, is a spiral shaped cemented tungsten carbide (WC) mill with chip breaker geometry and a diamond-like carbon coating (DLC). This was the only mill tested in this study that was coated. Owing to the DLC coating, lower cutting forces and higher quality surface finishes were expected to be found, however this was not seen when the relative data were examined. Looking at Figures 48 (A, B and E) makes it quickly apparent why higher performance was not obtained from the DLC coating, the DLC coating being seen to have completely worn off exposing a plain tungsten carbide (WC) mill. Figure 48 (A) shows the tool cutting edge where it shows that the DLC layer (dark grey) has been worn away to expose the cemented tungsten carbide (WC) (light grey). A moderate amount of BUEs are also shown. These BUEs may have led to the removal of the DLC layer by means of BUE induced edge

fractures and high abrasive wear. Figure 48 (B) shows another view of the tool edge, this time a larger partially severed BUE can be seen with chip retention also occurring. This BUE induced edge fracturing is believed to have led to rapid delamination of the DLC coating as well as edge chipping. Various loose chips are also shown adhered to the flute edges in Figure 48 (B). In Figure 48 (C) an enlarged section from Figure 48 (E) is shown. In this enlarged view the scale in which chips have adhered to the flute bodies is apparent. Furthermore, entangled chips can be seen hanging from the tool edge likely connected by the BUE. Figure 48 (D) shows a magnified image of the mill tip. A large amount of adhered chips, BUEs, edge chipping and general tool wear is visible. All edges of the tool show the DLC coating completely delaminated at this point and it can be stated that tool wear is higher at the tip of the mill than on the mill body.

5.1.11.1. Mill D: Meisinger HMB23G EDS

In order to verify the DLC coating had been worn on the tool edges, and that the eroded edges were what was believed to be shown in the previous images, an energy-dispersive X-ray spectroscopy (EDS) investigation was undertaken on the used mill. Two tests were undertaken with the used mill in this investigation. First, a two point, standard less, analysis scan was taken with one point on the exposed tungsten carbide (WC) surface, the other on the DLC layer. Secondly, a window scan was taken over an area showing the eroded tool edge and flute body where the DLC layer had not been delaminated. This scan was then mapped into the five key elements to show where the counts were found. Shown first is the two point test in Figures 49 and 50 and Table 12.

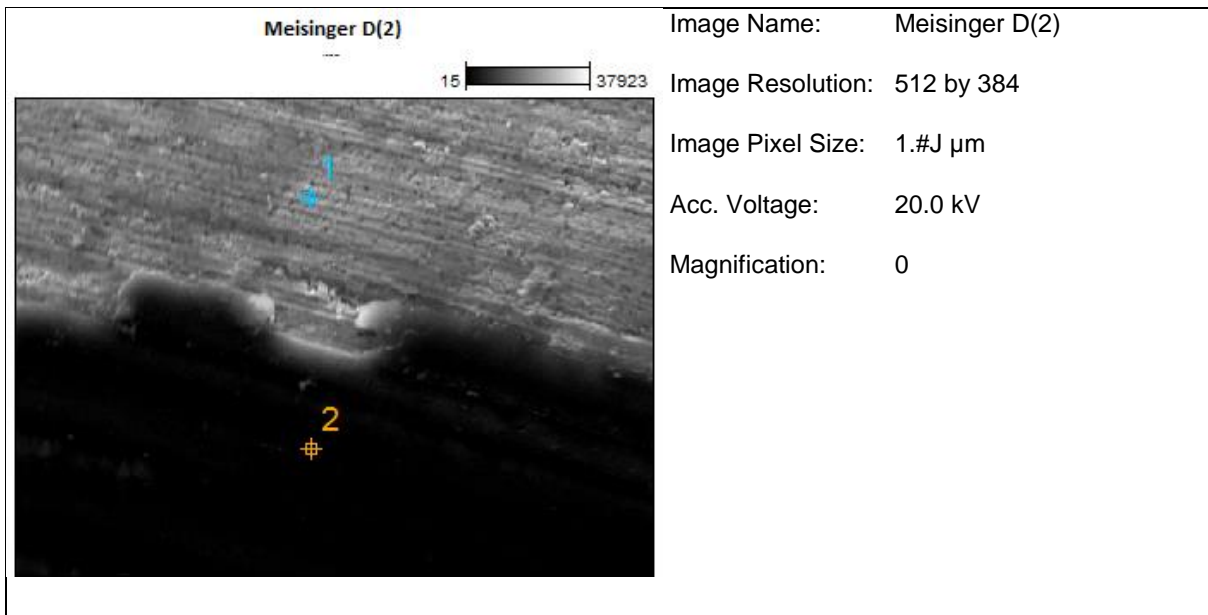


Figure 49 Mill D, DLC layer two point EDS test.

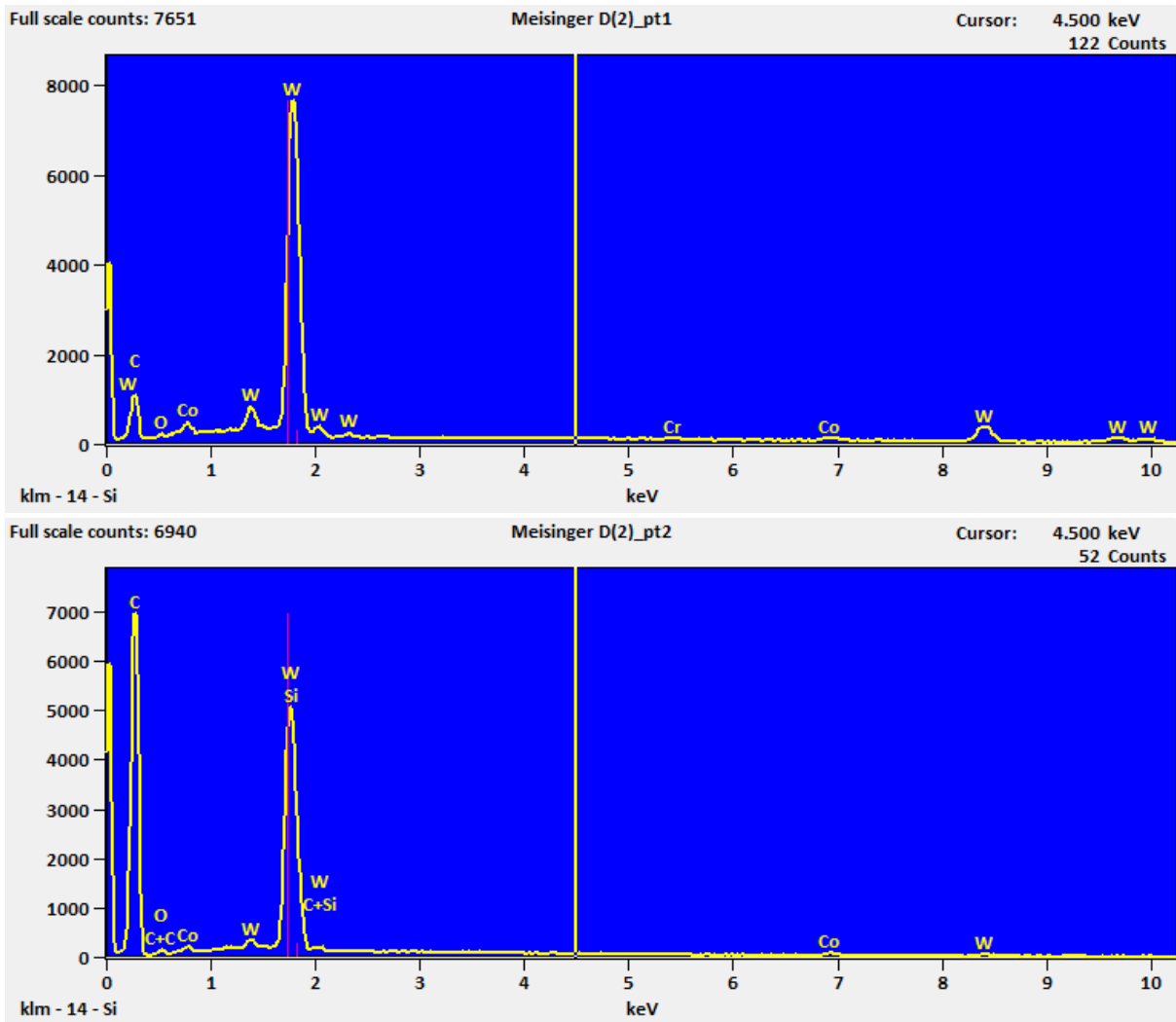


Figure 50 Mill D, DLC layer two point EDS test counts.

Table 12 Mill D, DLC layer two point EDS weight percentage.

	C-K	O-K	Si-K	Cr-K	Co-K	W-L
Meisinger D(2)_pt1	19.82	1.18		1.36	4.09	73.55
Meisinger D(2)_pt2	74.72	1.13	15.79		1.66	6.69

Figure 50 displays the EDS test counts for the two point test, while Table 12 lists the weight % values obtained from the converted count data. From the data listed in Table 12 it can be seen that point 1 consists of a high tungsten content, with moderate carbon content and low oxygen, chromium and cobalt contents. This aligns with the tungsten carbide mill composition, with trace elements of Co, and Cr most likely due to the contact with CoCrMo while milling the specimens. Point 2 exhibits a high carbon and moderate silicon composition with traces of cobalt, oxygen and tungsten content. This is thought to be the DLC layer, trace elements found in the scan can be explained by a combination of contact with the CoCrMo surface while milling and the fact that these tests are standard less which can offer some variation. The results obtained were confirmed by the SEM technician to be consistent enough to confirm the conclusions drawn relating to the DLC layer. In order to leave no doubt about the wearing of the DLC layer on the cutting edge a window scan was undertaken and the results were mapped to show the various element counts and their locations. This test is shown in Figures 51 and 52.

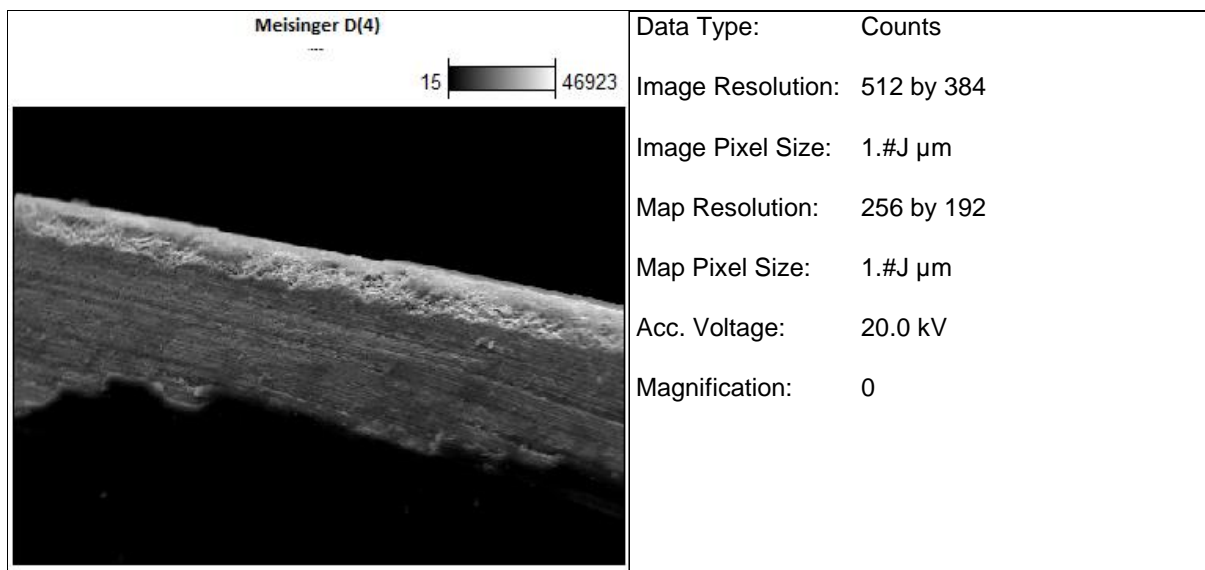


Figure 51 Mill D, DLC layer EDS window scan properties.

Figure 52 displays the mapped images of the data obtained from the EDS window scan shown in Figure 51. The four elements plotted were Tungsten (W), Cobalt (Co), Chromium (Cr), and Carbon (C). The light grey area in Figure 51 is believed to be the exposed cemented tungsten carbide (WC), with the dark black area below this being the DLC layer. The W and Co maps show the majority of these element counts occurring in the light grey area of the mill, with the Cr map showing this to a less defined extent. Co and Cr elements present on the mill would be due to the contact between the workpiece and tool during milling, therefore it is logical that the eroded area would show higher concentrations of these elements. Furthermore, since the majority of W in Table 12 was found in the mill composition, it is expected these element counts would appear on the light grey area (mill body). Most convincing is the map of C, showing the counts of C in a highly defined shape mimicking the dark area from Figure 51. Since DLC consists mainly of carbon, this leads to the conclusion that by using EDS analysis it can be definitively shown that the light grey area seen on the tool flutes is the tungsten carbide material of the mill where the DLC layer has been delaminated.

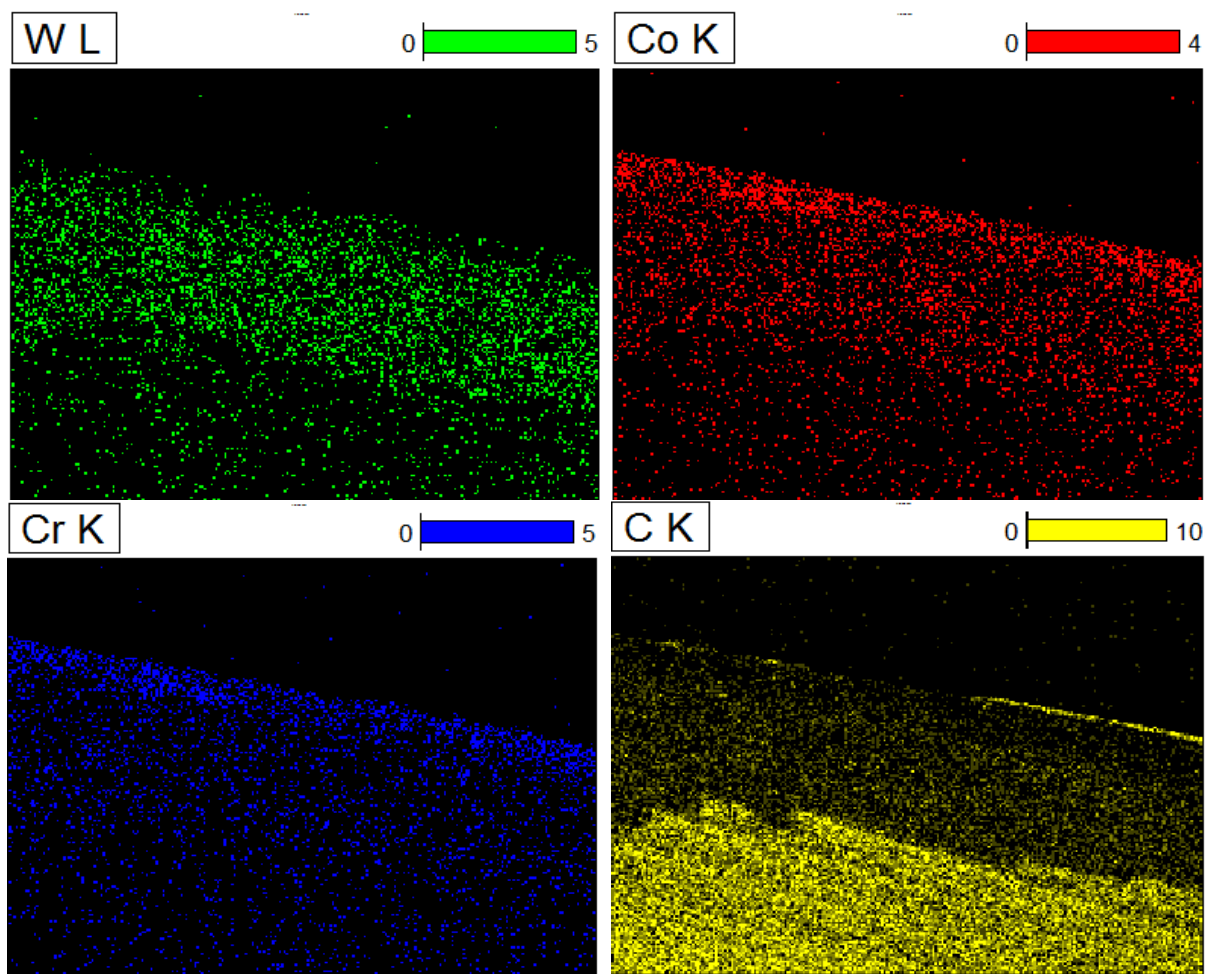


Figure 52 Mill D, DLC layer EDS window scan maps.

5.1.12. Chip Analysis

Samples of the machined chips were collected after milling to be viewed and analysed. These chips were mounted on carbon paper and viewed using SEM to see if there were any noticeable differences between chips from differing mills and/or spindle speeds. The author was unable to see any definitive differences between chips obtained from differing conditions (further analysis is recommended to be carried out). In order to illustrate this, five sets of chips from a spindle speed of 25,000 RPM are displayed, including chips collected from AR CoCrMo milled with Mill A, Figure 53 (a, b); Mill B, Figure 53 (c, d); Mill C Figure 54 (a, b); Mill D, Figure 54 (c, d) and HT4H CoCrMo milled with Mill B, Figure 54 (e, f). Images displaying the chips from AR CoCrMo milled with Mills A and B are shown with 300x and 100x magnifications, while the rest of the images are displayed with 100x and 30x magnifications. These images are shown in Figures 53 and 54.

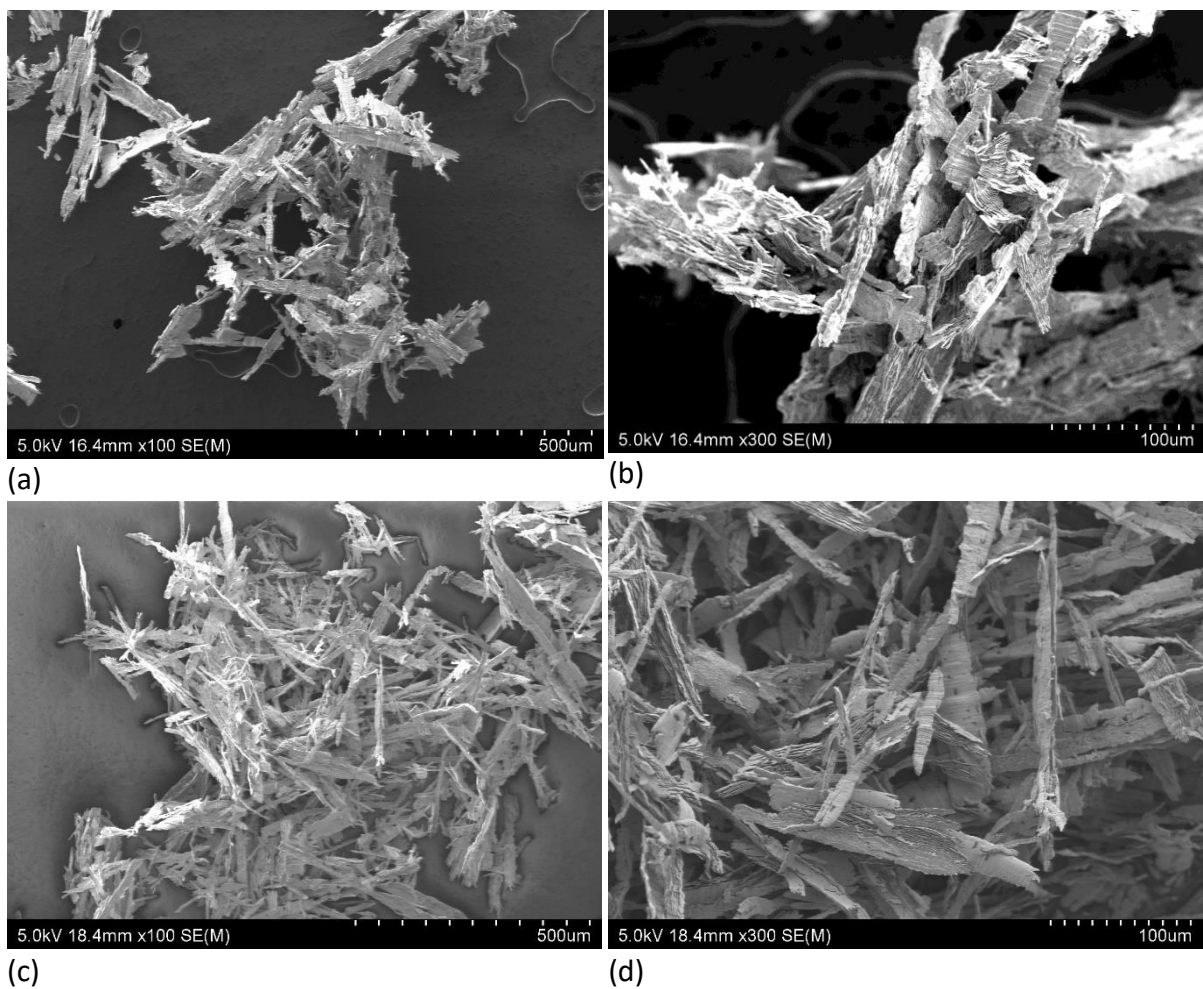


Figure 53 SEM images of chips obtained from AR CoCrMo milled at 25,000 RPM. (a, and b) chips from Mill A, (c, and d) chips from Mill B.

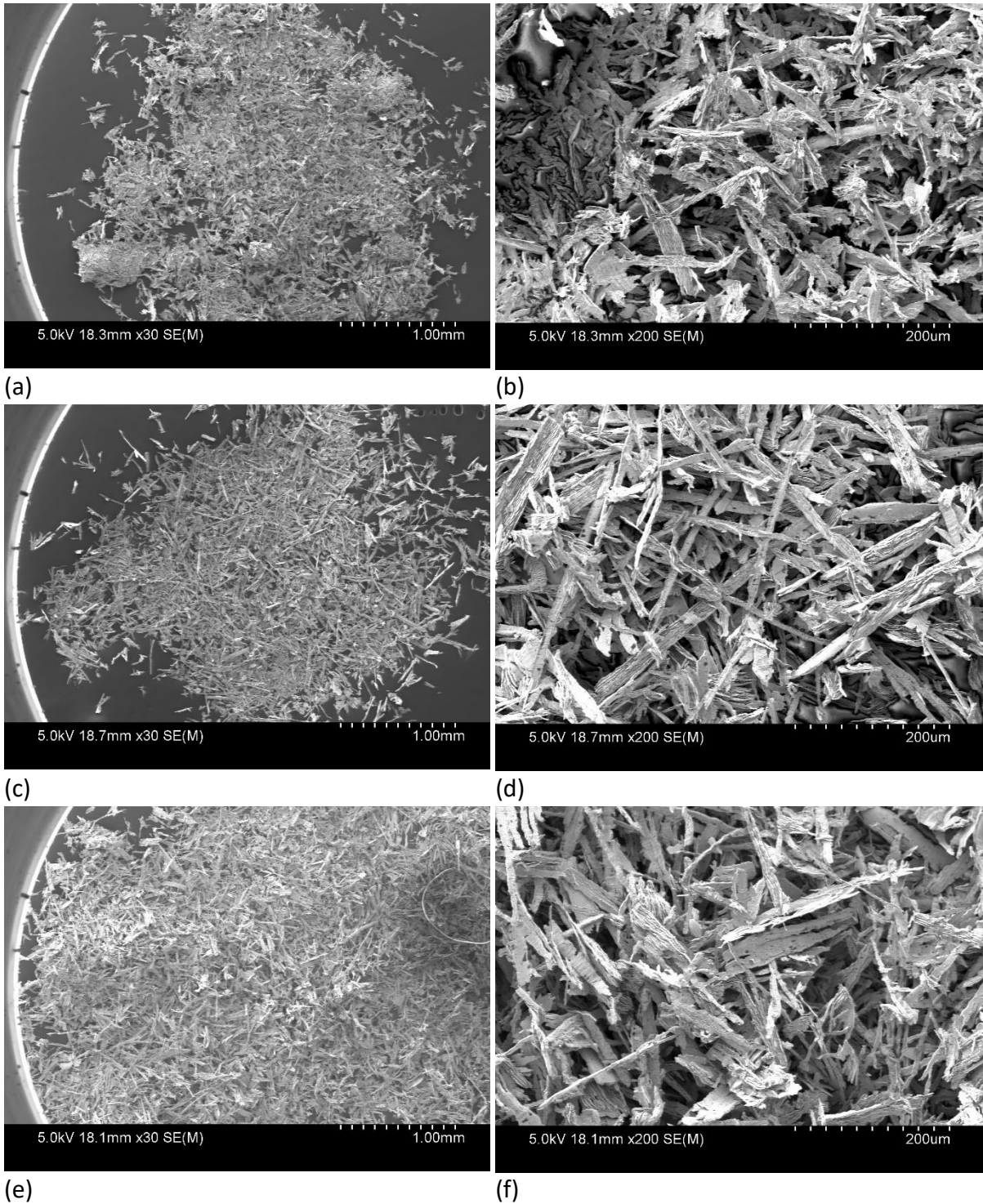


Figure 54 SEM images of chips obtained from milling; AR CoCrMo milled with Mill C (a, b), AR CoCrMo milled with Mill D (c, d) and HT4H CoCrMo milled with Mill B (e, f). All milling was undertaken at a spindle speed of 25,000 RPM.

As shown in Figures 53 and 54, there is little apparent difference to be seen from the chips collected. Four different mills were used, with two different material heat treatments, however no differences significant enough to draw conclusions from are shown. Thin needle-like chips are shown in all cases with slight variances in width and length occurring, however no major differences in geometry are noted. These chips were collected from milling passes

undertaken at 25,000 RPM. At this spindle speed major variances in surface finish were shown, with Mill C producing a relatively good surface finish, and Mill D producing a poor surface finish exhibiting high amounts of waviness and rewelded material. However, looking at Figure 54 (c, d) and (e, f) very little difference can be seen between chips obtained from these passes. This further backs up one of the underlying theories of this study that states mill vibrations, BUEs, and ploughing (related to the minimum chip thickness theory), are the main detriments to surface finish, rather than the tool geometry and related chip forming mechanism. To further illustrate this point, Figure 55 shows the surface finish and chips obtained from each test for Mill C, and Mill D milling AR CoCrMo at 25,000 RPM. It is apparent that Figure 55 (a) does appear to show slightly thicker and shorter chips than Figure 55 (c). However, this is only a small sample of the chips collected and despite these differences the author sees very little possibility that such minor differences in chip geometry could lead to such differing surfaces as shown in Figure 55 (b, and d).

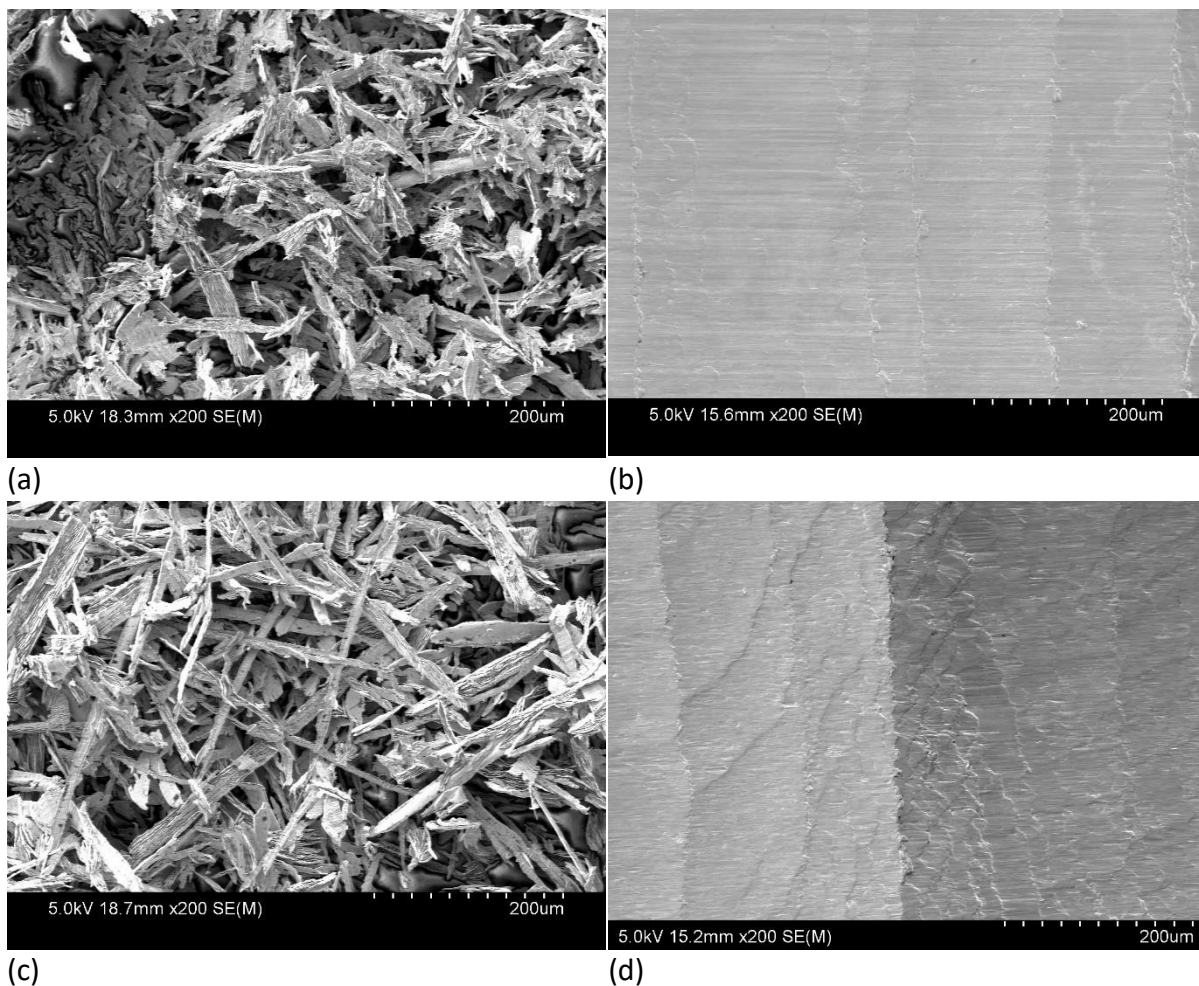


Figure 55 Chips vs corresponding surface finish for AR CoCrMo milled with Mills C, and D at 25,000 RPM.

5.2. Micro Hardness

Three indentations were made for each specimen while taking care to test uniformly for all specimens to allow a more reliable comparability. The complete data are shown in Table 13 showing the three readings as well as the average hardness for each specimen, HV300/10 was used as the testing standard.

Table 13 Micro hardness results.

Micro Hardness Tests			
Specimen	Measurement	Hardness (HV300/10)	Average Hardness (HV300/10)
CoCrMo As Received (AR)	1	403	402
	2	402	
	3	400	
CoCrMo 1200°C / 2H / Water Quench (HT2H)	1	373	368
	2	373	
	3	357	
CoCrMo 1200°C / 4H / Water Quench (HT4H)	1	366	356
	2	347	
	3	354	

The results shown in Table 13 show that CoCrMo has shown a reaction to the heat treatment. Heating to 1200°C for a sustained period of time followed by water quenching has affected the specimen's hardness by softening the material. The difference in hardness values between specimens annealed for 2 hours and specimens annealed for 4 hours is minimal, while the difference between the as-received specimen and the specimen annealed for 2 hours is quite significant. The spread of values also increases as the annealing time increases: the AR CoCrMo specimen has a spread of 3.1 HV300/10, the HT2H specimen has a spread of 15.9 HV300/10 and the HT4H specimen has a spread of 19.7 HV300/10. The hardness values are in line with what was expected with similar values to results found by A. Biomechaniki (23) for AR CoCrMo (402 HV300/10 vs 396 +/- 10HV respectively).

5.3. Metallography and Microstructure

Due to issues arising from the etching process there are no microstructure results to show. Aside from the milled specimens there were six other specimens prepared in total for this study. Two of each of the following heat treatments were prepared: as received CoCrMo (AR CoCrMo), CoCrMo annealed at 1200°C for 2 hours then water quenched (HT2H CoCrMo), and CoCrMo annealed at 1200°C for 4 hours then water quenched (HT4H CoCrMo). Two small samples of each material were cut from the larger specimens and mounted in polyfast resin. After this they were then ground and polished. This is further explained in previous methodology sections. Three of these specimens, one from each heat treatment, were successfully used for micro hardness testing, while the other three were designated for etching. However, as the etching process failed, these samples remain unused. These samples will remain available in the hope that whoever wishes to further this research is able to successfully etch them.

The results section contains discussions of the expected microstructures relating to the literature review content and linking in with the hardness testing data in an attempt to try predict the processes occurring during annealing. This is not an ideal outcome, but as the primary research focus is related to surface finish and tool wear, the microstructure can be considered of less importance. Further research into the etching of CoCrMo is recommended.

5.3.1 EDS Analysis of CoCrMo Specimen

A successful component of the metallography study was the EDS analysis of the chemical composition of an AR CoCrMo specimen. This was undertaken to confirm the composition of the specimen and compare the obtained results with the manufacturer's specifications. The analysis undertaken was a standard less window scan, on a freshly cut face of a CoCrMo ingot. The net count results, weight %, and atomic % are shown in Figure 56 and Table 14. The manufacturer's specifications are shown in Table 15 for comparison. The analysis shown in Figure 56 shows results which appear appropriate, aside from a mystery count peak at approx. 1.75Kev. At first it appeared to be tungsten (W), but since there are no W peaks at higher KeVs the software rejected it as a possibility. It is possible the peak could be an artefact of the counting process, or looking at the manufacturers spec it could potentially be a misread Si peak. Either way, the EDS analysis was done quickly without a reference standard so small variations from the manufacturers' specifications are reasonable. Comparing Table 14 and Table 15 shows the differences in recorded values and manufacturers specifications,

respectively. Aside from the mystery peak, the EDS showed a slightly higher Cr reading, and a slightly lower Mo reading, while the Co reading was fairly identical to the manufacturer's specifications. Furthermore, small trace elements like Ni, Fe, C, N, and Mn were not found in the obtained data, however due to the relative quickness of the test and it being standard less, the SEM technician recommended it was reasonable to conclude that the composition of the specimen is in line with the manufacturer's specifications and it can be confirmed to be CoCrMo.

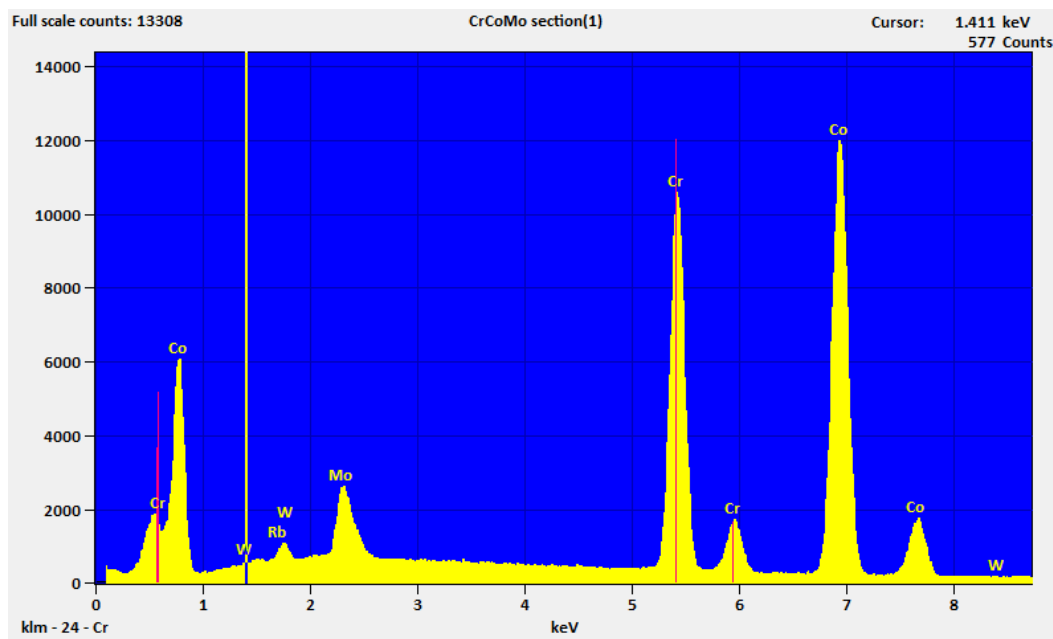


Figure 56 EDS composition scan of AR CoCrMo specimen.

Table 14 EDS composition of AR CoCrMo specimen.

Element Line	Net Counts	Weight %	Atom %
Cr K	178467	30.36	33.69
Cr L	24020	---	---
Co K	225156	64.53	63.20
Co L	73811	---	---
Rb K	231	---	---
Rb L	3396	0.47	0.32
Mo K	0	---	---
Mo L	38345	4.64	2.79
Mo M	3552	---	---
W L	0	0.00	0.00
W M	4675	---	---
Total		100.00	100.00

Table 15 Manufacturers composition specifications of AR CoCrMo.

Co	Cr	Mo	Ni	Fe	C	N	Mn	Si
Bal.	28.9	5.91	0.01	0.04	0.18	0.23	0.26	0.49

5.4. Roughness Testing

This section details and lists all the recorded roughness data in this study, the results being obtained from a Taylor Hobson Formtalysurf 5.0 roughness tester. In order for reliable and significant data to be collected, the machine needed approximately 6mm of milled surface to test. Due to the relatively short length of these experimental milling passes, 6mm of milled surface was only found on specimens with a completed milling pass. Because of mill instability, excessive forces and mill drop off, often the milling passes were not completed. Since only completed milling passes could be reliably tested the data sets acquired are often incomplete and offer readings for only some of the tested spindle speeds.

Tables for each specimen are displayed below, listing all measurable spindle speeds and the data acquired from these milled surfaces. The outputted data includes the arithmetic roughness average (Ra), the root mean squared roughness (Rq), and the maximum height of the profile (Rt). Ra is the most commonly used, and oldest, surface roughness measurement. Rq is also commonly used and therefore Ra and Rq are plotted for each specimen, with both Ra and Rq, (μm) vs spindle speed (RPM). These graphs allow for a graphical representation as to how the roughness values change as spindle speed progresses. In instances where a specimen has a single set of measurements from one spindle speed the graphs allow for little comparison; however all graphs use the same scales which allows for comparisons between specimens. Although Rt is not plotted, it does offer some insight into the extent of the peaks and valleys present in the surface profile and how they react as spindle speed increases. Rt should not be confused with waviness however, which is the source of the larger cyclic peaks and valleys seen in the previous SEM images section.

5.4.1. Annealed (HT4H) CoCrMo, Mill B: Shofu 21N

HT4H CoCrMo milled with Mill B: Shofu 21N was tested with the roughness tester, though milling at 10,000 RPM was the only pass completed to such an extent as to allow sufficient area for measurement. Interestingly, all spindle speeds were tested on this specimen from 10,000 to 35,000 RPM while milling. However after 10,000 RPM all the milling passes were stopped halfway and it is unknown if this was purposely done or due to machining difficulties. These shortened milling passes allowed enough milled surface for SEM analysis, however owing to the roughness testers need for 6mm of surface, only the 10,000 RPM pass could be analysed. Shown below in Table 16 is the data obtained for HT4H CoCrMo milled with Mill B listing Ra, Rq, and Rt (μm) in the columns, with spindle speed (RPM) listed in rows. Below this is Figure 57, displaying the Ra and Rq values (μm) vs spindle speed (RPM). As mentioned previously, with data obtained from only one spindle speed the graph does not offer much comparability on its own, however with identical scales for all measurements it is possible to gain some understanding of how this specimen compares to others.

Table 16 Roughness testing values for HT4H CoCrMo laterally milled with Mill B: Shofu 21N.

Roughness Test: HT4H CoCrMo, Mill B, Shofu 21N			
Spindle Speed (RPM)	Ra (μm)	Rq (μm)	Rt (μm)
10,000	3.5477	4.6222	25.7413

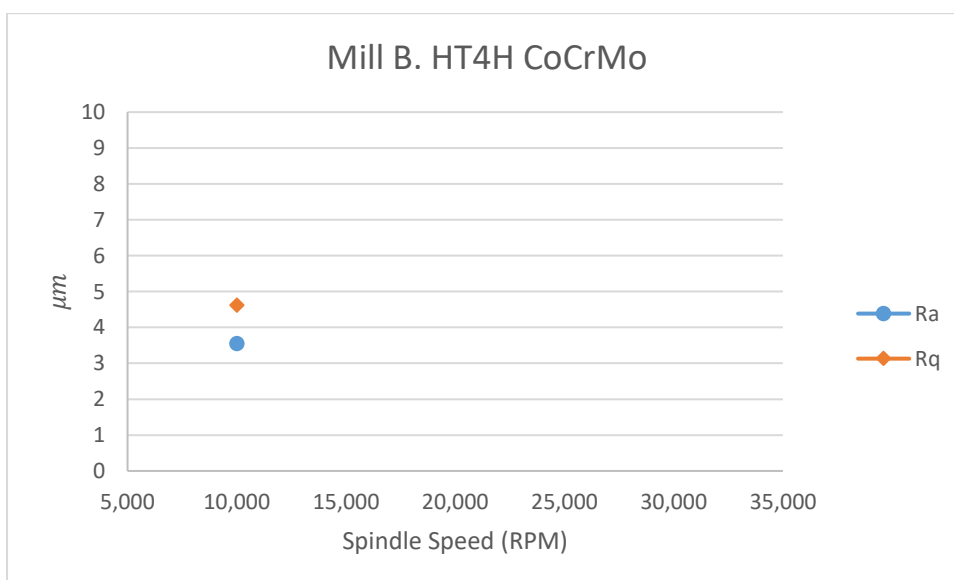


Figure 57 Ra and Rq roughness values for HT4H CoCrMo laterally milled with Mill B: Shofu 21N.

5.4.2. As-received (AR) CoCrMo, Mill A: Meisinger HM23LR

As-received CoCrMo milled with Mill A: Meisinger HM21LR, had three milling passes completed before drill instability shortened the achievable milling length. This resulted in 25,000 RPM to 35,000 RPM not being tested. Data acquired from surfaces milled with spindle speeds of 10,000 RPM to 20,000 RPM are listed in Table 17. Figure 58 displays Ra and Rq (μm) vs spindle speed (RPM). Although not definitive, a trend is observed showing roughness increasing as the spindle speed increases. Both Ra and Rq increased more than double in size from 10,000 RPM to 15,000 RPM. Though the increase from 15,000 RPM to 20,000 RPM is significantly less, it still shows roughness increasing with increasing spindle speed. Rt more than doubles in value from 10,000 RPM to 20,000 RPM, though it drops slightly from 15,000 RPM to 20,000 RPM. Despite the apparent trend, limited data limits any conclusions.

Table 17 Roughness testing values for AR CoCrMo laterally milled with Mill A: Meisinger HM23LR.

Roughness Test: AR CoCrMo, Mill A, Meisinger HM23LR			
Spindle Speed (RPM)	Ra (μm)	Rq (μm)	Rt (μm)
10,000	2.0357	2.5969	12.7177
15,000	4.5289	6.1757	33.0573
20,000	5.3502	6.3821	27.5016

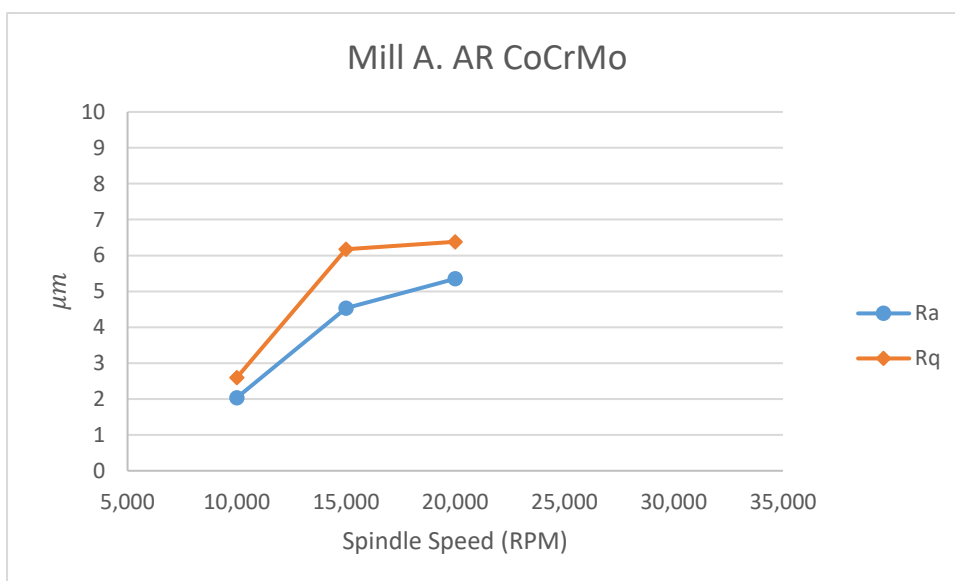


Figure 58 Ra and Rq roughness values for AR CoCrMo laterally milled with Mill A: Meisinger HM23LR.

5.4.3. As-received (AR) CoCrMo, Mill B: Shofu 21N

As-received CoCrMo milled with Mill B: Shofu 21N, completed all milling passes from 10,000 RPM to 35,000 RPM and allowed for a good insight into the progression of roughness vs spindle speed. Obtained data are displayed in Table 18, while Ra and Rq (μm) is plotted vs spindle speed (RPM) in Figure 59. A general trend of roughness increasing with increasing spindle speed is seen. Ra follows Rq fairly closely and an increase in values from 10,000 RPM to 15,000 RPM is shown. This is continued with a very slight increase in value from 15,000 RPM to 20,000 RPM. 20,000 RPM to 25,000 RPM provides a steep increase in values following the trend of roughness increasing with increase of spindle speed. 30,000 RPM shows an odd exception to this trend with roughness values dropping to values similar to those seen at 20,000 RPM. The change from 30,000 RPM to 35,000 RPM shows a very steep increase in roughness values. Rt follows the trend of Ra and Rq and even drops at 30,000 RPM.

Table 18 Roughness testing values for As Received CoCrMo laterally milled with Mill B: Shofu 21N.

Roughness Test: AR CoCrMo, Mill B, Shofu 21N			
Spindle Speed (RPM)	Ra (μm)	Rq (μm)	Rt (μm)
10,000	1.9757	2.4843	12.8995
15,000	2.9215	3.5988	15.7498
20,000	2.9819	3.6504	16.5817
25,000	4.4131	5.3851	22.7010
30,000	2.9997	3.7006	15.9031
35,000	8.0722	9.4908	40.2728

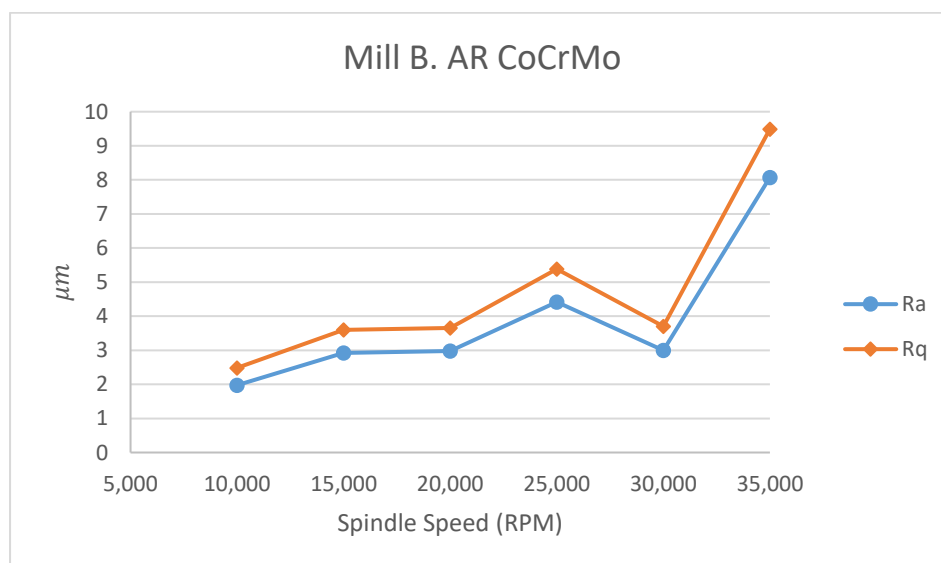


Figure 59 Ra and Rq roughness values for AR CoCrMo laterally milled with Mill B: Shofu 21N.

5.4.4. As-received (AR) CoCrMo, Mill C: Meisinger HM23GX

As-received CoCrMo milled with Mill C: Meisinger HM23GX provided six complete milling passes allowing for roughness data to be measured for all speeds from 10,000 RPM to 35,000 RPM. This was the first set of data which did not display a generally increasing trend for the roughness values. From 10,000 RPM to 25,000 RPM Ra and Rq show a similar pattern. Values at 10,000 RPM are relatively high and decrease significantly to values at 15,000 RPM, from 15,000 RPM to 25,000 RPM there is a slight continuous increase in values. From this point Ra and Rq differ significantly. Ra very slightly decreases in value from 25,000 RPM to 35,000 RPM. However Rq values continue to rise from 25,000 RPM to 30,000 RPM, and then fall to a lower value at 35,000 RPM. Rt values tend to follow the path of Rq in respect of increasing and decreasing as spindle speeds change. This is shown in Table 19, and Figure 60.

Table 19 Roughness testing values for AR CoCrMo laterally milled with Mill C: Meisinger HM23GX.

Roughness Test: AR CoCrMo, Mill C, Meisinger HM23GX Mill			
Spindle Speed (RPM)	Ra (μm)	Rq (μm)	Rt (μm)
10,000	4.8347	5.8314	24.4296
15,000	3.7242	4.6178	20.2374
20,000	4.0244	4.9417	23.2939
25,000	4.9818	6.3546	31.5474
30,000	4.8834	6.9656	38.0055
35,000	4.8005	5.9001	29.5654

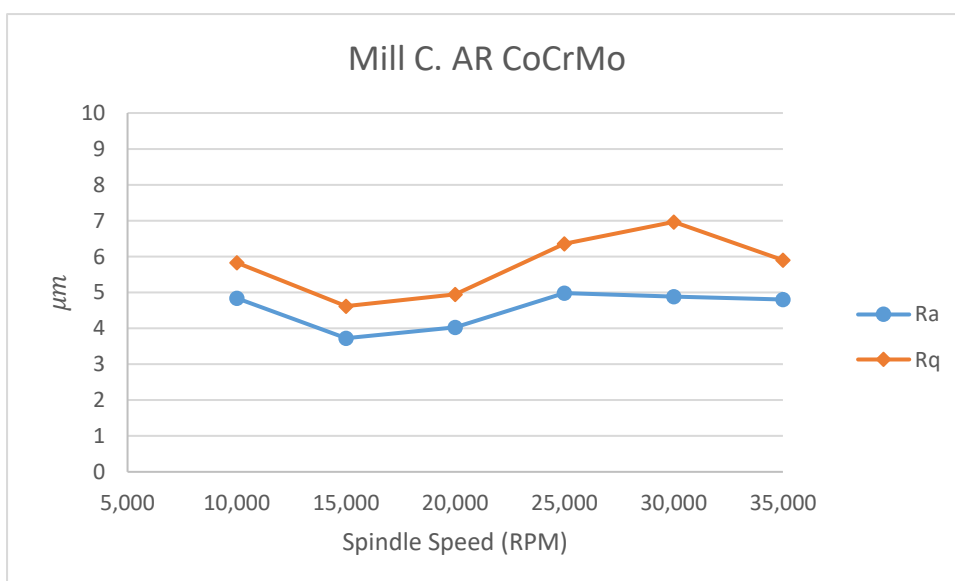


Figure 60 Ra and Rq roughness values for AR CoCrMo laterally milled with Mill C: HM23GX.

5.4.5. As-received (AR) CoCrMo, Mill D, Meisinger HMB23G

As-received CoCrMo milled with Mill D: Meisinger HMB23G faced large amounts of mill instability. Only passes at 10,000 RPM and 15,000 RPM where milled sufficiently to allow roughness testing to be undertaken. Extreme differences are seen in the recorded roughness data. At 10,000 RPM the Ra, Rq and Rt values were the lowest values at any spindle speed for all mills, however at 15,000 RPM the Ra, Rq and Rt values are the second highest in all experiments, only beaten by Mill B at 35,000 RPM. This enormous jump at first suggests unreliable roughness measurements may have occurred, though another explanation lies in the difference of this mill vs the others. This Meisinger HMB23G was coated in a DLC layer, which was expected to lead to superior machining, however it was shown by the surface obtained with Mill D that this did not occur. This sharp change from 10,000 RPM to 15,000 RPM could suggest that the DLC coating was rapidly worn during the pass at 10,000 RPM leaving exposed tungsten carbide (WC) cutting edges, these exposed edges causing significantly higher forces at 15,000 RPM. The data is shown in Table 20, and in Figure 62.

Table 20 Roughness testing values for AR CoCrMo laterally milled with Mill D: Meisinger HMB23G.

Roughness Test: AR CoCrMo, Mill D, Meisinger HMB23G Mill			
Spindle Speed (RPM)	Ra (μm)	Rq (μm)	Rt (μm)
10,000	1.2075	1.7529	10.5443
15,000	6.8298	8.3366	34.4139

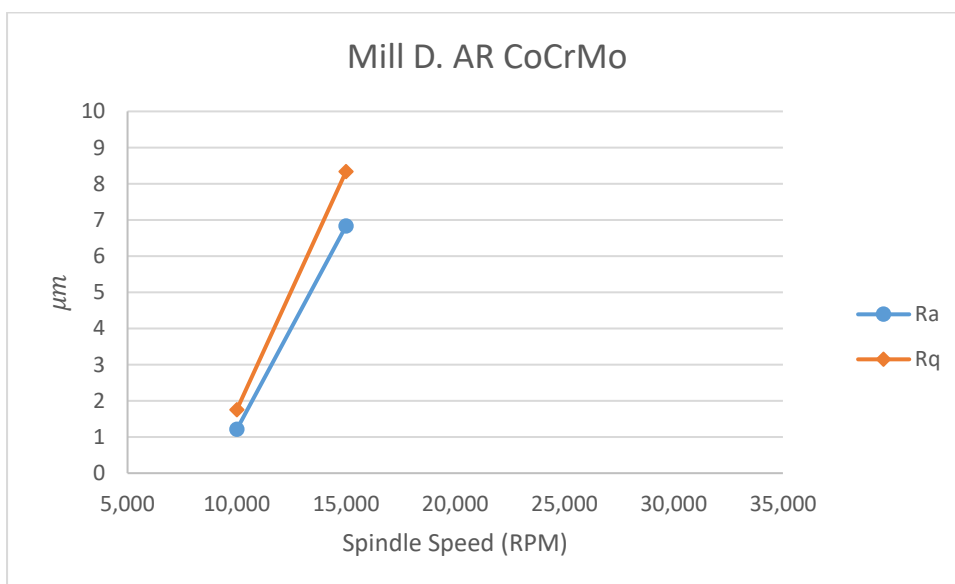


Figure 61 Ra and Rq roughness values for AR CoCrMo laterally milled with Mill D: Meisinger HMB23G.

5.5. Cutting Forces

Cutting forces for all milled surfaces were measured and supplied by Akita University. The specimens to be milled were placed on top of a 200N load cell in order to measure the cutting forces during milling. Generally forces in three dimensions (F_x , F_y and F_z) would be captured to calculate the overall resultant force. Unfortunately due to limitations of the load cell used for these measurements, only vertical forces (F_z) were measured. A diagram shows the milling setup, including the load cell, dental alloy, high speed spindle and the force axis in Figure 62. Where possible, multiple force measurements were taken throughout the pass at periodic intervals which allowed for average forces and standard deviations to be calculated.

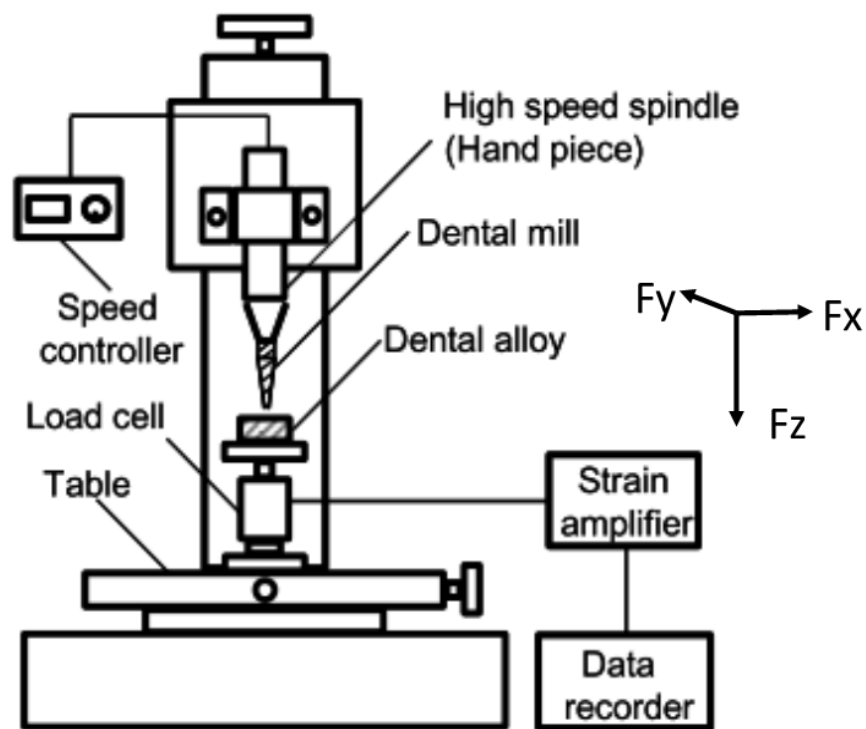


Figure 62 Milling diagram with force directions. M. Takahashi et al. (29)

Five sets of data were recorded and inserted into tables. The data sets are as follows: AR CoCrMo milled with Mill A, B, C and D, and HT4H CoCrMo milled with Mill B. Cutting Force (N) is the field of interest. Furthermore, in case of mill drop off or mill fractures occurring, the corresponding forces are not taken into consideration while calculating the average forces and standard deviation values.

HT4H CoCrMo	Mill B	Shofu 21N		
Clockwise	with OIL	1st		Ave. Cutting-Force
				Standard Deviation
drop off fracture	10000rpm [N]	-10.35618		
	Initial value [N]	-9.6979		
	Cutting Force [N]	-0.65828		0.658282599
	15000rpm [N]	-10.36321		
	Initial value [N]	-9.8333		
	Cutting Force [N]	-0.52991		0.529909878
	20000rpm [N]	-10.08491638		
	Initial value [N]	-9.6979		
	Cutting Force [N]	-0.387016384		0.387016384
	25000rpm [N]	-10.17579736		
	Initial value [N]	-9.8125		
	Cutting Force [N]	-0.363297359		0.363297359
30000rpm [N]	-10.22540032			
Initial value [N]	-9.8958			
Cutting Force [N]	-0.329600324		0.329600324	
35000rpm [N]	-10.25851363			
Initial value [N]	-9.7813			
Cutting Force [N]	-0.477213629		0.477213629	

Table 21 Cutting forces of HT4H CoCrMo laterally milled with Mill B: Shofu 21N

AR CoCrMo	Mill B	Shofu carbide burr 21N					Ave. Cutting-Force	Standard Deviation
Clockwise	with OIL	1st	2nd	3rd	4th	5th		
fracture	10000rpm [N]	-11.348215	-10.69886	-10.21549	-10.06399959	-10.3154607		
	Initial value [N]	-10.292	-9.7187	-9.3646	-9.4479	-9.5208		
	Cutting Force [N]	-1.056215	-0.98016	-0.85089	-0.61610	-0.79466	0.859606384	0.170863973
	15000rpm [N]	-10.9207322	-10.03708	-9.94039	-10.1032885	-10.46600326		
	Initial value [N]	-10.104	-9.2188	-9.2813	-9.5833	-9.5208		
	Cutting Force [N]	-0.816732195	-0.81828	-0.65909	-0.51999	-0.94520	0.751857571	0.164600193
	20000rpm [N]	-10.87269433	-9.85973	-10.07747	-10.24065416	-10.44163536		
	Initial value [N]	-10.187	-9.2708	-9.3229	-9.3958	-9.3958		
	Cutting Force [N]	-0.685694325	-0.58893	-0.75457	-0.84485	-1.04584	0.783977802	0.173811368
	25000rpm [N]	-11.07494945	-9.93174	-10.11357	-10.18954935	-10.3756948		
Initial value [N]	-10.208	-9.3646	-9.3021	-9.5	-9.375			
Cutting Force [N]	-0.866949447	-0.56714	-0.81147	-0.68955	-1.00069	0.78715999	0.166202102	
30000rpm [N]	-10.75522713	-10.01039	-10.26061	-10.26719056	-10.377730542			
Initial value [N]	-10.219	-9.0938	-9.4583	-9.4167	-9.2917			
Cutting Force [N]	-0.536227128	-0.91659	-0.80231	-0.85049	-1.08561	0.838244658	0.199988387	
35000rpm [N]	-10.6672339	-9.91901	-10.41200	-10.27439029	-10.39380217			
Initial value [N]	-10.229	-9.2813	-9.3438	-9.4583	-9.3854			
Cutting Force [N]	-0.438233896	-0.63771	-1.06820	-0.81609	-1.00840	0.793727627	0.261072771	

Table 23 Cutting forces of AR CoCrMo laterally milled with Mill B: Shofu 21N.

AR CoCrMo	Mill D	HMB23G(DLC)					Ave. Cutting-Force	Standard Deviation
Clockwise	with OIL	1st	2nd	3rd	4th			
drop off fracture	10000rpm [N]	-11.80344	-10.70196	-10.5041891	-11.09435854			
	Initial value [N]	-10.104	-9.3229	-9.2708	-9.4167			
	Cutting Force [N]	-1.69944	-1.37906	-1.23332	-1.67766		1.497369945	0.228807768
	15000rpm [N]	-11.61477	-10.50242	-11.00651438	-11.27630133			
	Initial value [N]	-10.177	-9.4375	-9.2917	-9.4792			
	Cutting Force [N]	-1.43777	-1.06492	-1.71481	-1.79710		1.503650762	0.330420072
	20000rpm [N]	-11.47693	-11.55178	-10.64106722	-11.02795856			
	Initial value [N]	-10.292	-9.4583	-9.2708	-9.4062			
	Cutting Force [N]	-1.18493	-2.09348	-1.37027	-1.62176		1.695168957	0.367153094
	25000rpm [N]	-11.07541	-10.93652	-10.68639374	-11.07210243			
	Initial value [N]	-10.229	-9.375	-9.4167	-9.3646			
	Cutting Force [N]	-0.84641	-1.56152	-1.26969	-1.70750		1.512904524	0.222915952
	30000rpm [N]	-10.78964	-10.77974	-10.1207886	-10.70976554			
	Initial value [N]	-10.177	-9.3958	-9.125	-9.4479			
	Cutting Force [N]	-0.61264	-1.38394	-0.99579	-1.26187		1.322903964	0.086321364
	35000rpm [N]	-10.27189	-10.71801		-9.418993626			
	Initial value [N]	-10.177	-9.375		-9.2813			
	Cutting Force [N]	-0.09489	-1.34301		-0.13769			

Table 25 Cutting forces of AR CoCrMo laterally milled with Mill D: Meisinger HMB23G.

5.6. Minimum Chip Thickness Evaluation

A major component of the minimum chip thickness theory and surrounding studies concerns the cutting thickness per tool edge (h) and the tool edge radius (r) leading to the well documented h/r ratio. Many sources in literature have focused on experimentally and theoretically calculating the minimum h/r ratio for a chip to form, and it has been found to be approximately 0.3 for all materials and mills (32,34,35,54). This section looks at SEM images of the unused milling tools in order to measure an average tool edge radius by looking at the edge diameter. Since these diameters will change along the tool's length the measurement has been taken near the tip of the mill as this is the part of the mill making contact with the workpiece. By finding this radius and using the known feed rate, spindle speed and number of flutes, the h/r ratio can be theoretically found. SEM images of the edge measurements are shown with a table listing the h/r values for various spindle speeds; furthermore a sample calculation is shown below to better understand how these values were achieved. Finally a graph of all h/r values for the four mills is shown plotting the h/r ratio vs spindle speed (RPM).

5.6.1. Sample Calculation – Mill B: Shofu 21N

The sample calculation below is for Mill B: Shofu 21N. The feed rate, spindle speed and number of flutes is known, while the tool edge radius is roughly calculated from SEM images.

Feed Rate = 0.15 mm/s (Constant across all experiments) Spindle Speed = 10,000 RPM

$$\therefore \text{Feed / Rev} = \frac{0.15 \text{ mm/s}}{10,000 \text{ rpm} \frac{1 \text{ min}}{60 \text{ sec}}} = 0.900 \mu\text{m}.$$

The number of flutes per revolutions is known as = 10

$$\therefore \text{Cutting Depth / Tool Edge (h)} = \frac{0.900 \mu\text{m}}{10} = 0.090 \mu\text{m}$$

Tool Edge Radius (r) = 4 μm

Therefore $h/r = \frac{0.090 \mu\text{m}}{4} = 0.0225$ for Mill B: Shofu 21N at 10,000 RPM.

Table 26 Sample minimum chip thickness calculations.

Mill B - Shofu 21N						
Feed Rate (mm/s)	Rotation Rate (RPM)	Feed/rev (μm)	Flute per Rev.	Cut Depth/Edge h (μm)	Tool Edge Radius r (μm)	h/r
0.15	10,000	0.900	10	0.090	4	0.0225
0.15	15,000	0.600	10	0.060	4	0.0150
0.15	20,000	0.450	10	0.045	4	0.0113
0.15	25,000	0.360	10	0.036	4	0.0090
0.15	30,000	0.300	10	0.030	4	0.0075
0.15	35,000	0.257	10	0.026	4	0.0064

5.6.2. Mill A: Meisinger HM23LR

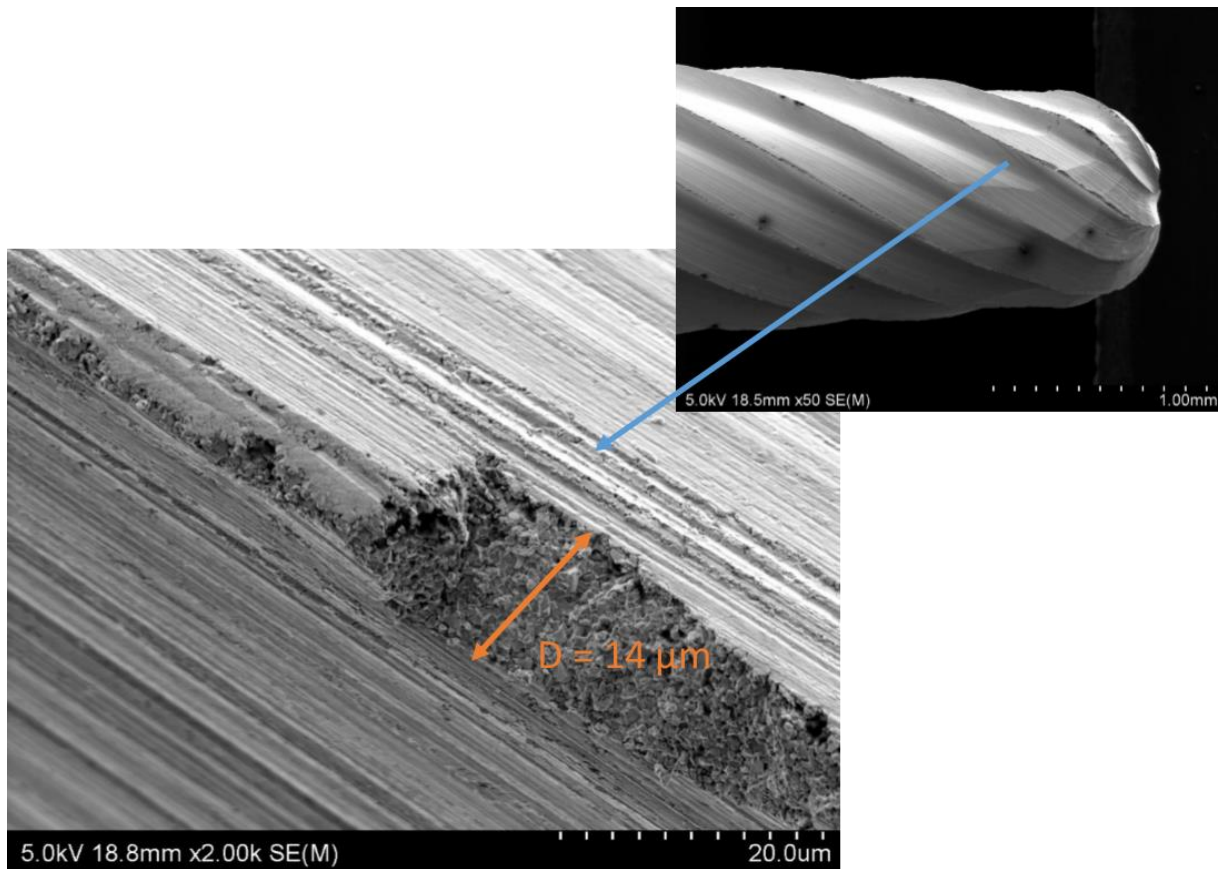


Figure 63 Mill A: Meisinger HM23LR cutting edge radius (r).

Using a fractured tool edge to find an edge diameter in Figure 63, leads to a tool edge diameter of $14 \mu m$ and therefore a tool edge radius (r) of $7 \mu m$. This is then plotted into an excel spreadsheet to show the h/r values for all spindle speeds from 10,000 RPM to 35,000 RPM in 5000 RPM increments. These values are shown below in Table 27.

Table 27 Mill A: Meisinger HM23LR h/r ratio calculations.

Mill A - Meisinger HM23LR						
Feed Rate (mm/s)	Rotation Rate (RPM)	Feed/rev (μm)	Flute per Rev.	Cut Depth/Edge h (μm)	Tool Edge Radius r (μm)	h/r
0.15	10,000	0.900	10	0.090	7	0.0129
0.15	15,000	0.600	10	0.060	7	0.0086
0.15	20,000	0.450	10	0.045	7	0.0064
0.15	25,000	0.360	10	0.036	7	0.0051
0.15	30,000	0.300	10	0.030	7	0.0043
0.15	35,000	0.257	10	0.026	7	0.0037

5.6.3. Mill B: Shofu 21N

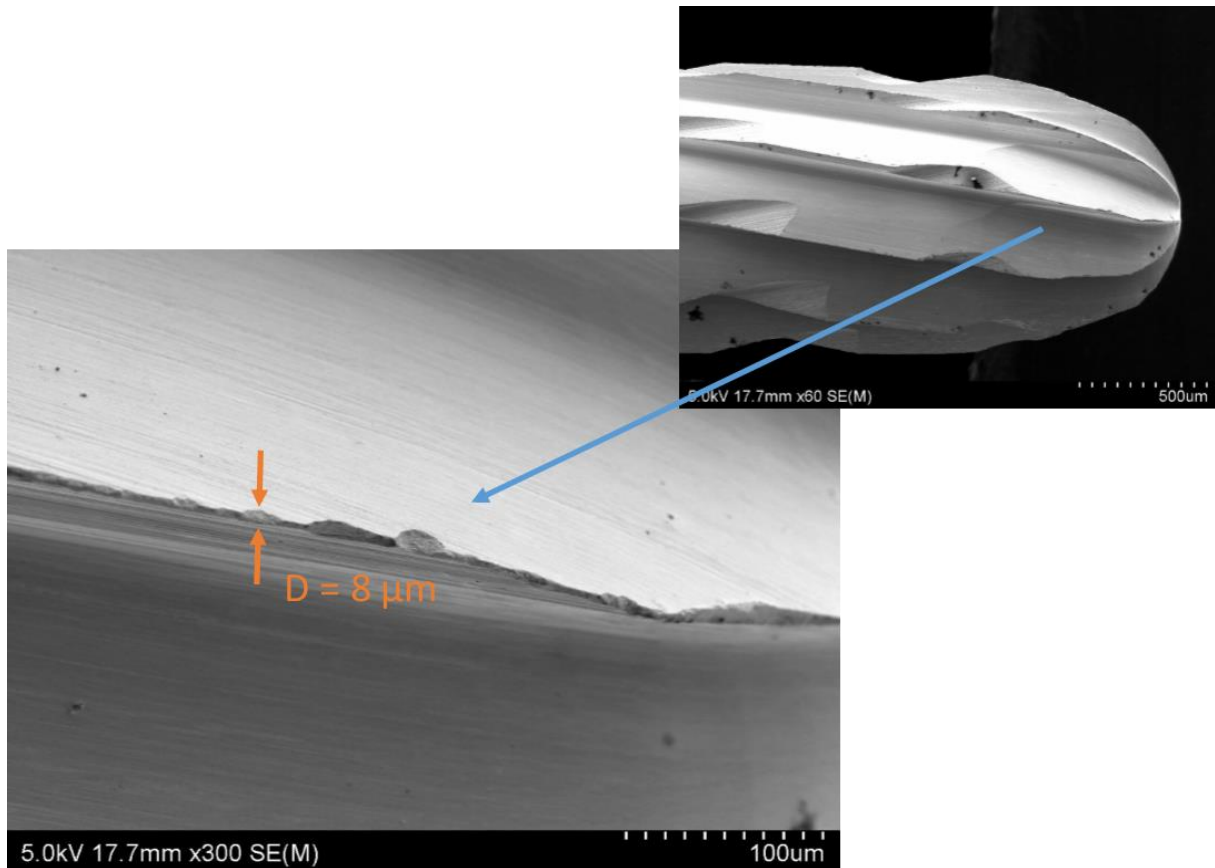


Figure 64 Mill B: Shofu 21N cutting edge radius (r).

The same technique is used here as was previously for Mill A, by using a fractured tool edge to find an edge diameter. Figure 64 shows the unused mill. Note that the magnification is relatively low, best estimations finding that a tool edge diameter of $8\mu\text{m}$ is seen and therefore a tool edge radius (r) of $4\mu\text{m}$. This was also plotted below in into an excel spreadsheet to show the h/r values for all spindle speeds from 10,000 RPM to 35,000 RPM in 5000 RPM increments and are shown in Table 28.

Table 28 Mill B: Shofu 21N h/r ratio calculations.

Mill B - Shofu 21N						
Feed Rate (mm/s)	Rotation Rate (RPM)	Feed/rev (μm)	Flute per Rev.	Cut Depth/Edge h (μm)	Tool Edge Radius r (μm)	h/r
0.15	10,000	0.900	10	0.090	4	0.0225
0.15	15,000	0.600	10	0.060	4	0.0150
0.15	20,000	0.450	10	0.045	4	0.0113
0.15	25,000	0.360	10	0.036	4	0.0090
0.15	30,000	0.300	10	0.030	4	0.0075
0.15	35,000	0.257	10	0.026	4	0.0064

5.6.4. Mill C: Meisinger HM23GX

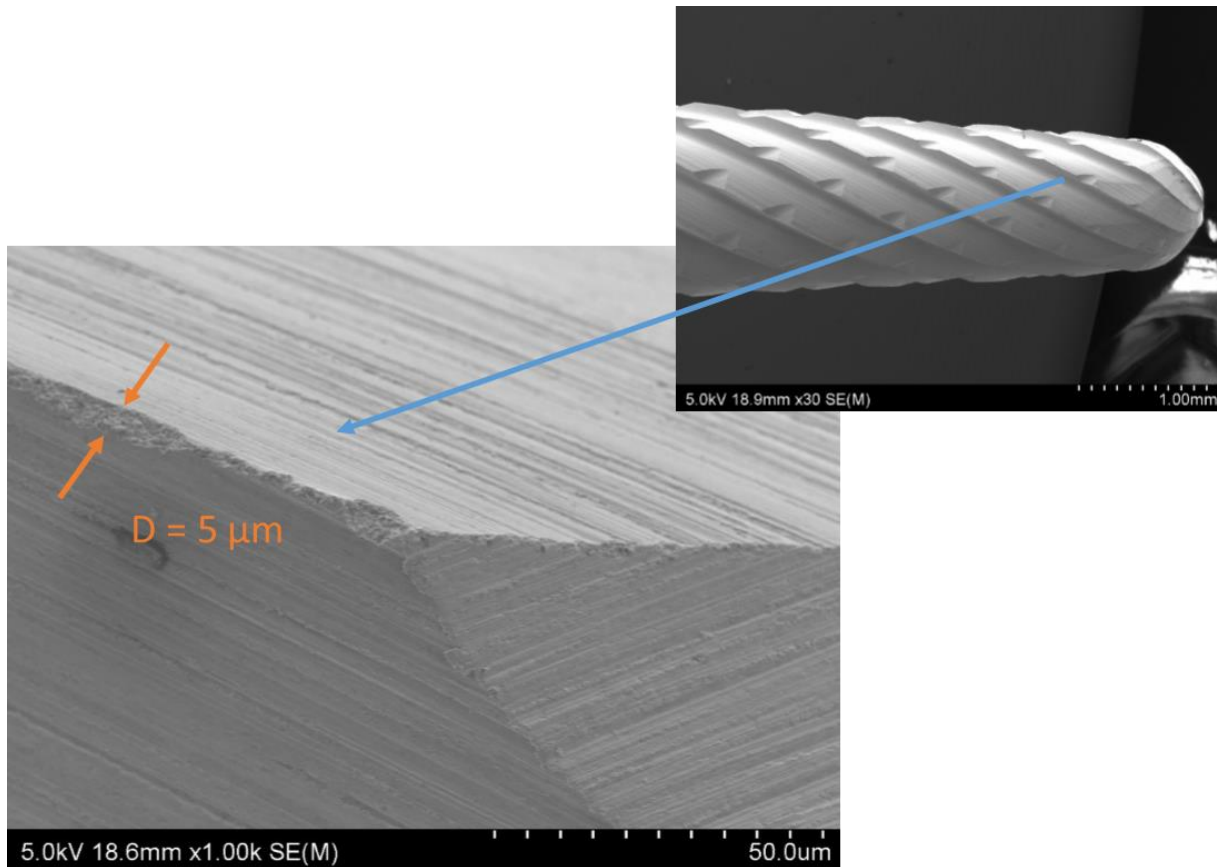


Figure 65 Mill C: HM23GX cutting edge radius (r).

Once again the SEM images of Mill C are used to find and estimate the tool edge radius (r). Figure 65 shows the unused mill, with a 1000x magnification allowing for accurate estimation. A tool edge diameter of $5\mu m$ is seen and therefore a tool edge radius (r) of $2.5\mu m$ can be estimated. As before the data is plotted into an excel spreadsheet to show the h/r values for all spindle speeds from 10,000 RPM to 35,000 RPM in 5000 RPM increments shown in Table 29.

Table 29 Mill C: Meisinger HM23GX h/r ratio calculations.

Mill C - Meisinger HM23GX							
Feed Rate (mm/s)	Rotation Rate (RPM)	Feed/rev (μm)	Flute per Rev.	Cut Depth/Edge h (μm)	Tool Edge Radius r (μm)	h/r	
0.15	10,000	0.900	10	0.090	2.5	0.0360	
0.15	15,000	0.600	10	0.060	2.5	0.0240	
0.15	20,000	0.450	10	0.045	2.5	0.0180	
0.15	25,000	0.360	10	0.036	2.5	0.0144	
0.15	30,000	0.300	10	0.030	2.5	0.0120	
0.15	35,000	0.257	10	0.026	2.5	0.0103	

5.6.5. Mill D: Meisinger HMB23G

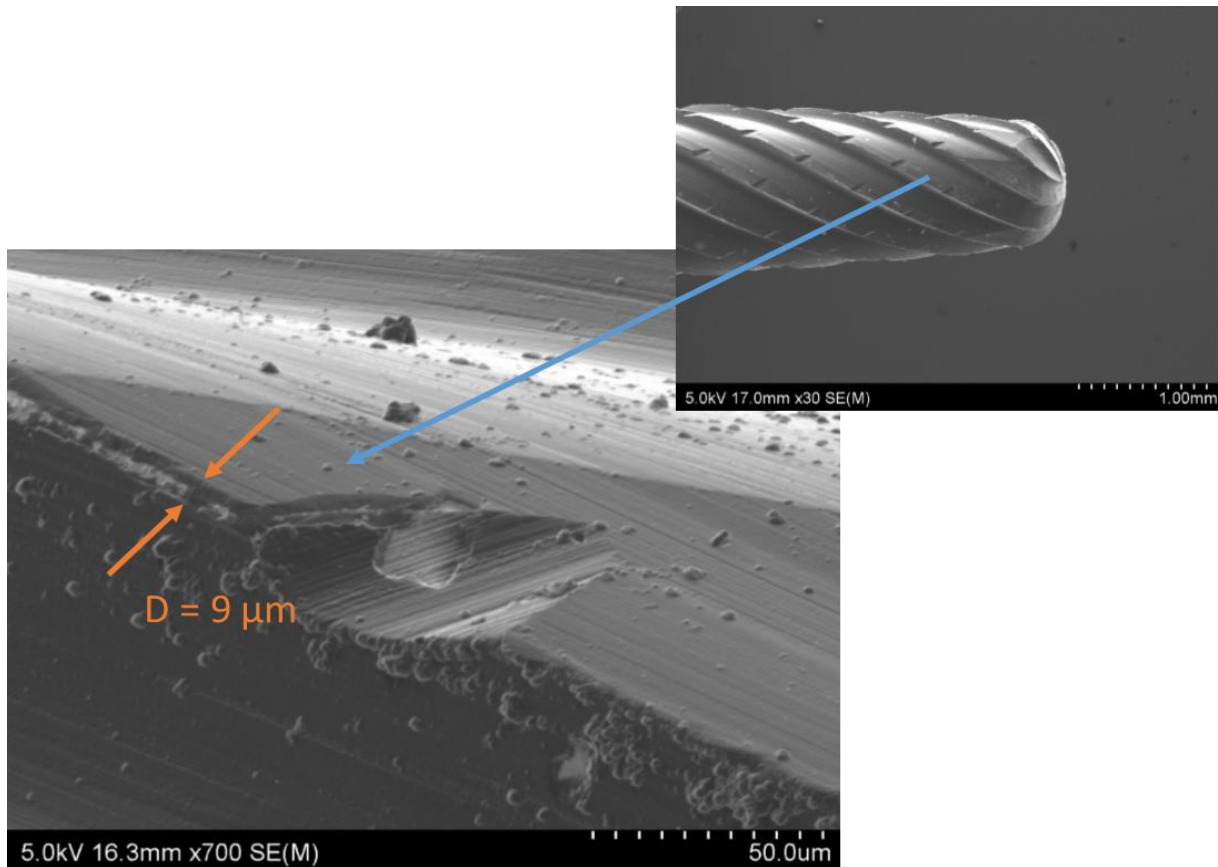


Figure 66 Mill D: HMB23G cutting edge radius (r).

The same method of tool edge estimation was employed for Mill D. Owing to the mill's DLC coating there was an appearance of two tool edge diameters: the DLC coating edge and the tungsten carbide edge. The overall diameter of the DLC coating was taken as shown in Figure 66. A tool edge diameter of $9 \mu\text{m}$ was found and therefore a tool edge radius (r) of $4.5\mu\text{m}$. This is plotted below into an excel spreadsheet to show the h/r values for all spindle speeds from 10,000 RPM to 35,000 RPM in 5000 RPM increments in Table 30.

Table 30 Mill D: Meisinger HMB23G h/r ratio calculations.

Mill D - HMB23G						
Feed Rate (mm/s)	Rotation Rate (RPM)	Feed/rev (μm)	Flute per Rev.	Cut Depth/Edge h (μm)	Tool Edge Radius r (μm)	h/r
0.15	10,000	0.900	10	0.090	4.5	0.0200
0.15	15,000	0.600	10	0.060	4.5	0.0133
0.15	20,000	0.450	10	0.045	4.5	0.0100
0.15	25,000	0.360	10	0.036	4.5	0.0080
0.15	30,000	0.300	10	0.030	4.5	0.0067
0.15	35,000	0.257	10	0.026	4.5	0.0057

5.6.6. Theoretical h/r Values for Mills A, B, C, D vs. Spindle Speed (RPM)

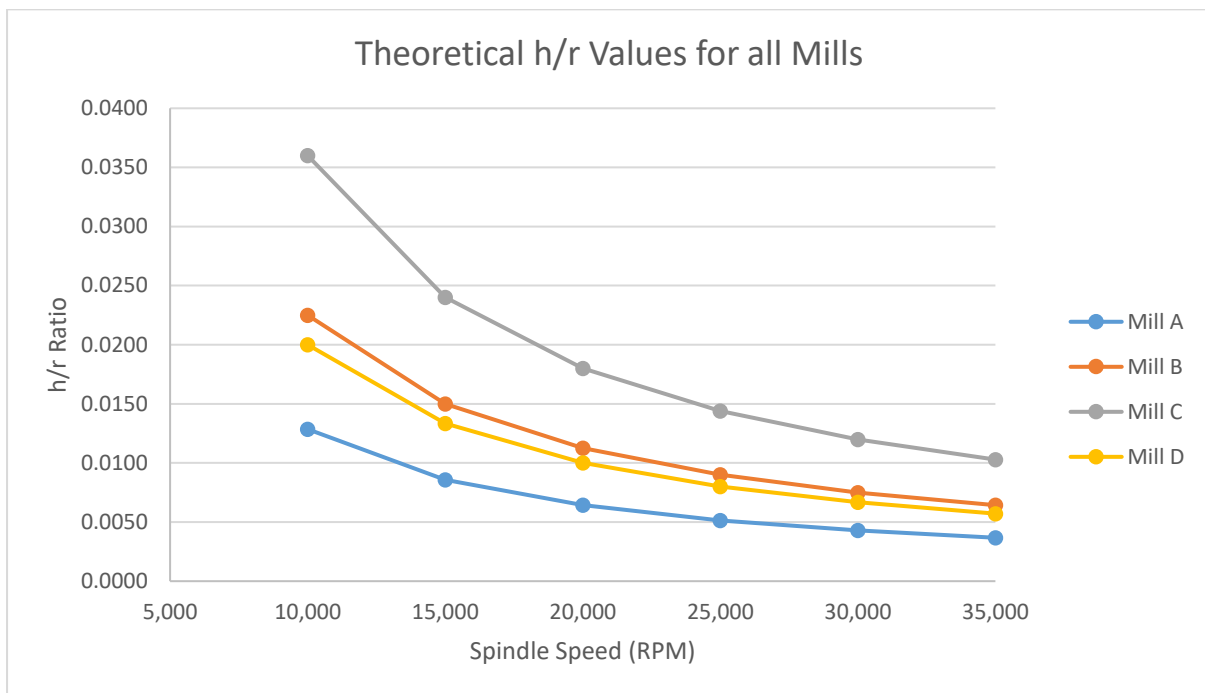


Figure 67 Theoretical h/r Values vs spindle speed (RPM) for all mills.

Figure 67 displays the theoretically calculated h/r values from the previous sections for Mills A, B, C and D, plotted against spindle speed (RPM). As seen in Figure 67, Mill C: Meisinger HM23GX showed significantly better results than other mills in these calculations. However, even at the lowest spindle speed of 10,000 RPM, and therefore highest h/r ratio, Mill C still has an h/r value equal to roughly a tenth of what is recommended (0.0360 vs 0.3 respectively).

The calculations undertaken in this section serve to further reinforce the author's belief that the minimum chip thickness effect is having significant effects on the surface finishes obtained in this study. The method used to obtain tool edge radii has been imprecise and was employed simply to provide rough calculations and a basic grasp of the potential for further investigation. If the effect of minimum chip thickness is to be investigated further, a more accurate method will be needed to obtain the tool edge radius.

6.0. Discussion

The following section discusses and presents results of interest obtained during this study, relevant to each individual section. SEM analysis, micro-hardness testing, roughness testing, cutting forces and minimum chip thickness theory are all evaluated individually. Next, a section of further thoughts discusses potential links and conclusions between obtained results and offers insights into the author's thoughts on the study's outcome. Finally, the implications and limitations of the study are discussed.

6.1. Scanning Electron Microscopy (SEM) Images

This section discusses results relating to the SEM images and conclusions drawn from the analysis in respect to spindle speed and surface finish quality. Instead of being organised by spindle speed, as the images were first displayed, this section is organised into discussions involving each mill and the obtained surface qualities separately. Finally, a summary of the mills and their performance relating to surface quality and spindle speed is discussed.

6.1.1. Mill A: Meisinger HM23LR

Mill A was used to mill an AR CoCrMo specimen from 10,000 RPM to 35,000 RPM in increments of 5000 RPM, though the 35,000 RPM pass was unsuccessful due to mill drop off. Furthermore, the 30,000 RPM pass was only partially completed. Since Mill A was the only mill without chip breaker geometry it was expected that significant amounts of material rewelding on the milled surface and chip adhesion on the mill would occur. At 10,000 RPM a fairly adequate surface was shown, roughness values were low and no major waviness or drill instability seemed present. There was however a lot of ripples/ridges and rewelded material on these ridges. Furthermore moderate gouging was present thus indicating ploughing was having a significant effect on the surface finish. Mill A was highly susceptible to chatter and vibrations, and at 15,000 RPM the formation of waviness peaks was already a prominent issue. Ripples/ridges were less pronounced and more widespread than at 10,000 RPM, however these large waviness peaks were synonymous with rewelded chips occurring. Ploughing appeared less severe, though it could have been overshadowed with the large waviness peaks. The surface quality had definitely decreased from the surface at 10,000 RPM, and the roughness testing values reflected that. Surface finish at 20,000 RPM continued the trend of decreasing surface quality, with even larger waviness peak ridges and further chip rewelding occurring on these peak ridges. Small cavities, tearing and gouging could also be

seen, yet were considered secondary issues when faced with the amount of rewelding and waviness occurring. Ploughing and ripples/ridges were more prominent at this speed than at previous speeds. The surface finish at 25,000 RPM had an interesting change where the waviness peak height and spacing increased, however the surface between these peaks improved. Ridges were shallower, less rewelding occurred and gouging was significantly less prominent. This is a perfect example of an underlying theory of this study, in which it is thought that the mill vibrations have led to unreliable results and complex mechanisms occurring that may not have been present without the excess vibrations. The surface finish obtained at 30,000 RPM showed a variety of surface quality and defects, however major drill instability led to an incomplete pass and an unreliable result. For that reason this surface is not discussed.

As stated previously, Mill A had no chip breaker geometry and as such it was not unexpected that a large amount of material build-up would be found on the used mill in both BUE form and entangled chips/adhered chips attached to the flutes and edges. A significant amount of layered BUEs were found on the tool's cutting edges and slightly chipped edges were shown, believed to be due to BUE induced edge fracturing. Large amounts of sporadically adhered chips were also seen on the mill body. Although edge wear did occur and chipped tool edges were common, the damage was far from catastrophic. Had the amount of BUE not been so severe it is believed this mill would have performed substantially better, however with materials like CoCrMo, BUE is always going to be an issue and therefore a mill with chip breaker geometry is crucial.

6.1.2. Mill B: Shofu 21N

Mill B: Shofu 21N was used to mill both AR CoCrMo and HT4H CoCrMo from 10,000 RPM to 35,000 RPM. In both cases all speeds were able to be milled to completion.

For AR CoCrMo milled at 10,000 RPM, a surface finish with distinct horizontal bands of varying surface finishes ranging from smooth with no ridges, to areas littered with horizontal belts of fractured craters was shown. The crater edges had large amounts of chip rewelding occurring, as well as rough fractured edges, leading to a very poor surface. Evidence of ploughing and gouging was also shown. Areas outside of these crater belts showed surfaces with relatively good quality, with small vertical ridges free from rewelded material. These horizontal bands of varying surface finish were bordered by large horizontal ridges and gouges almost

separating the areas of differing surface finish. The surface obtained at 15,000 RPM showed improvement with reduced amounts of craters, this resulting in less rewelded material overall, and the horizontal ridges/ploughing/gouging were also minimized leading to a fairly good surface finish. Surface finish quality at 20,000 RPM showed a decrease in quality from the previous spindle speed, the same characteristics being present as found in the 10,000 RPM surface, with large crater formations, defined horizontal boundaries and high amounts of ploughing/gouging occurring. There was however slightly less rewelded chips than at 10,000 RPM. At 25,000 RPM the surface finish drastically changed and although the same typical features were present, their extent exponentially increased. The large crater formations were deep, rugged and fractured. Deep, thick horizontal gouging could be seen across the entire surface and rewelded material on the exposed ridges was much more frequent than with any other spindle speed. It is uncertain what caused this sudden change in quality, perhaps a natural frequency was found in mill vibration, though the cutting force was comparable to other spindle speeds. The surface finish was far worse than at 20,000 RPM. Spindle speeds of 30,000 RPM showed a surface very similar to the quality shown at 20,000 RPM and the features and detriments were comparable and even Ra values recorded showed similar values. This further emphasises the question of what occurred at 25,000 RPM to create such a drastic change in quality. The surface found at 35,000 RPM showed major fracturing, large craters and deep gouging/ploughing occurring. Rewelded material was extremely high and the overall surface was easily identifiable as very poor.

While milling HT4H CoCrMo with Mill B, a very different surface finish to that of AR CoCrMo milled with Mill B was shown. Instead of the predominant pattern being horizontal bands of varying surface finish, HT4H CoCrMo was dominated with large vertical ridges. At spindle speeds of 10,000 RPM a vague cyclic pattern of vertical ridges was shown combined with heavy ploughing/gouging, and occasional thin horizontal bands of crater formations. No rewelding was seen occurring at this speed, despite the extremely rough surface finish. Surface quality at 15,000 RPM showed closer spaced vertical ridges that were both steeper and more fractured than at 10,000 RPM. Large semi-detached chips were shown hanging from these ridges, while thin horizontal belts of craters were also present in lower regions. Although the width of these craters was less than in AR CoCrMo, their depth and frequency created a substantially rougher surface finish. Horizontal gouging was still heavily present

indicating significant ploughing was occurring. At a spindle speed of 20,000 RPM a noticeable decrease in the amount of vertical ridges was shown; however the ridges present were deeper than at 15,000 RPM. They appeared mainly towards the start of the milling pass though, indicating that they could be due to initial instability when the mill first contacted the surface. Long needle-like chips were shown hanging from these ridges and it is unknown whether they were rewelded, or semi-detached material that had not sheared completely. The ductility of this HT4H CoCrMo was shown to be higher than AR CoCrMo from the micro-hardness results where it was found AR CoCrMo was harder than HT4H CoCrMo. This increased ductility in HT4H CoCrMo can be seen in the way the mill bites into these vertical ridges, often squeezing material out behind it creating a plastically deformed ridge. The surface finish shown at 25,000 RPM was a major improvement over previous passes with the almost complete removal of the vertical ridges, though ploughing and horizontal gouging was still heavily shown. The amount of rewelded material also dropped significantly due to the substantially lower occurrence of vertical ridges. The crater formations typical of Mill B were minor, though there were horizontal belts of deep fractured crater surfaces near the bottom of the milled section, most likely due to excess vibrations in the mill tip. The surface obtained at 30,000 RPM showed no significant change from 25,000 RPM, with the exception of a slightly rougher bottom half owing to the severe crater belts seen, presumably created due to mill vibration increasing as the spindle speed increased. Milling at 35,000 RPM showed major mill instability and excess vibrations, vertical ridges once again formed as well as deep gouging and ploughing. The horizontal width of the crater belts increased, as did the depth. Rewelding also increased significantly due to the increased ridges and as a result an overall much poorer surface finish was shown, though this was not unexpected as no mill has provided a good surface finish at 35,000 RPM in this study.

The Shofu 21N mills were shown to be well manufactured and had the sharpest cutting edges in the study, though they suffered significantly worse tool wear than the Meisinger mills. In both cases, with AR CoCrMo and HT4H CoCrMo there was significant damage done to the flutes and cutting edges. Large chunks of material were chipped off exposing the bare cemented tungsten carbide matrix. BUE formation did occur; however the chunks of material chipped off were many times larger than the BUE and much larger than any edge fractures in other mills. The fractures and chipping shown had a very brittle nature. Edge wear near the

tip of the mill was most extensive, suspected to be due to excess vibrations in the thinner section of the mills which could also lead to the crater formations which occurred more frequently towards the surface milled by the tip of the mill. These mills would not be able to be reused due to this severe edge wear. Large oil burn marks were shown across the mill body also which indicates that high temperatures were reached during milling. A noticeable difference between these mills and the Meisinger mills, was the lack of adhered chips on the mill bodies. Aside from the occasional small BUE, the mills themselves were relatively clean. In terms of tool life, Mill B used to mill AR CoCrMo showed significantly less damage than the Mill B used to mill HT4H CoCrMo. This was most likely due to the increased BUE that comes with softer material.

6.1.3. Mill C: Meisinger HM23GX

Mill C was used to mill AR CoCrMo specimens from 10,000 RPM to 35,000 RPM and was one of two mills able to complete all milling passes without drill drop off or instability leading to milling cancelation. A spindle speed off 10,000 RPM produced a relatively poor surface, waviness spacing and peak height being both low; however large amounts of angled ridges were shown, as well as chip rewelding occurring on these ridges and on the larger waviness peak ridges. Some ploughing was present though it was overshadowed by the ridges, rewelding and waviness severity. A spindle speed of 15,000 RPM provided an improved surface finish with a general reduction in waviness peak height, though spacing did increase and towards the end of the pass mill instability was illustrated with the rise of waviness peak heights. Moderate gouging was also present and slight chip rewelding on the waviness peak ridges, though noticeably less than at 10,000 RPM. The major difference was found in the surfaces between these waviness peaks where ridges were minimal and a smooth surface was shown. Chip rewelding was also minimal in these areas and the only defect was slight ploughing and the occasional ridge. Surface quality at 20,000 RPM continued this trend of improving surface finish with both waviness peak height and spacing smaller than at 15,000 RPM. Internal ridges were not seen and only slight ridges occurred on the waviness peaks. Minimal chip rewelding was shown occurring on the waviness peaks and none occurred between them. The only detriment, aside from the slight waviness, was evidence of some ploughing and tearing occurring. This is the best surface shown in this study. At a spindle speed of 25,000 RPM the images showed signs of a declining surface finish, waviness peak

height increasing and the formation of valleys and peaks becoming noticeably visible. Occasional ridges formed inside these larger peaks and chip rewelding increased from the amount shown at 20,000 RPM. One observation is that ploughing and tearing seemed significantly less than at 20,000 RPM, though different contrast levels in each image could have hidden the flaws. Surfaces at both 30,000 RPM and 35,000 RPM showed significantly lower surface quality. The surface at 30,000 RPM showed large waviness peaks, high amounts of chip rewelding, and deep ripple/ridges. Furthermore ploughing left significant horizontal gouging across the entire surface. The surface at 35,000 RPM exhibited all the same as 30,000 RPM but to more of an extent, especially rewelded material, which was a severe issue.

Mill C, like Mill A, suffered BUE formation along all cutting edges. Furthermore BUE induced edge fracturing was believed to occur. Entangled chips and adhered chips were seen across the mill body, to less of an extent than Mill A however, which is believed to be attributed to the chip breaker geometry present on Mill C. Oil burn marks were shown across the body of the mill indicating that high temperatures were reached during machining, specifically towards the tip of the mill. Adhered chips, oil stains, BUE and chipped tool edges were the main detriments of the used mill, however no catastrophic failure occurred and the mill seems to have performed with adequate tool life. Furthermore, the highest quality surface finish was achieved with this mill.

6.1.4. Mill D: Meisinger HMB23G

Mill D was coated in a diamond-like carbon (DLC) layer and used to mill AR CoCrMo from 10,000 RPM to 35,000 RPM. However due to mill instability the 35,000 RPM pass was cancelled. The milling pass at 30,000 RPM was only partially completed, and even at 25,000 RPM the milling pass was significantly shorter than the others. This indicates high cutting forces and mill instability forced the manual cancellation of these milling passes. At 10,000 RPM the mill provided a very good surface finish with the lowest Ra value in the entire study. Small ridges were shown with approximately 40 to 80 μm between each; these were very shallow, however minor chip rewelding did occur along the ridges. Ploughing also occurred between ridges leaving distinctive gouge marks. No waviness was seen occurring however, and aside from the minor chip rewelding occurring on the ridges the surface was relatively good. The change to a spindle speed of 15,000 RPM though, saw a dramatic drop in quality as large waviness peaks appeared leaving a completely different surface finish. Chip rewelding

around the waviness peaks was common and significantly detrimental with many smaller ridges appearing between the larger peaks. Gouging and ploughing was present on the uphill rises of these large peaks, as well as layers of rewelded material which formed a rough flaky surface. At 20,000 RPM the surface finish obtained showed a slight improvement with the amount of rewelded material dropping. Waviness peak height and spacing was similar, maybe slightly lower than at 15,000 RPM. Gouging and tearing was still present indicating ploughing was occurring. The amount and depth of the minor ridges had dropped leaving a cleaner surface than at 15,000 RPM, despite still experiencing waviness. At 25,000 RPM, major mill instability was visible, alternating waviness peak heights and spacing were present combined with mill drop off and huge amounts of reweld and deep gouging were present. This is another occasion where the surface finish inside the waviness peaks was significantly better than the overall finish so a potentially good surface finish might have been achievable if mill vibrations were minimised. The surface finish at 30,000 RPM was the same as 25,000 RPM, with the potential for a semi decent finish if mill vibrations were controlled, although at 30,000 RPM instability was so bad that less than 2mm of surface was able to be milled.

The most noticeable aspect of the SEM images of Mill D was the wearing of the DLC layer, even at magnifications as low as 30x the difference in the dark grey DLC coating and the light grey tungsten carbide material of the mill body being apparent. Cutting edges had been completely stripped off the coating after the milling had been completed. Though it is not known at which spindle speed this major wear occurred, it is speculated that it could have worn off as early as after the 10,000 RPM pass (due to roughness data collected and SEM images of the surfaces). Large BUEs can be seen leading to BUE induced edge fractures which seem to have accelerated the removal of the DLC layer. Entangled chips and loose adhered chips are also shown attached to the mill. The edge wear in itself is not so severe and certainly not a catastrophic failure, but because the DLC coating has been worn it renders this mill's unique properties useless. Furthermore, with the coating removed it showed worse performance than the uncoated mills. It is convincingly observed during this study that a DLC coating is not suitable for milling CoCrMo. The cutting forces were much larger than Mill B which is uncoated, and furthermore generally obtained surface finishes were no better than any other mills (excluding the pass at 10,000RPM). In the case of Mill D, except for perhaps the surface milled at 10,000 RPM, no benefit has been shown for this DLC coating.

6.1.5. Overall Evaluation

It can be concluded from the aforementioned discussions on each specimen that rewelding and mill gyration were the top two issues facing the obtainability of a high quality surface finish. Chip rewelding was generally observed across all specimens with trends showing an increase in rewelded material as the spindle speed was increased. This is likely due to increased heat and vibrations occurring at higher spindle speeds. Increased vibrations at higher spindle speeds will affect the way chips are retained and ejected from the mill flutes. Increased heat will affect the frictional re-welding occurring. Furthermore, this increased vibration leads to increased waviness and therefore an increased amount of exposed ridges, which is where chip rewelding was most likely to occur. This is a self-feeding cycle which is extremely detrimental to the surface finish. The results potentially link rewelding to cyclic and non-cyclic mill vibration, though this statement would need to be investigated further.

Waviness was shown to significantly affect Mills A, C and D. Some vibration was shown in Mill B, specifically with HT4H material, however it seemed not to form the generic cyclic waviness. Despite the lack of waviness, vibrations did cause obvious damage in specimens milled with Mill B. Since all AR CoCrMo specimens milled were the same in terms of mechanical properties and machining parameters, the difference in mill vibrations is therefore thought to be due to the differences in mill geometries. The pattern in waviness occurring was observed to be similar to re-welding, in which the general trend showed severity increased with increasing spindle speed, particularly above speeds of 25,000 RPM where it exponentially worsened. Further on this, is the fact that very few positive results were observed at spindle speeds of 30,000 RPM and 35,000 RPM.

Specimen C milled at 20,000 RPM (with Mill C) was found to exhibit the overall best surface finish. Specimen D at 10,000 RPM and specimen C at 15,000rpm were found to be the second and third best surfaces respectively. Specimen B showed low cutting forces and low roughness values, and produced moderate surfaces at 10,000 RPM to 25,000 RPM. However the nature of the extensive crater belts and differences in horizontal finishes, which was only noticeable under microscopic analysis, led to a lower overall evaluation. Re-welded material is minimal in all three cases of the best surfaces, although minor re-welding occurs on the ridge edges in specimen C at 20,000 RPM and specimen D at 10,000 RPM.

The HM23LR mill (Mill A) is an uncoated spiral shaped mill without chip breakers while the HMB23G (Mill D) mill is a spiral shaped DLC coated mill with chip breakers. Aside from the

coating and chip breakers, they both have similar geometry. Mill D showed less re-welding than Mill A despite the significantly higher mill vibrations, though it is believed this can be attributed mainly to the presence of chip breakers rather than the DLC coating. However, the DLC coating would lower the coefficient of friction which could potentially lower the machining temperatures leading to less material being re-welded. The use of tool coatings and the effect on rewelding and waviness would need to be investigated further in future studies.

The S21N and HM23GX mills are both cross shaped mills with chip breakers. Despite the similarities they produced distinctly different surfaces which led to few conclusions being drawn between the two. Further research is needed on this to identify how mill geometry is affecting surface finish.

Overall, Mill C: Meisinger HM23GX, was the best performing mill. Mill B: Shofu 21N showed good promise with low Ra values and low cutting forces, however it showed the worst tool life of all four mills and significant microscopic surface defects were found on the milled surfaces. Mill D produced underwhelming results considering the presence of a DLC coating. Owing to this it can be stated a DLC coating is not suitable for milling CoCrMo. Mill A performed poorly and this was expected with the lack of chip breaker geometry and it can be concluded that chip breaker geometry is crucial while milling CoCrMo.

Annealing CoCrMo led to material softening, shown in the hardness results. The milling of this alloy led to a very different surface finish than was seen while milling AR CoCrMo. There were large deep ridges, huge amounts of rewelded material and significant gouging indicating large amounts of ploughing was taking place. V. Huntrupl (53) stated that with materials such as CoCrMo, a softer workpiece can lead to larger BUE formations on the milling tool which in turn will lead to a poorer surface finish. This fits in well with the observations seen as it is known that large BUE formations cause significant ploughing, and therefore gouging, to occur. This was the case with HT4H CoCrMo where ploughing was significantly worse than that present in AR CoCrMo. BUE on the cutting tool is also linked to rewelding, which was also significantly more detrimental in HT4H CoCrMo than it was in AR CoCrMo. And finally, BUEs are known to lead to tool wear and edge chipping and this was also shown in the mill used to mill HT4H CoCrMo. It can be concluded that most likely the softened material led to the formation of larger BUEs which caused a poor surface finish and accelerated tool wear.

6.2. Micro-Hardness Testing

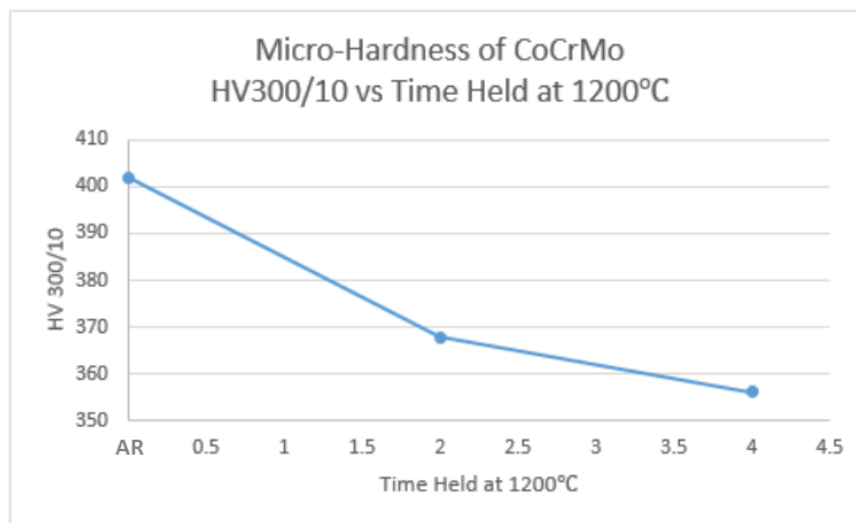


Figure 68 Micro-hardness of CoCrMo vs annealing time.

The difference between the hardness values obtained for the as-received, HT2H, and HT4H specimens as shown in Figure 68, is believed to be due to second phase dissolution (the removal of the HCP phase) and carbide shrinkage occurring during the annealing of CoCrMo. The homogenization occurring wants to remove the HCP phase and create a full FCC structure. As-cast CoCrMo exhibits roughly 0.05 volume fraction HCP (15) and after 2 hours at 1200°C the majority of the HCP structure is believed to have homogenized and carbide reduction has occurred. Once this change has occurred, rapid cooling due to water quenching forces an FCC structure due to the sluggish kinetics. This second phase dissolution explains the significant difference in hardness values between the as-received (AR) specimen and the HT2H specimen. However, since a majority of the HCP phase is believed to have been removed after 2 hours annealing, further dissolution will be minimal between annealing for 2 hours and annealing for 4 hours. This led to little difference in the hardness values between the HT2H specimen and the HT4H specimen. Although not tested further, an annealing limit is expected to be found around the 6 hour mark if the trend in decreasing HV300/10 was to continue. Originally a secondary aim of this study was to etch the specimens to confirm the changes in carbides, grain size and interdendritic structures after annealing. However since etching was not possible the only data obtained are the hardness values. These values definitively conclude that successful softening of the CoCrMo specimens has been achieved by annealing at 1200°C for 2-4 hours then water quenching. Following the extensive literature review this was expected to occur.

6.3. Roughness Testing

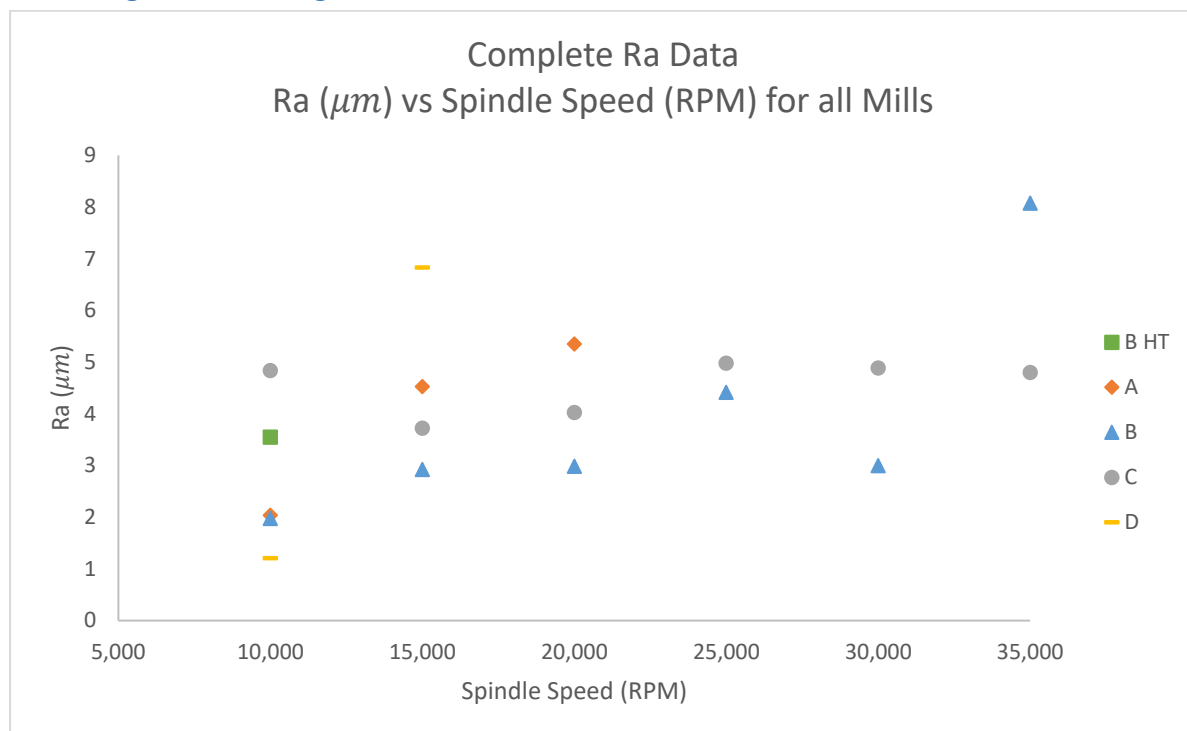


Figure 69 Complete Ra data for lateral milling of CoCrMo with all mills.

Shown in Figure 69 is the complete data acquired for the arithmetic average of the roughness profile, Ra (μm) vs cutting speed (RPM) for all mills and specimens. As mentioned earlier, some passes could not be measured due to the need for a completed milling pass so, as such, the data lacks any obvious conclusions, though some definitive trends can be seen. Mill A: Meisinger HM21LR, is shown to sharply increase from 2.036 μm at 10,000 RPM to 4.53 μm at 15,000 RPM, from here a more modest increase is shown to 5.35 μm at 20,000 RPM. Spindle speeds above this proved unstable and no more completed milling passes could be measured. It can safely be stated that Mill A exhibited a trend of increasing surface roughness with increasing spindle speeds.

Mill B: Shofu 21N successfully completed all milling passes and, aside from Mill C, was the only mill to do this. This allows a better insight as to how roughness reacted to increasing spindle speeds. It should be noted that the cutting forces for Mill B seemed unaffected by spindle speed. Mill B at 10,000 RPM had the second lowest overall roughness with a Ra of 1.98 μm , from here there is a slight increase to 2.92 μm at 15,000 RPM. 15,000 RPM to 20,000 RPM showed little change (2.92 μm and 2.98 μm respectively), next there was a large jump to 4.41 μm at 25,000 RPM. This did drop back down to 3.00 μm at 30,000 RPM though. This does mimic the obtained surface finishes which saw a huge decrease in quality from 20,000

RPM to 25,000 RPM. 35,000 RPM shows an extraordinarily high Ra value of $8.07 \mu m$, however cutting forces were no higher than usual at 35,000 RPM. This data appears to be able to be concluded two ways: first, and probably most logically, the Ra at 30,000 RPM can be dismissed as an anomaly and then it could be concluded that Mill B also shows a general trend of roughness increasing with spindle speed increasing. Secondly, perhaps a little unreasonably, is the possibility to conclude that 25,000 RPM was an anomaly and state that from 15,000 RPM to 30,000 RPM the roughness values are consistent and independent of spindle speed. The first situation seems more sensible; however the issue with Mill B is the horizontal bands of varying surface finish that are typical of its milled surfaces. Depending on which point the stylus made contact with it could lead to very different Ra readings.

Mill C: Meisinger HM23GX was one of two mills to complete all milling passes sufficiently at all tested spindle speeds, which gives a good insight into how roughness reacts to increasing spindle speeds. A Ra value of $4.83 \mu m$ occurs at 10,000 RPM, this drops steeply to $3.72 \mu m$ at 15,000 RPM. From here it increases to $4.02 \mu m$ at 20,000 RPM and $4.98 \mu m$ at 25,000 RPM. 25,000 RPM to 35,000 RPM shows a slight decrease from $4.98 \mu m$ to $4.88 \mu m$ and $4.80 \mu m$. Unlike other data seen before, Mill C does not at first glance seem to conform to the trend of increasing roughness as spindle speeds increase, in fact Ra even decreases in value from 25,000 RPM to 35,000 RPM. As far as comparison to other mills; Ra at 10,000 RPM for Mill C is the highest recorded, the Ra values at 15,000 RPM and 20,000 RPM are mid-range, and then once again with exception to Mill B at 30,000 RPM, the remaining Ra values are the highest for each speed respectively. This is despite the SEM image analysis finding that the best surface finish microscopically occurred by Mill C at 20,000 RPM. This is a clear example of the dangers of micro-machining where surfaces that appear smooth, and even provide low roughness values, may be microscopically rough.

Mill D: Meisinger HMB23G was the only coated mill in the study and was coated with a DLC layer. It was believed this would lead to lower cutting forces, lower Ra values and a high quality surface finish. Only two milling passes were completed to sufficient levels to allow the surfaces to be analysed by the surface roughness tester however, and the results obtained from these two passes were far from what was predicted. With only two measured surfaces, Mill D provided both the lowest Ra value measured at any speed (10,000 RPM, $1.21 \mu m$), and the second highest value measured at any speed (15,000 RPM, $6.83 \mu m$). This definitely agreed with the trend of increasing Ra with increasing spindle speed, however there needs to

be a reason for such extreme changes, and they are believed to be due to the DLC coating. SEM images confirm the DLC coating was worn after all milling passes completed, however this data may suggest that the DLC coating was worn even after one pass at 10,000 RPM. SEM images of the milled specimen agrees with this showing a good surface finish at 10,000 RPM, then a major decrease in quality to a very poor surface at 15,000 RPM with large amounts of waviness and rewelding present.

Mill B HT showed Shofu 21N milling HT4H CoCrMo, only one milling pass was completed to a sufficient extent that allowed roughness testing, this with a spindle speed of 10,000 RPM. With a softer material (due to annealing), it was hoped that a better surface finish would be acquired. However the roughness results show the second to worst Ra at 10,000 RPM with $3.55 \mu\text{m}$, second only to Mill C with $4.83 \mu\text{m}$ at 10,000 RPM. While the lack of data does not offer much insight into this material, it can be definitively stated that for a spindle speed of 10,000 RPM the softer material did not lead to a better surface finish. This was concluded with an Ra value of almost double the size of AR CoCrMo milled with Mill B ($3.55 \mu\text{m}$ vs $1.98 \mu\text{m}$ respectively).

Figure 70 plots the average Ra (arithmetic average of the roughness profile) and Rq (root mean squared average of the roughness profile) values for all recorded data, plotting μm vs spindle speed (RPM). The issue arising from this graph is that there are significantly more data at spindle speeds of 10,000 RPM, 15,000 RPM, and 20,000 RPM than there are at spindle speeds above this. Specimens B and C were the only specimens to be completely milled at all speeds. This lack of data at higher RPMs throws the graph off. If the incomplete passes were able to be tested with the roughness tester there is no doubt they would provide very high Ra values, but without this data the average values at these higher speeds are relatively low. It is believed to still be reasonable to state that roughness values increased as the spindle speed increased. This was found to be completely proven in specimens A and D. Specimen B showed an almost complete increase of surface roughness with increasing spindle speeds, with the only exception being at 30,000 RPM. Specimen C provided mixed results and was the only specimen to not comply with the theory of surface roughness increasing with increasing spindle speeds. However Rq values showed a continuous increase from 15,000 RPM to 30,000 RPM, with Ra values showing an increase from 15,000 RPM to 25,000 RPM for Mill C. Overall the results showed that in general it was widely shown that as spindle speed increased so did

the various surface roughness parameters, though this is most likely due to increased rewelding instead of cutting kinematics. One thing to be noted is the increase in waviness as spindle speed increased. Theoretically the roughness tester should ignore waviness and separate Ra from the recorded data, though on such a small milling scale with reasonably low calibration and small experience operating the tester it is possible some waviness formations could be added to the Ra values.

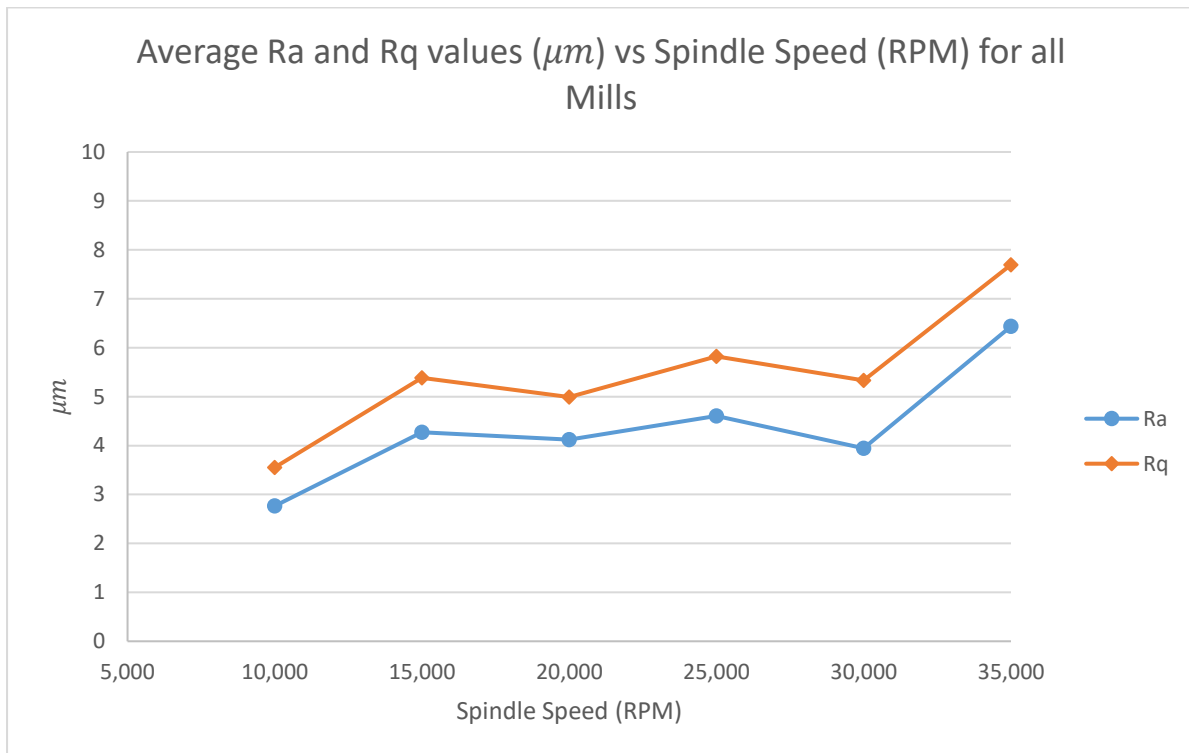


Figure 70 Average Ra and Rq values (μm) vs Spindle Speed (RPM) for all mills.

6.4. Cutting Forces

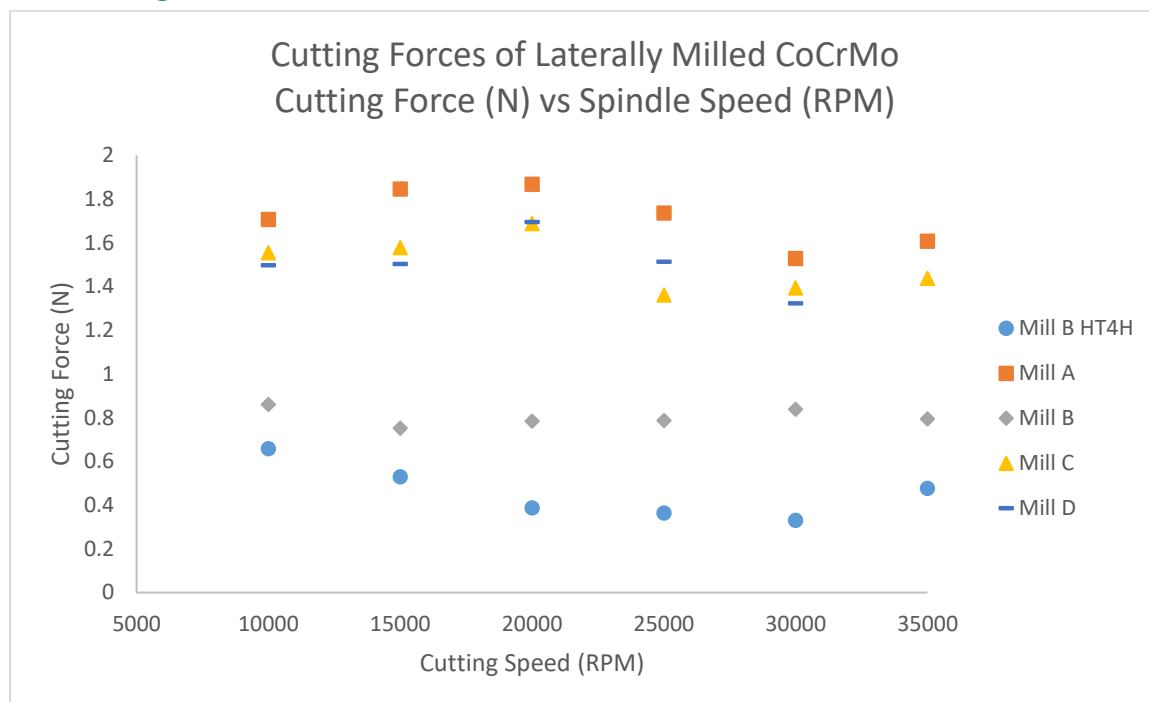


Figure 71 Cutting forces of laterally milled CoCrMo displaying Cutting Force (N) vs Spindle Speed (RPM) for all mills.

Figure 71 shows the cutting forces for all specimens in this study, plotting cutting force (N) vs spindle speed (RPM). While milling AR CoCrMo, Mills A, C and D showed cutting forces that were fairly similar ranging from approximately 1.3 N to 1.9N across all spindle speeds. Cutting forces for Mill B were significantly lower with forces ranging from 0.7N to 0.9N for AR CoCrMo, and even lower for HT4H CoCrMo with forces of 0.3N to 0.7N approximately. Measurements for Mill D at 35,000 RPM are not shown due to severe drop off occurring and no reliable measurements taken. Mill A also suffered extensive drop off at 35,000 RPM however one reliable measurement was taken on the second interval. Aside from these two, the measurements were able to be acquired reliably with only momentary drop off occurring. These momentary drop offs include 2/5 intervals for Mill A and Mill D at 30,000 RPM, 1/5 intervals for Mill C and Mill D at 20,000 RPM and 1/5 intervals for Mill D at 20,000 RPM. The drop off occurring for Mill C seems to be an anomaly, while Mill A and D suffered multiple times at higher RPMS. The drop offs frequently occurred upon early contact with the material which is believed to be due to the jarring nature of initial contact. Further explanations of these drop offs and patterns are shown in Section 5.6.

Mill A: Meisinger HM23LR was the only mill without chip breaker geometry and unsurprisingly shows the highest cutting forces out of all mills used in this study. Initially the forces increased

as speed increased from 10,000 RPM (1.71N) to 20,000 RPM (1.85N), then the forces decrease almost linearly from 1.85N at 20,000 RPM to 1.53N at 30,000 RPM, which is lower than at 10,000 RPM (1.71N). At 35,000 RPM the force increased to 1.60N though large drop offs occurred here and only one measurement interval was able to be used leading to moderately unreliable data. One interesting observation is that at 25,000 RPM, where the cutting forces start to decline, is where the start of major drill instability occurs in the SEM images, possibly linking the decrease in forces to the increase in mill instability.

Mill B: Shofu 21N (AR CoCrMo) showed significantly lower cutting forces than the other three mills used to mill AR CoCrMo. Forces for Mill B were relatively constant regardless of spindle speeds ranging between 0.75N at the lowest, at 0.85N at the highest, at 10,000 RPM and 15,000 RPM respectively. The other values obtained at various spindle speeds fall in between these limits. There is a slight trend of force decreasing from 10,000 RPM to 15,000 RPM, then slightly increasing up to 30,000 RPM before slightly dropping to 35,000 RPM, though with such minor differences it can be concluded that cutting forces for Mill B remained relatively stable regardless of spindle speed.

Mill B: Shofu 21N (HT4H CoCrMo) showed even lower cutting forces than Mill B with AR CoCrMo. This is to be expected as the annealing process for CoCrMo is documented to soften the material. The cutting forces were less linear in their progression and declined quite steeply from 0.65N at 10,000 RPM to 0.35N at 20,000 RPM, from which it was relatively stable, only decreasing slightly until 30,000 RPM. From 30,000 RPM it increased sharply from 0.33N to 0.48N at 35,000 RPM.

Mill C: Meisinger HM23GX experienced relatively high cutting forces considering it was responsible for the some of the best surface finishes obtained. Forces were stable at first with 1.55N at 10,000 RPM, and 1.57N at 15,000 RPM. However, the force quickly jumped to 1.68N at 20,000 RPM. It should be noted that this spindle speed is where the best surface finish was found, also with one of the lowest waviness peak heights in all experiments. From here the force plummeted to 1.36N at 25,000 RPM. Interestingly the shift in forces also mimics the shift in waviness where it was practically non-existent at 20,000 RPM, to being a major detriment at 25,000 RPM. This shows potentially that lower forces could be related to drill instability. From here the forces slowly increase as the spindle speed increases, however so did waviness in the SEM images, suggesting that cutting forces may not be linked to waviness.

Mill D: Meisinger HMB23G was the only coated mill used in these studies and was coated with

a DLC layer. Owing to its coating, lower coefficients of friction, superior edge wear and lower cutting forces were expected. Although it did show lower cutting forces at 10,000 RPM and 15,000 RPM (1.50N and 1.50N respectively) than Mills A and C, they were nowhere near as low as the values found for Mill B. Furthermore high amounts of mill drop off occurred, with partial drop off at 20,000 RPM, 25,000 RPM, 30,000 RPM and complete drop off at 35,000 RPM. Mill D followed the pattern of Mill A where it jumped up to a maximum cutting force value at 20,000 RPM (1.70N) and then fell almost linearly to a minimum value at 30,000 RPM (1.33N). Despite earlier beliefs from SEM images and roughness data that the DLC coating had worn off after the 10,000 RPM, the cutting force values either do not seem to reflect this, or do not seem to be affected by the presence of the DLC coating.

It was mentioned earlier about the possibility of the increase of drill instability leading to a decrease in cutting force. This was partially shown with Mills A and D dropping significantly in force from 20,000 RPM to 30,000 RPM, and Mill C following this trend to a lower extent. However one thing that is unanimously seen is the increase in drill instability from 30,000 RPM to 35,000 RPM, and cutting forces for Mills A and C increase from 30,000 RPM to 35,000 RPM while Mill D experienced a complete drop off and could not sufficiently mill CoCrMo at this speed. This seems to oppose the belief that instability leads to lower cutting forces. Though for unknown reasons, Mills A, C and D did experience the highest milling forces at 20,000 RPM. While Mill B has a completely different reaction and seems generally unaffected by spindle speed in AR CoCrMo, and generally decreases in cutting forces while spindle speed increases while milling HT4H CoCrMo, with exception of 35,000 RPM where it increases in value from the value at 30,000 RPM.

6.5. Minimum Chip Thickness Effect

The minimum chip thickness effect is an issue believed to be deeply relevant to this study, though still relatively new in literature, with no direct research found relating to CoCrMo. The key features of this theory are the transition from ploughing to chip formation when the h/r ratio reaches a certain limit, often approximated to 0.3 with multiple materials and tool geometry. Unfortunately milling with multi-faced conical mills creates such a complex and intertwined mechanism that it is hard to identify just one effect occurring. Mill vibrations were the major detriment in this study, making it hard to identify mill performance and separate it from chatter and general instability. One area this was possible was very low speeds where excess vibrations had not yet taken effect. In a perfect milling experiment with complete stability and no interference it is stated that a saw tooth-like profile would be present indicating that minimum chip thickness effect is occurring, as shown in Figure 72.

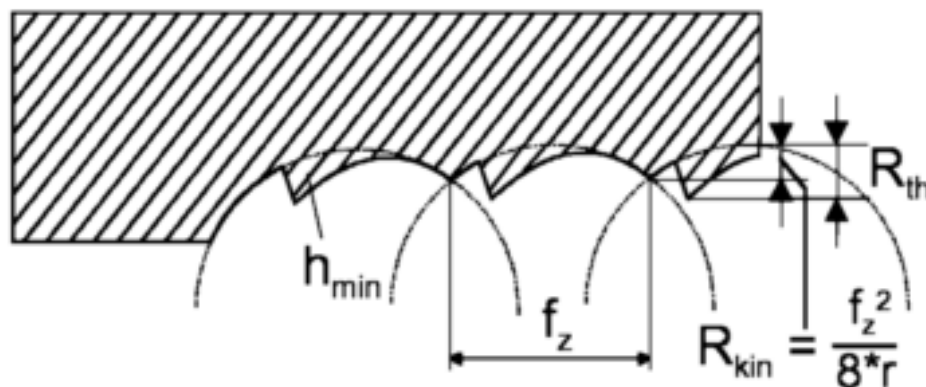


Figure 72 Saw tooth profile typical of the minimum chip thickness effect. V. Huntrup et al. (53).

Figure 72 shows the saw tooth profile; note milling is occurring from right to left as in this study, however the milling occurring in the image is up-milling while in this study down-milling was used. The overall profile will be similar, but reversed due to the mill cutting in the opposite direction. One example of a surface finish like this was in the surface milled by Mill A at 10,000 RPM. Calculations in Section 5.7.2 led to an h/r ratio of 0.0129 for Mill A at 10,000 RPM, well below the recommended 0.3. In this case it would be expected to see ploughing and compression to have occurred until such time that a chip thickness had built up at which point it would be sheared off. This would lead to the saw tooth-like profile shown in Figure 72. Figure 73 shows the surface milled by Mill A at 10,000 RPM, where both conditions of the minimum chip thickness can be seen with 'ripple bands' making up the saw tooth-like profile

and heavy gouging in between these bands likely caused by ploughing from the BUE on the mill. Although ploughing is indicated by arrows in the lower section of the image it should be noted that this occurs across the whole image and only an example of ploughing is being pointed to. Chip rewelding is also shown, though this is believed to be due to excess frictional heat and the way in which the chips were retained in the mill flutes. However, ploughing would certainly lead to excess frictional heat. This is believed to be a good example of the effects of minimum chip thickness and shows probable cause that the minimum chip thickness effect was occurring. This also further reinforces the theory that an adequate h/r value had not been reached with the selected spindle speeds, feed rate and mill geometry used in this study. Unfortunately at higher spindle speeds waviness and mill vibration led to chaotic surfaces, and analysis became increasingly difficult. Heavy gouging was shown in nearly every specimen indicating that ploughing was occurring heavily throughout this study, and it is known ploughing occurs when h/r is below the minimum value required to form complete chips.

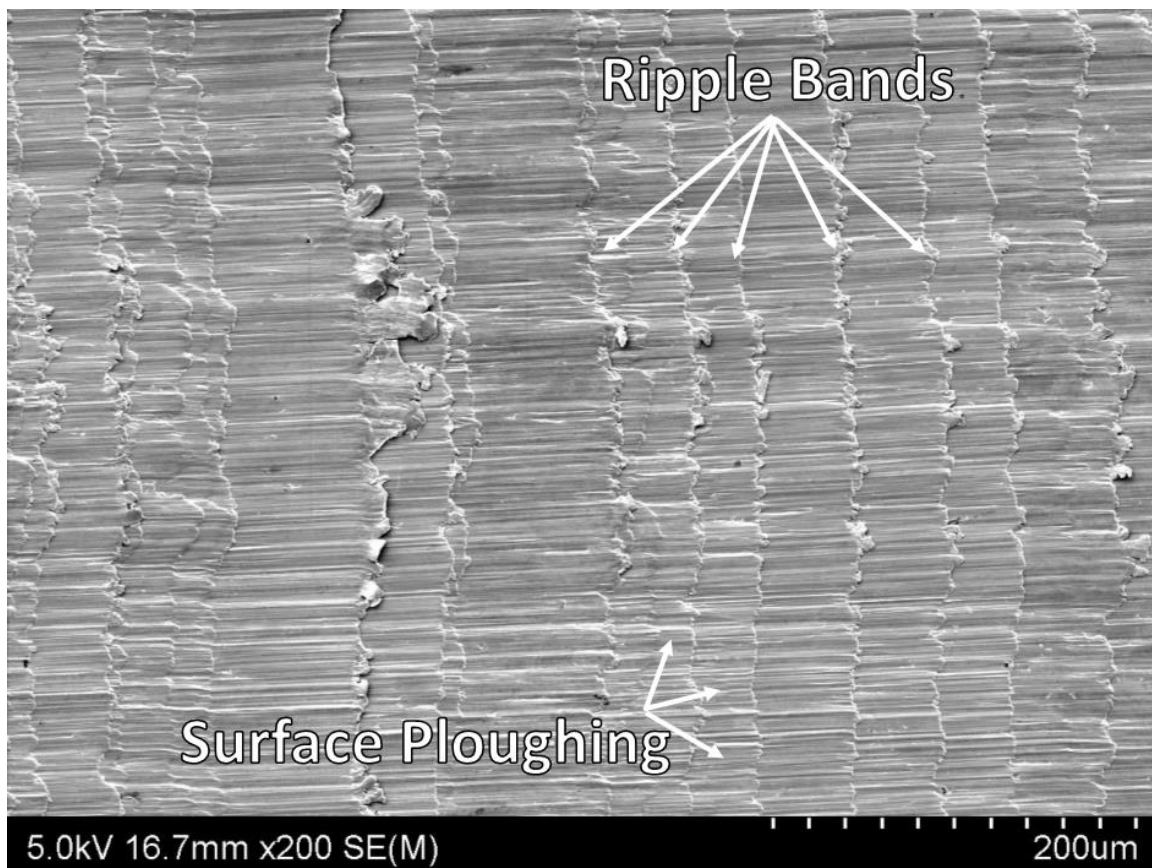


Figure 73 Minimum chip thickness analysis of the surface milled by Mill A at 10,000 RPM.

Although the tool edge radius measurements shown in the previous section are largely inaccurate, even with high allowances for errors it is clearly shown that the h/r values in this experiment are far below the recommended ratios of approximately 0.3. The highest calculated h/r value was of Mill C at 10,000 RPM, where a value of 0.0360 was calculated. This is just under a tenth of the recommended value. Very slow feed speeds are recommended for milling CoCrMo, however 0.15 mm/s is near a practical minimum. It would appear that other parameters such as edge radius, or flutes per revolution need to be investigated. Though this is not definitive proof, the author strongly believes that the minimum chip thickness effect is playing a crucial role in the acquired surface and needs to be further investigated.

6.6. Mill Gyration and Run-out

Run-out deviation is an issue of particular relevance in micro-machining. Whereas in conventional macro-milling operations, a small runout will have insignificant effects on the forces and mill wear, tool run-out in micro-machining can be extremely detrimental. This is especially so when the feed per tooth is as low as $0.257\ \mu\text{m}$ (value at 35,000 RPM in this study), as at such small feeds even a run-out of nanometres will have a significant effect on the mechanism between the mill and the surface. In face milling this run-out can lead to some of the tool flutes cutting chips thicker than expected while others fail to make contact with the surface. Run-out can never be completely avoided, it can only be minimised. In macro-machining this is usually enough, however in the case of micro-machining this minimization may need to be investigated further. No measurements of run-out were undertaken during this study but as the calculations were done and the feed per tooth was revealed to be as low as $0.257\ \mu\text{m}$ it became quite unreasonable to believe run-out was not having some significant effect. Run-out deviation is caused by bearing size deviations in the spindle assembly and clamping errors, this causes the mill to rotate not coaxially to the bearings. This is explained in Figure 74 sourced from work done by P. Connor et al. (57).

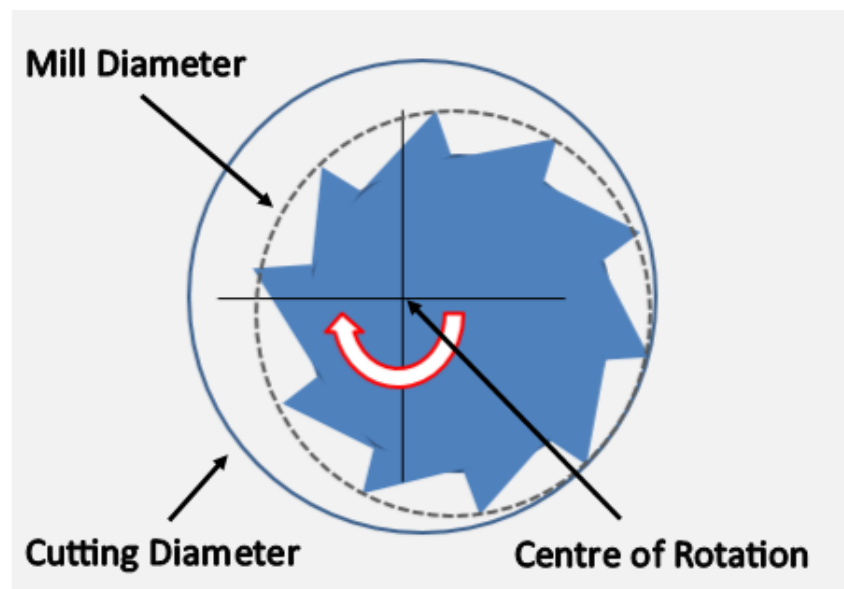


Figure 74 Run-out deviation diagram. P. Connor et al (57)

Figure 74 illustrates the principle of run-out deviation due to the spindle system of the milling tool, the mill diameter is shown as well as the direction of rotation. Further you can see the centre of rotation, notice how this is not in line with the mill's centre, this leads to run-out and the cutting diameter being larger than the diameter of the mill. Owing to the off-balance

rotation excessively thick chips will be cut by some edges while other edges do not make contact with the surface at all. As mentioned earlier, though this was not directly measured in this study the author strongly believes that with such miniscule feeds per tooth this needs to be investigated further. J. Pathak et al. (33) also shared this belief and investigated the use of air bearings in their ultra-high-speed micro milling spindle, however even then they found the run-out experienced in their design to be too severe.

Mill gyration is another mechanism that occurs during machining which is hugely detrimental to the surface finish. One factor that is believed to be responsible for mill gyration is the relatively long slender shape that makes up these mills. This long slender design leads to limited stiffness in bending and torsion. While milling is undertaken, the unsteady forces normal and parallel to the workpiece surface cause the mill to vibrate against the contact surface. This can almost certainly be stated to be occurring due to the significant amount of waviness shown in the previous SEM images. This is demonstrated in Figure 75 from work done by P. Connor et al. (57).

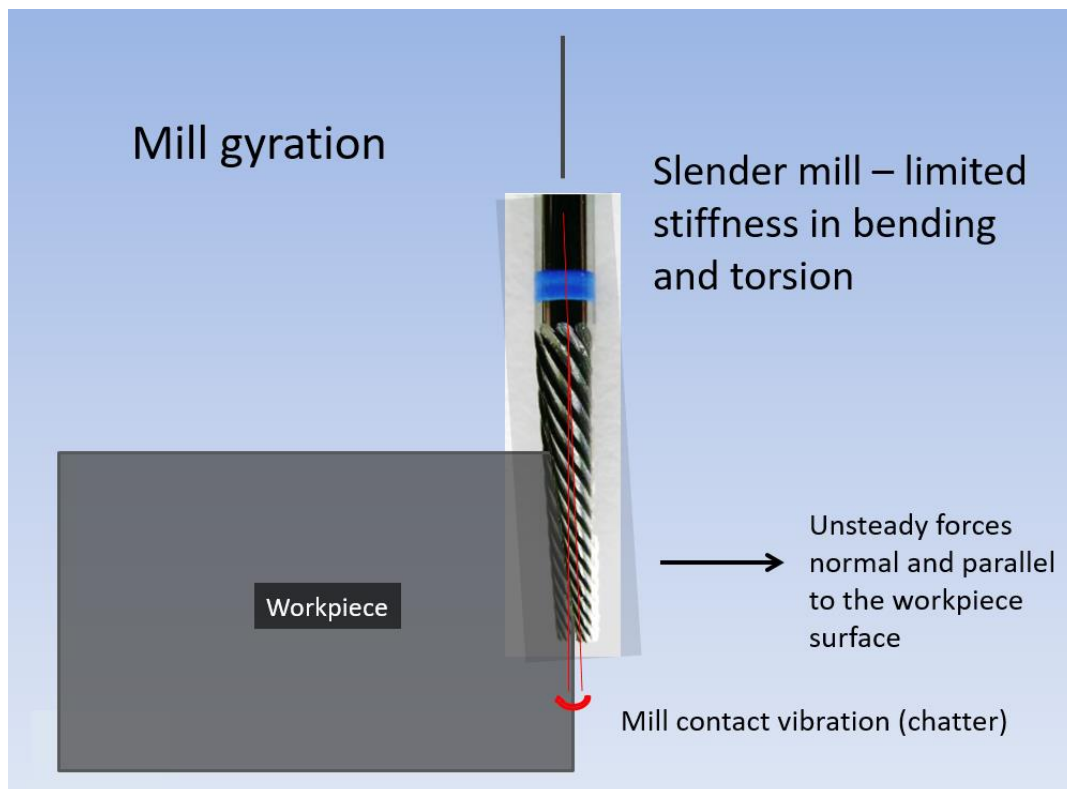


Figure 75 Mill gyration diagram. P. Connor et al. (57)

Poor clamping, mill run-out deviation and mill gyration occur in sync with each other leading to the hugely detrimental condition known as chatter occurring. Chatter is a form of self-

continued vibration that occurs when the tool, tool holder and spindle vibrate at natural frequencies. The assembly will often vibrate at multiple natural frequencies at the same time causing what is known as waviness, this variable load feeds the already existing vibrations which exponentially increase in severity as it feeds on itself. The fact that both waviness and incomplete milling passes increased in severity with increasing spindle speeds shows that these excess forces and run-out were leading to massive amounts of chatter occurring at higher spindle speeds.

6.7. Implications and Limitations of Study

The goal of this study was to fill the gap in the literature relating to the milling of CoCrMo alloys. A lack of literature exists concerning the milling of CoCrMo, and since this is a common dental alloy, information relating to optimal machining parameters should be well documented in order for dental implants to meet the highest obtainable surface finish quality.

The research methodology used in this study can be thought of as an experimental approach where the experiment-observation-conclusion strategy was employed. This strategy is a common occurrence in all areas of scientific research and the advantages of this method are the ease of implementation and the potential for very good results to be obtained. There are some negative aspects of this methodology though and they are generally to do with the ease in which the experiment can lead to unexpected results due to the many complex phenomena and factors occurring in milling. Also, due to the equipment used and the speciality in each study, there is little general applicability of the conclusions drawn. Regardless of the speciality of this study, or the lack of general applicability, the author believes that a reasonable area of machining CoCrMo has been evaluated and therefore the lack of literature has been slightly reduced. The aim of this study was to observe the milled CoCrMo specimens and combine these evaluations with recorded cutting force data and roughness testing data to draw conclusions as to the parameters required to provide the best surface finish. Furthermore, by identifying common defects and discussing the believed causations, future improvements in the milling of CoCrMo can be made.

Owing to the complex nature of interacting mechanisms occurring during the milling in this study, there were no definite optimal milling parameters found that would result in an ideal surface finish. This could be considered as a limitation of the research undertaken. The research did however provide strong insights into the common detriments and speculated on the causation of these. Furthermore, cutting force data, roughness data and a large library of SEM images have been captured allowing further research to move forward from this point. A second limitation of this study was its generally wide scope. Various research has been undertaken into cutting forces, surface analysis and roughness testing with multiple mills at varying spindle speeds. This work combined with the inquiries into the annealed samples involving etching and micro-hardness testing means that a vast amount of knowledge has

been obtained, though no specific area has been thoroughly investigated. In conclusion it can be said that though the vast scope of this study provides a solid foundation for further research, it does limit the impact and certainty of the conclusions drawn.

The biomedical field, specifically the dental industry, requires implants to be of the highest standards acquirable for successful implant performance, as well as patient health and comfort. Multiple studies have shown that a poor surface finish can lead to plaque retention and oral disease. This study showed that despite the surfaces appearing smooth and even showing low Ra values, they are microscopically rough and can lead to poor performance in respect to biocompatibility. This research contributes to the available literature offering insight into potentially hazardous and unnoticed microscopic defects. By releasing this information the implications are safer and better performing dental and medical implants for patients worldwide.

6.8. Further Thoughts

Throughout this study there have been no exceptionally well performing milling operations. Trends showed lower speeds (<25,000 RPM) provided a better surface finish but no obviously superior parameters were revealed. For example roughness testing and cutting forces showed Mill B was superior, however visible inspection of SEM images showed surfaces milled by Mill B were relatively poor and tool life was the lowest. SEM analysis showed the surface milled by Mill C at 20,000 RPM was the best achieved and Mill C exhibited good tool life, however roughness values and cutting forces show Mill C did not perform better than any other mill. Mill D was coated in a DLC coating and was expected to show significantly lower cutting forces and better surface finishes, however neither of these were shown.

From these mixed and seemingly random results it cannot be said with any confidence that one set of parameters should be used over another. Milling with multi faced conical mills is an extremely complex process and there was no obvious pattern found. The main issue arises from the amounts of chatter and vibration experienced during these experiments. It can be quite confidently said that better surfaces were found at lower speeds, due to the lack of chatter, however it is not definitively known whether these mills at higher spindle speeds would have produced better results if the chatter was minimised.

Controlling these vibrations will be crucial to further studies. Long slender mills with limited stiffness can be thought to be a contributing factor to the excessive vibrations. Another area that needs investigation is tool run-out deviation. An axial run-out, even on a nanoscale could be leading to the mill striking the surface harder part way through each revolution. This off-balance rotation could potentially be creating mill vibration, and this, combined with the gyration of the slender mills, could lead to all sorts of harmonic vibrations.

Previous studies done by T. Pasang et al. (28) and M. Takahashi (29) showed that chip rewelding was the most detrimental mechanism occurring while milling CoCrMo. As expected, chip rewelding proved to be one of the most significant issues faced in this study. In general, chip rewelding seemed to increase with increasing spindle speed, which is logical due to the increasing frictional heat generated at higher speeds. However, this rewelded material was generally found on both the peak ridges of the large waviness formations and the smaller ridges inside these formations. This could potentially link rewelding to mill chatter and vibrations, rather than strictly to spindle speed. It is believed also that excessive vibration will affect the way chips are retained in the mill flutes and thus effect how they are frictionally

rewelded.

One of the most significant realisations throughout this study was how severely the effects of micro-machining can change the milling dynamics. Micro-machining is still widely discussed with no definitive answer for h/r values. Various values have been reported though and values of approximately 0.3 seem generally accepted (32,34,35,54). Very basic calculations were undertaken in this study with tool edge measurements estimated from SEM images. The author accepts that these measurements are inaccurate at best and only serve as a guideline, though the huge difference between theoretical h/r values calculated in this study and recommended h/r values is apparent. Areas of the minimum chip thickness arguments are often confusing and contradicting. Various authors state that by increasing the spindle speed the minimum h/r value is decreased, however increasing spindle speed leads to a lower cutting thickness per tool edge and therefore further drops the achieved h/r value. One way to achieve a lower value is to lower the spindle speed, though speeds below 10,000 RPM are likely to increase cutting forces significantly. Slowing the feed rate would result in a lower h/r ratio, though the feed rate is already minimal at 0.15mm/sec. It seems that less tool flutes is the most reasonable option to increase h/r . One final possibility is entering the experimental area of ultra-high-speed milling with spindle speeds of approximately 200,000 RPM, though it is hard to imagine mill vibration would be able to be controlled at this speed.

Perhaps the most logical way to progress from this study is to focus on controlling mill vibration and chatter as this should lead to improved surface finishes overall, and lower tool wear. Also without excess vibrations, the obtained results will be more reliable and drawing conclusions should be more impactful. If vibrations are linked to chip rewelding then this should also lead to a minimized amount of chip rewelding. Furthermore, chip rewelding can be further minimised by the addition of flood milling to aid in lubrication and lower the temperatures of the workpiece, mill and formed chips. Finally, tool coatings should be further investigated as R. Polini et al. (31) showed that CVD diamond coated mills exhibited lower cutting forces than non-coated mills as well as a longer tool life while milling CoCrMo. The combination of lower chatter/vibrations, less rewelding and lower cutting forces is expected to lead to significantly better surface finishes. Furthermore the data obtained will be of more relevance and serve to remove some of the complexity that occurred in this study. If all the above is controlled and progress is made then effects involving the minimum chip thickness theory can be investigated with a reliable base platform already existing.

7.0. Conclusion

In this study the examination of laterally face milled cobalt-chromium-molybdenum (CoCrMo) specimens was undertaken. Milled specimens were provided for analysis along with cutting force measurements taken during milling. SEM images were captured of each surface. Furthermore, micro-hardness testing and roughness testing were undertaken where available.

- Mill B showed significantly lower cutting forces for both AR CoCrMo and HT4H CoCrMo, than all three other mills. Mill B with AR CoCrMo was generally unaffected by spindle speed and forces remained consistent around approximately 0.8N. Mill B with HT4H CoCrMo showed approximately 0.7N at 10,000 RPM then continued decreasing up to spindle speeds of 30,000 RPM where it reached approximately 0.4N. It then increased slightly at 35,000 RPM. Mills A, C and D increased in cutting force from 10,000 RPM to a max value at 20,000 RPM. From here they dropped to a minimum value at 30,000 RPM, then they once again increased in value to 35,000 RPM (where applicable). These forces occurred between the ranges of 1.4N to 1.9N approximately. Mills A and D experienced some drop off where the mill geometry and cutting forces led to the spindle loosening.
- Roughness testing data suggested a trend in roughness increasing as spindle speeds increased, though at higher speeds a fair amount of milling passes were not completed leading to incomplete data sets. Individually the results mostly conclude that increasing spindle speed leads to increasing roughness. Mill A and D agree completely with this trend. Mill B showed a continuous increase with exception of a spindle speed of 30,000 RPM. Mill C was the only mill to not agree with this trend and showed a decrease in value from 10,000 RPM to 15,000 RPM, then a consistent increase in value to 30,000 RPM before dropping slightly at 35,000 RPM. Since only two completed data sets are available, and one agrees with this trend (Mill B) and one does not (Mill C), the trends in roughness vs spindle speeds need to be investigated further. Mill B provided the lowest roughness values, with Mill C in second place.
- Micro-hardness testing showed a decrease in hardness as the time spent at 1200°C increased. As-received (AR) CoCrMo showed a HV300/10 hardness average of 402HV, with CoCrMo annealed for two hours (HT2H) showing a value of 368HV, and CoCrMo annealed for four hours (HT4H) showing 356HV.

- While many surfaces visually appeared smooth, and showed low Ra values, they were microscopically rough. The roughness levels were heavily affected by chip rewelding, mill vibrations, mill wear and the minimum chip thickness effect. Both chip rewelding and waviness increased as spindle speed increased. The majority of chip rewelding occurred on/or near the waviness peaks, suggesting that mill vibration affects the way chips are retained in the flutes and are frictionally rewelded to the surface.
- Specimens milled with Mill A showed high amounts of rewelding and waviness. Mill B provided low Ra values and low cutting forces though under microscopic investigation regions of craters, ploughing and horizontal gouging were shown to lead to a detrimental surface. Mill C provided the best surface finish at 20,000 RPM, with very little rewelded material and signs of minimal mill vibrations. However, at 25,000 RPM and above, vibrations and waviness led to very detrimental surfaces for Mill C. Mill D provided a good surface at 10,000 RPM with low amounts of rewelded material and mill vibrations, however at 15,000 RPM and above, mill instability and high amounts of rewelded material led to poor surfaces. HT4H CoCrMo milled by Mill B showed far lower quality surface finishes than AR CoCrMo milled with Mill B, with high amounts of mill instability, gouging, ploughing and rewelded material present.
- Tool life for mills A, C and D were comparable with BUE formations, entangled chips, adhered material and BUE induced edge fractures occurring, however they were not catastrophically damaged. Mill B showed the lowest tool life with large edge fractures and major chipping leading to a complete failure.
- A DLC coating was shown to be inappropriate for milling CoCrMo. Though low roughness values and a microscopically good surface finish at 10,000 RPM with mill D showed that tool coatings had potential if not rapidly worn. Mill D showed the lowest recorded Ra at 10,000 RPM before showing the second highest Ra value at any speed at 15,000 RPM, this indicating the DLC coating was worn as early as after the 10,000 RPM pass. The SEM analysis showed a good surface finish obtained at 10,000 RPM while at 15,000 RPM it was very poor, this tending to agree with the theory of the DLC coating was worn early.
- Minimum chip thickness was evaluated and showed that, with the tool edge radii, feed rates, spindle speeds and feed depth per edges used in this study, the calculated h/r ratios were far below the recommended values for chip formation to occur.

8.0. Further Work

- Mill chatter needs to be eliminated in order to truly understand how surface roughness changes with spindle speed. The obtained information regarding surface finish and mill tool life is complex and intertwined with events occurring due to chatter and excess vibrations. Although conclusions have been drawn, the removal of mill vibration would lead to more impactful results and conclusions.
- R. Polini et al. (31) showed that CVD diamond coated mills exhibited lower cutting forces than non-coated mills as well as a longer tool life while milling CoCrMo. Despite exhibiting good results at 10,000 RPM, the DLC coated mill showed no significantly lower cutting forces, tool life or better surface finishes than the non-coated mills. SEM images showed major edge wear had removed the DLC coating. There is a need to investigate diamond coated mills further in order to obtain the best possible surface finish. TiN and AlCrN coated tools are recommended.
- Mill run-out deviation needs to be investigated on a micro-scale as this could potentially be contributing to chatter, excessive tool wear and poor surface finish. The spindle system visually appears to securely hold the mill in position; however with such small cutting depth per tool edge (less than $1\mu\text{m}$) even deviations of a few nanometres could be detrimental.
- Milling with lubrication was recommended by M. Takahashi et al. (29) to reduce chip rewelding. In this study milling oil was manually sprayed onto the surface and although a reduction did occur, chip rewelding was still a significant issue. Flood milling is recommended to be investigated along with other cooling/lubrication methods.
- In order to further understand how annealing affected the CoCrMo specimens' mechanical properties it is recommended that a successful etchant be found. This is an area lacking significant literature and investigating this would be beneficial to the engineering community.
- The minimum chip thickness theory is recommended to be evaluated and investigated further. A more detailed tool edge radius should be obtained to lead to more accurate h/r values being found. By use of different mill geometry, forward speeds, spindle speeds or a combination of all, an h/r value of 0.3 should be obtained and the resulting surface finish and force measurements analysed.

References

1. Bordin A, Ghiotti A, Bruschi S, Facchini L, Bucciotti F. Machinability characteristics of wrought and EBM CoCrMo alloys. *Procedia CIRP* [Internet]. Elsevier B.V.; 2014;14:89–94. Available from: <http://dx.doi.org/10.1016/j.procir.2014.03.082>
2. Viennot S, Francis D, Malquarti G, Grosogeat B. Combination fixed and removable prostheses using a CoCr alloy: A clinical report. *J Prosthet Dent*. 2006;96(2):100–3.
3. Chun K, Prior DJ, Waddell JN, Swain M V, Cam CAD. Comparison of the microstructure and phase stability of as-cast, CAD / CAM and powder metallurgy manufactured Co – Cr dental alloys. *Dent Mater* [Internet]. The Academy of Dental Materials; 2015;31(12):e306–15. Available from: <http://dx.doi.org/10.1016/j.dental.2015.10.010>
4. Takaichi A, Nakamoto T, Joko N, Nomura N. Microstructures and mechanical properties of Co – 29Cr – 6Mo alloy fabricated by selective laser melting process for dental applications. *J Mech Behav Biomed Mater* [Internet]. Elsevier; 2013;21:67–76. Available from: <http://dx.doi.org/10.1016/j.jmbbm.2013.01.021>
5. Yamanaka K, Mori M, Chiba A. Assessment of precipitation behavior in dental castings of a Co – Cr – Mo alloy. *J Mech Behav Biomed Mater* [Internet]. Elsevier; 2015;50:268–76. Available from: <http://dx.doi.org/10.1016/j.jmbbm.2015.06.020>
6. Bellfontaine G. The Corrosion of CoCrMo Alloys for Biomedical Applications [Internet]. University of Birmingham; 2010. Available from: <papers2://publication/uuid/D3611780-AA0A-4FAA-8CC8-4651D8B48A2B>
7. Bordin A, Bruschi S, Ghiotti A. The effect of cutting speed and feed rate on the surface integrity in dry turning of CoCrMo alloy. *Procedia CIRP* [Internet]. Elsevier B.V.; 2014;13:219–24. Available from: <http://dx.doi.org/10.1016/j.procir.2014.04.038>
8. Cawley J, Metcalf JEP, Jones AH, Band TJ, Skupien DS. A tribological study of cobalt chromium molybdenum alloys used in metal-on-metal resurfacing hip arthroplasty. *Wear*. 2003;255:999–1006.
9. Chiba A. Pin-on-disk wear behavior in a like-on-like configuration in a biological environment of high carbon cast and low carbon forged Co – 29Cr – 6Mo alloys. *Acta Mater*. 2007;55:1309–18.
10. Ezugwu EO. Key improvements in the machining of difficult-to-cut aerospace superalloys. *Int J Mach Tools Manuf*. 2005;45:1353–67.
11. Giacchi J V, Morando CN, Fornaro O, Palacio HA. Microstructural characterization of as-cast biocompatible Co – Cr – Mo alloys. *Mater Charact* [Internet]. Elsevier Inc.; 2010;62(1):53–61. Available from: <http://dx.doi.org/10.1016/j.matchar.2010.10.011>
12. Henriques B, Soares D, Silva FS. Microstructure, hardness, corrosion resistance and porcelain shear bond strength comparison between cast and hot pressed CoCrMo alloy for metal-ceramic dental restorations. *J Mech Behav Biomed Mater* [Internet]. Elsevier Ltd; 2012;12:83–92. Available from: <http://dx.doi.org/10.1016/j.jmbbm.2012.03.015>
13. Isik M, Niinomi M, Cho K, Liu H, Nakai M, Yilmazer H, et al. Microstructural evolution and mechanical properties of biomedical Co-Cr-Mo alloy subjected to high-pressure torsion. *J Mech Behav Biomed Mater* [Internet]. Elsevier; 2015;59:226–35. Available from: <http://dx.doi.org/10.1016/j.jmbbm.2015.11.015>

14. Karpuschewski B, Pieper HJ, Krause M, Döring J. Future Trends in Production Engineering: Proceedings of the First Conference of the German Academic Society for Production Engineering (WGP), Berlin, Germany, 8th-9th June 2011. In: Schuh G, Neugebauer R, Uhlmann E, editors. Berlin, Heidelberg: Springer Berlin Heidelberg; 2013. p. 261–74. Available from: http://dx.doi.org/10.1007/978-3-642-24491-9_26
15. Saldivar-Garcia AJ, Lopez HF. Microstructural effects on the wear resistance of wrought and as-cast Co-Cr-Mo-C implant alloys. Wiley InterScience. 2005. p. 269–74.
16. Mori M, Yamanaka K, Chiba A. Cold-rolling behavior of biomedical Ni-free Co – Cr – Mo alloys : Role of strain-induced ϵ martensite and its intersecting phenomena. J Mech Behav Biomed Mater [Internet]. Elsevier; 2016;55:201–14. Available from: <http://dx.doi.org/10.1016/j.jmbbm.2015.10.021>
17. Buford A, Goswami T. Materials & Design Review of wear mechanisms in hip implants : Paper I – General. Mater Des. 2004;25:385–93.
18. Niinomi M, Nakai M, Hieda J. Acta Biomaterialia Development of new metallic alloys for biomedical applications. Acta Biomater [Internet]. Acta Materialia Inc.; 2012;8(11):3888–903. Available from: <http://dx.doi.org/10.1016/j.actbio.2012.06.037>
19. Liao Y, Pourzal R, Stemmer P, Wimmer MA, Jacobs JJ, Fischer A, et al. New insights into hard phases of CoCrMo metal-on-metal hip replacements. J Mech Behav Biomed Mater [Internet]. Elsevier Ltd; 2012;12:39–49. Available from: <http://dx.doi.org/10.1016/j.jmbbm.2012.03.013>
20. Wataha JC. Alloys for prosthodontic restorations. J Prosthet Dent. 2002;87(4):351–63.
21. Mori M, Yamanaka K, Kuramoto K, Ohmura K, Ashino T, Chiba A. Effect of carbon on the microstructure , mechanical properties and metal ion release of Ni-free Co – Cr – Mo alloys containing nitrogen. Mater Sci Eng C [Internet]. Elsevier B.V.; 2015;55:145–54. Available from: <http://dx.doi.org/10.1016/j.msec.2015.05.058>
22. Yan Y, Neville A, Dowson D. Tribo-corrosion properties of cobalt-based medical implant alloys in simulated biological environments. Wear. 2007;263(7-12 SPEC. ISS.):1105–11.
23. Biomechaniki AP. METALLOGRAPHIC ANALYSIS OF SELECTED COBALT-. Aktual Probl Biomech. 2011;(5):183–90.
24. Bollen CM, Lambrechts P, Quirynen M. Comparison of surface roughness of oral hard materials to the threshold surface roughness for bacterial plaque retention: a review of the literature. Dent Mater. England; 1997 Jul;13(4):258–69.
25. Quirynen M, Bollen CM. The influence of surface roughness and surface-free energy on supra- and subgingival plaque formation in man. A review of the literature. J Clin Periodontol. DENMARK; 1995 Jan;22(1):1–14.
26. Grossner-Schreiber B, Griepentrog M, Haustein I, Muller WD, Lange KP, Briedigkeit H, et al. Plaque formation on surface modified dental implants. An in vitro study. Clin Oral Implants Res. Denmark; 2001 Dec;12(6):543–51.
27. Tanner J, Carlen A, Soderling E, Vallittu PK. Adsorption of parotid saliva proteins and adhesion of *Streptococcus mutans* ATCC 21752 to dental fiber-reinforced composites. J Biomed Mater Res B Appl Biomater. United States; 2003 Jul;66(1):391–8.
28. Pasang T, Takahashi M, Shinohara D, Connor P, Tanaka K, Kamiya O. Machining of Metallic

- Biomaterials: Comparisons between Co-Cr-Mo and Ti-Al-Nb. In: 26th European Conference on biomaterials. Liverpool; 2014.
29. Takahashi M, Pasang T, Conor P, Ono H, Tanaka K, Kamiya O. Machining Cobalt-Based Dental Alloys with Tungsten Carbide Millis. *Int J Soc Mater Eng Resour.* 2014;Vol.20(No.2):163–9.
 30. Deshpande A, Yang S, Puleo D, Pienkowski D, Dilon O, Outeiro JJ, et al. Minimized Wear and Debris Generation Through Optimized Machining of Co-Cr-Mo Alloys for Use in Metal-on-Metal Hip Implants. In: *ASME International Manufacturing Science and Engineering Conference.* Notre Dame, Indiana.: ASME; 2012. p. 297–305.
 31. Polini R, Allegri A, Guarino S, Quadrini F, Sein H, Ahmed W. Cutting force and wear evaluation in peripheral milling by CVD diamond dental tools. *Thin Solid Films.* 2004;470:161–6.
 32. Brandão F, Oliveira D, Roger A, Teixeira R, Fagali A, Souza D. International Journal of Machine Tools & Manufacture Size effect and minimum chip thickness in micromilling. *Int J Mach Tools Manuf* [Internet]. Elsevier; 2015;89:39–54. Available from: <http://dx.doi.org/10.1016/j.ijmachtools.2014.11.001>
 33. Pathak JP. DESIGN, ASSEMBLY, AND TESTING OF AN ULTRA-HIGH-SPEED MICRO-MILLING SPINDLE. UNIVERSITY OF FLORIDA; 2003.
 34. Ducobu F, Rivière-lorphèvre E, Filippi E. Chip Formation in Micro-cutting. *J Mech Eng Autom.* 2013;3:441–8.
 35. Lai X, Li H, Li C, Lin Z, Ni J. Modelling and analysis of micro scale milling considering size effect , micro cutter edge radius and minimum chip thickness. *Int J Mach Tools Manuf.* 2008;48:1–14.
 36. Aslantas K, Hopa HE, Percin M. Cutting performance of nano-crystalline diamond (NCD) coating in micro-milling of Ti 6 Al 4 V alloy. *Precis Eng.* 2016;45:55–66.
 37. Beruvides G, Castaño F, Quiza R, Haber RE. Surface roughness modeling and optimization of tungsten – copper alloys in micro-milling processes. *MEASUREMENT* [Internet]. Elsevier Ltd; 2016;86:246–52. Available from: <http://dx.doi.org/10.1016/j.measurement.2016.03.002>
 38. Autenrieth H, Strauß T, Deuchert M, Hoffmeister J, Schulze V. Journal of Materials Processing Technology Characterization of the transition from ploughing to cutting in micro machining and evaluation of the minimum thickness of cut. *J Mater Process Tech* [Internet]. Elsevier B.V.; 2012;212(3):594–600. Available from: <http://dx.doi.org/10.1016/j.jmatprotec.2011.07.007>
 39. U.S. Food and Drug Administration. Implants and Prosthetics [Internet]. 2015 [cited 2016 May 12]. p. 1. Available from: <http://www.fda.gov/MedicalDevices/ProductsandMedicalProcedures/ImplantsandProsthetics/>
 40. Lucchetti MC, Fratto G, Valeriani F, Vittori E De. Cobalt-chromium alloys in dentistry : An evaluation of metal ion release. *J Prosthet Dent* [Internet]. Editorial Council for the Journal of Prosthetic Dentistry; 2015;114(4):602–8. Available from: <http://dx.doi.org/10.1016/j.prosdent.2015.03.002>
 41. Jabbari YS Al, Koutsoukis T, Barmpagadaki X, Zinelis S. Metallurgical and interfacial characterization of PFM Co – Cr dental alloys fabricated via casting ,. *Dent Mater* [Internet]. The Academy of Dental Materials; 2014;30(4):e79–88. Available from:

- <http://dx.doi.org/10.1016/j.dental.2014.01.008>
42. Oberg E, Jones FD, Horton HL, Ryffel HH. Machinery's Handbook. 26th ed. New York: Industrial Press Inc.; 2000. 699-702 p.
 43. Benardos PG, Vosniakos G. Predicting surface roughness in machining : a review. *Int J Mach Tools Manuf.* 2003;43:833–44.
 44. Deutsches Institut für Normung. Form deviations: concepts, classification system : DIN 4760. Berlin: DIN Deutsches Institut für Normung; 1982. 1-3 p.
 45. Zahouani H. Proceedings of the 10th International Conference on Metrology and Properties of Engineering Surfaces. In: Zahouani H, editor. Proceedings of the 10th International Conference on Metrology and Properties of Engineering Surfaces. Saint-Etienne: Université de Saint-Etienne; 2005. p. 145.
 46. Tefan T, Stach S, Klaić B. Morphology of Co – Cr – Mo Dental Alloy Surfaces Polished by Three Different Mechanical Procedures. *Microsc Res Tech.* 2015;78(May):831–9.
 47. Gough JE, Clupper DC, Hench LL. Osteoblast responses to tape-cast and sintered bioactive glass ceramics. *J Biomed Mater Res A. United States;* 2004 Jun;69(4):621–8.
 48. Aydin AK. Evaluation of finishing and polishing techniques on surface roughness of chromium-cobalt castings. *J Prosthet Dent. UNITED STATES;* 1991 Jun;65(6):763–7.
 49. Ishida K, Nishizawa T. The Co-Cr (Cobalt-Chromium) system. *Bull Alloy Phase Diagrams [Internet].* 1990;11(4):357–70. Available from: <http://dx.doi.org/10.1007/BF02843315>
 50. Matković T, Matković P, Malina J. Effects of Ni and Mo on the microstructure and some other properties of Co–Cr dental alloys. *J Alloys Compd [Internet].* 2004 Mar 10;366(1–2):293–7. Available from: <http://www.sciencedirect.com/science/article/pii/S0925838803007618>
 51. López HF, Saldivar-Garcia AJ. Martensitic Transformation in a Cast Co-Cr-Mo-C Alloy. *Metall Mater Trans A [Internet].* 2008;39(1):8–18. Available from: <http://dx.doi.org/10.1007/s11661-007-9370-8>
 52. Onderka F, Kadlec J. Microstructural Characterization, Chemical Composition and Hardness of As-Cast Biocompatible CoCrMo Alloy. *Littera Scr - Tech Nat Sci Sect.* 2013;6(2):184–94.
 53. Huntrupl V, Tritschlerl H, Weule H. Steel to Meet New Requirements in Miniaturization. *CIRP Ann - Manuf Technol.* 2001;50(1):61–4.
 54. Malekian M, Mostofa MG, Park SS, Jun MBG. Journal of Materials Processing Technology Modeling of minimum uncut chip thickness in micro machining of aluminum. *J Mater Process Tech [Internet].* Elsevier B.V.; 2012;212(3):553–9. Available from: <http://dx.doi.org/10.1016/j.jmatprotec.2011.05.022>
 55. Hassanpour H, Sadeghi MH, Rasti A, Shajari S. Investigation of surface roughness , microhardness and white layer thickness in hard milling of AISI 4340 using minimum quantity lubrication. *J Clean Prod [Internet].* Elsevier Ltd; 2016;120:124–34. Available from: <http://dx.doi.org/10.1016/j.jclepro.2015.12.091>
 56. mdpi. 3D Surface Scan [Internet]. 2016 [cited 2016 Jul 13]. p. 1. Available from: http://www.mdpi.com/sensors/sensors-13-04906/article_deploy/html/images/sensors-13-04906f6-1024.png

57. Conor P, Takahashi M, Pasang T, Ono H, Tanaka K, Kamiya O. Machining cobalt-based dental alloys with tungsten carbide mills. In: NZ Microscopy Conference. Dunedin; 2015. p. 1–17.

Glossary

AC = As-cast

AR CoCrMo = CoCrMo specimens as supplied by the manufacturer

BUE = Built up Edge

CoCr = Cobalt Chromium Alloys

CoCrMo = Cobalt-chromium-molybdenum Alloys

CVD = Chemical Vapour Deposition

DLC = Diamond-like carbon Coating

DOC = Depth of Cut

EDS = Energy-dispersive X-ray spectroscopy

h = Cutting thickness

h_{min} = Minimum thickness of cut

HC = High Carbon

HT = Heat Treatment Undergone

HT2H = CoCrMo specimens annealed at 1200°C for 2 hours then water quenched.

HT4H = CoCrMo specimens annealed at 1200°C for 4 hours then water quenched.

LC = Low carbon

LS = Laser Sintering

MUCT = Minimum uncut chip thickness

NiCr = Nickel Chromium

R = Tool edge radius

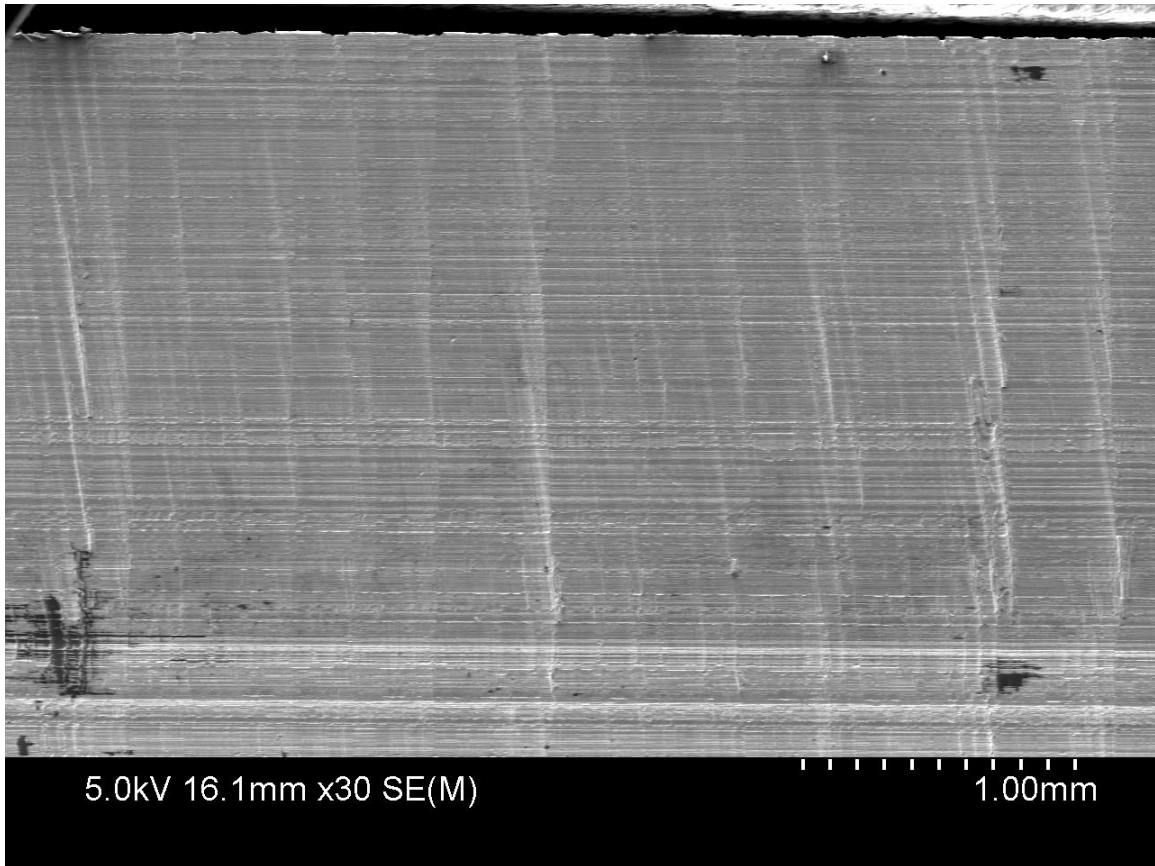
Ti = Titanium

SEM = Scanning Electron Microscopy

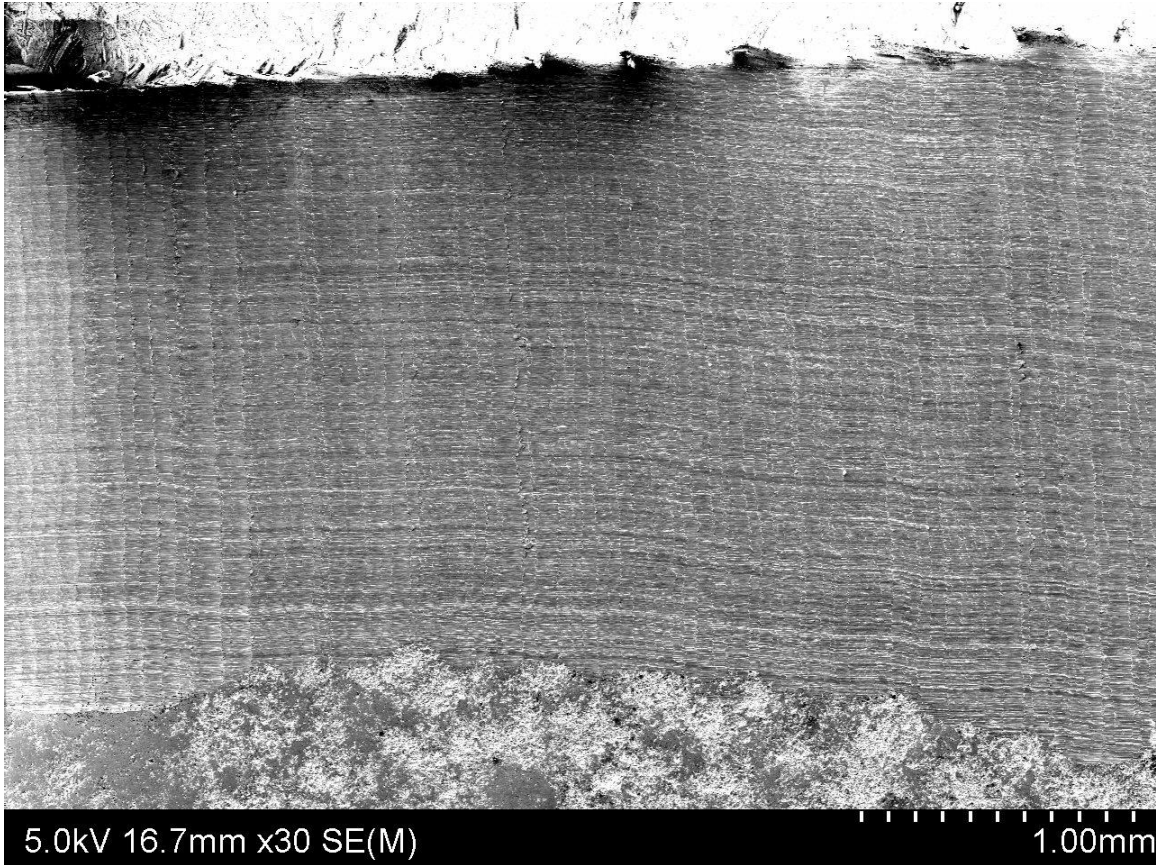
WC = Tungsten Carbide

Appendices

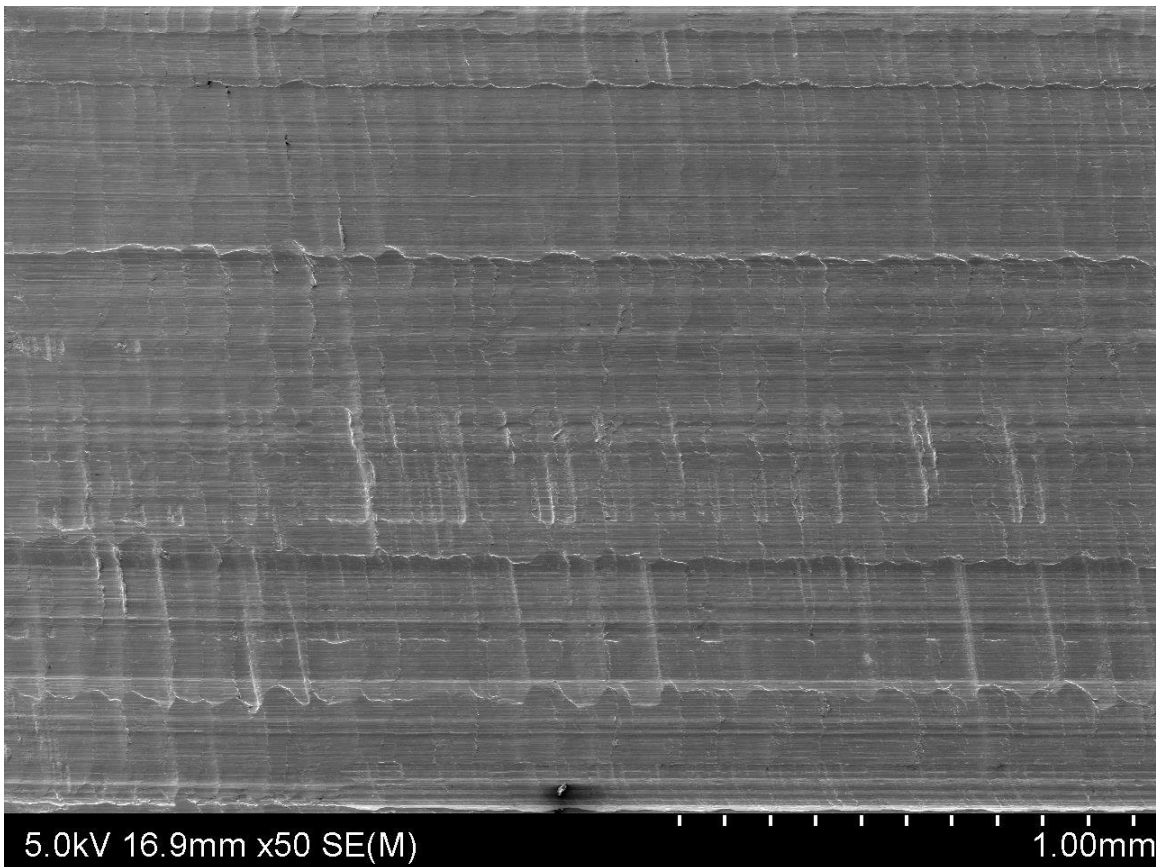
Appendices A1: SEM Images of surfaces milled at 10,000 RPM.



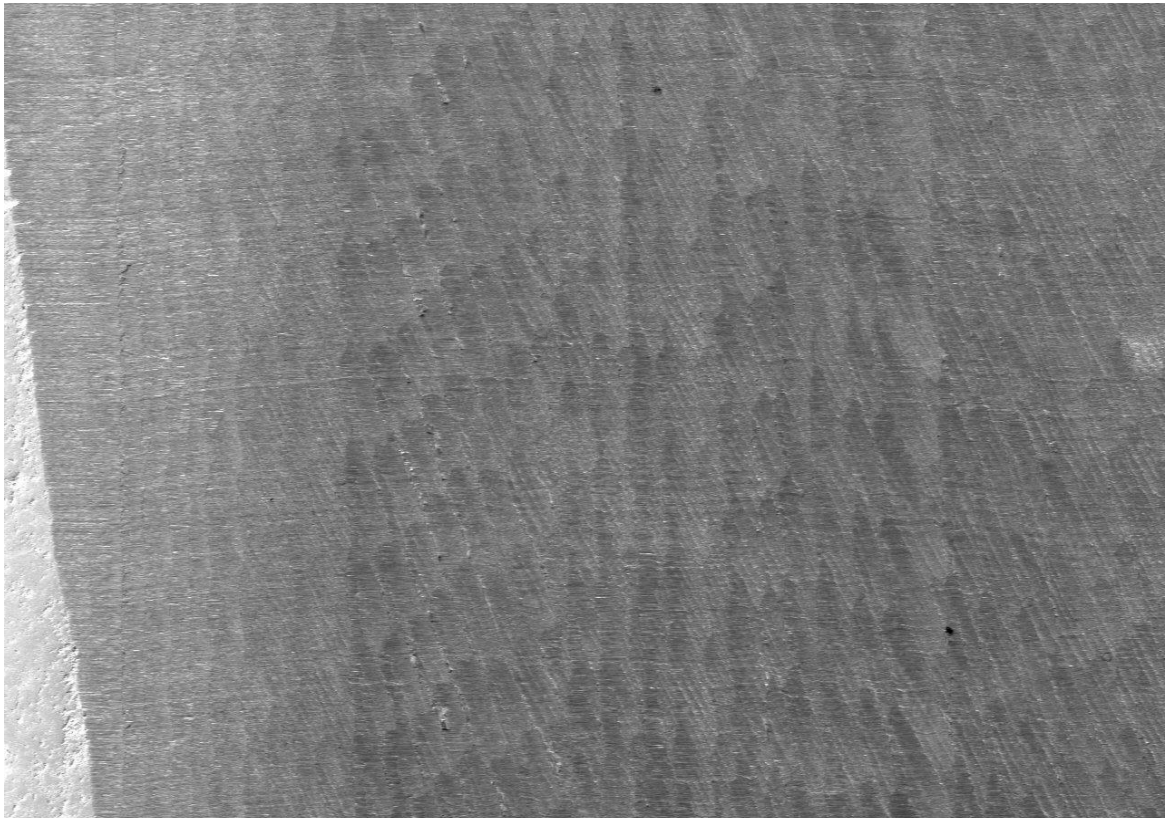
HT4H CoCrMo milled with Mil B.



AR CoCrMo milled with Mill A.



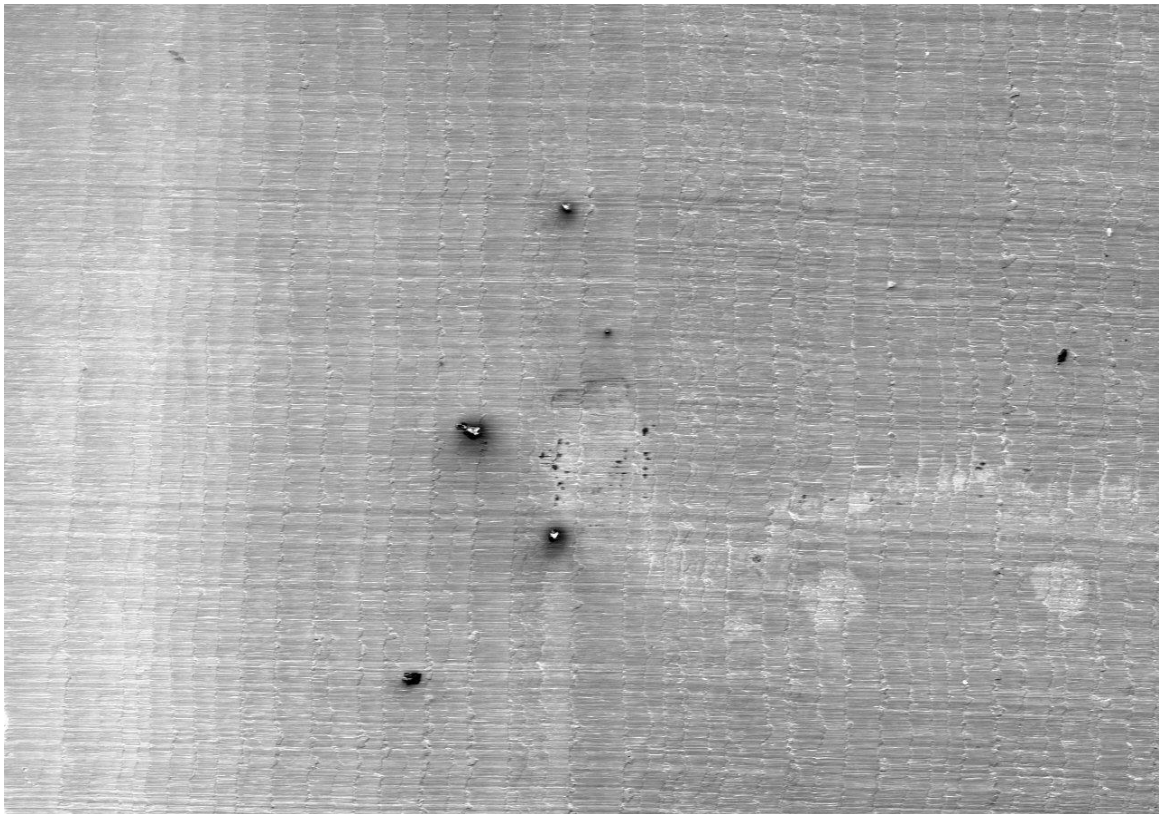
AR CoCrMo milled with Mill B.



5.0kV 16.5mm x30 SE(M)

1.00mm

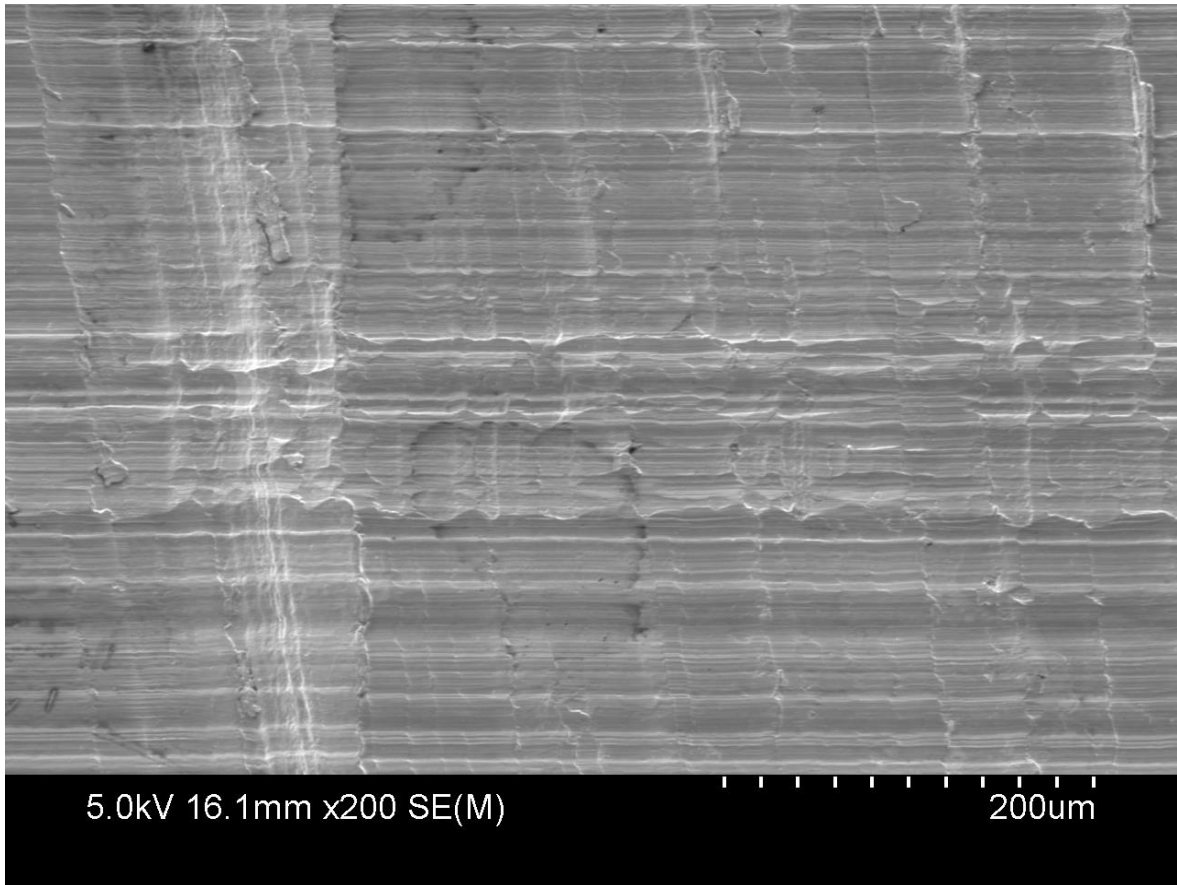
AR CoCrMo milled with Mill C.



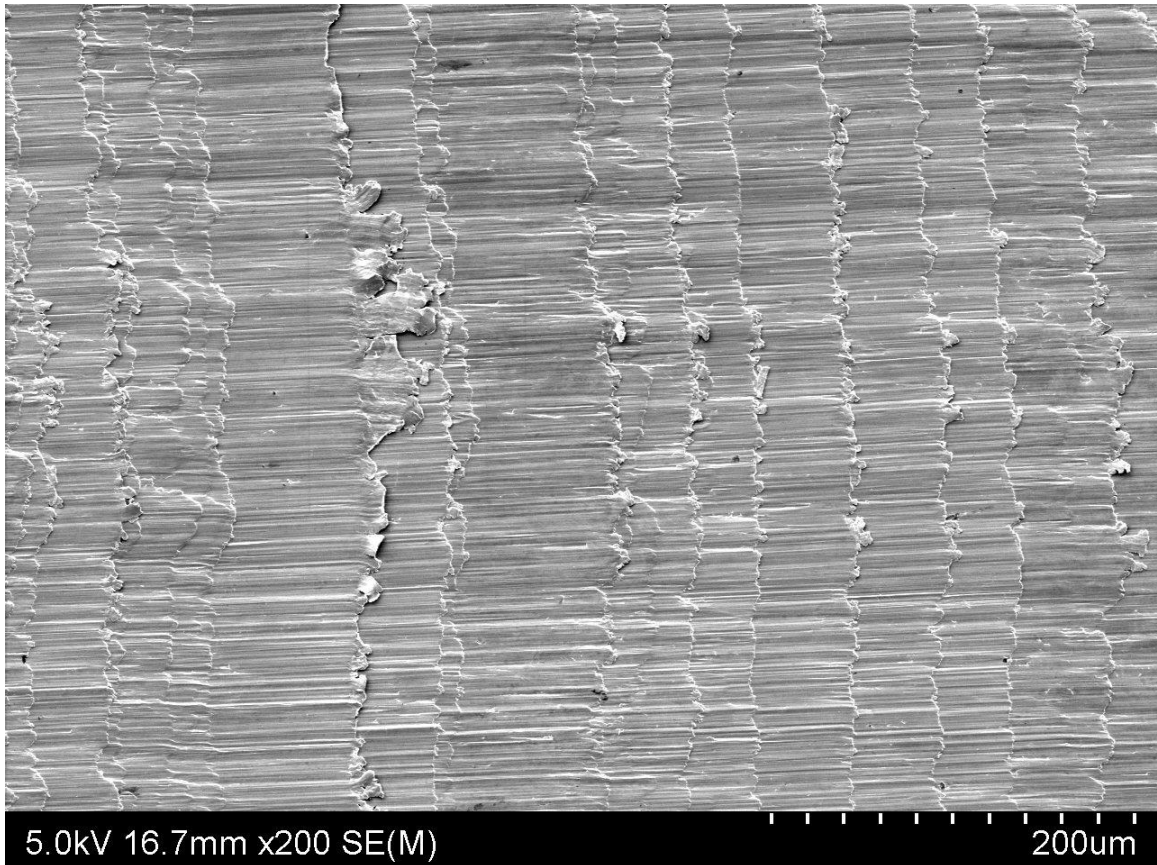
5.0kV 16.8mm x50 SE(M)

1.00mm

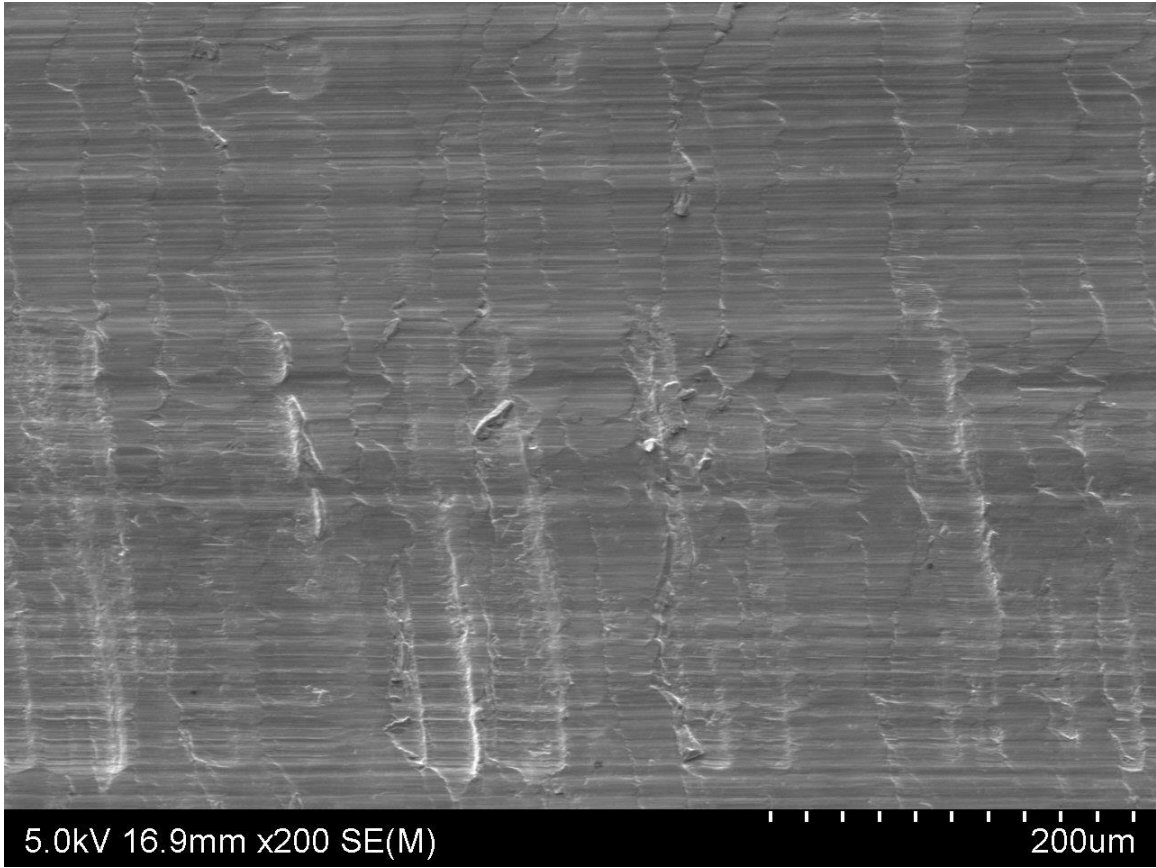
AR CoCrMo milled with Mill D.



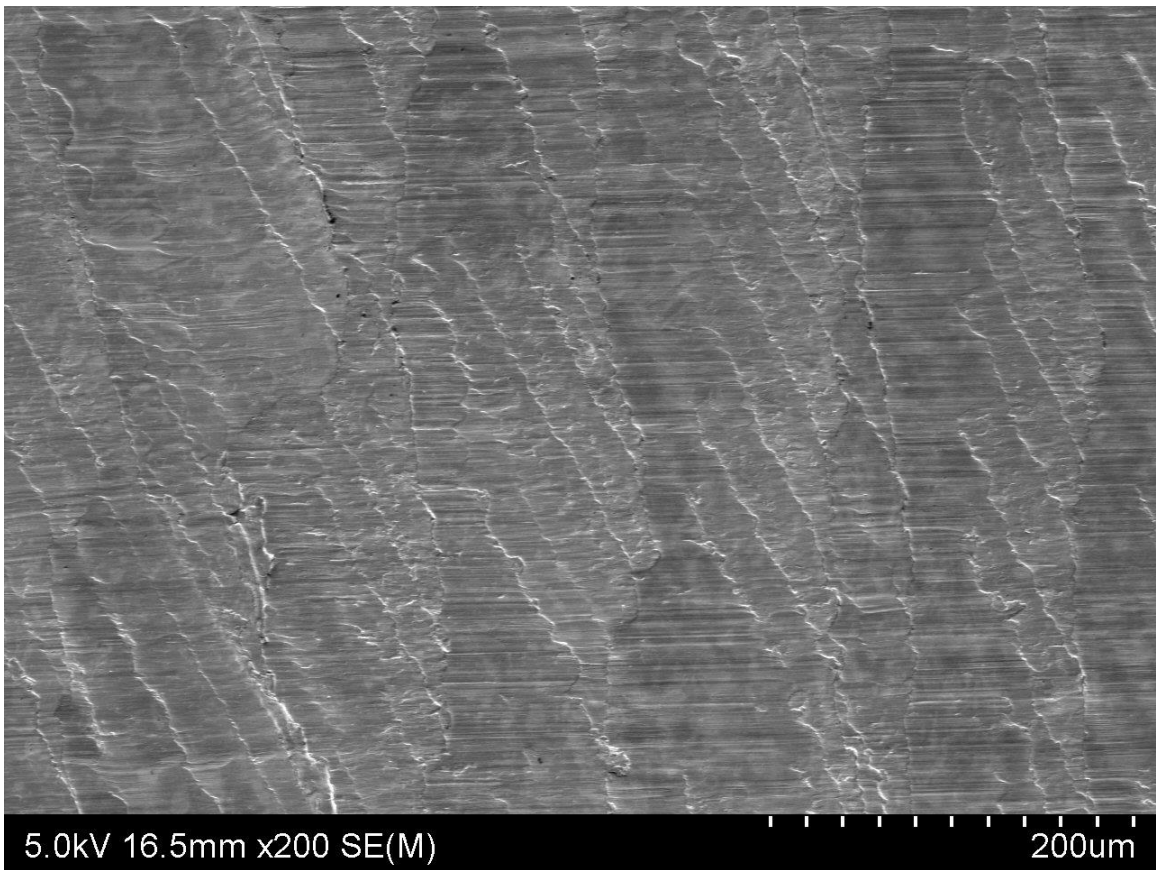
HT4H CoCrMo milled with Mill B.



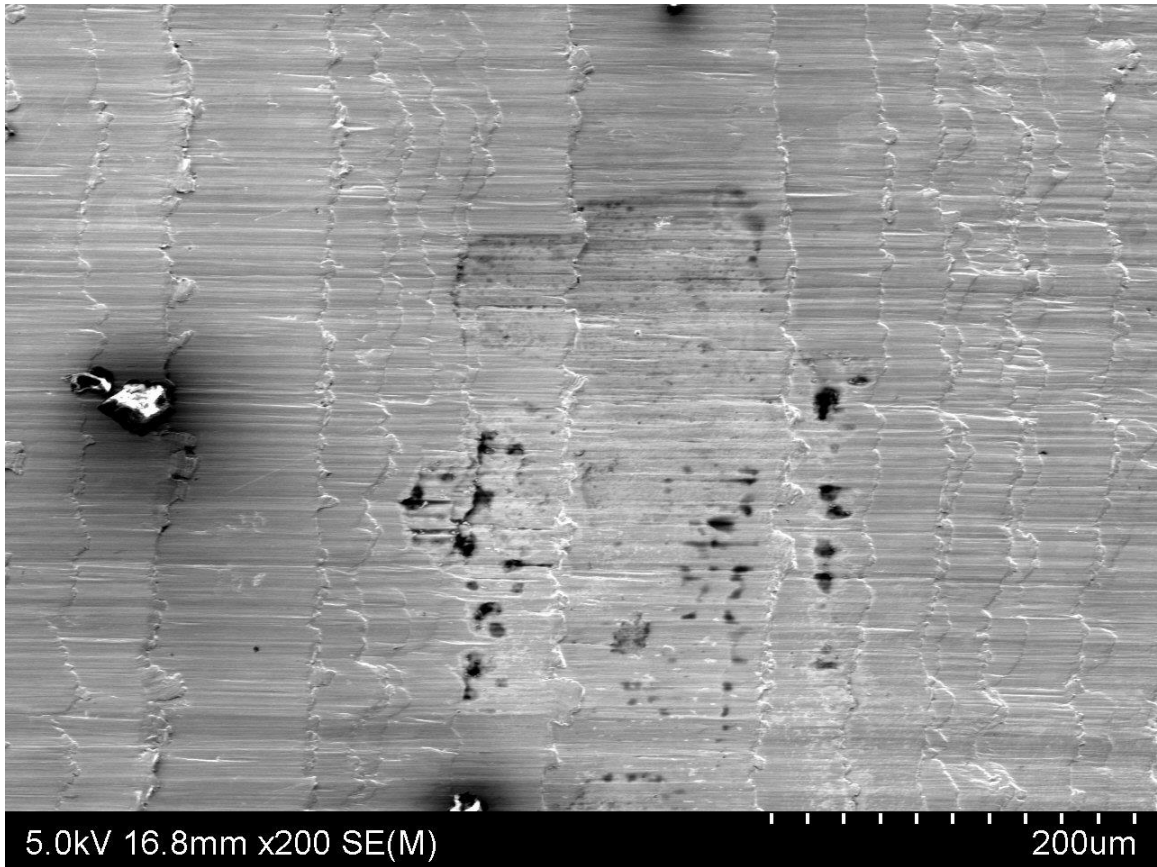
AR CoCrMo milled with Mill A.



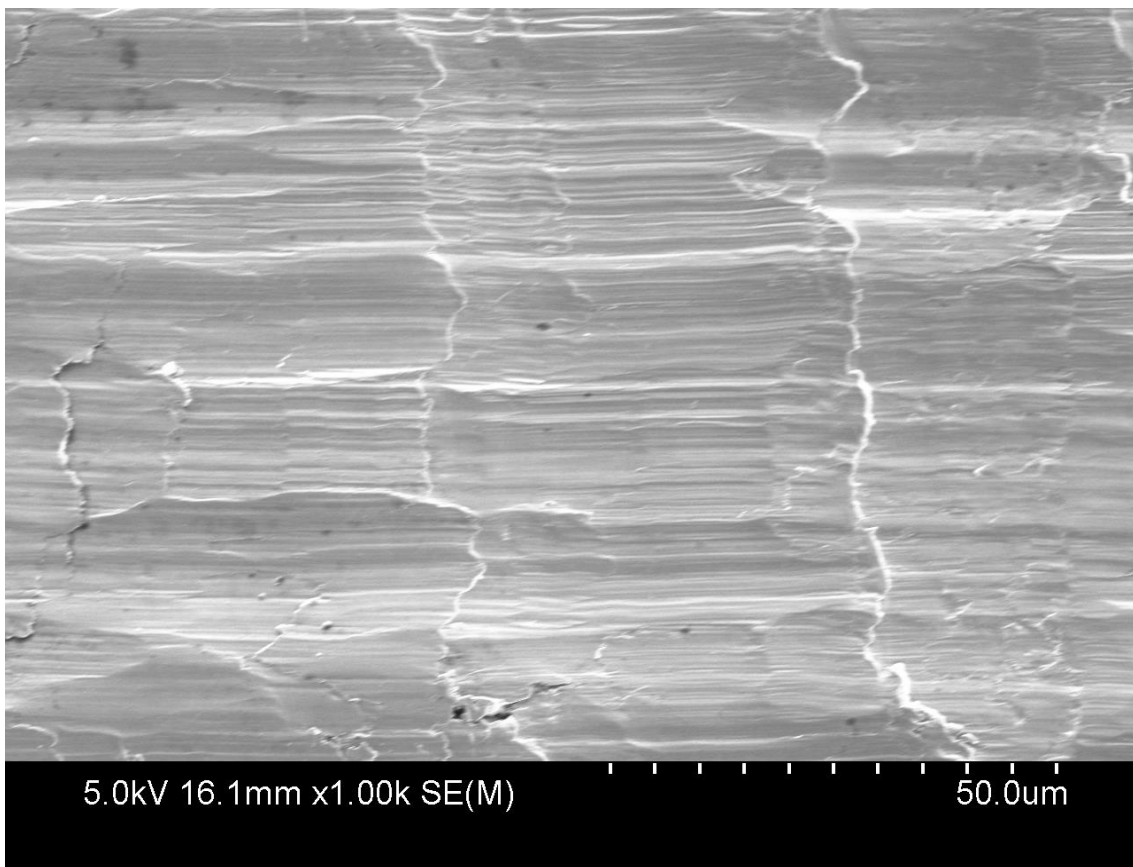
AR CoCrMo milled with Mill B.



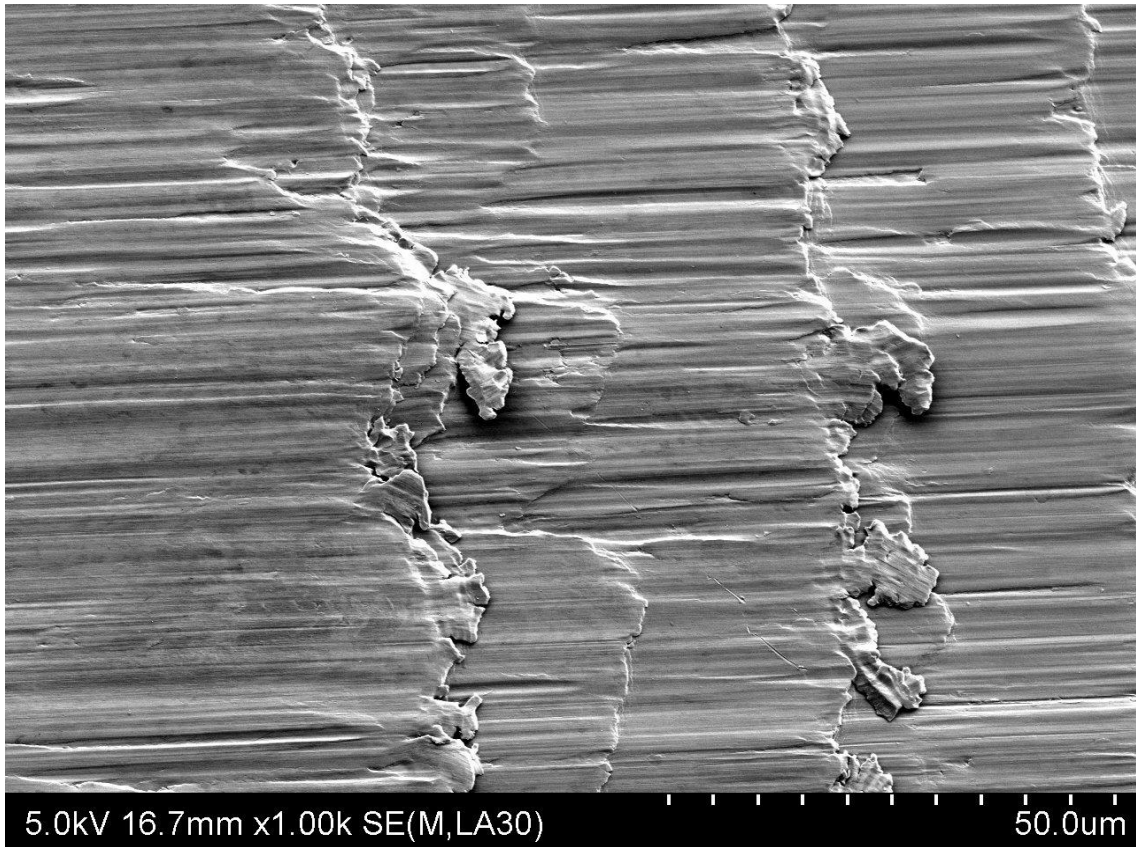
AR CoCrMo milled with Mill C.



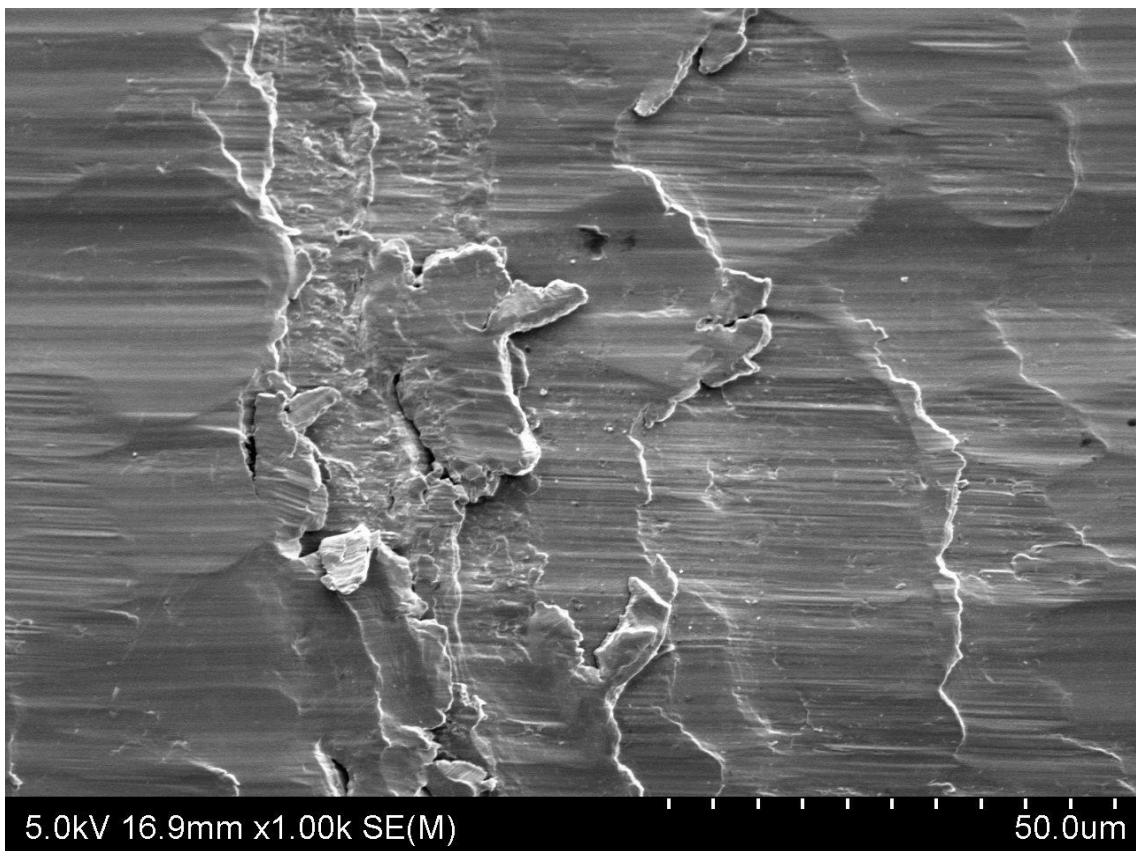
AR CoCrMo milled with Mill D.



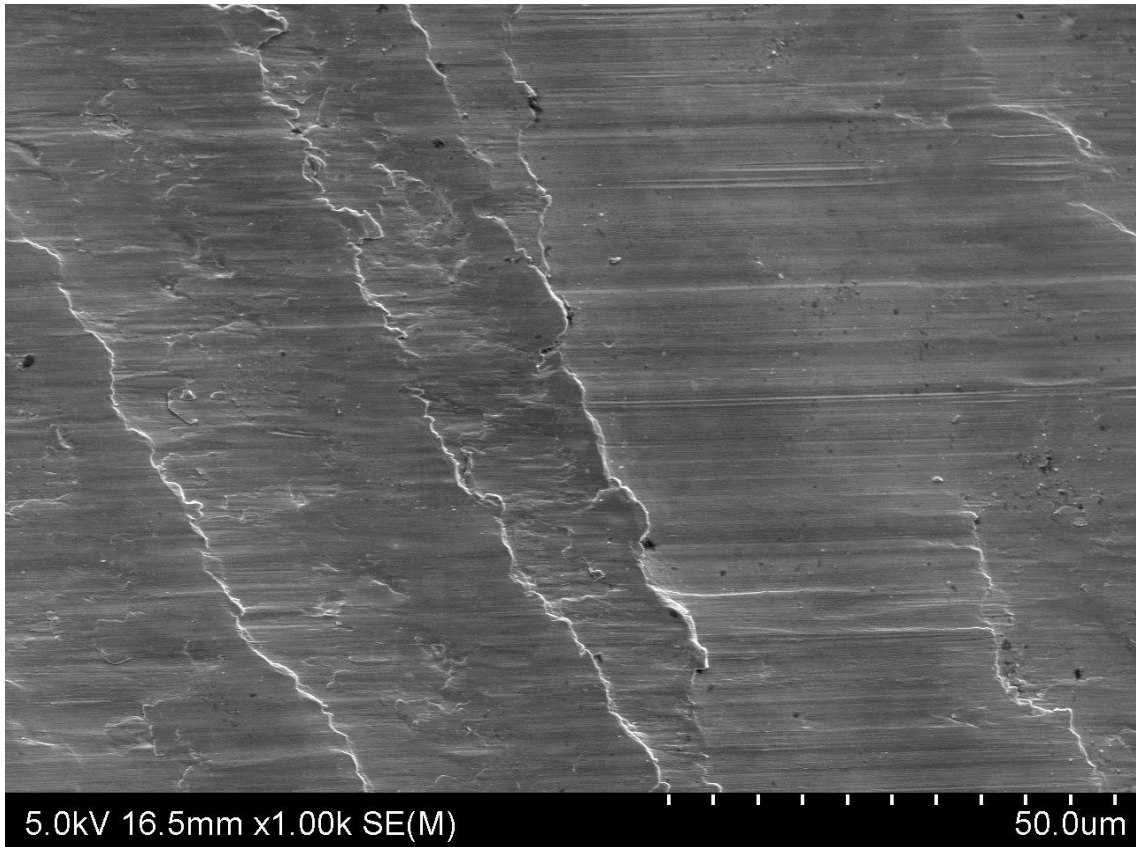
HT4H CoCrMo milled with Mill B.



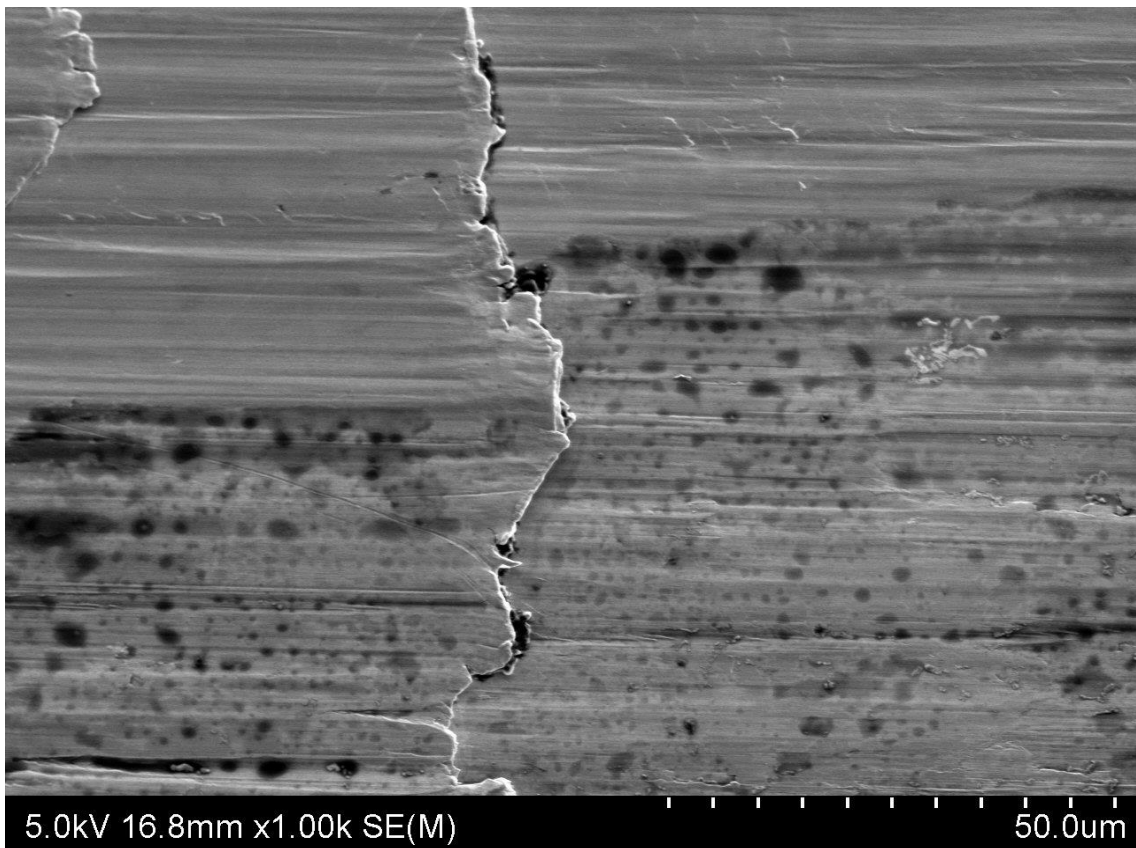
AR CoCrMo milled with Mill A.



AR CoCrMo milled with Mill B.

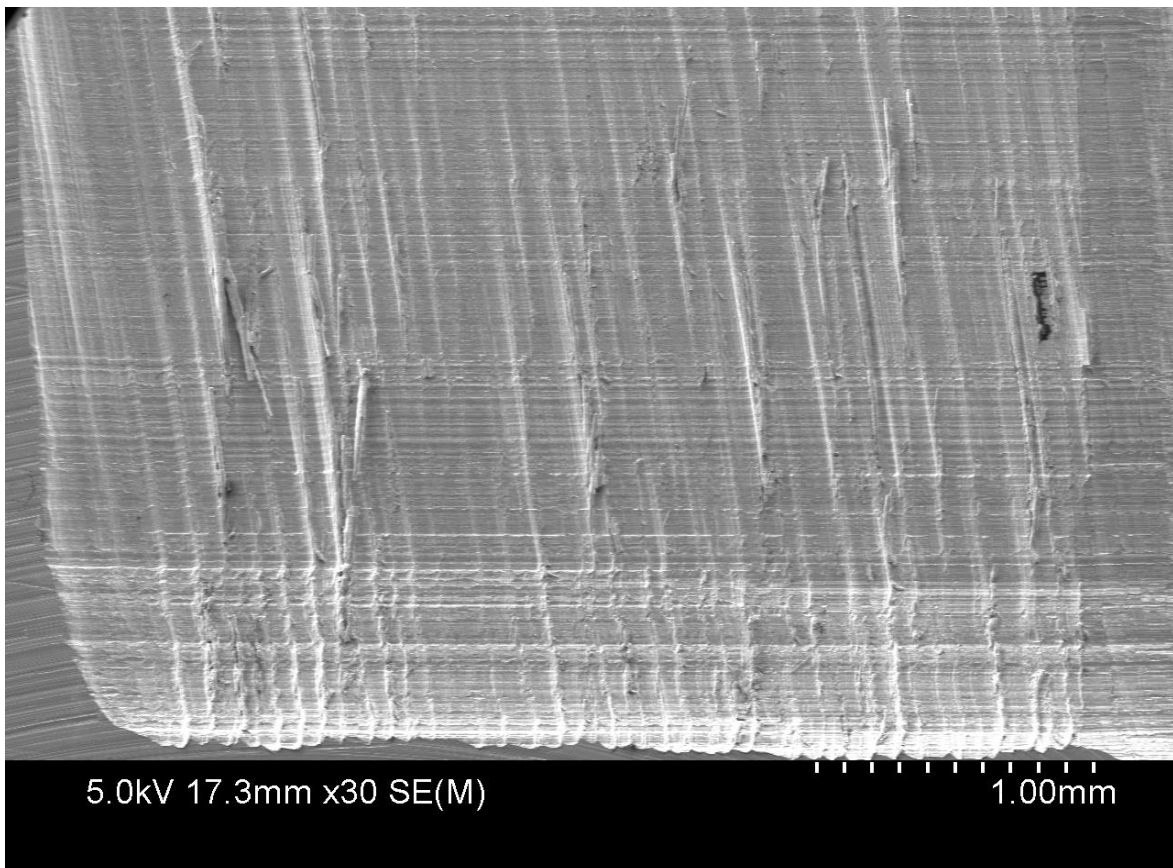


AR CoCrMo milled with Mill C.

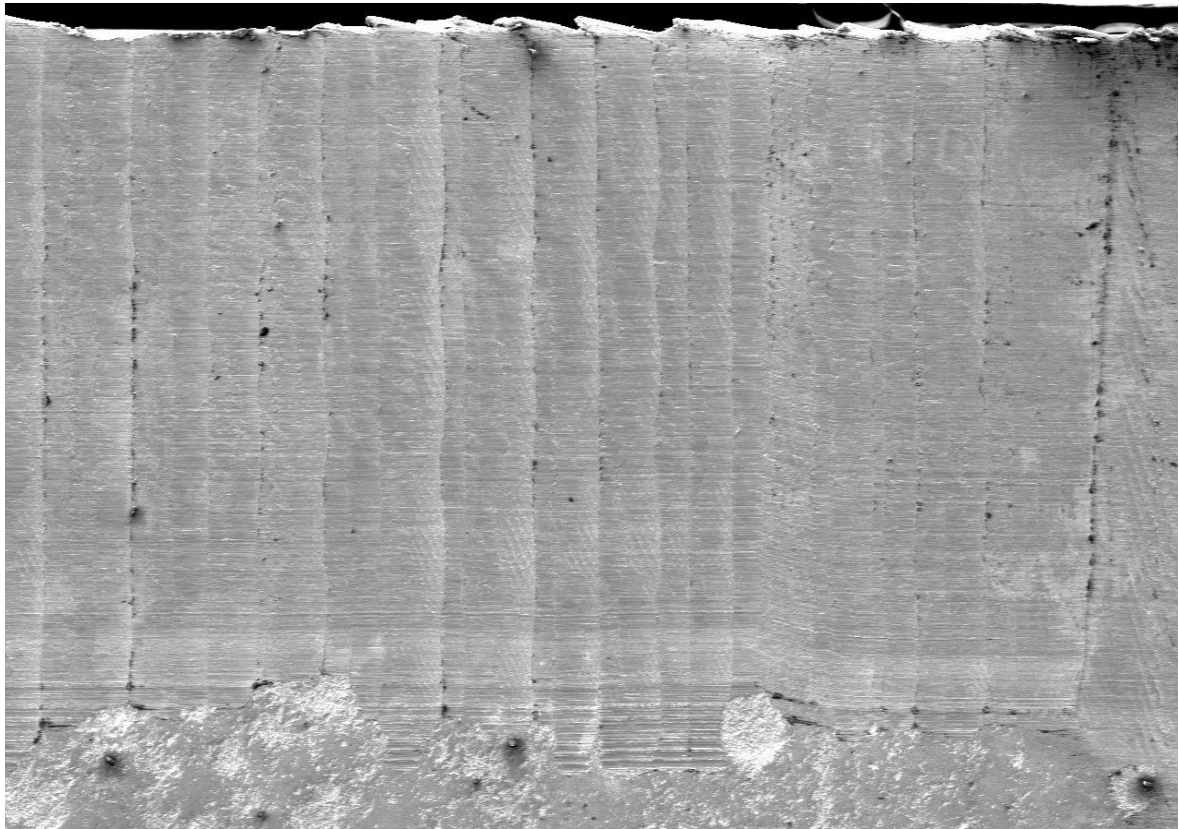


AR CoCrMo milled with Mill D.

Appendices A2: SEM Images of surfaces milled at 15,000 RPM.



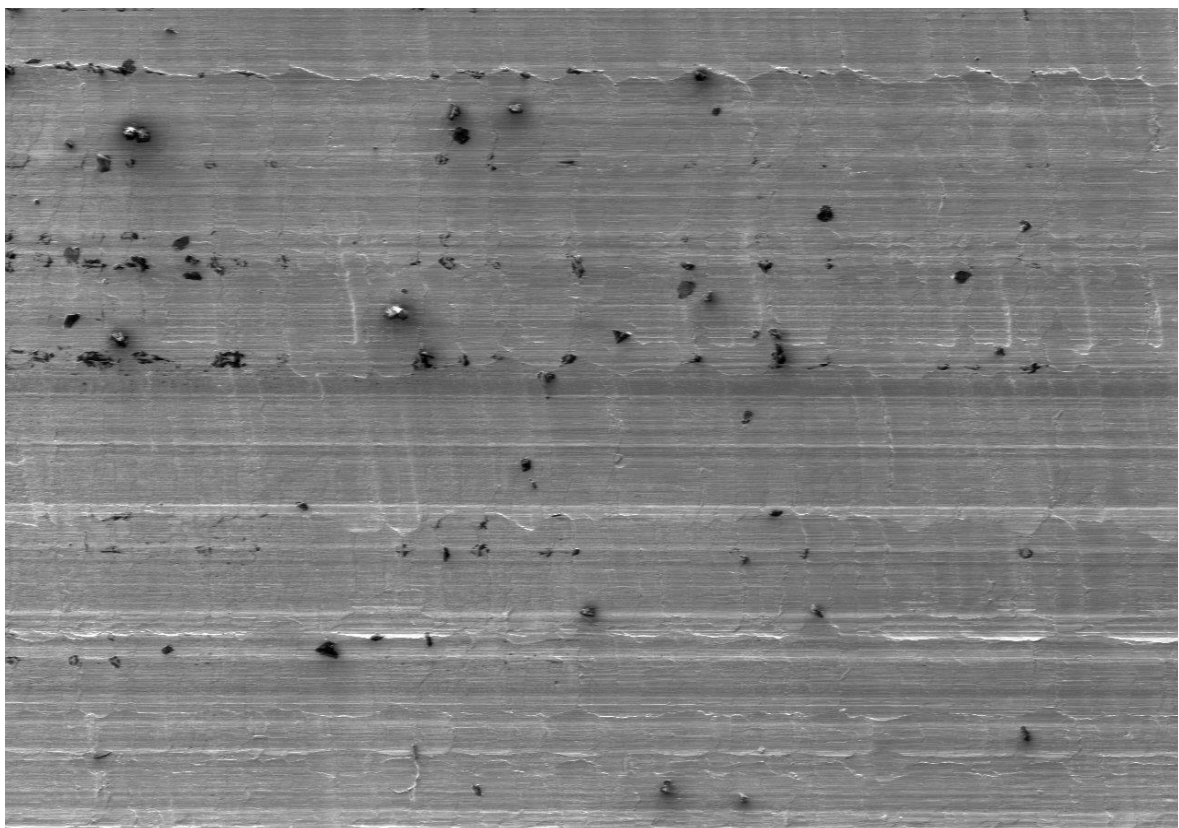
HT4H CoCrMo milled with Mill B.



5.0kV 16.6mm x30 SE(M)

1.00mm

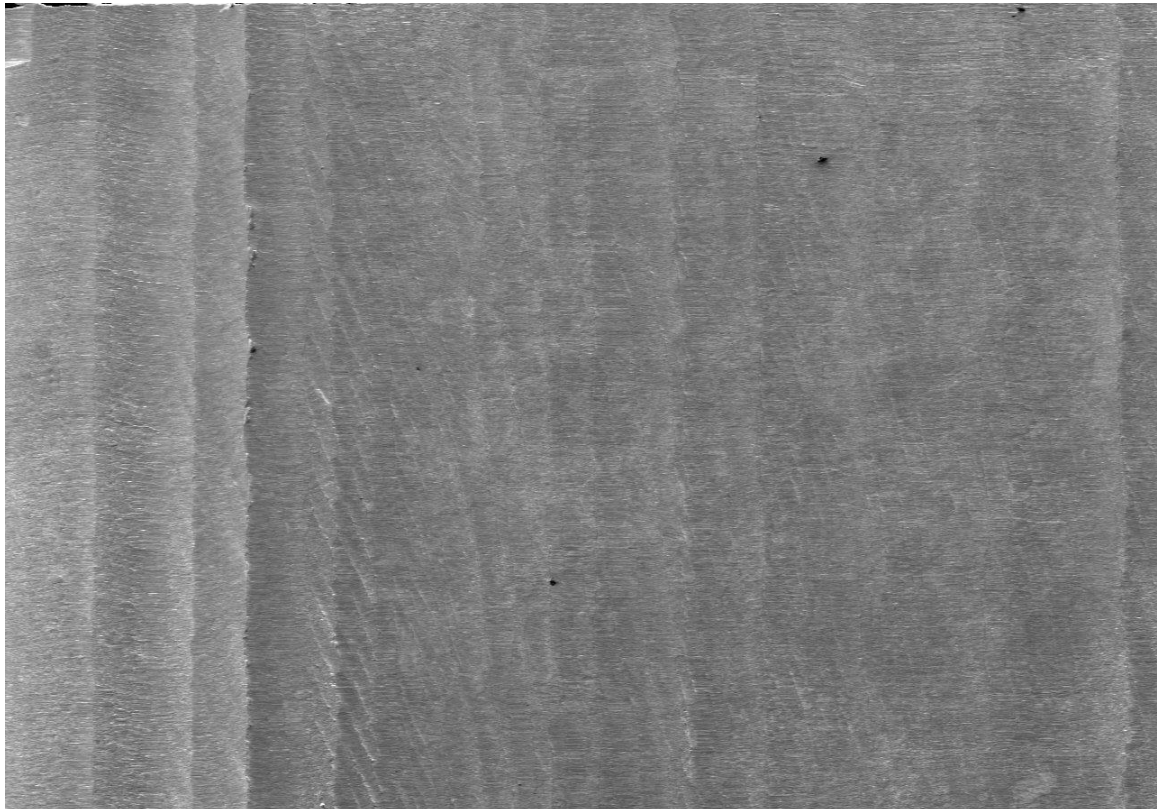
AR CoCrMo milled with Mill A.



5.0kV 16.8mm x50 SE(M)

1.00mm

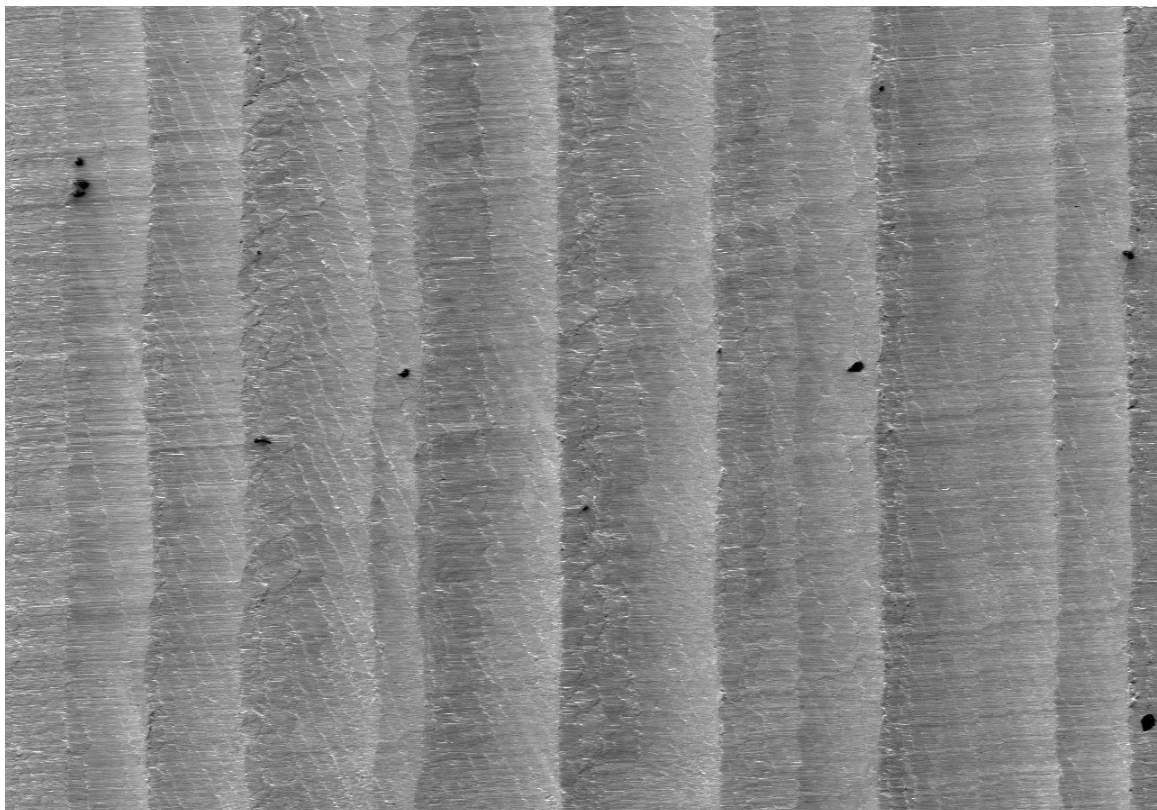
AR CoCrMo milled with Mill B.



5.0kV 16.7mm x30 SE(M)

1.00mm

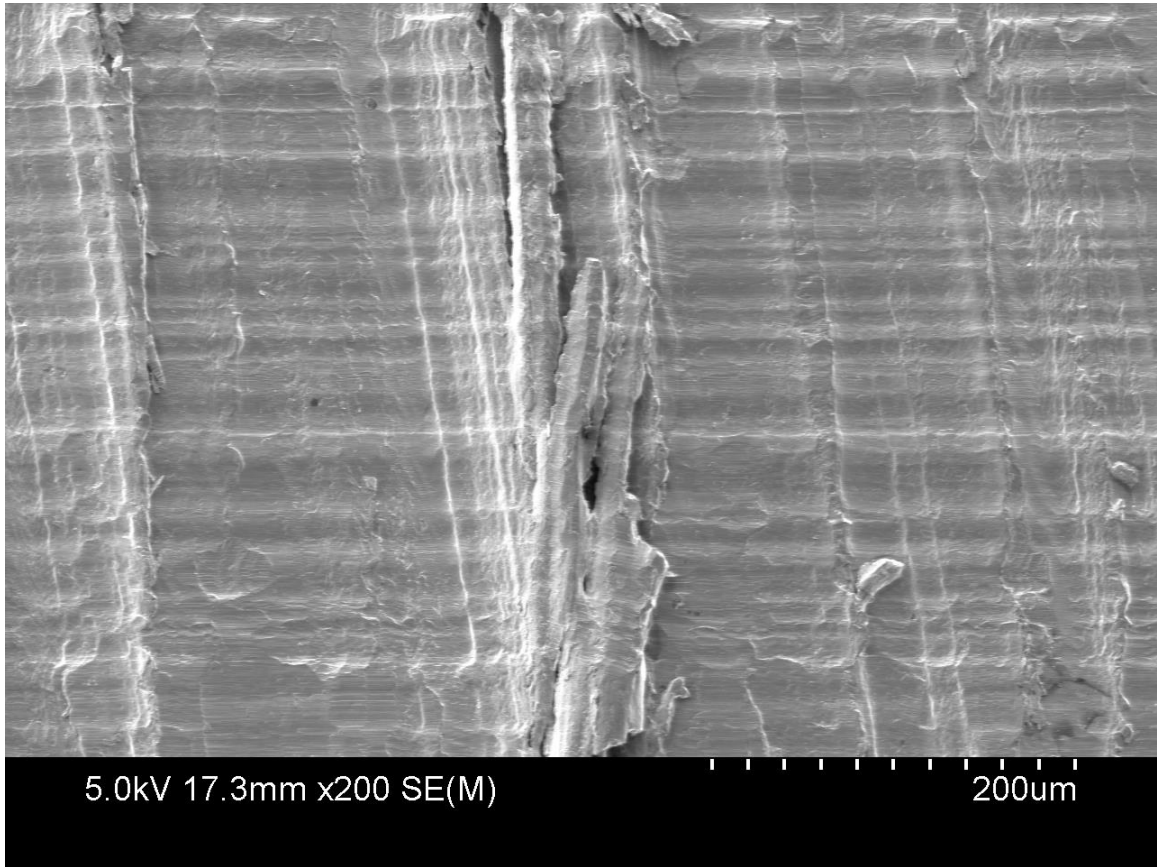
AR CoCrMo milled with Mill C.



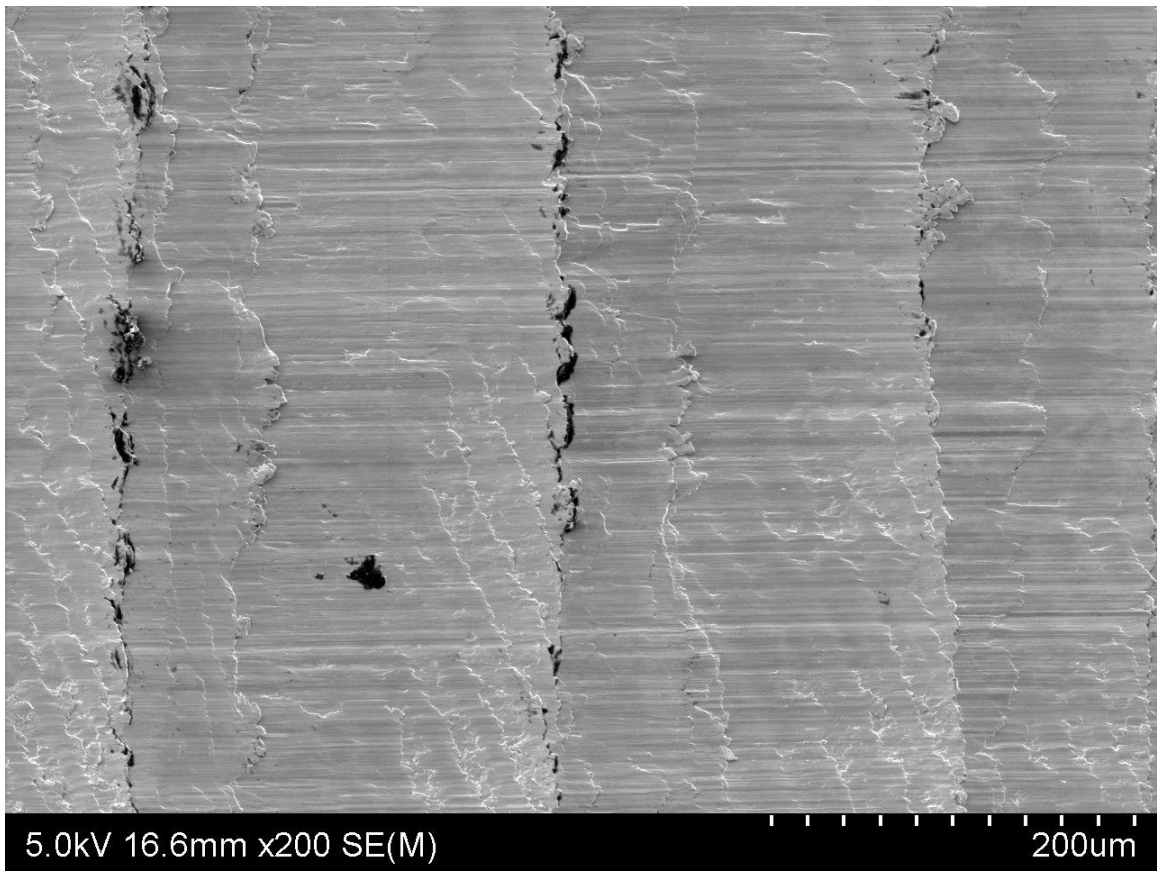
5.0kV 15.4mm x50 SE(M)

1.00mm

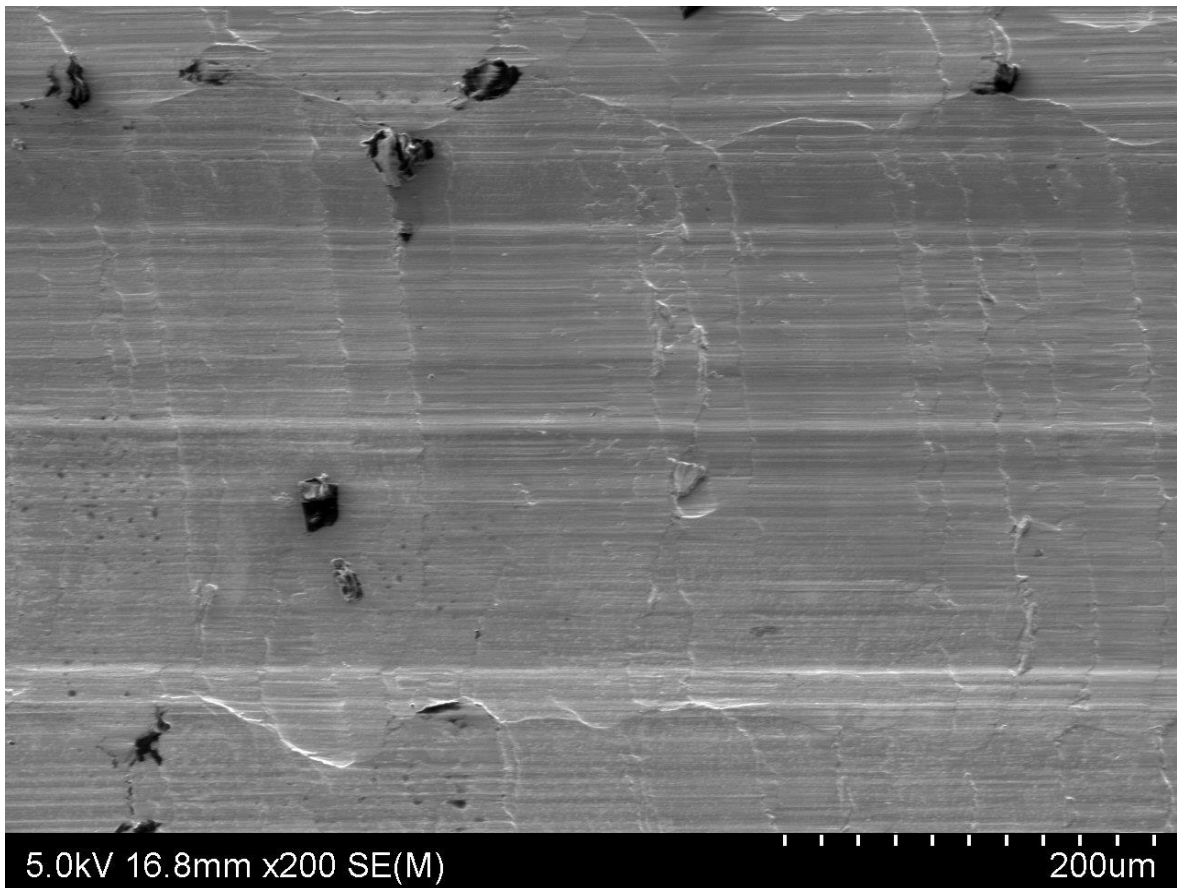
AR CoCrMo milled with Mill D.



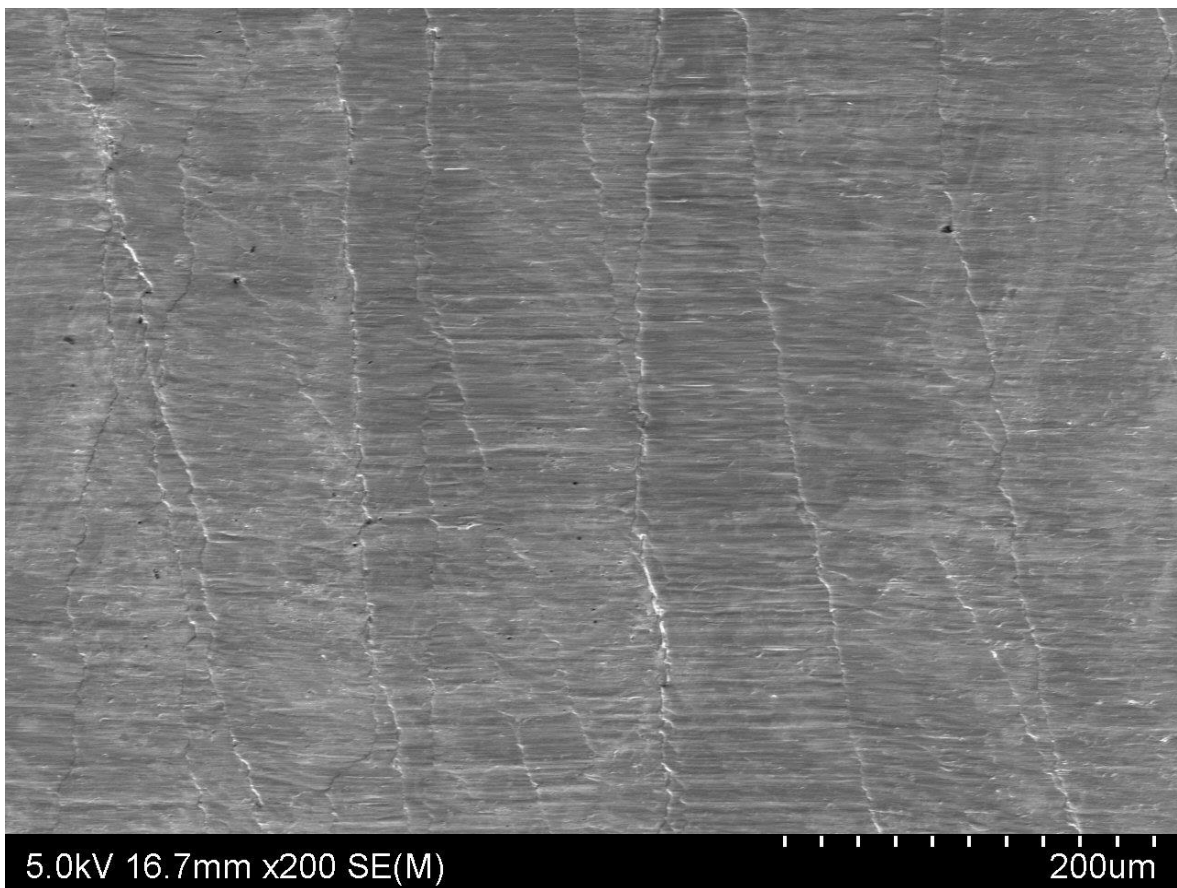
HT4H CoCrMo milled with Mill B.



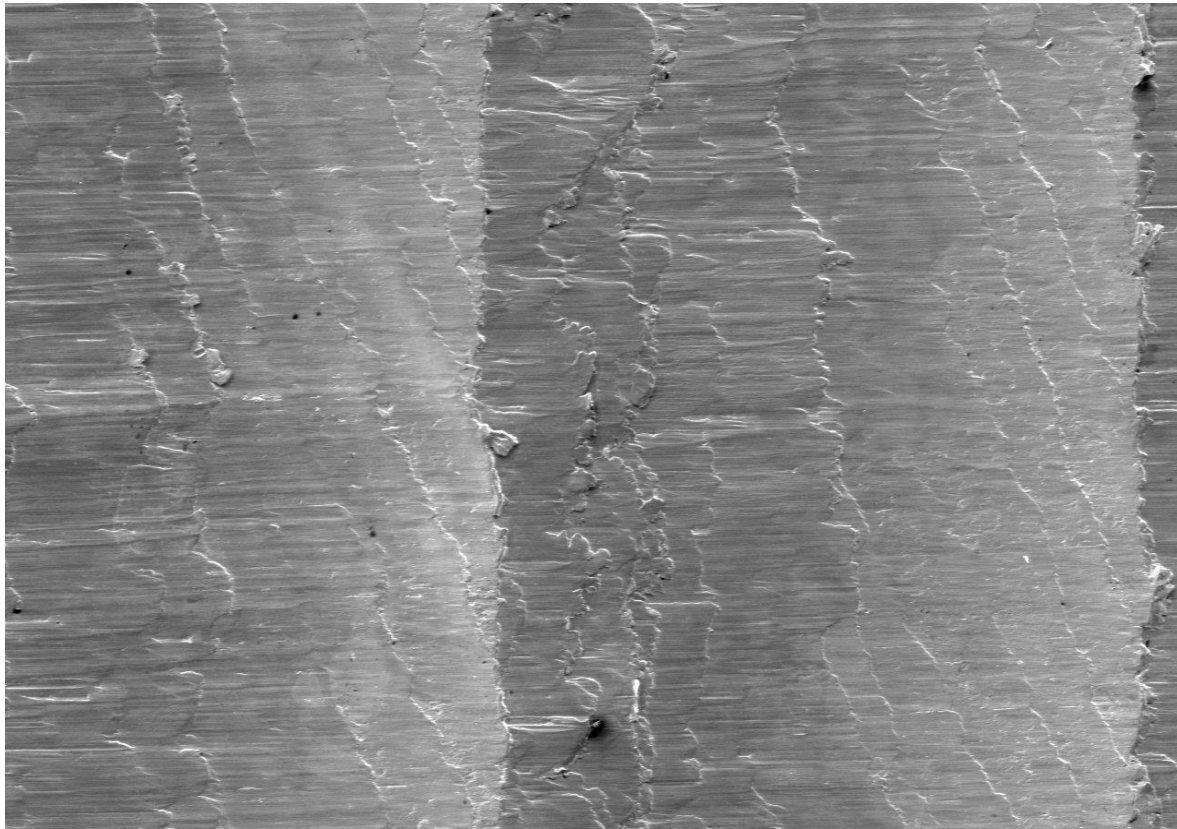
AR CoCrMo milled with Mill A.



AR CoCrMo milled with Mill B.



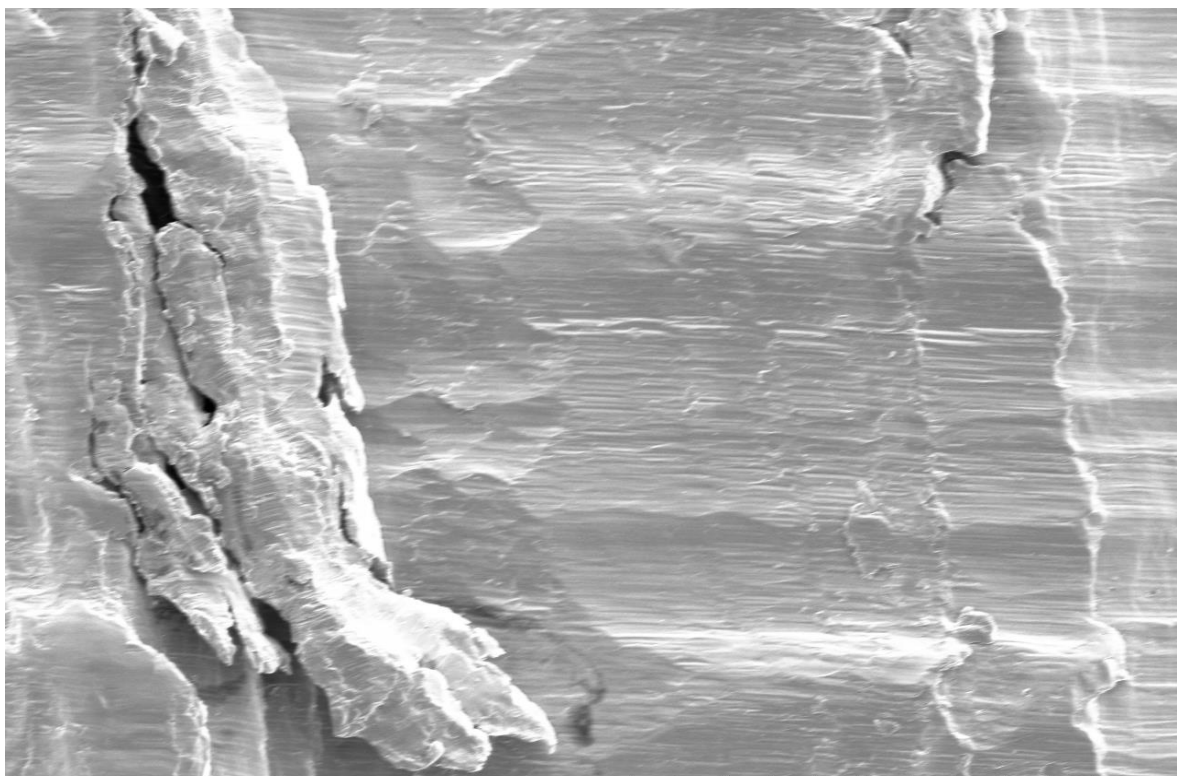
AR CoCrMo milled with Mill C.



5.0kV 15.4mm x200 SE(M)

200um

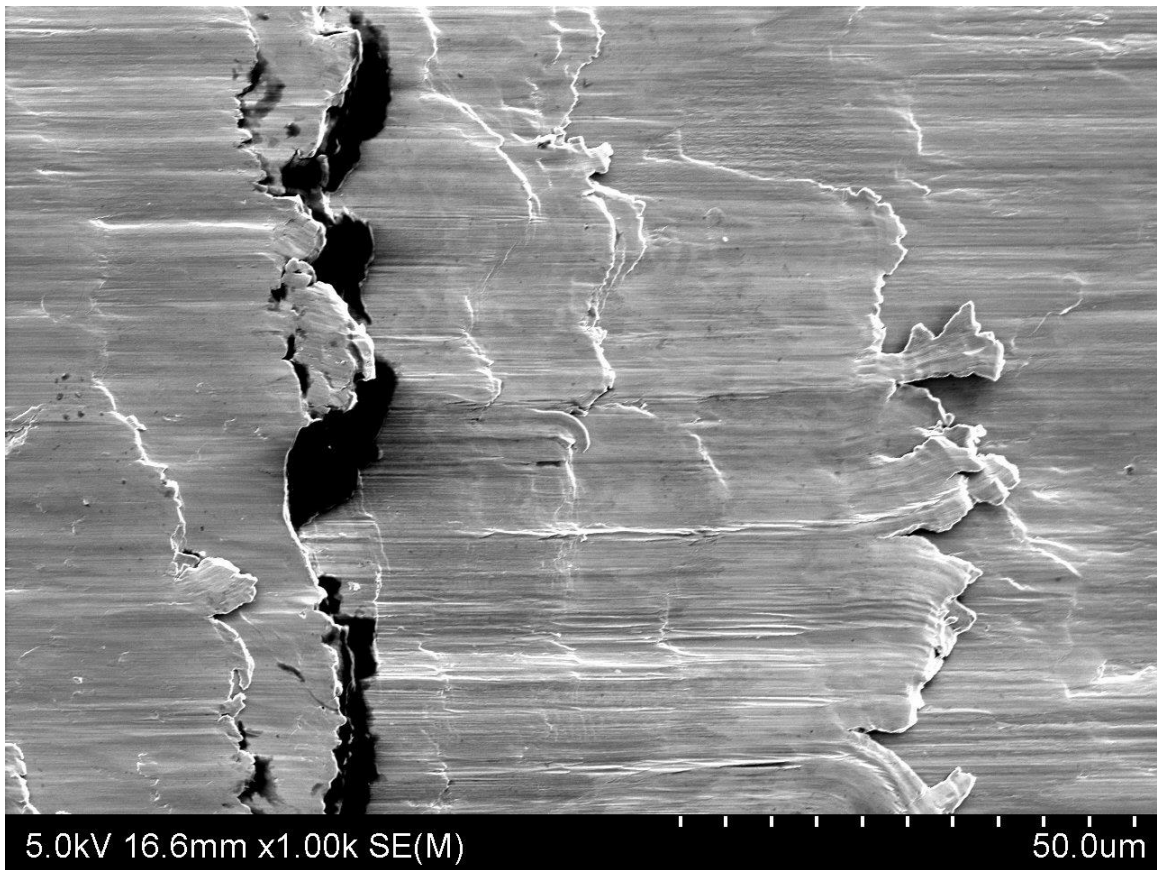
AR CoCrMo milled with Mill D.



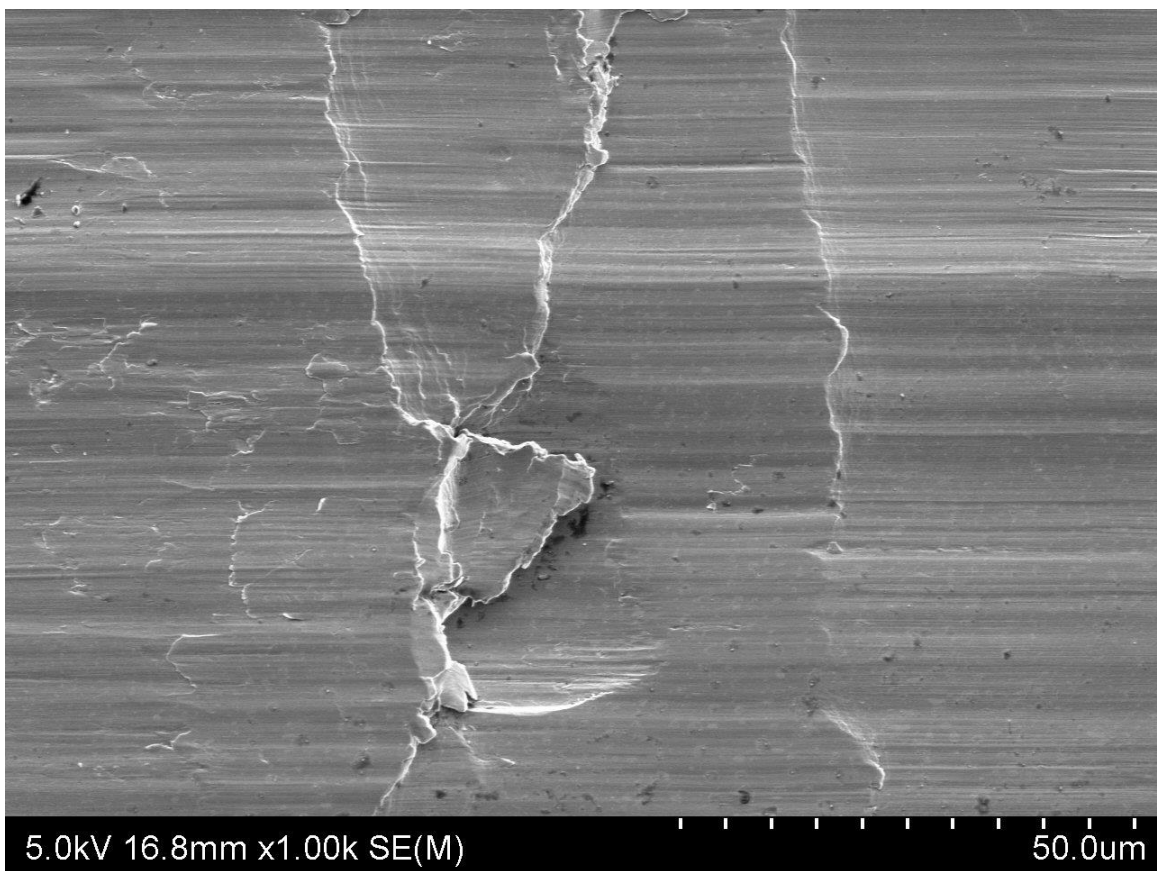
5.0kV 17.1mm x1.00k SE(M)

50.0um

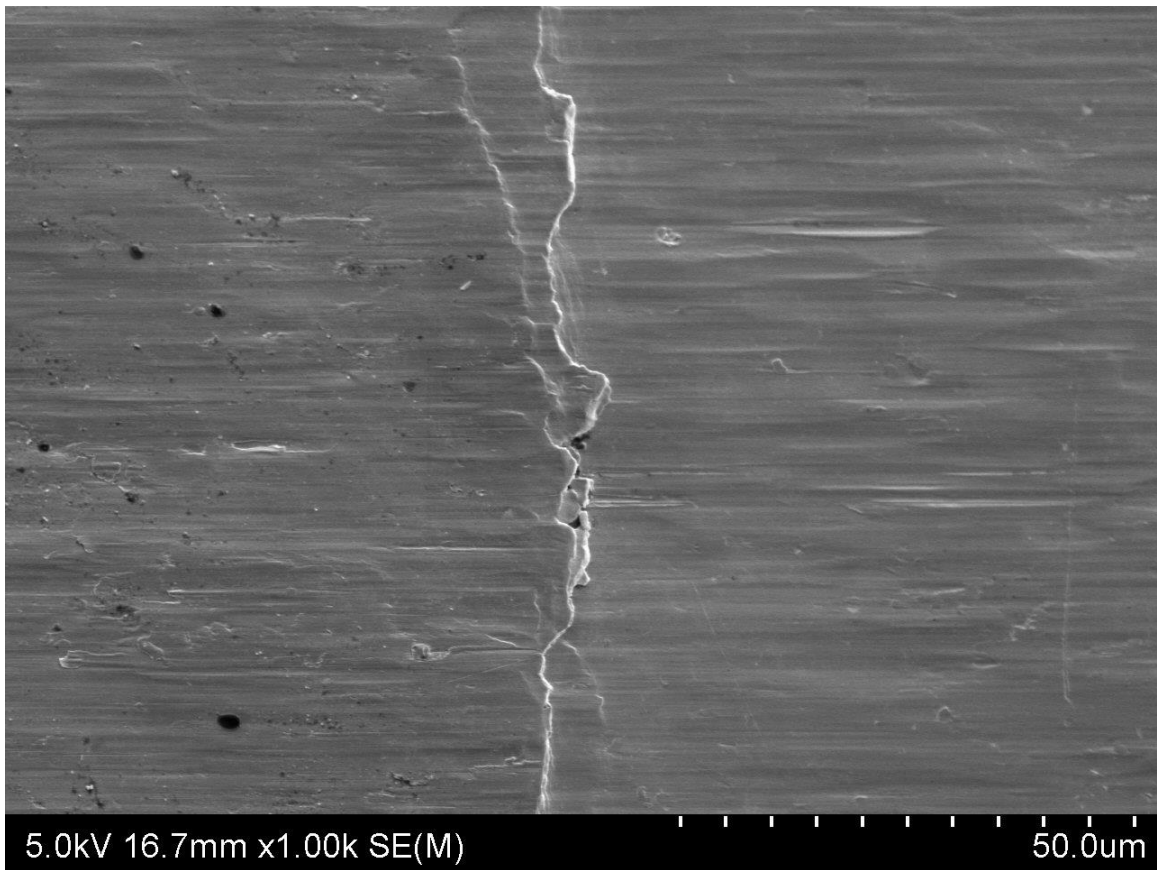
HT4H CoCrMo milled with Mill B.



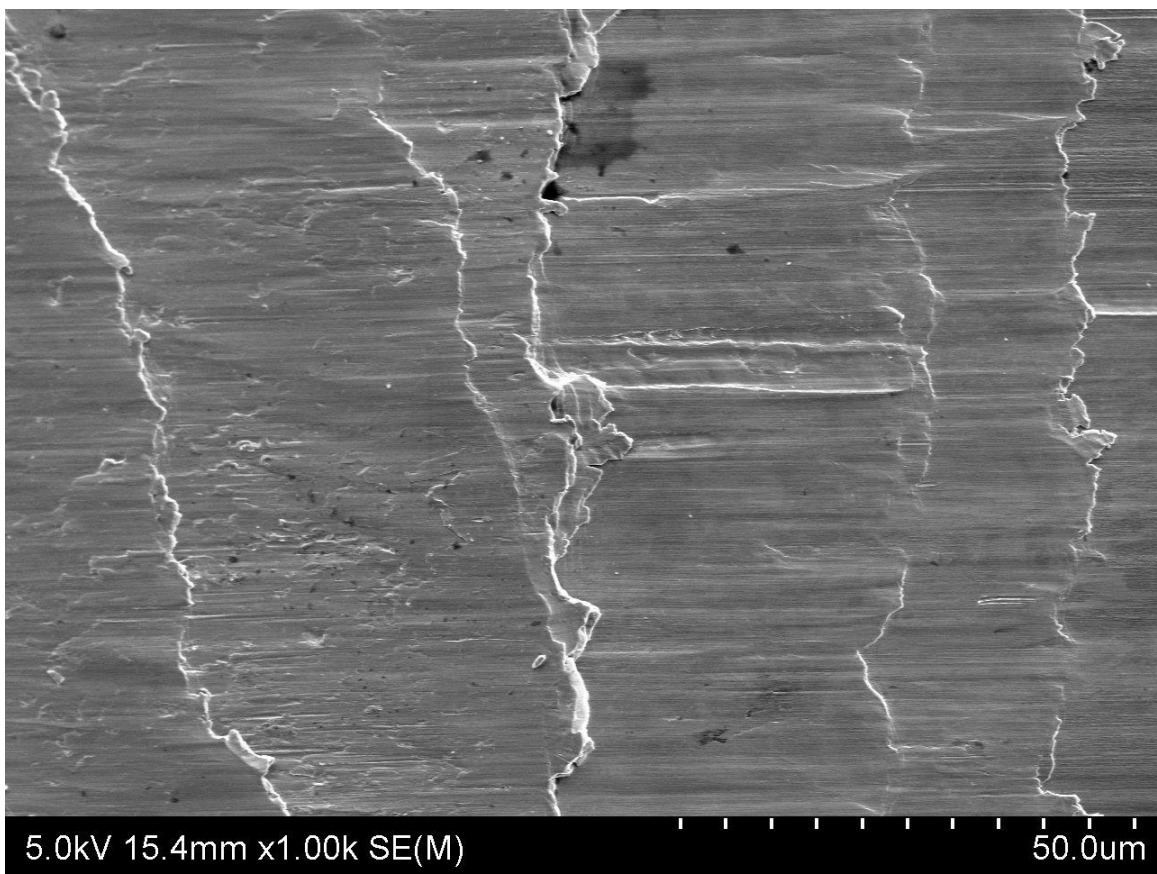
AR CoCrMo milled with Mill A.



AR CoCrMo milled with Mill B.

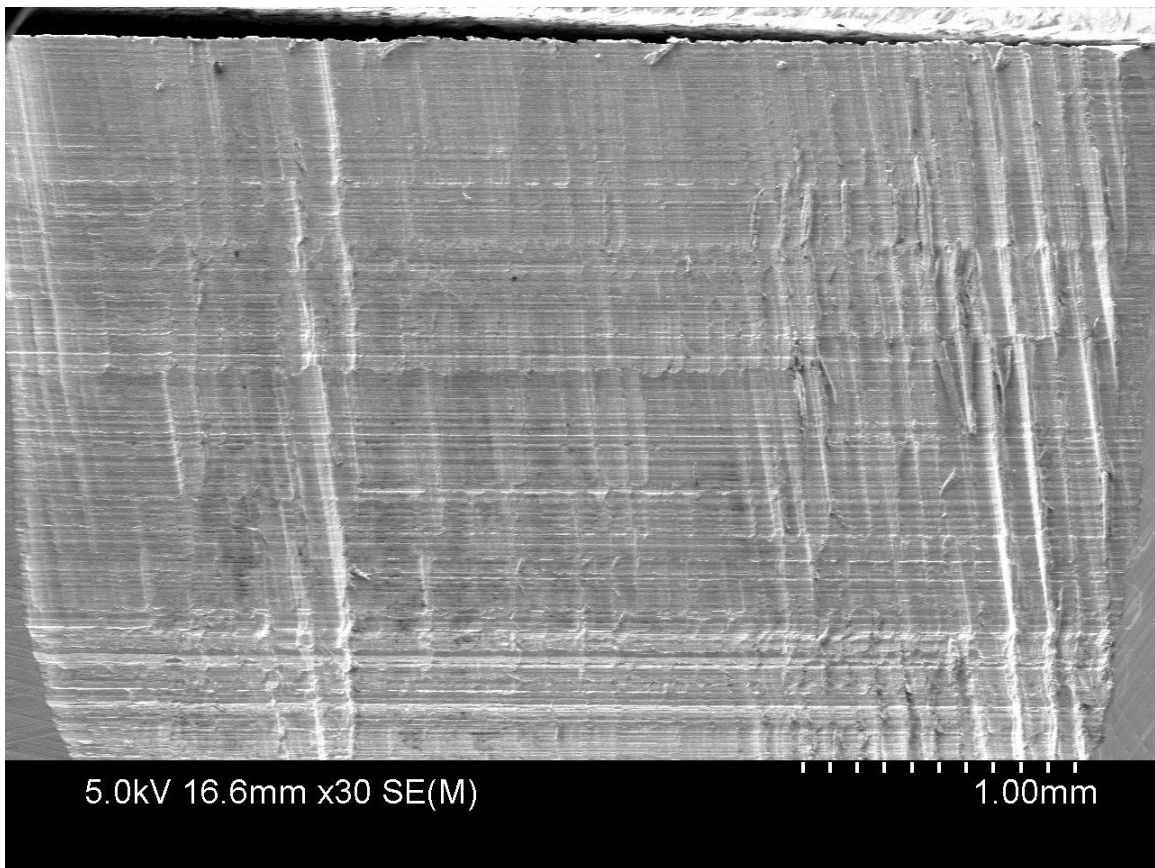


AR CoCrMo milled with Mill C.

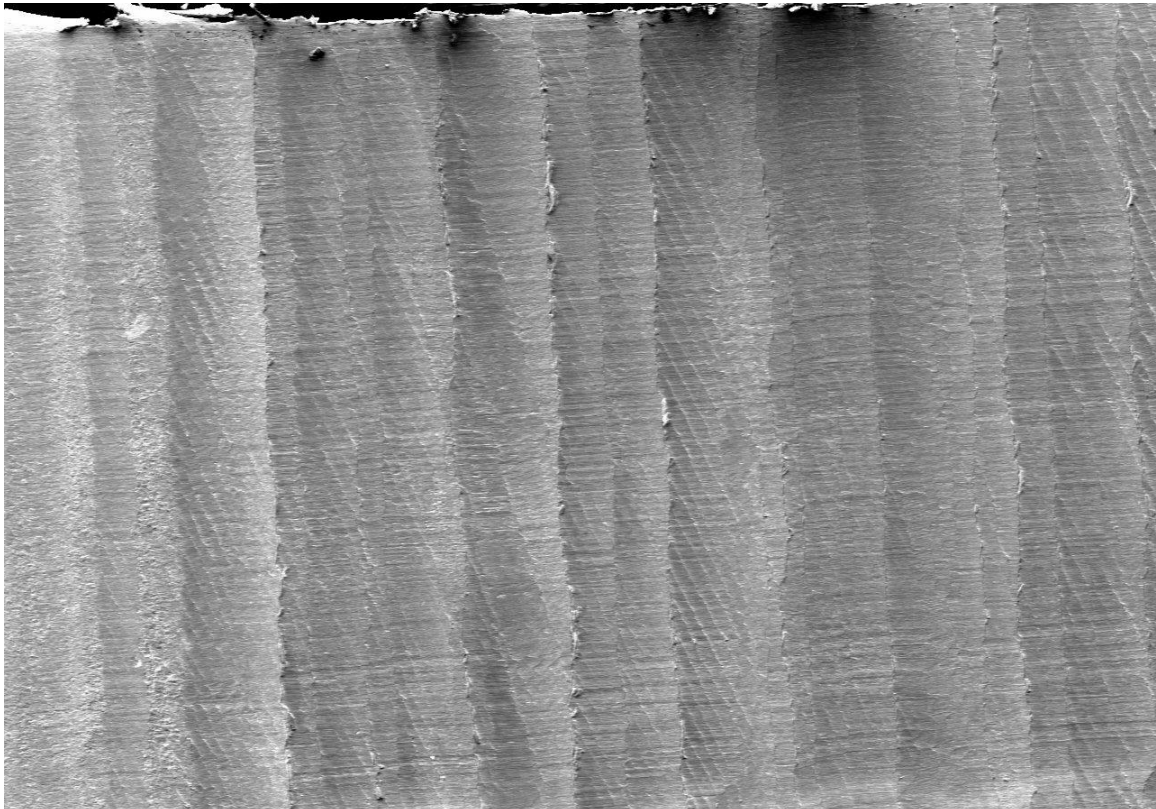


AR CoCrMo milled with Mill D.

Appendices A3: SEM Images of surfaces milled at 20,000 RPM.



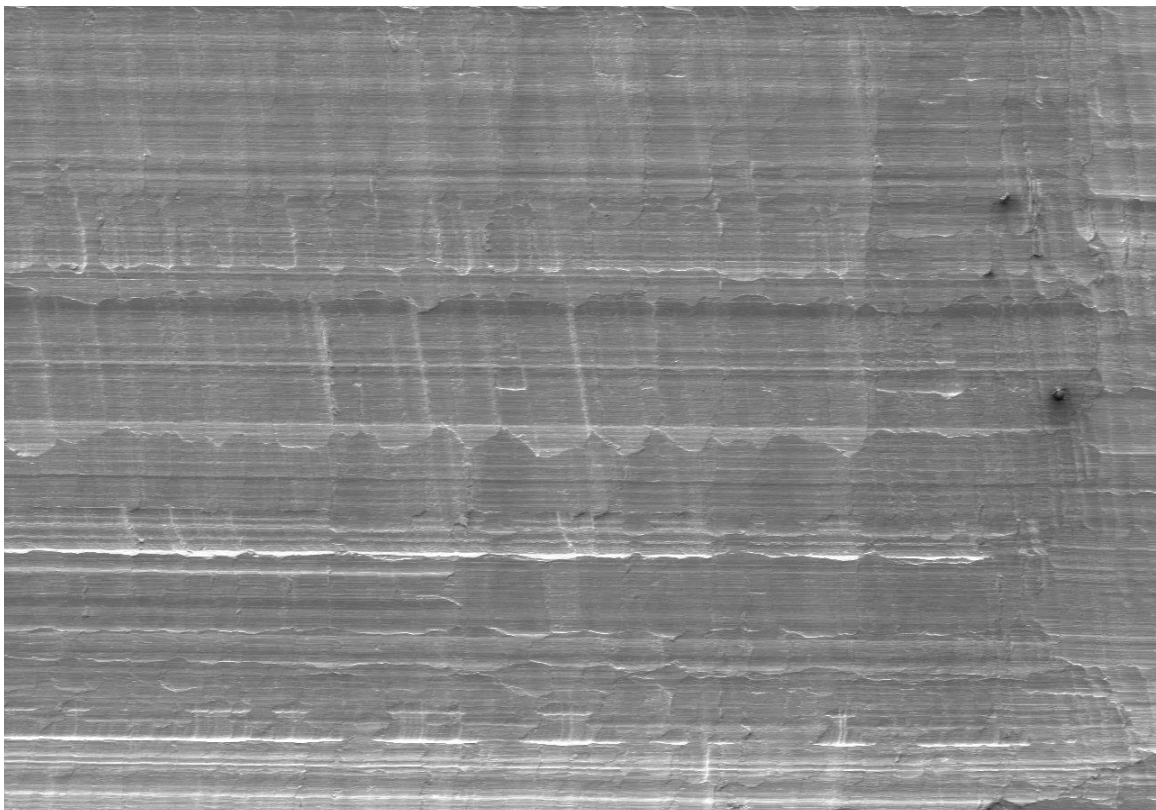
HT4H CoCrMo milled with Mill B.



5.0kV 16.8mm x40 SE(M)

1.00mm

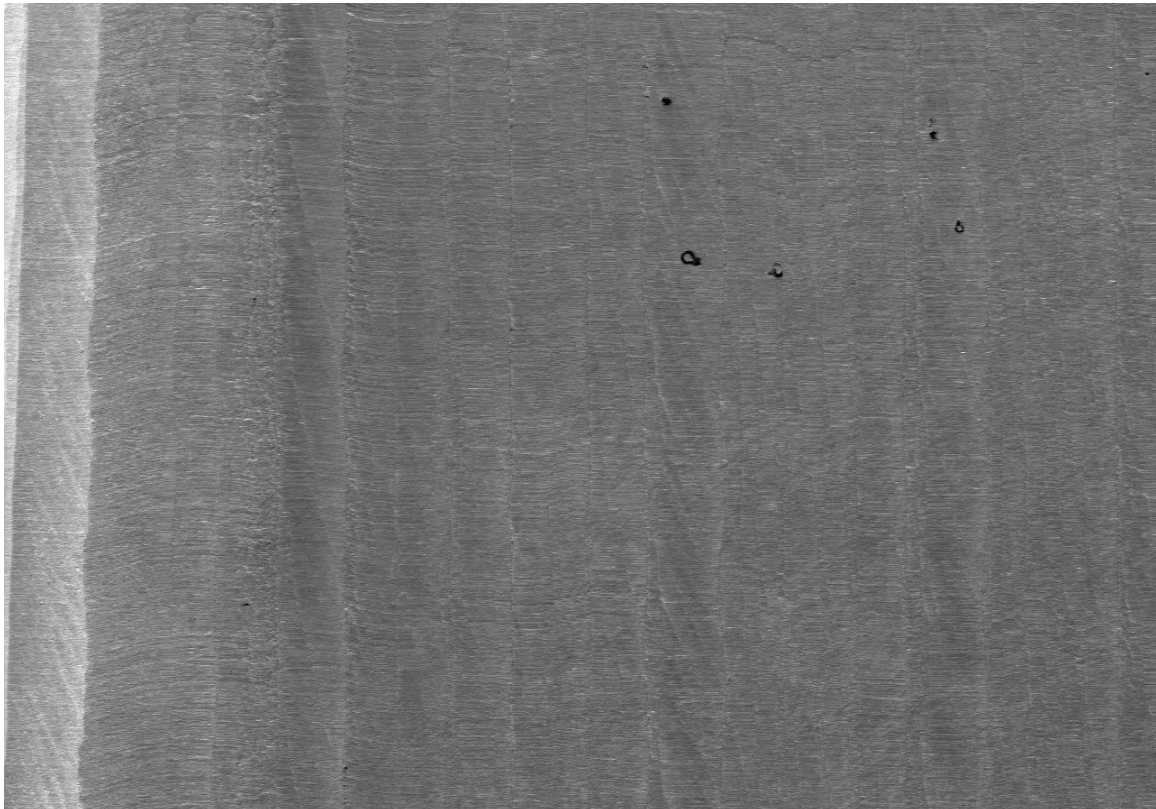
AR CoCrMo milled with Mill A.



5.0kV 17.0mm x50 SE(M)

1.00mm

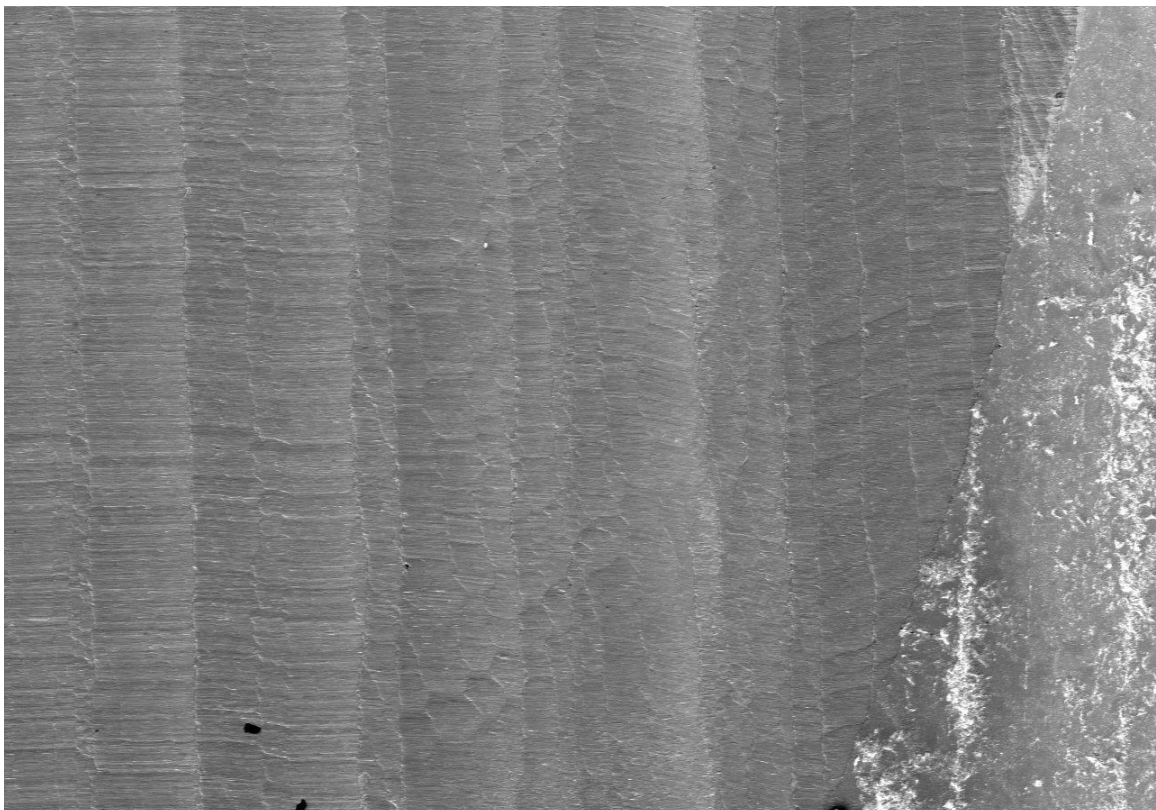
AR CoCrMo milled with Mill B.



5.0kV 16.1mm x30 SE(M)

1.00mm

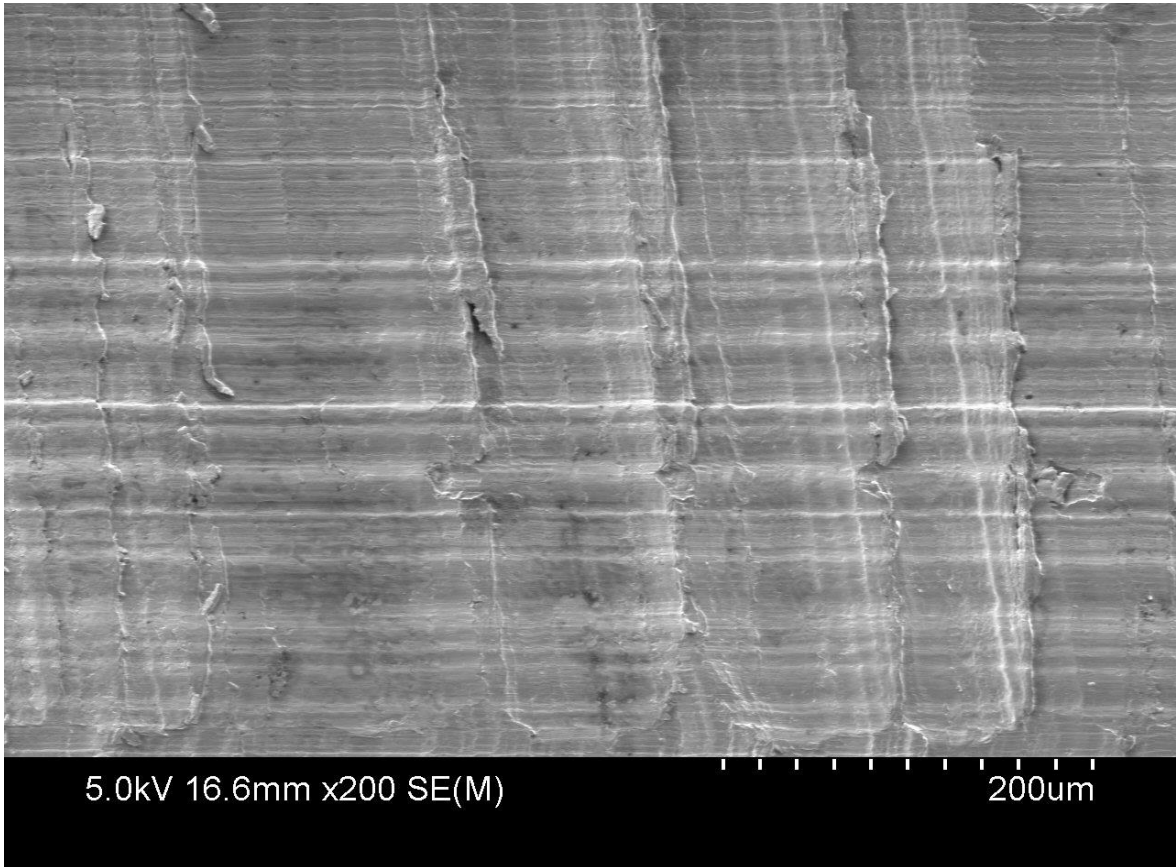
AR CoCrMo milled with Mill C.



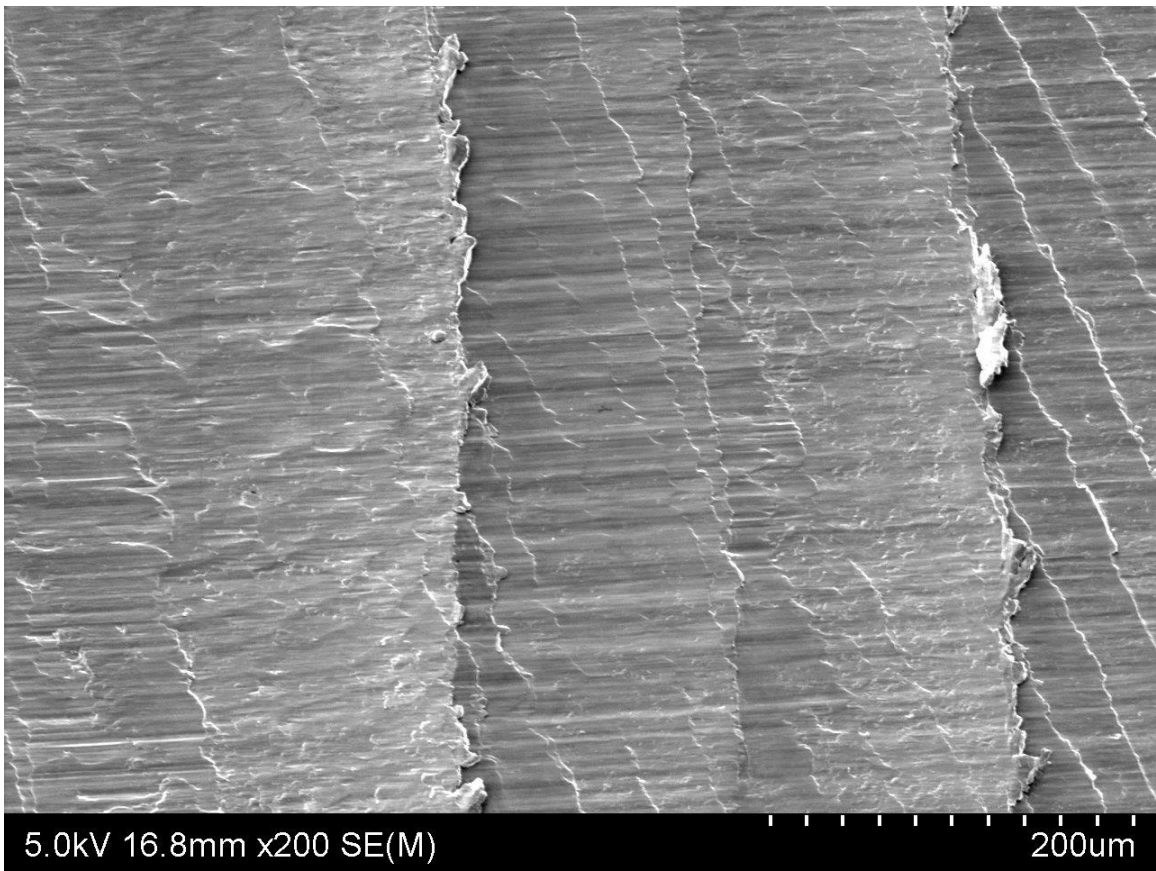
5.0kV 15.4mm x50 SE(M)

1.00mm

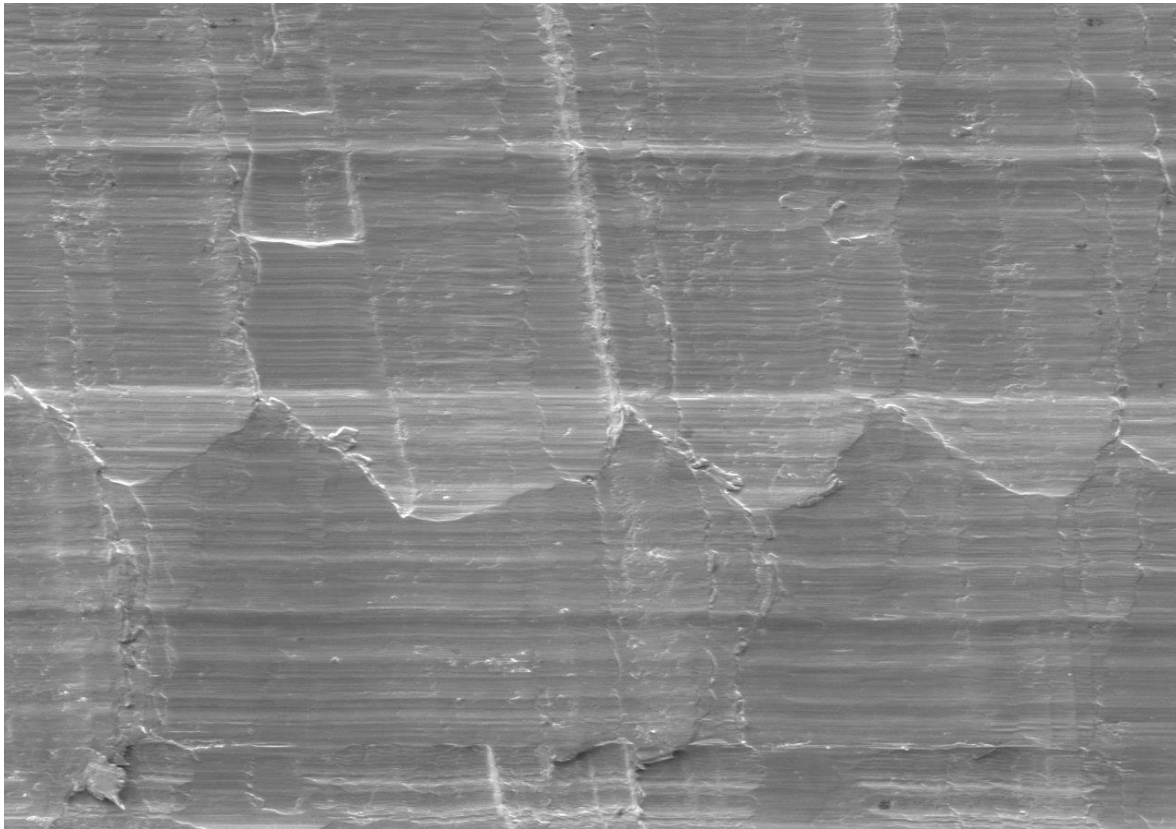
AR CoCrMo milled with Mill D.



HT4H CoCrMo milled with Mill B.



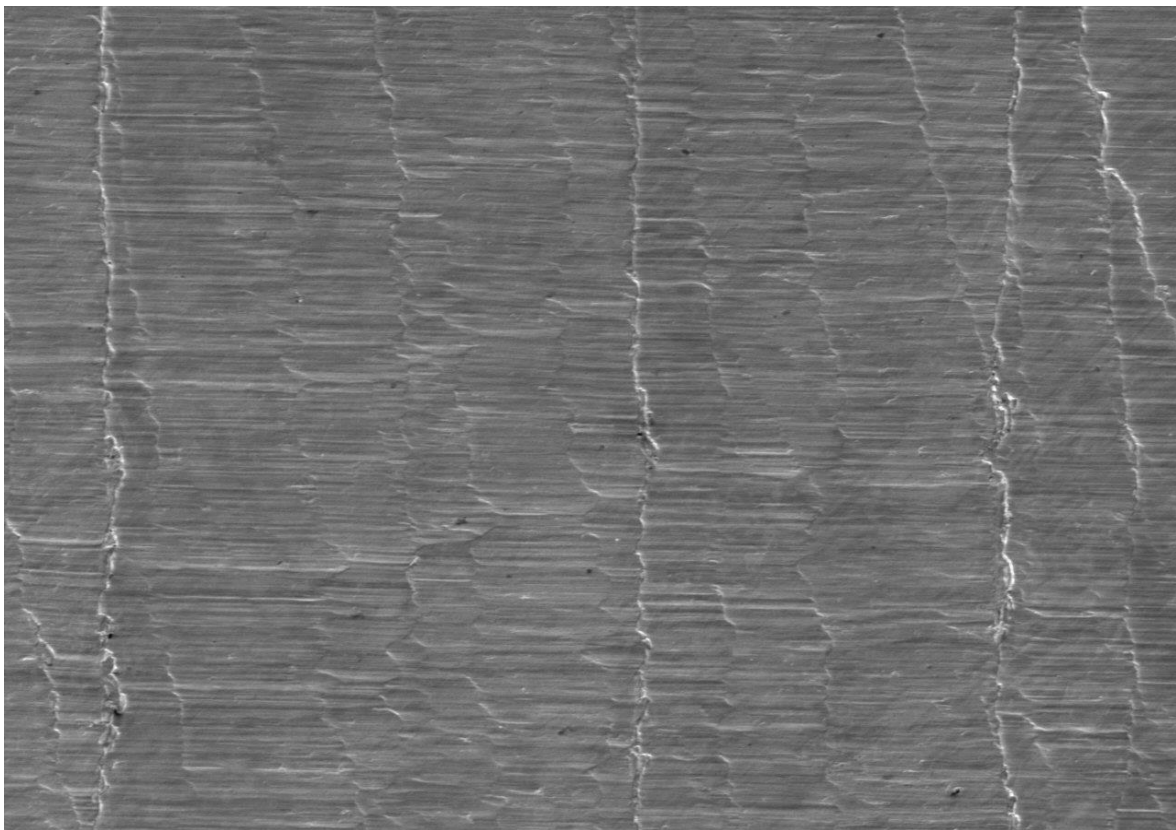
AR CoCrMo milled with Mill A.



5.0kV 17.0mm x200 SE(M)

200um

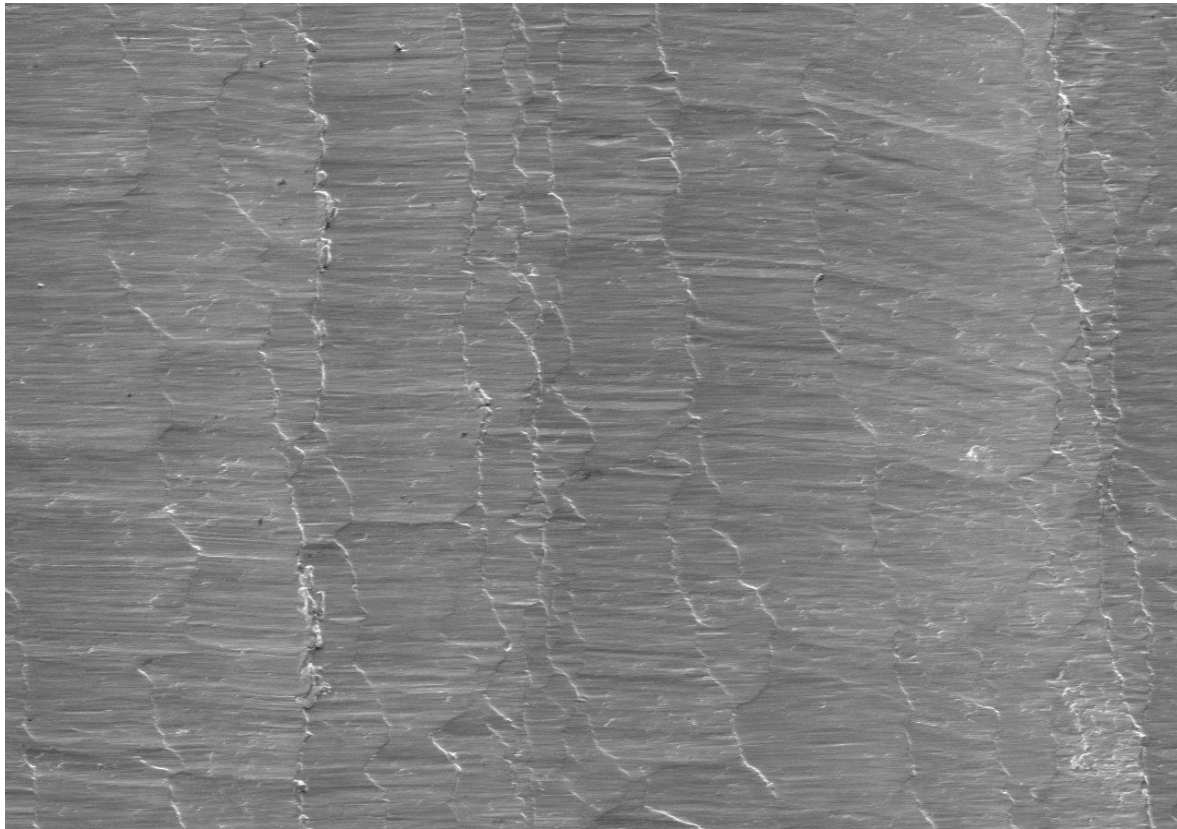
AR CoCrMo milled with Mill B.



5.0kV 16.1mm x200 SE(M)

200um

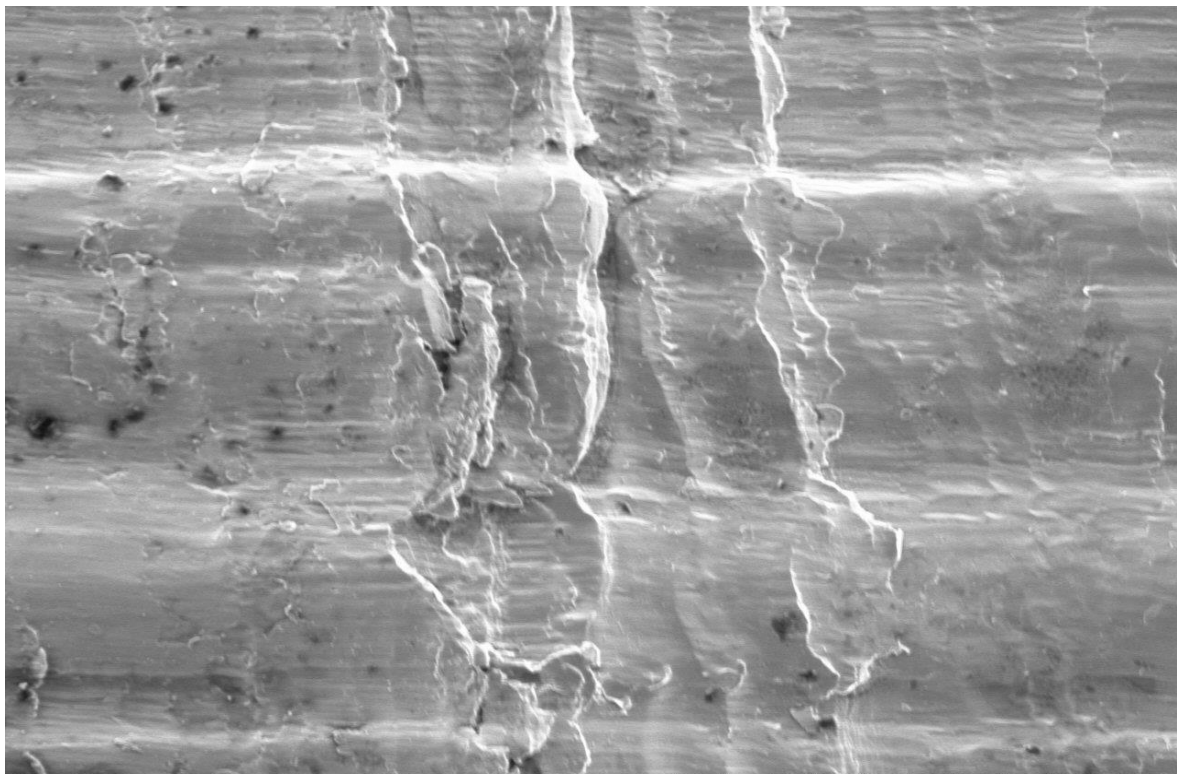
AR CoCrMo milled with Mill C.



5.0kV 15.4mm x200 SE(M)

200um

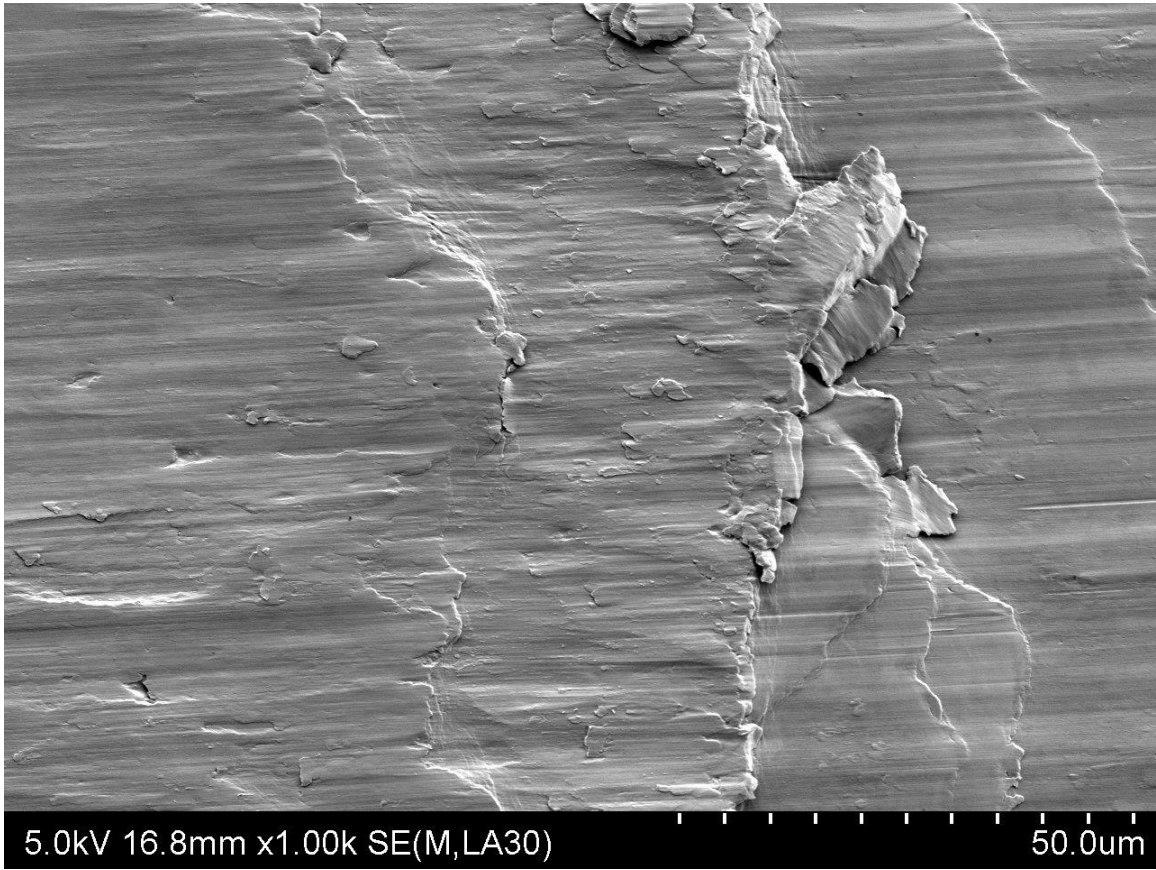
AR CoCrMo milled with Mill D.



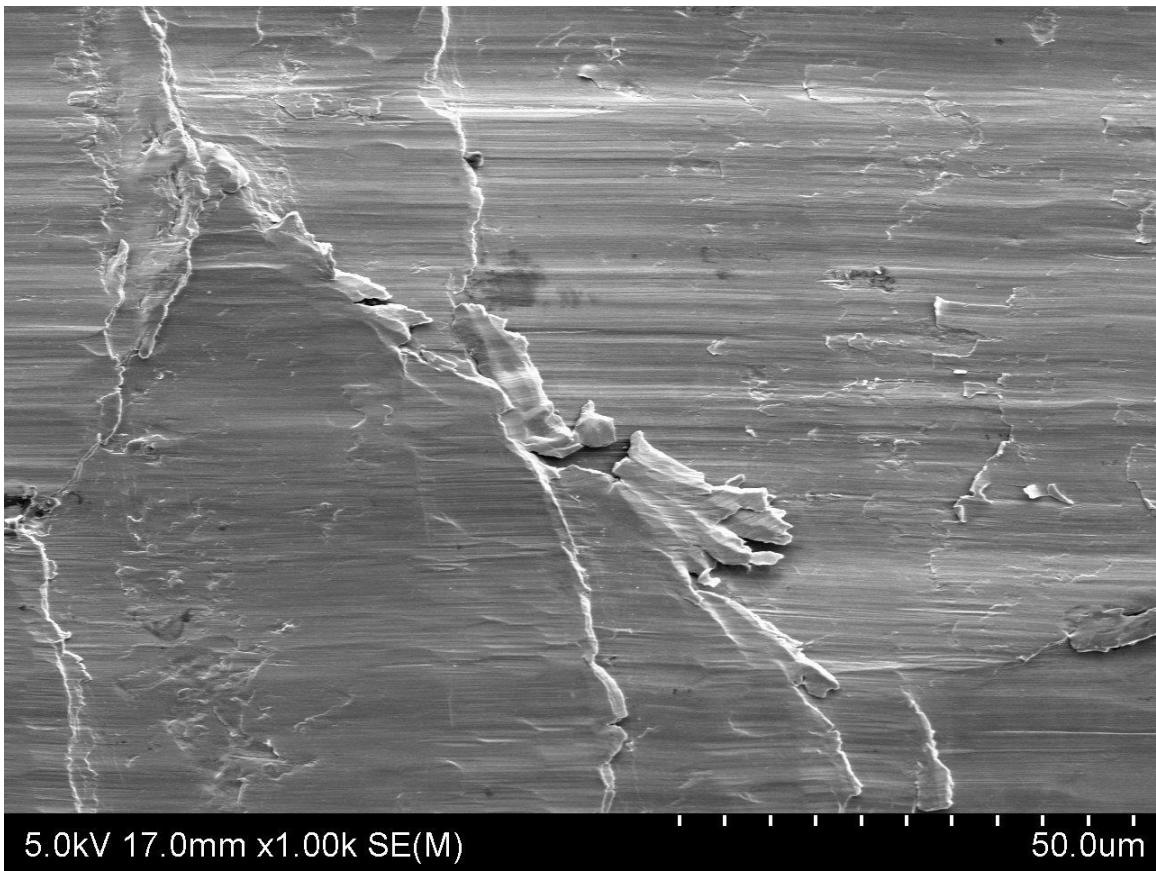
5.0kV 16.6mm x1.00k SE(M)

50.0um

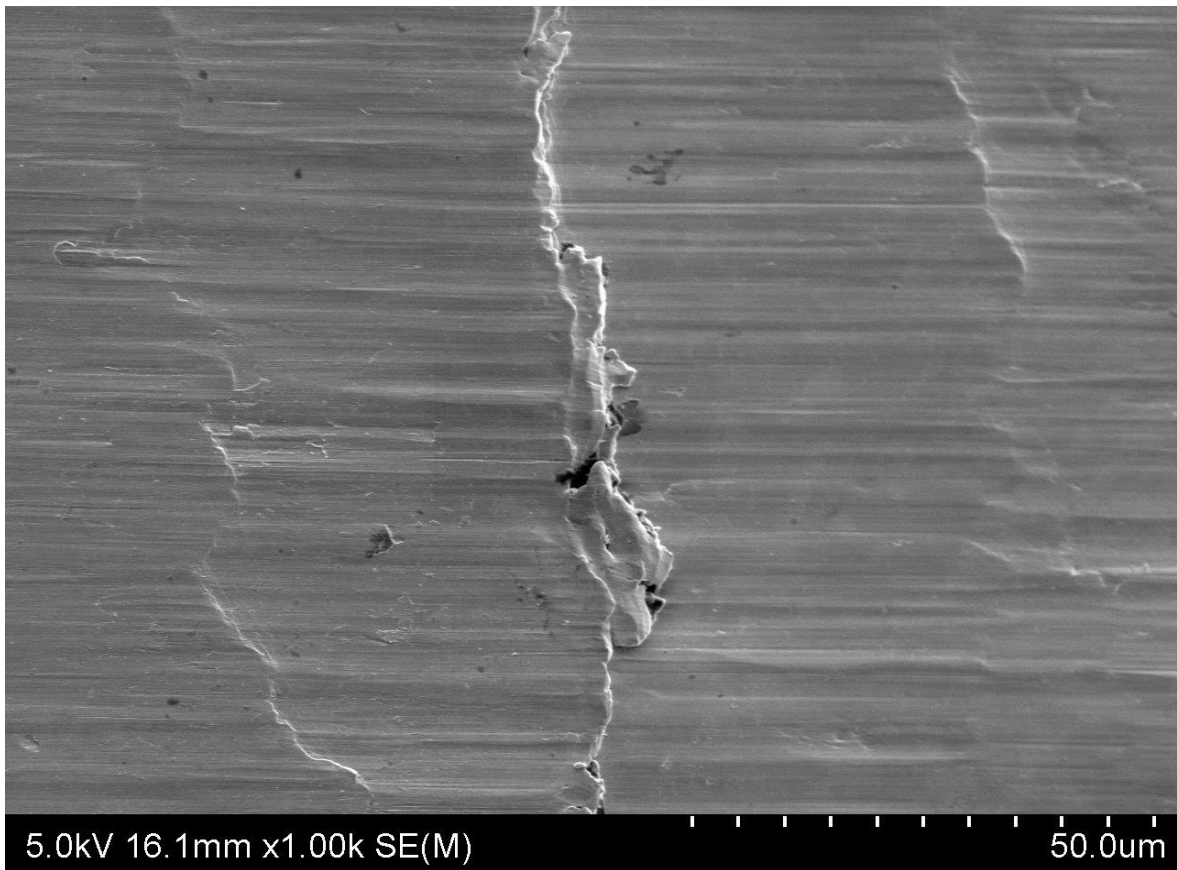
HT4H CoCrMo milled with Mill B.



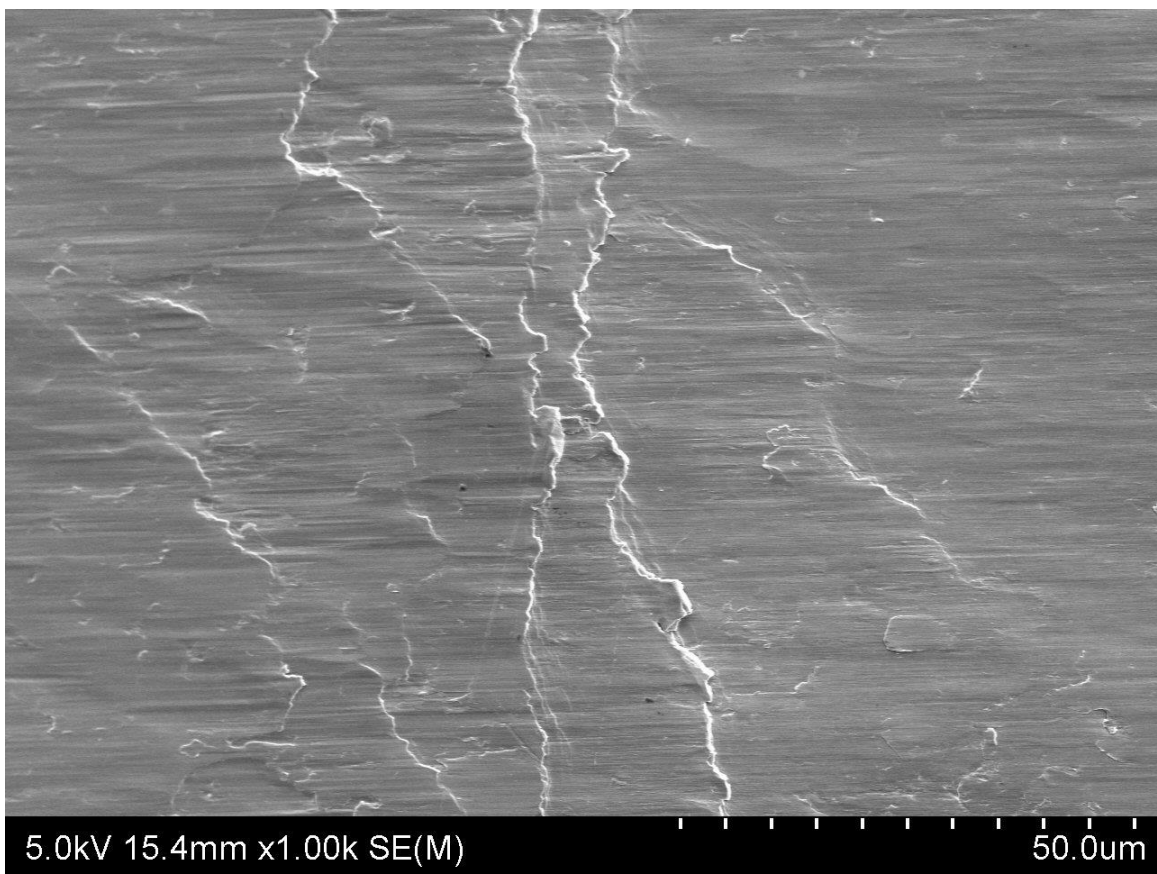
AR CoCrMo milled with Mill A.



AR CoCrMo milled with Mill B.

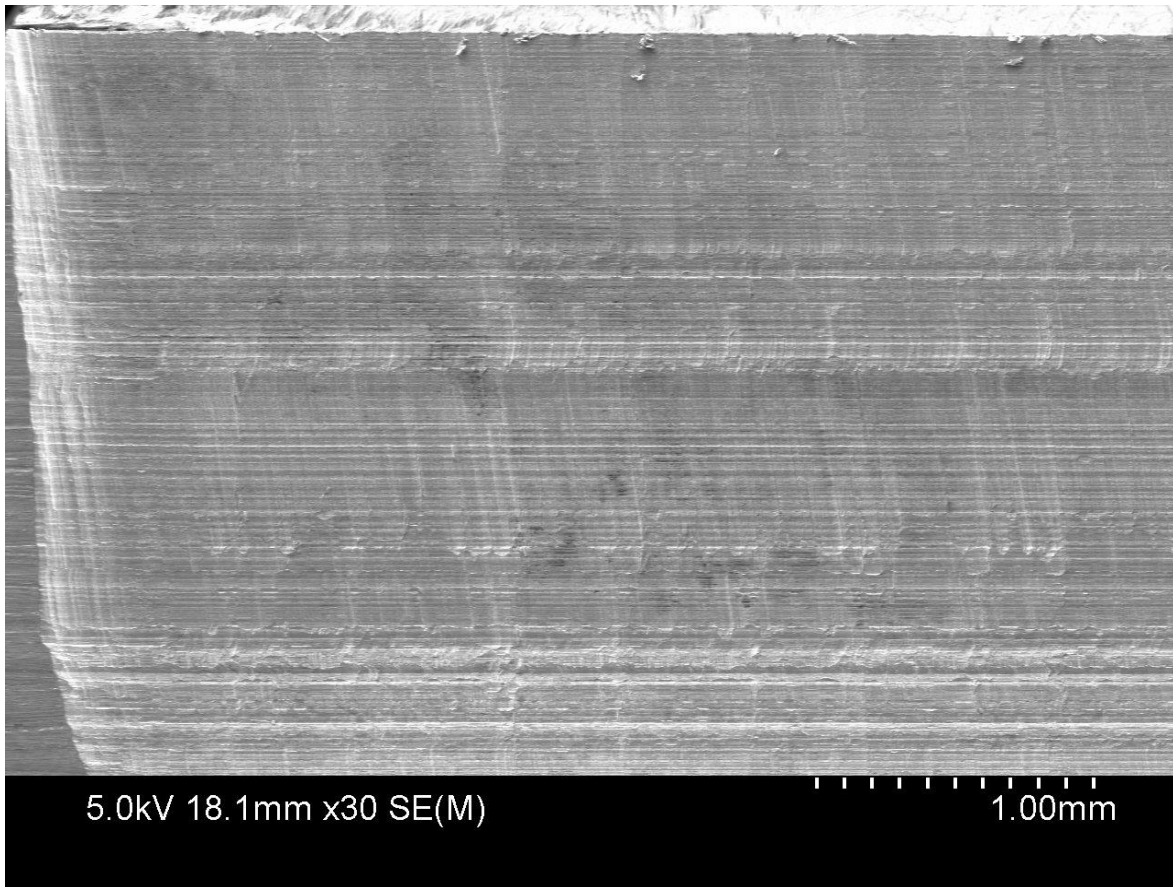


AR CoCrMo milled with Mill C.

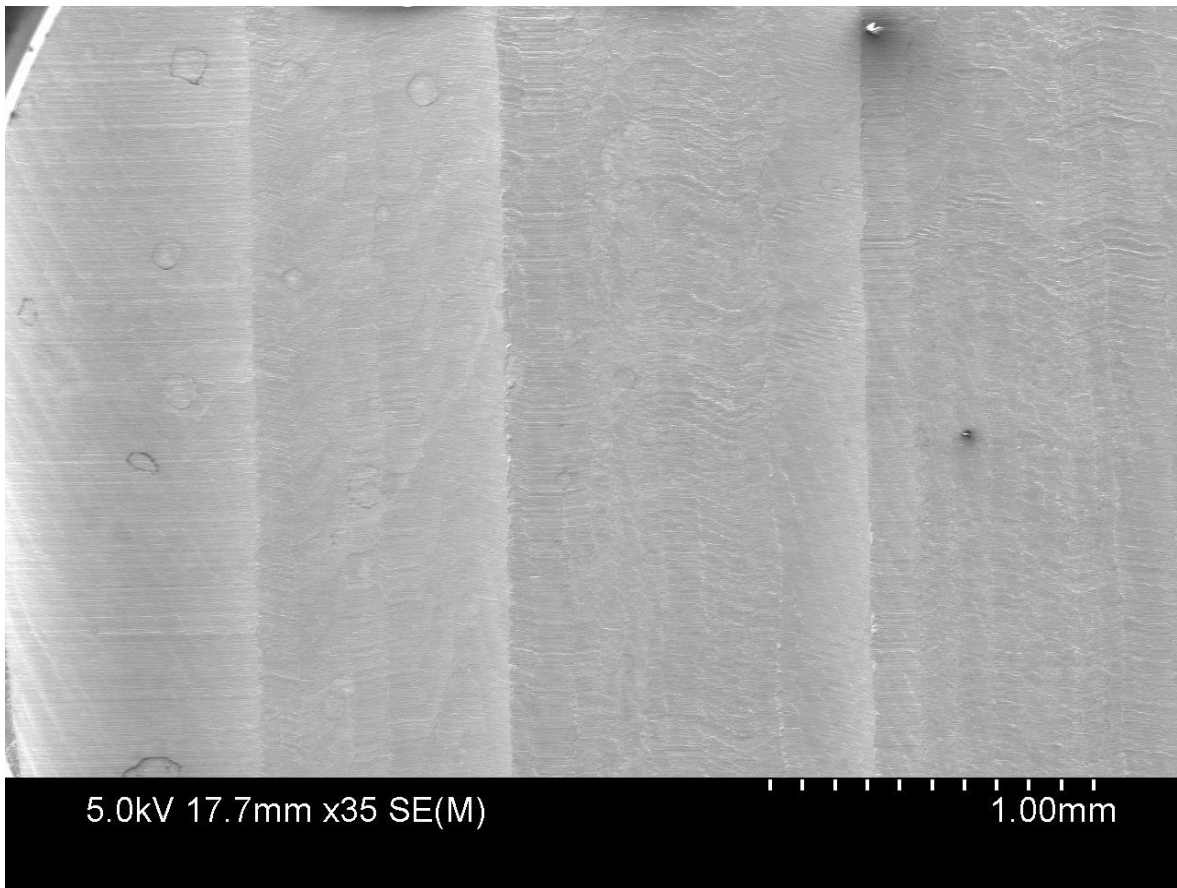


AR CoCrMo milled with Mill D.

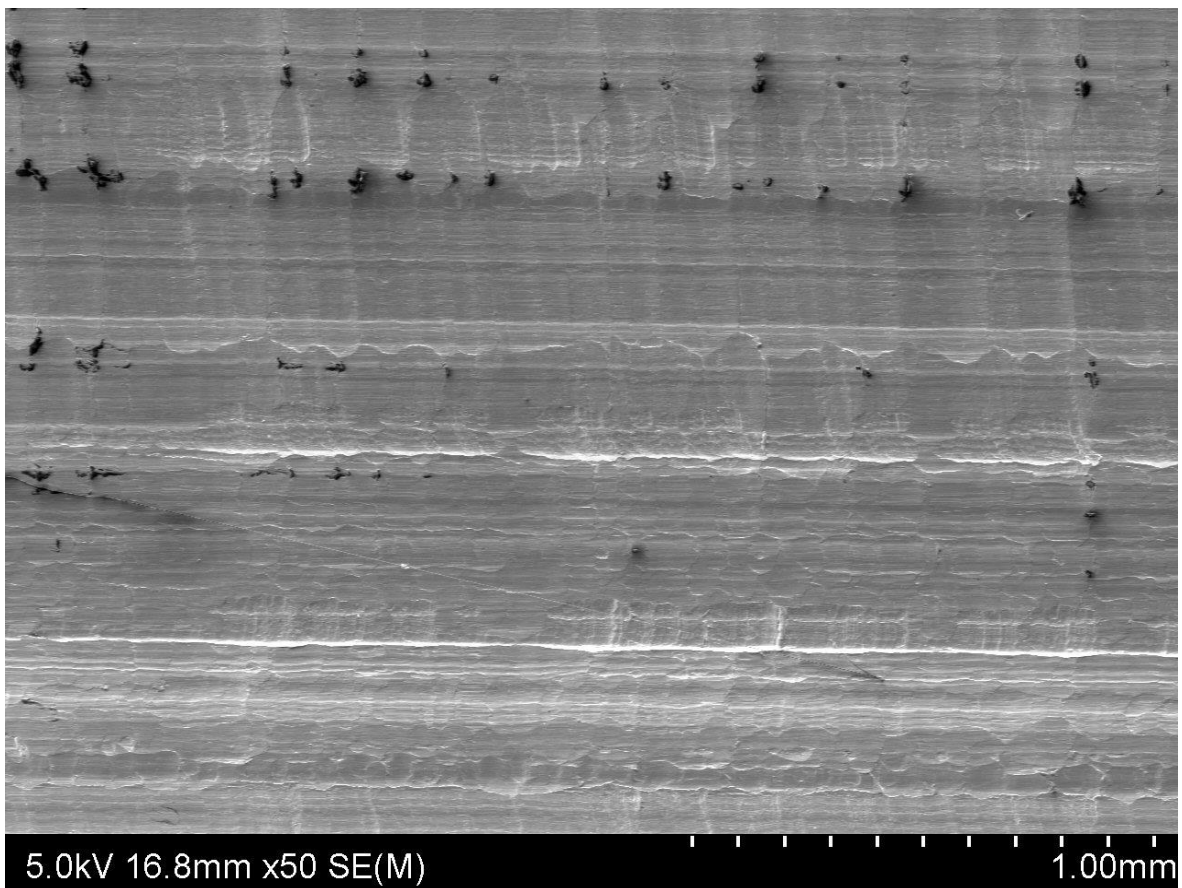
Appendices A4: SEM Images of surfaces milled at 25,000 RPM.



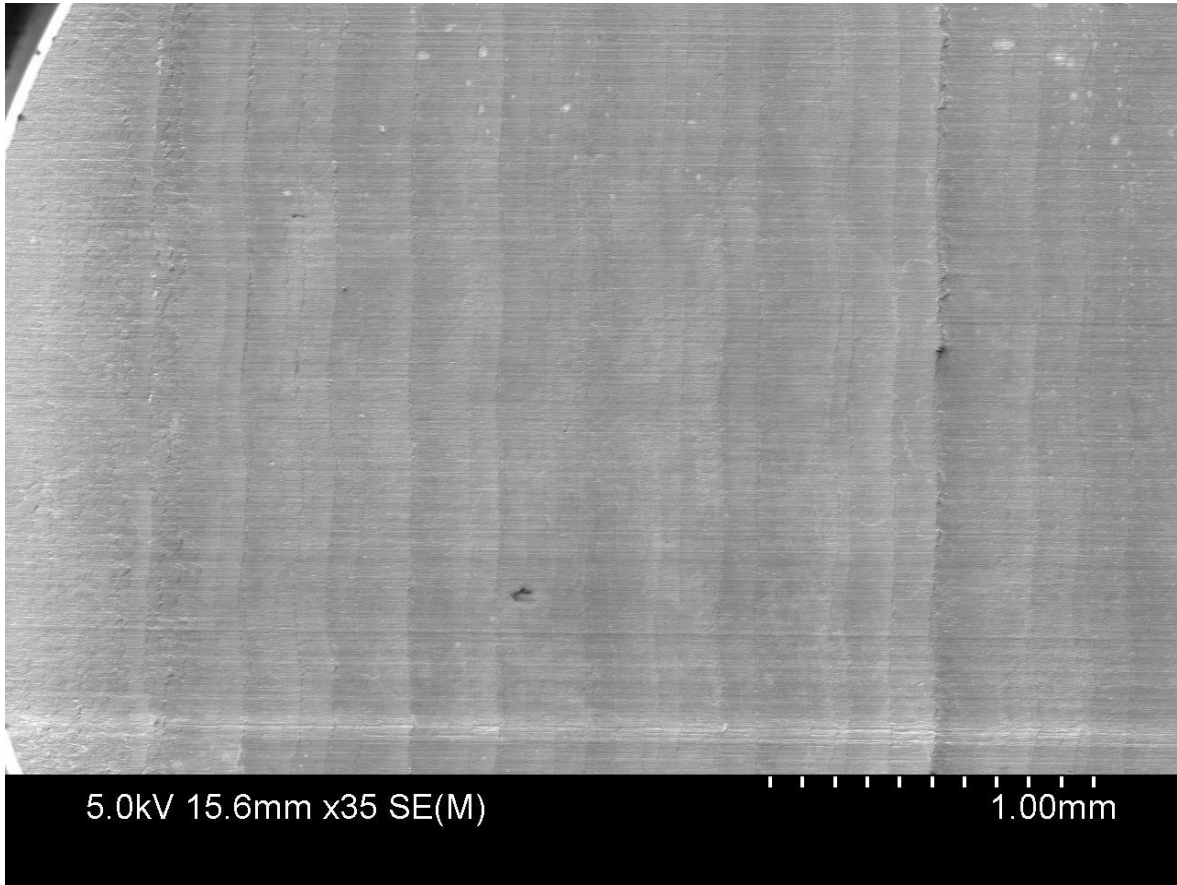
HT4H CoCrMo milled with Mill B.



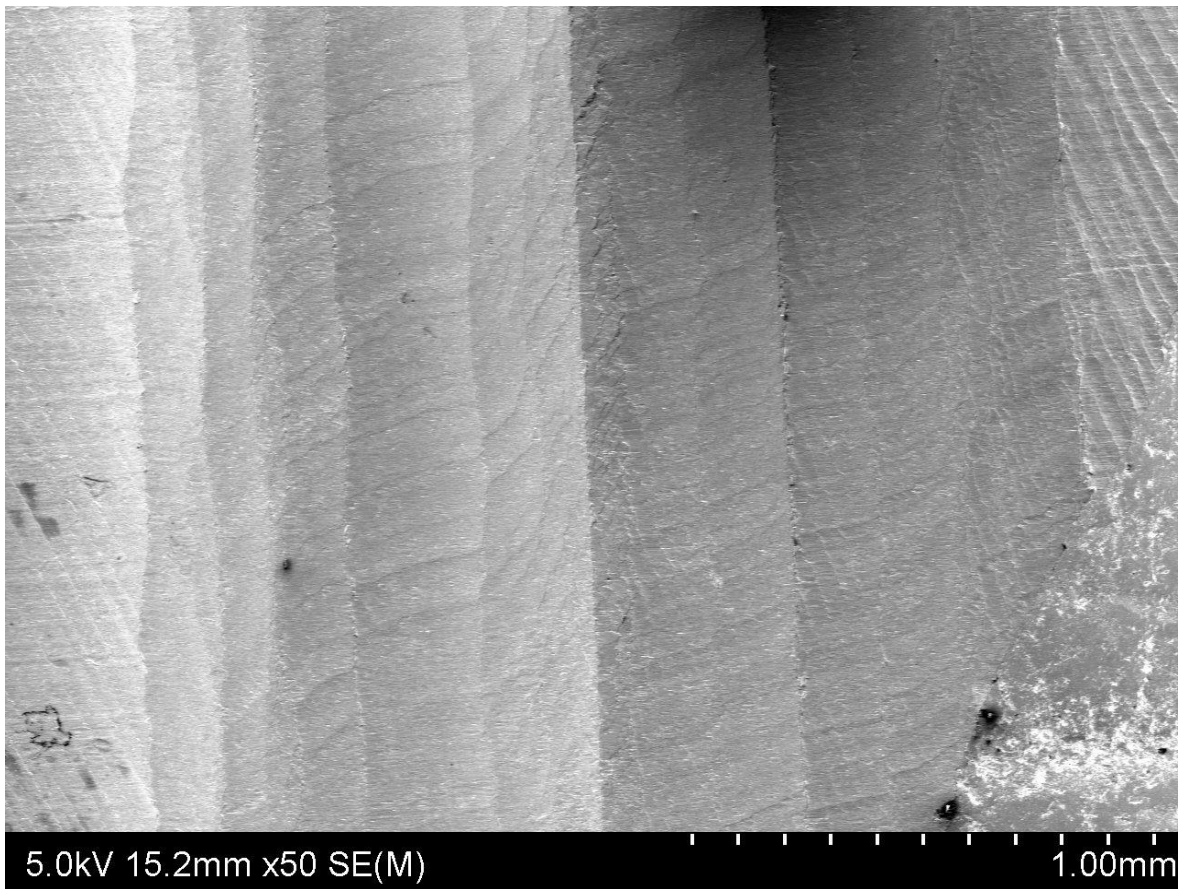
AR CoCrMo milled with Mill A.



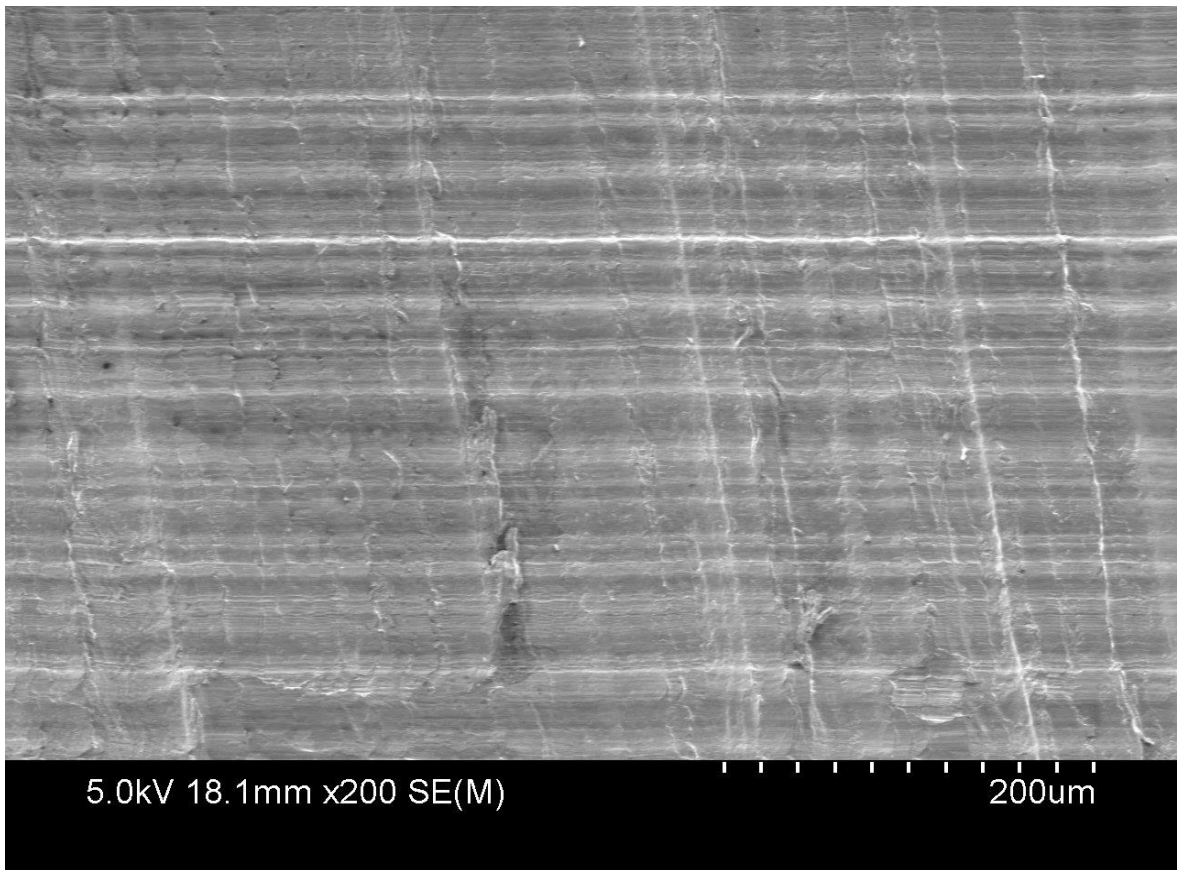
AR CoCrMo milled with Mill B.



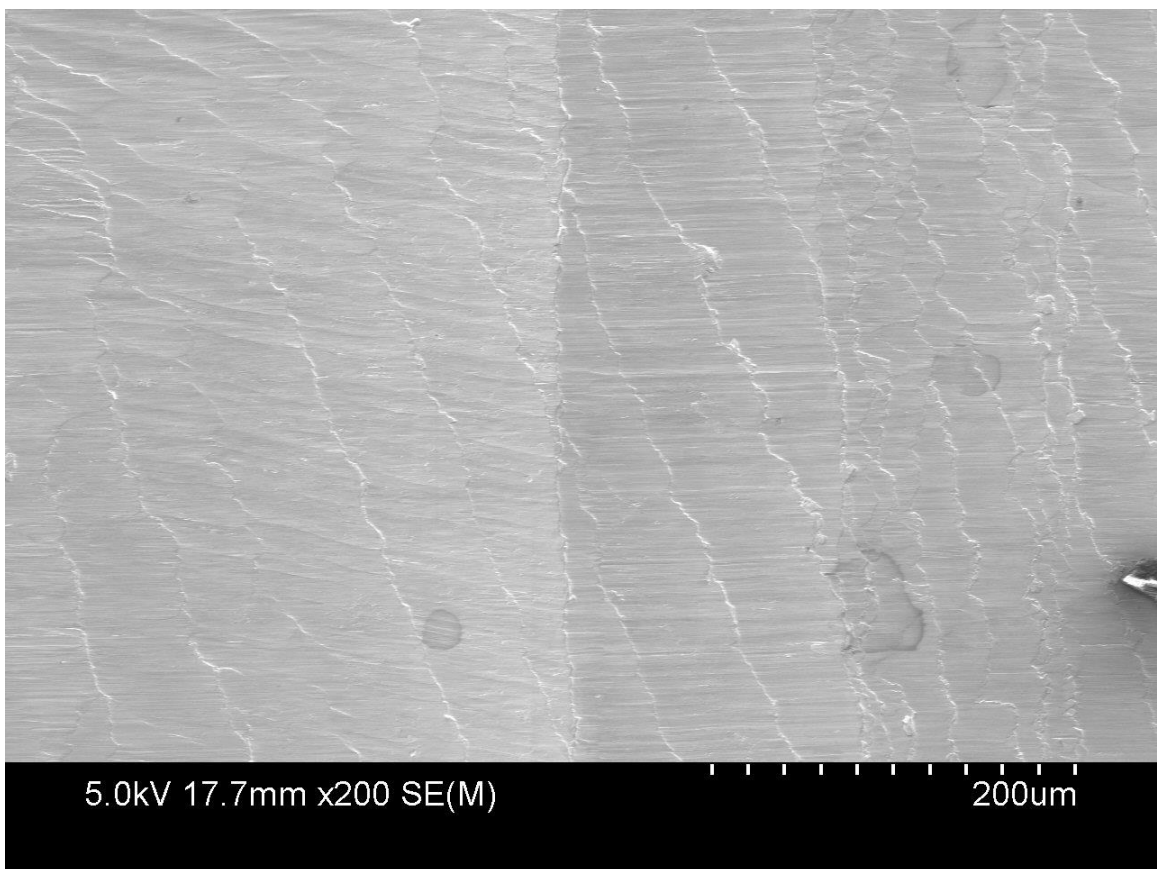
AR CoCrMo milled with Mill C.



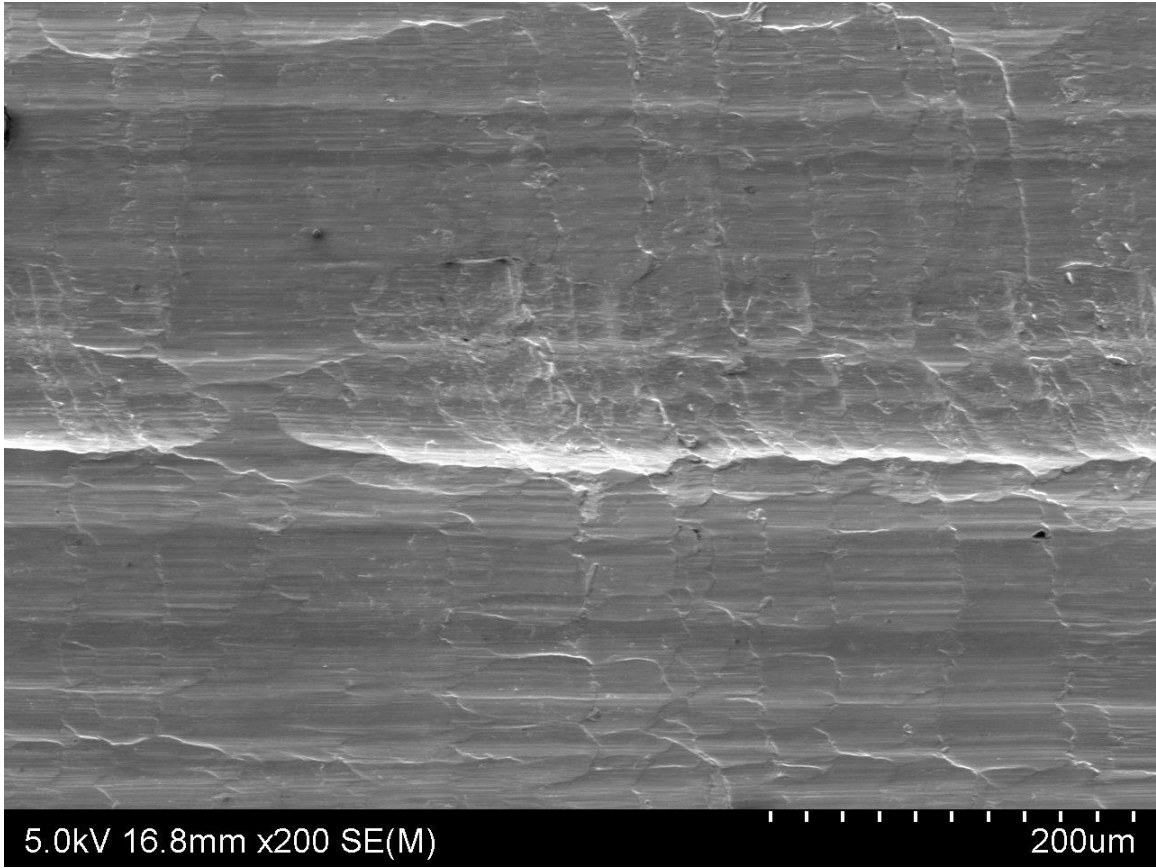
AR CoCrMo milled with Mill D.



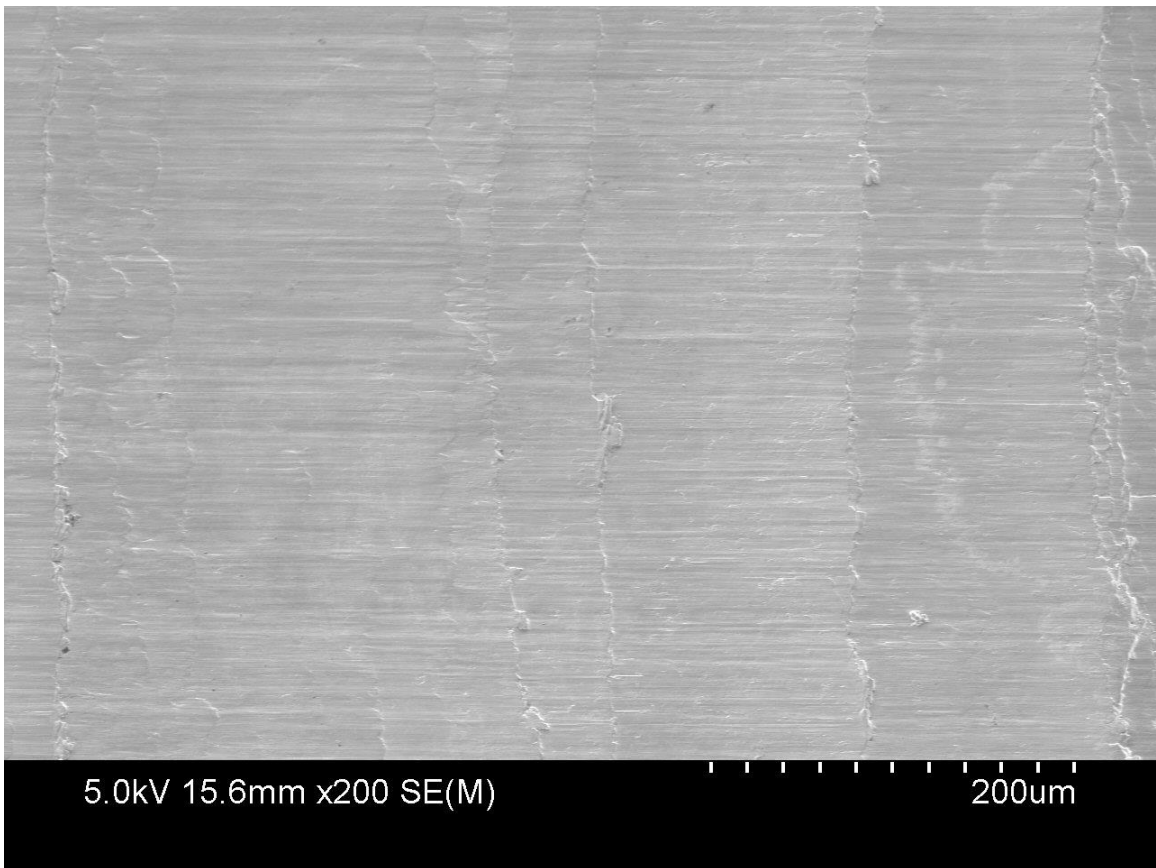
HT4H CoCrMo milled with Mill B.



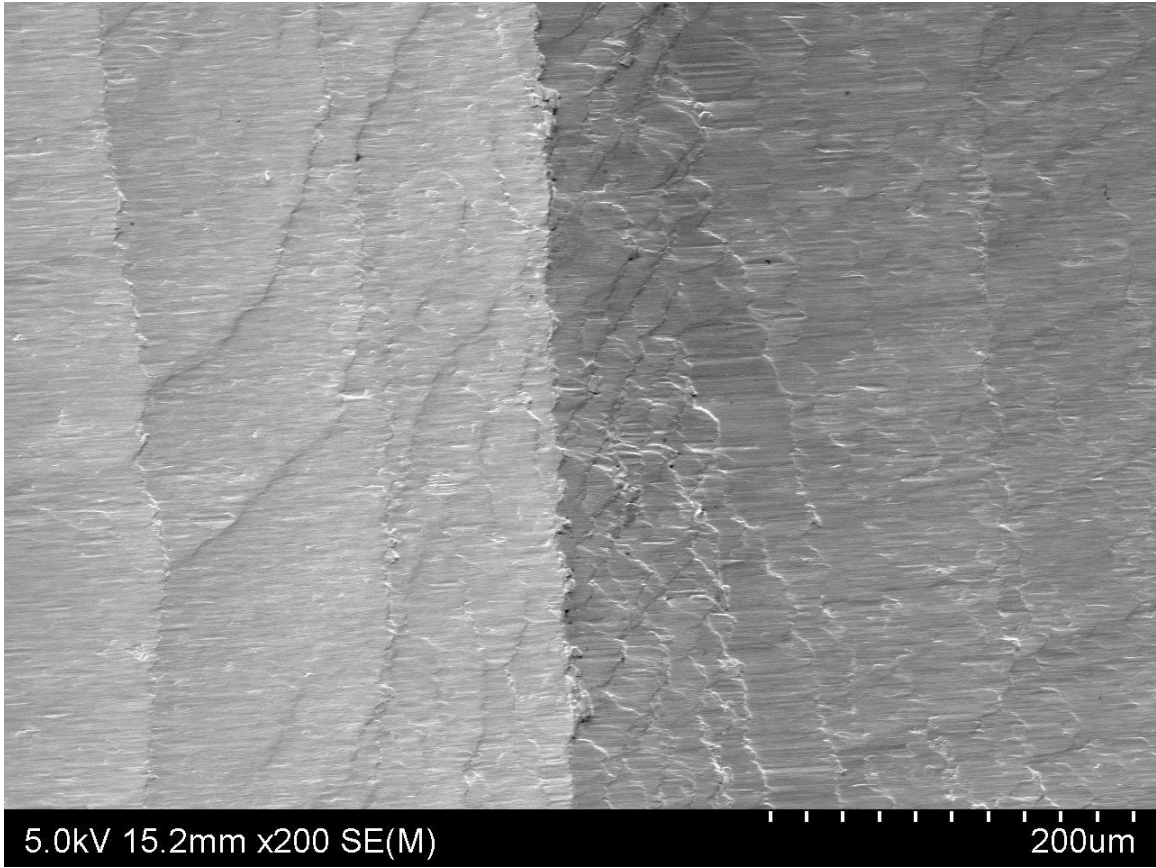
AR CoCrMo milled with Mill A.



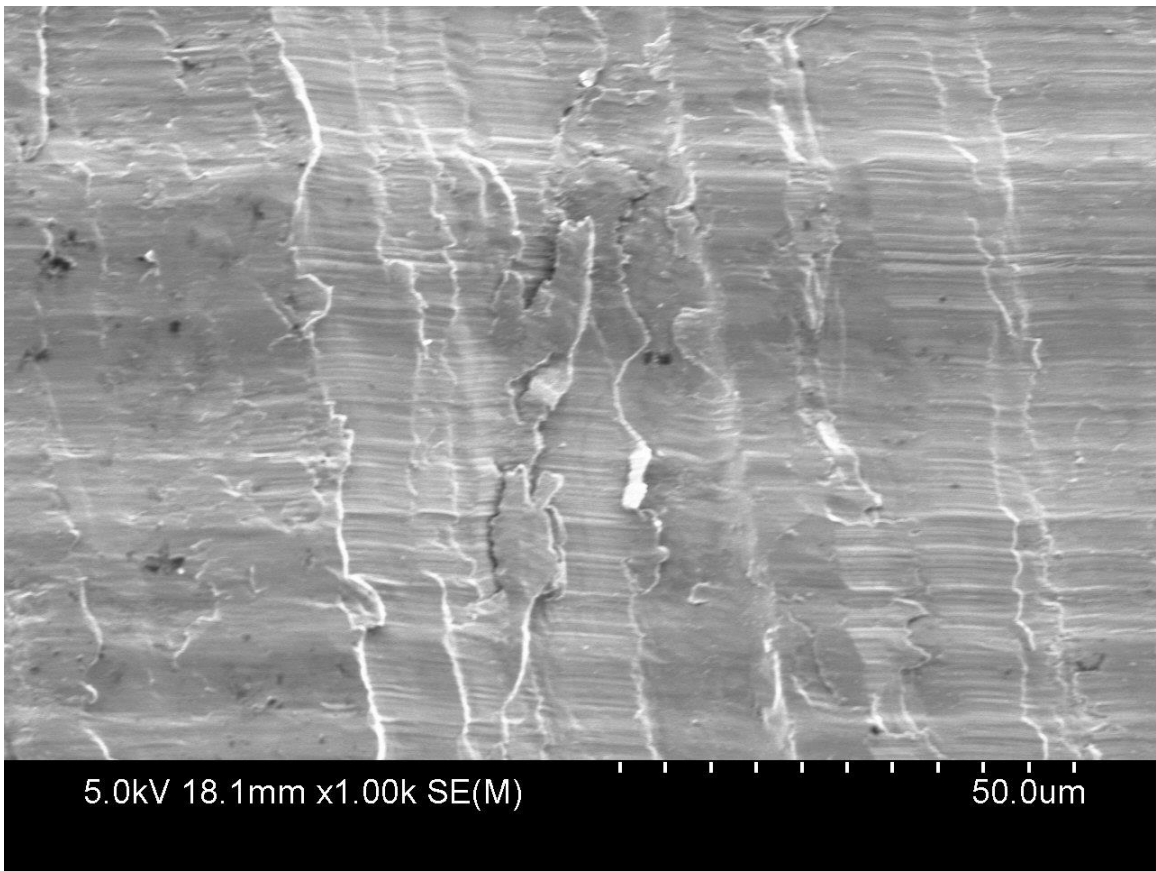
AR CoCrMo milled with Mill B.



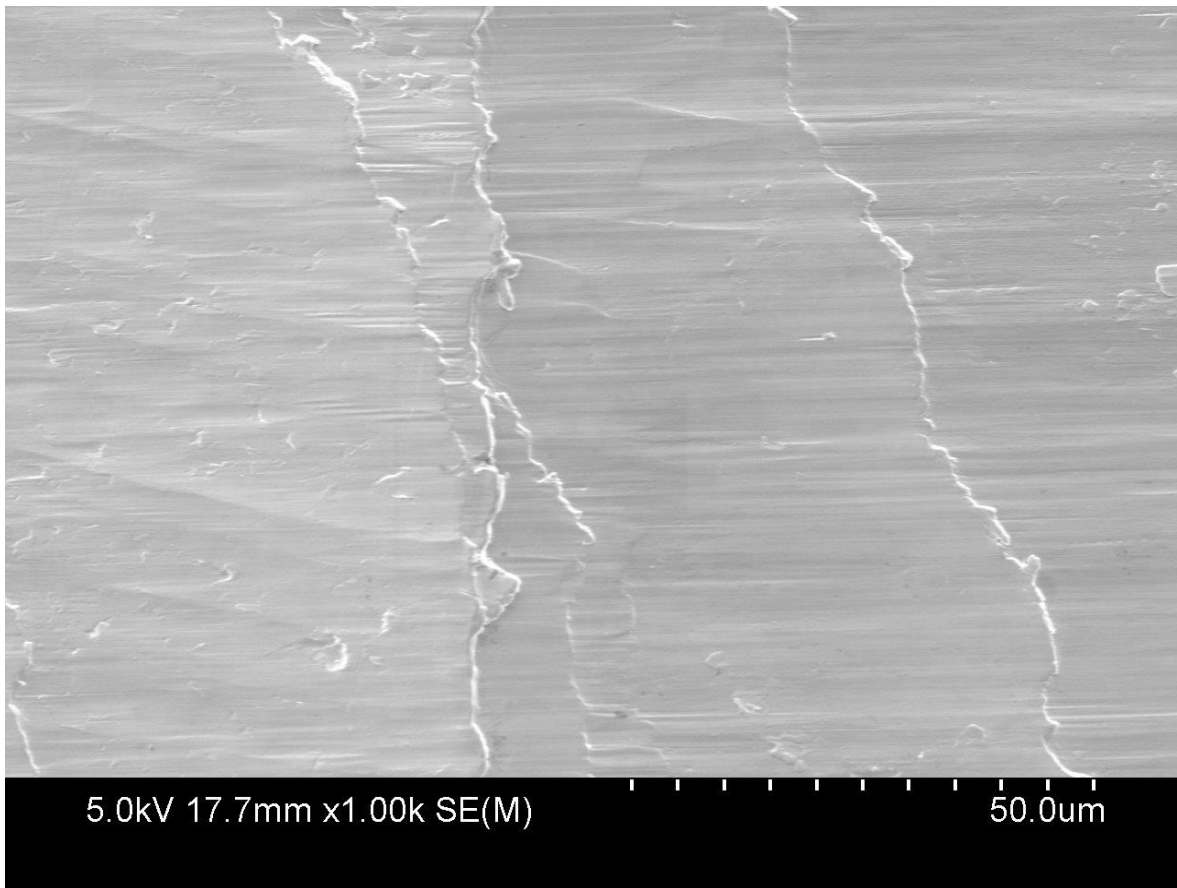
AR CoCrMo milled with Mill C.



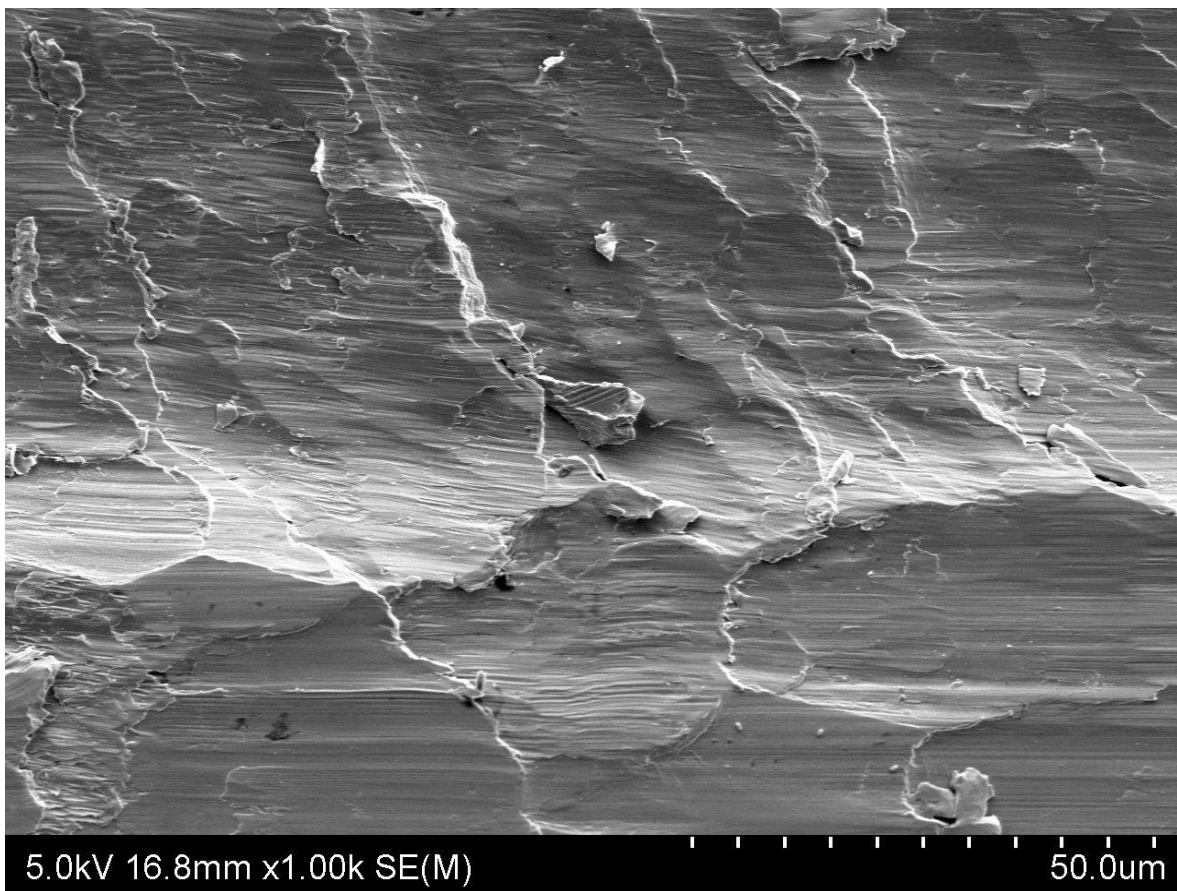
AR CoCrMo milled with Mill D.



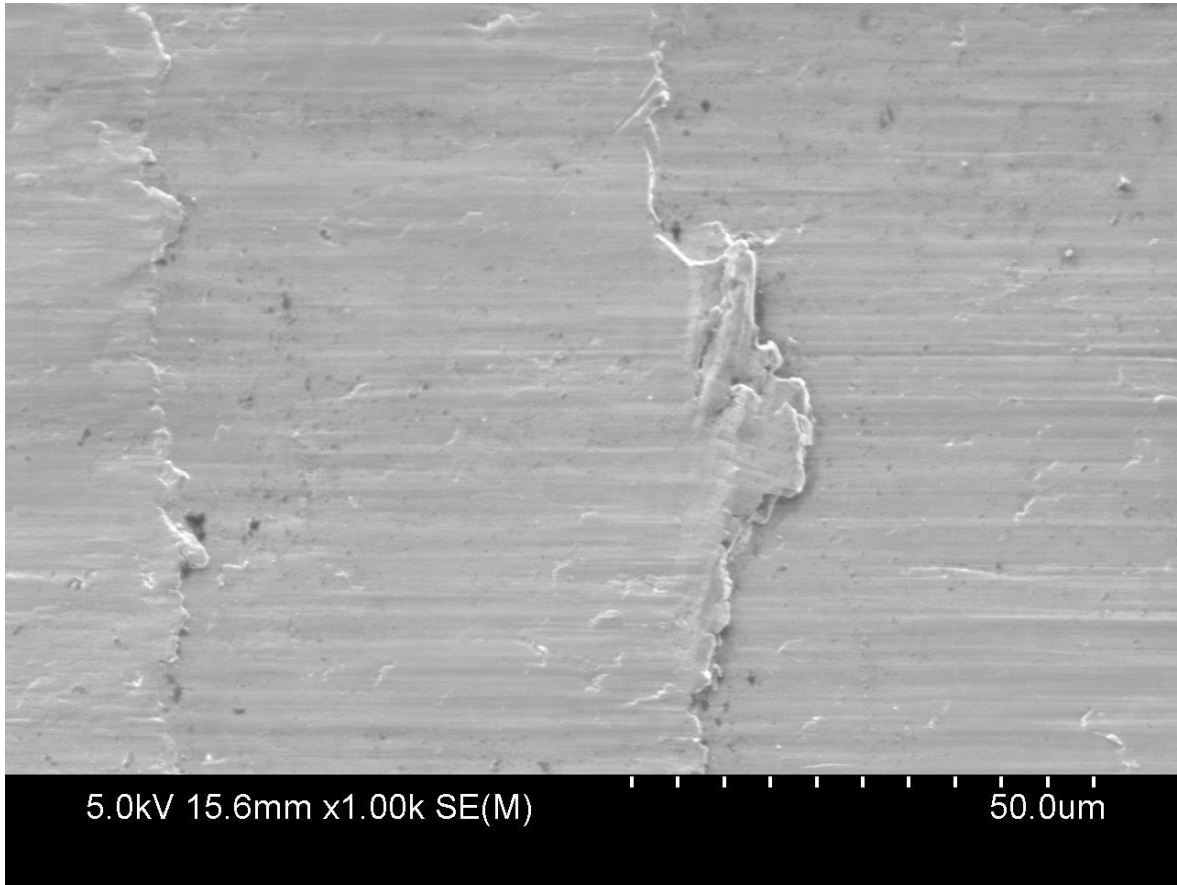
HT4H CoCrMo milled with Mill B.



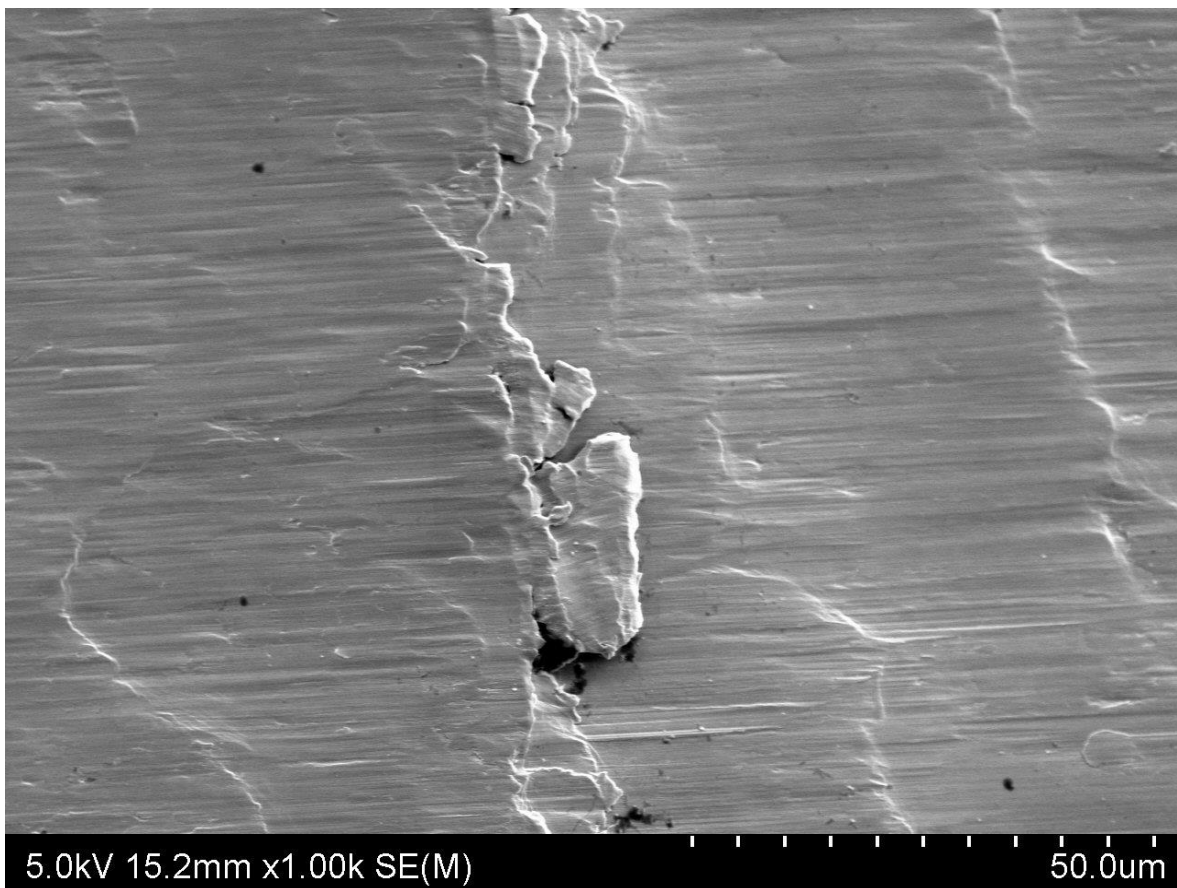
AR CoCrMo milled with Mill A.



AR CoCrMo milled with Mill B.

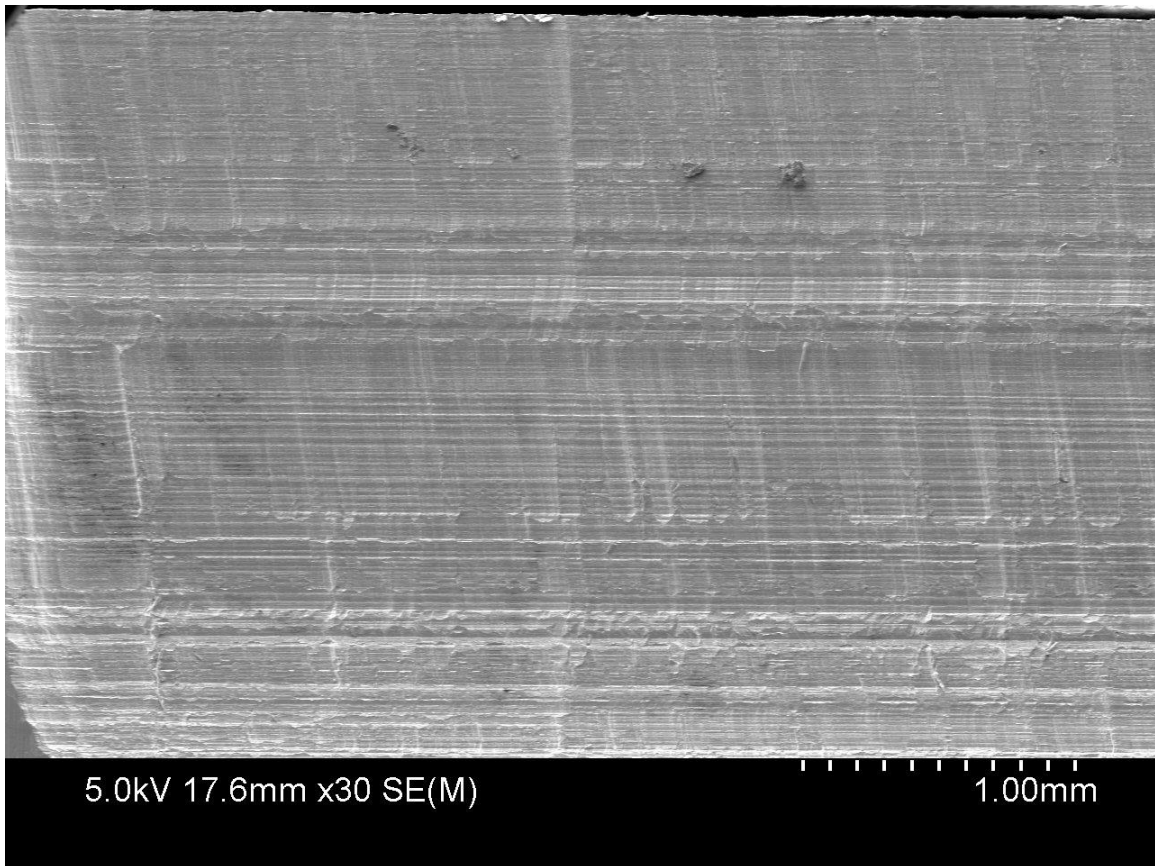


AR CoCrMo milled with Mill C.

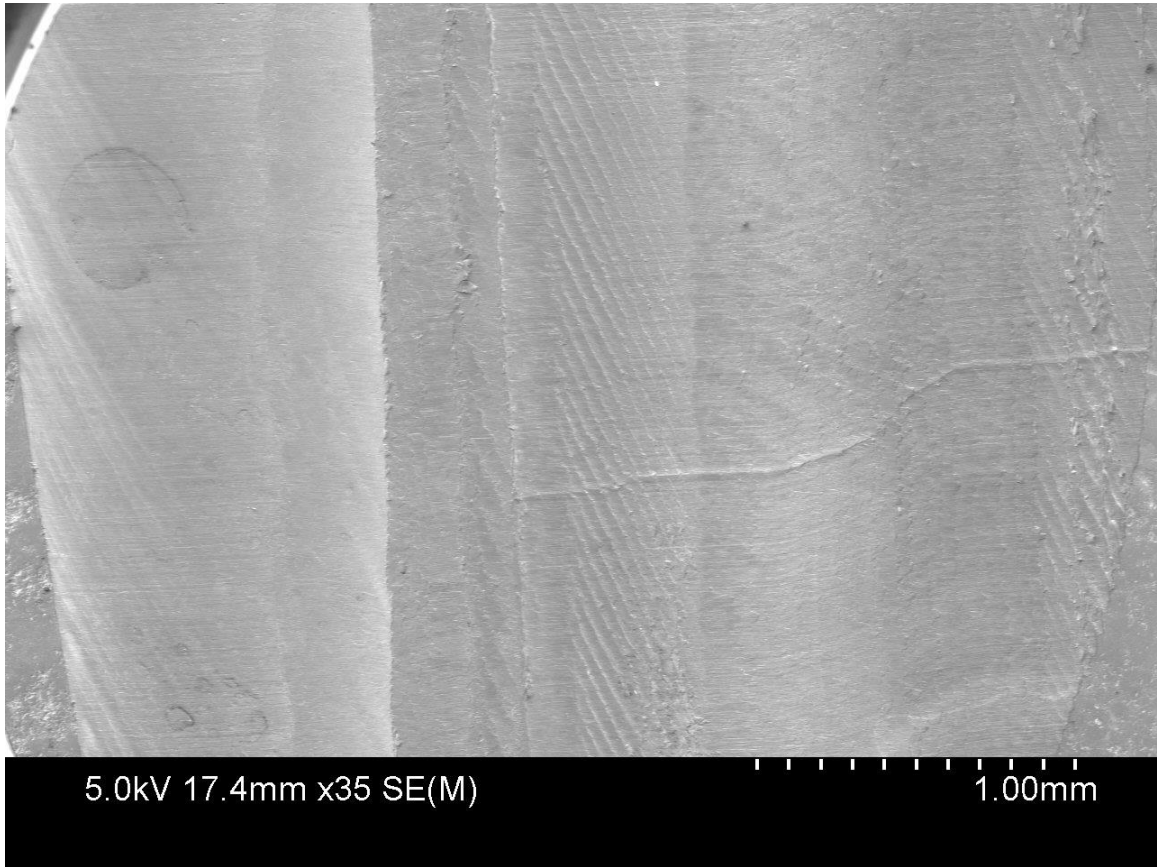


AR CoCrMo milled with Mill D.

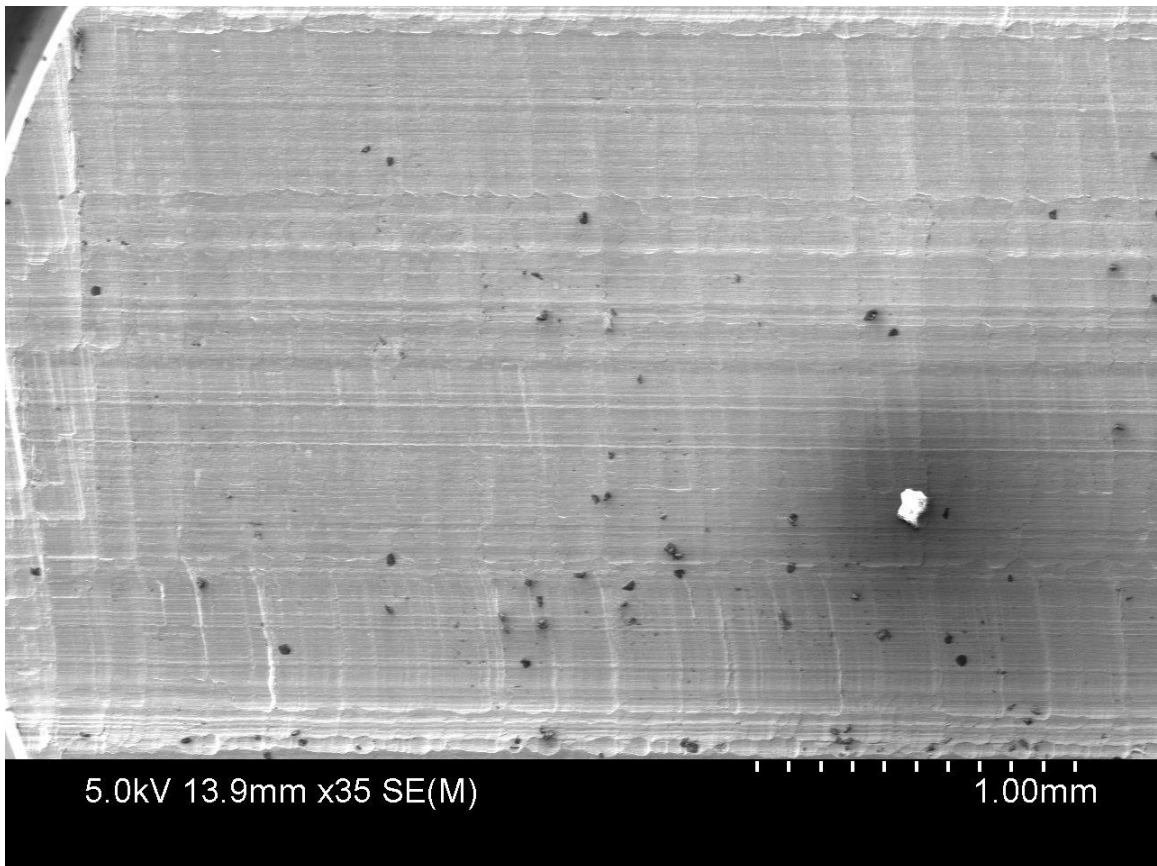
Appendices A5: SEM Images of surfaces milled at 30,000 RPM.



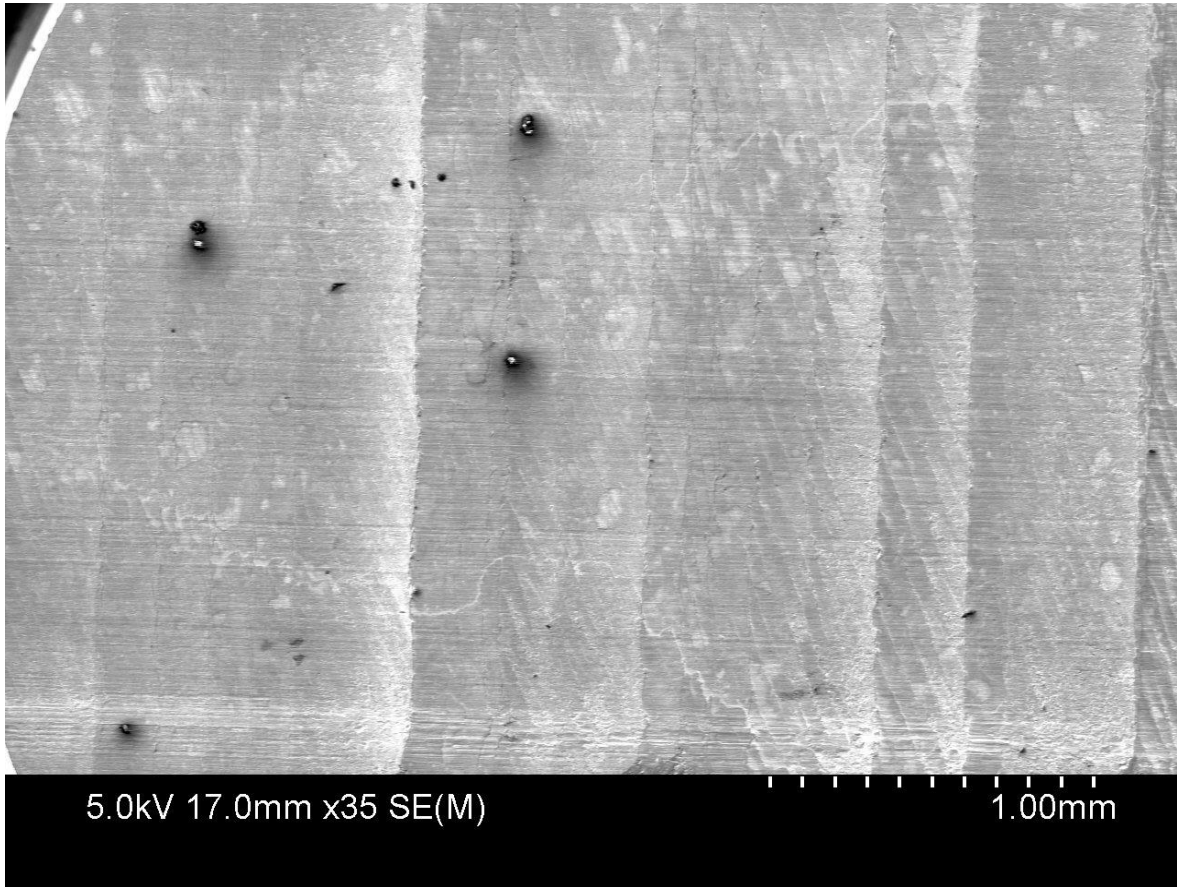
HT4H CoCrMo milled with Mill B.



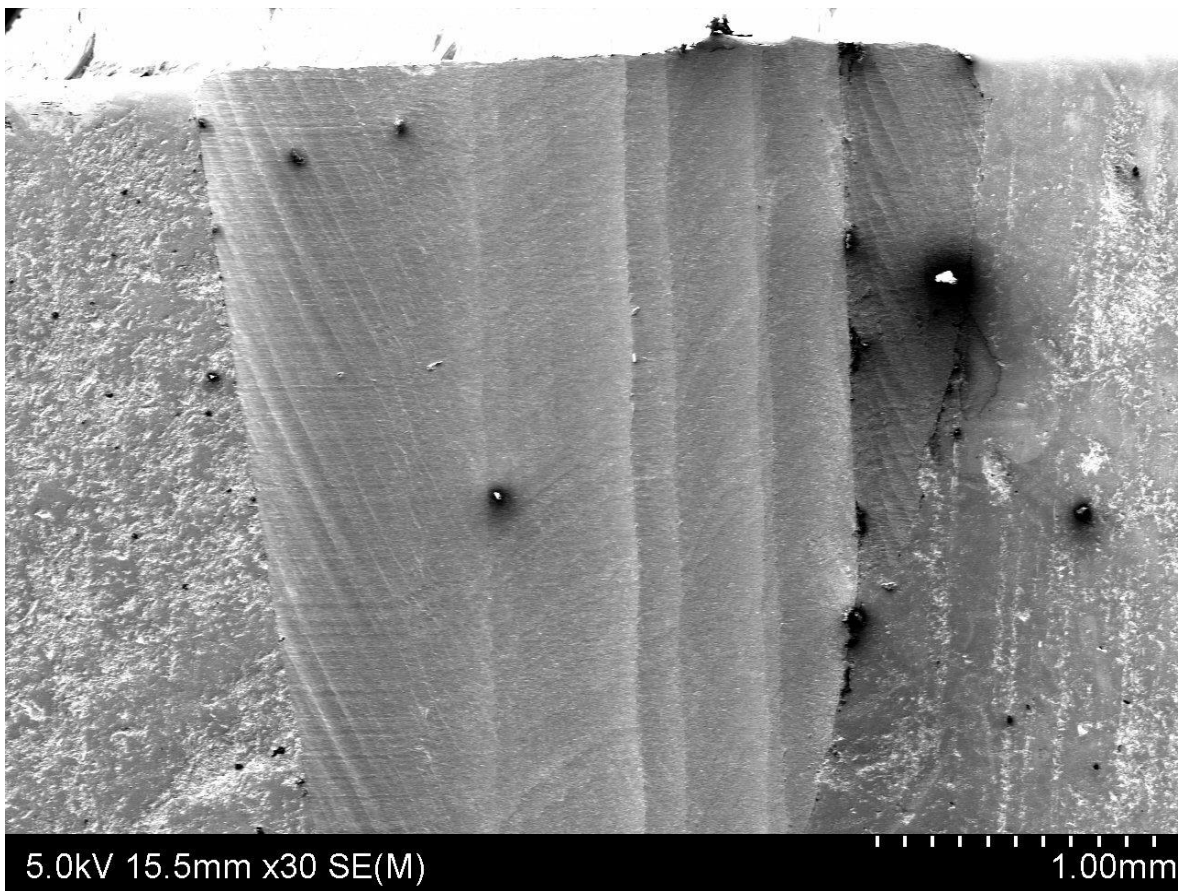
AR CoCrMo milled with Mill A.



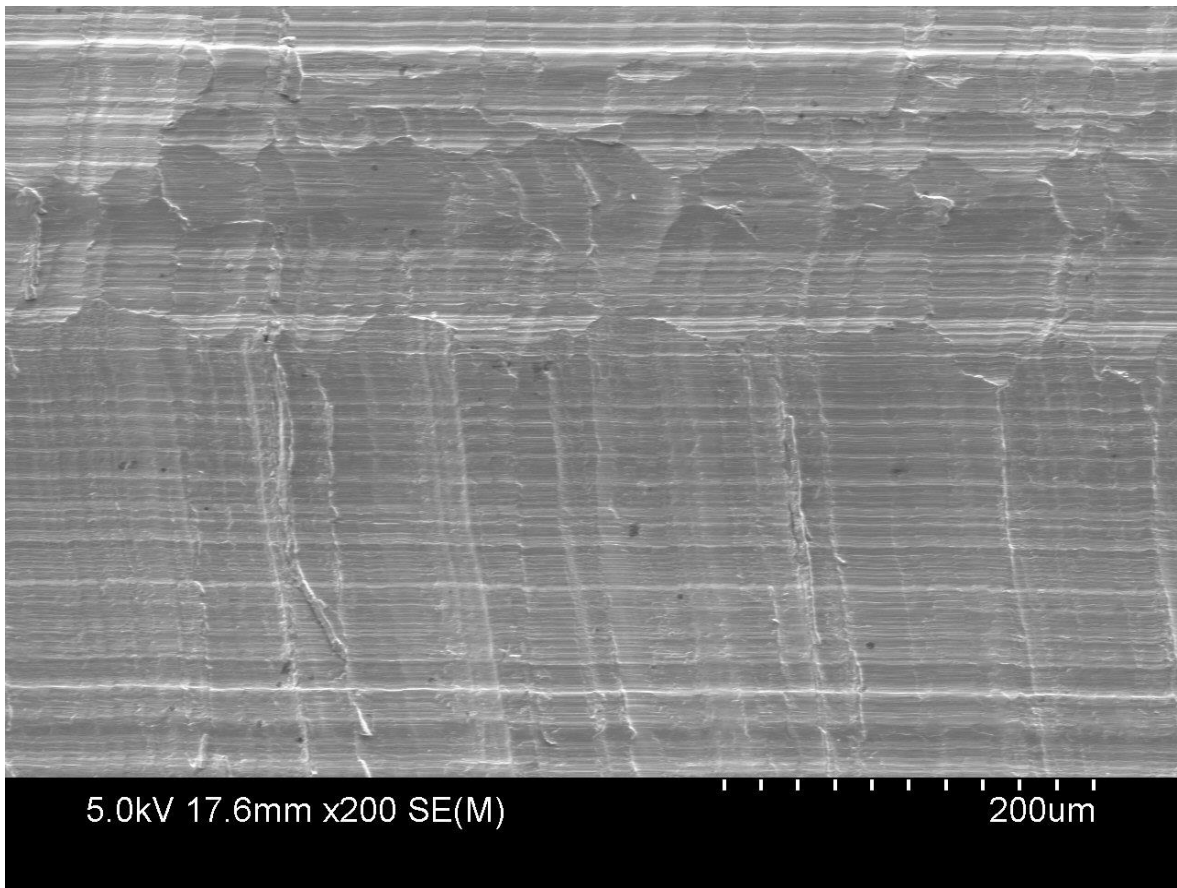
AR CoCrMo milled with Mill B.



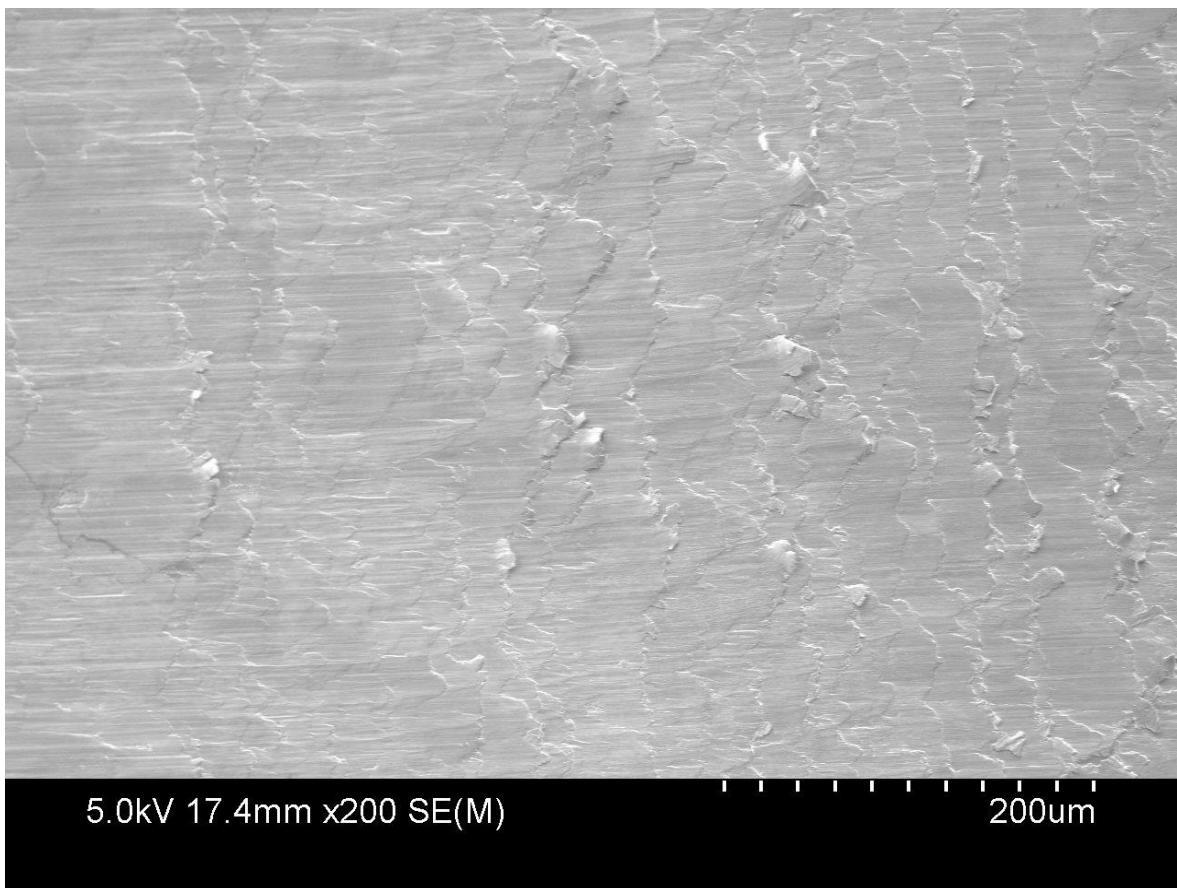
AR CoCrMo milled with Mill C.



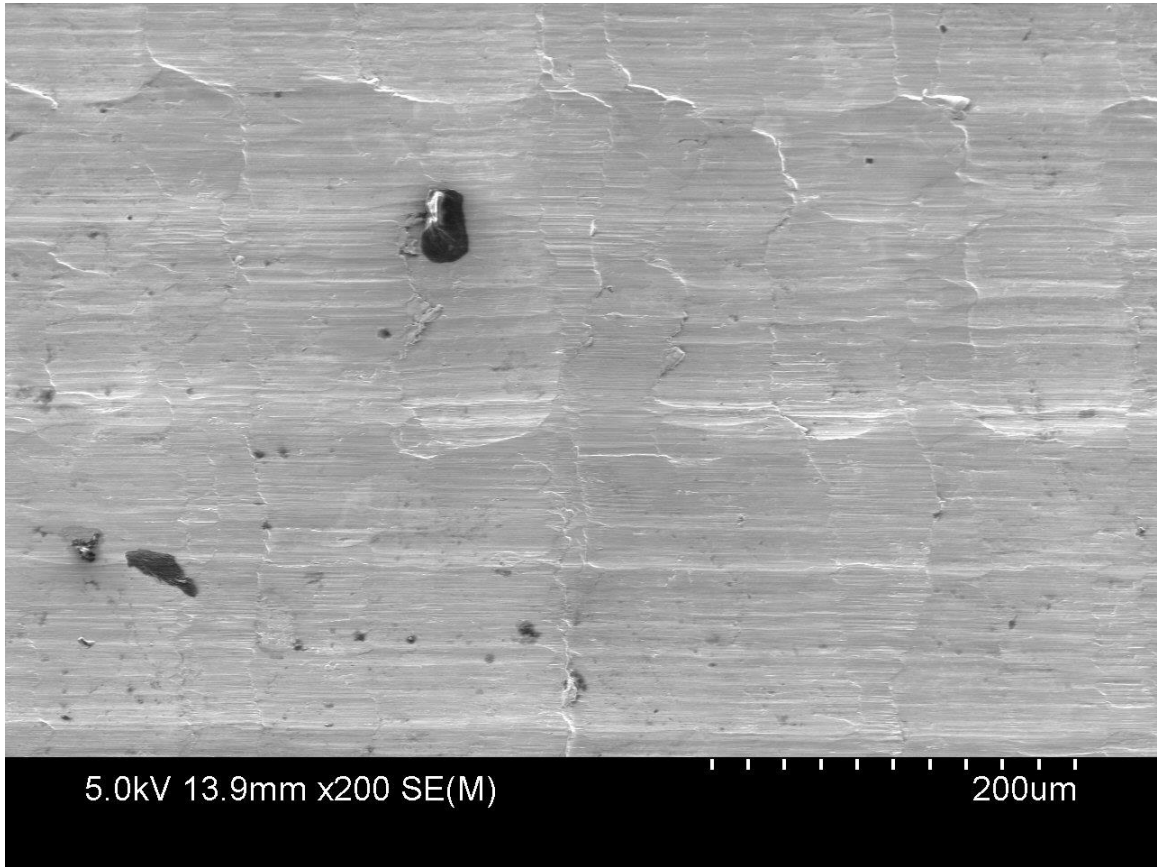
AR CoCrMo milled with Mill D.



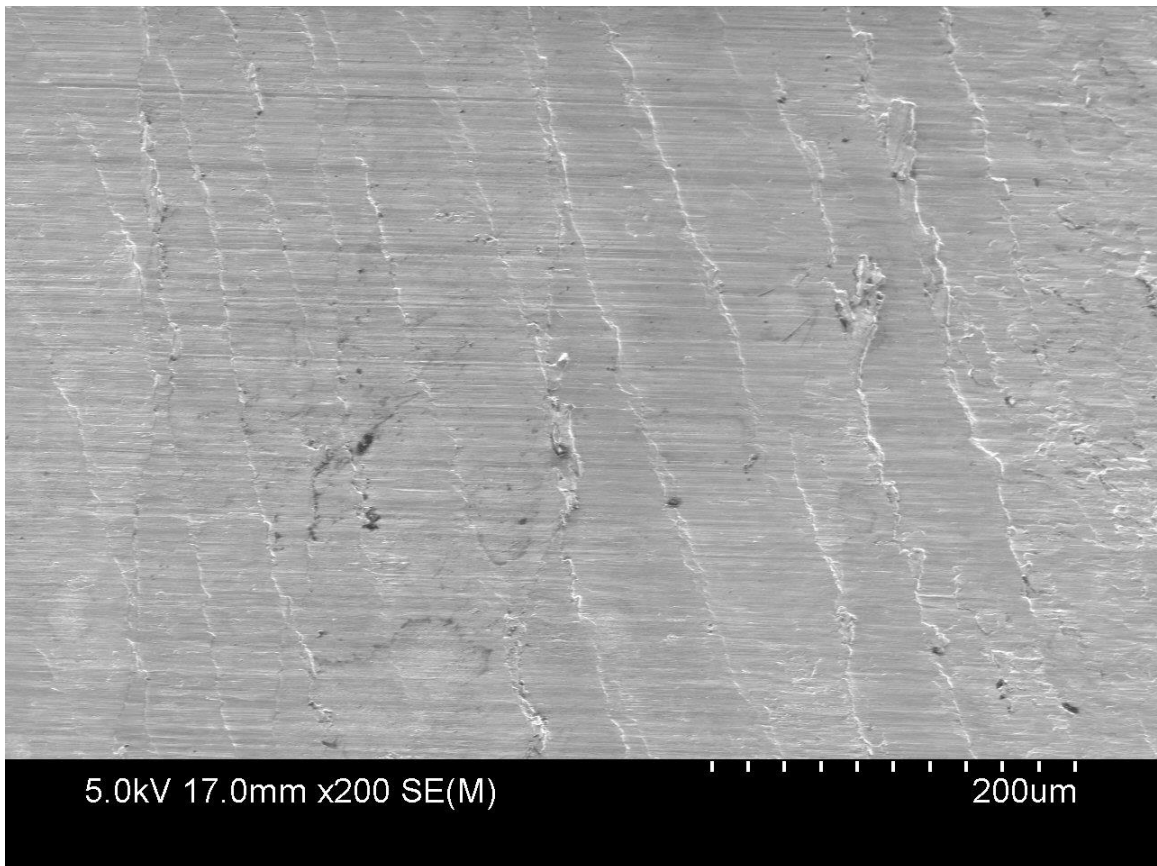
HT4H CoCrMo milled with Mill B.



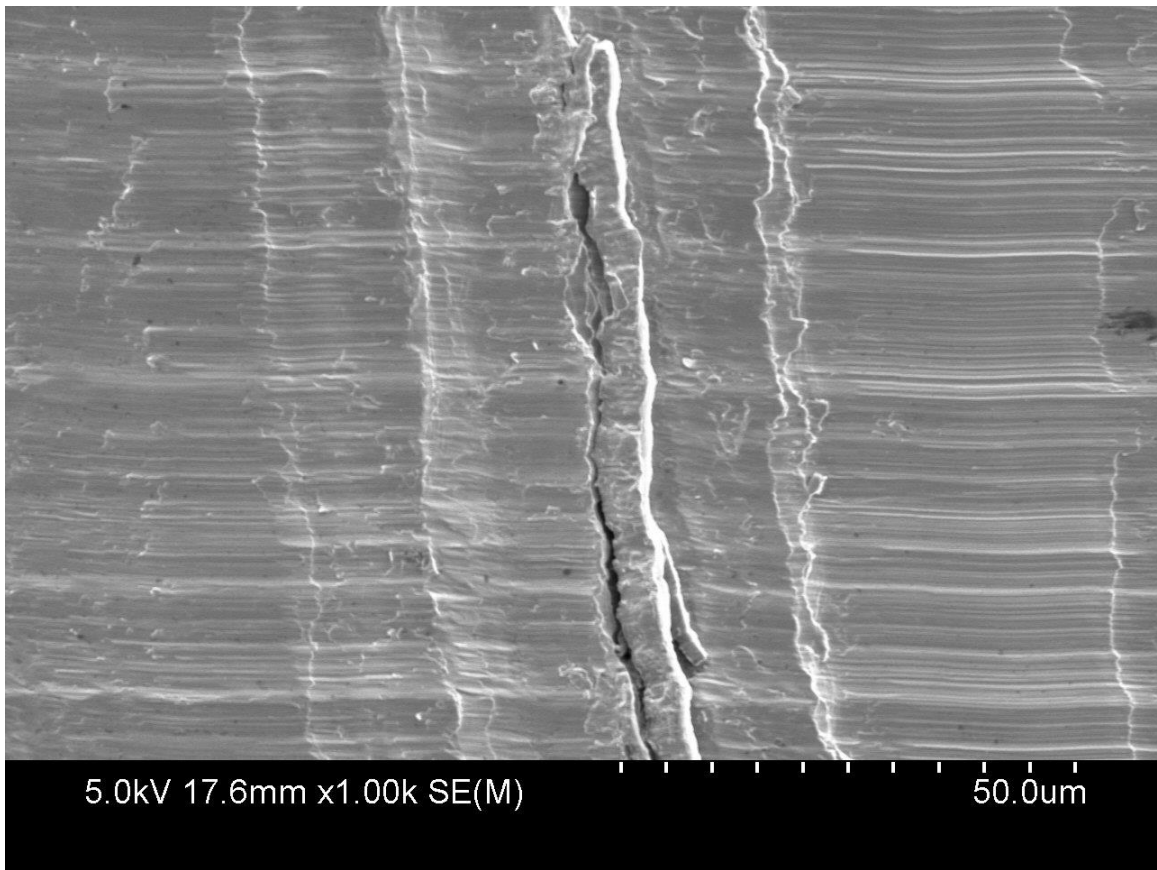
AR CoCrMo milled with Mill A.



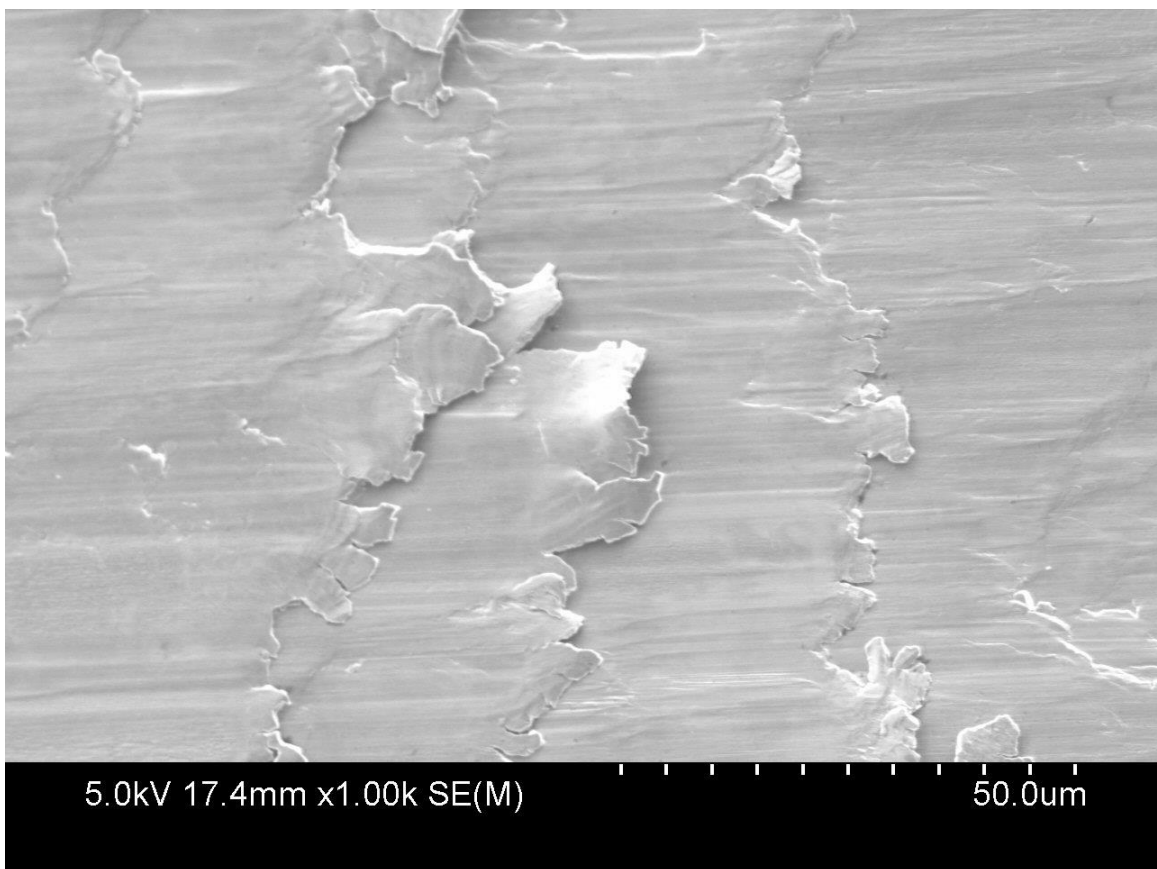
AR CoCrMo milled with Mill B.



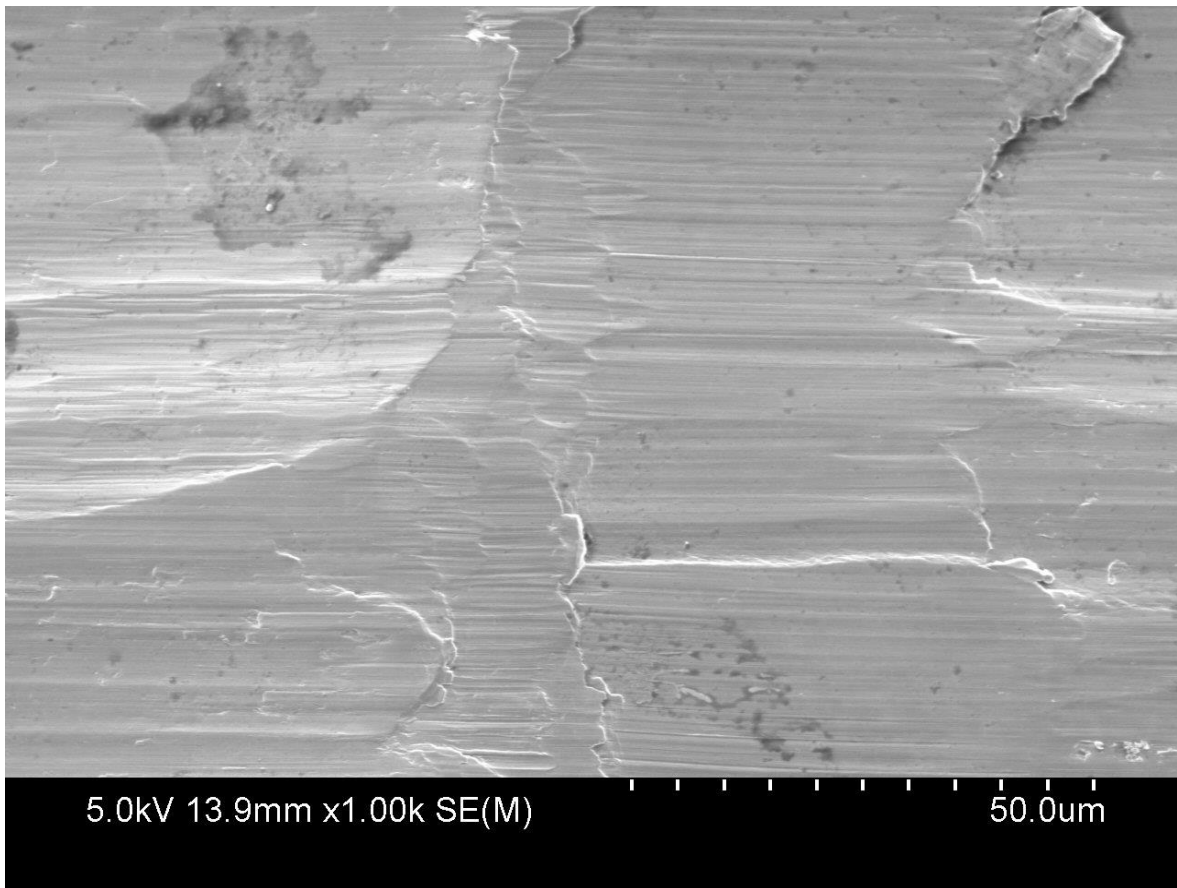
AR CoCrMo milled with Mill C.



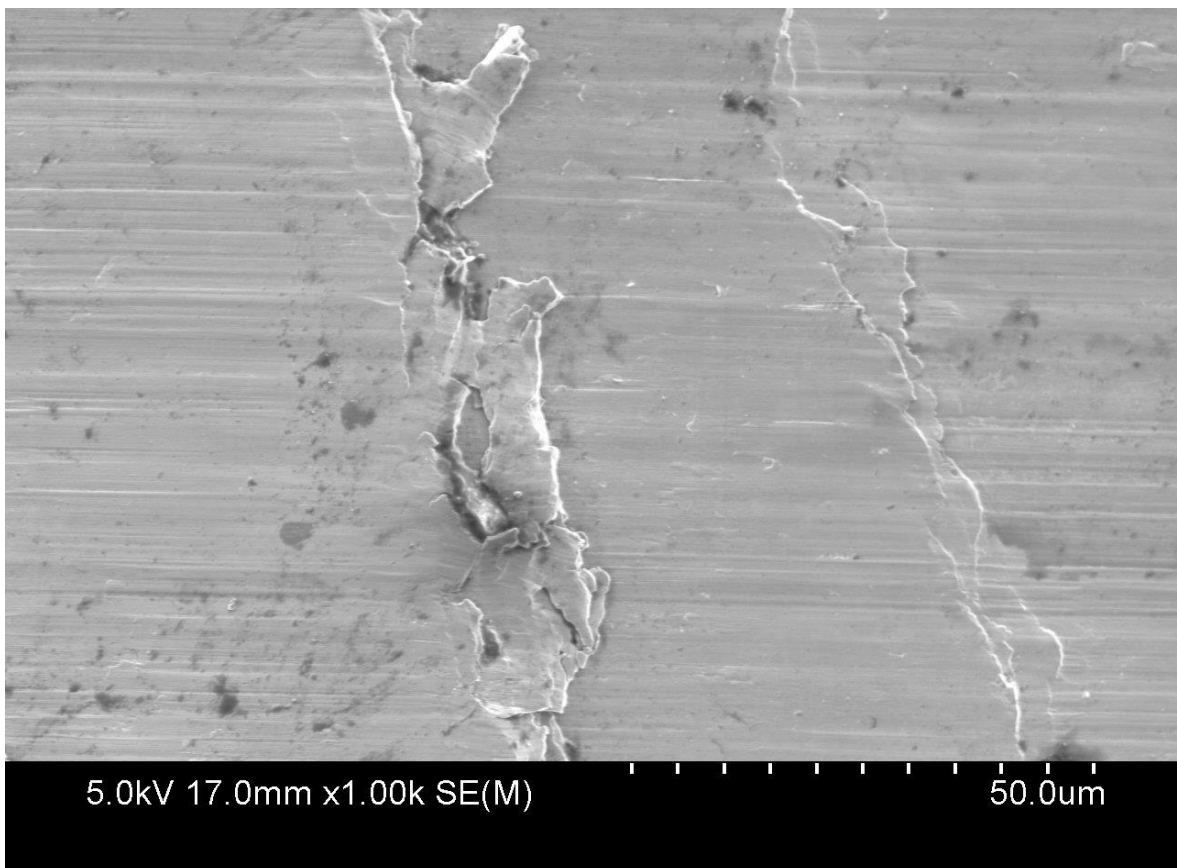
HT4H CoCrMo milled with Mill B.



AR CoCrMo milled with Mill A.

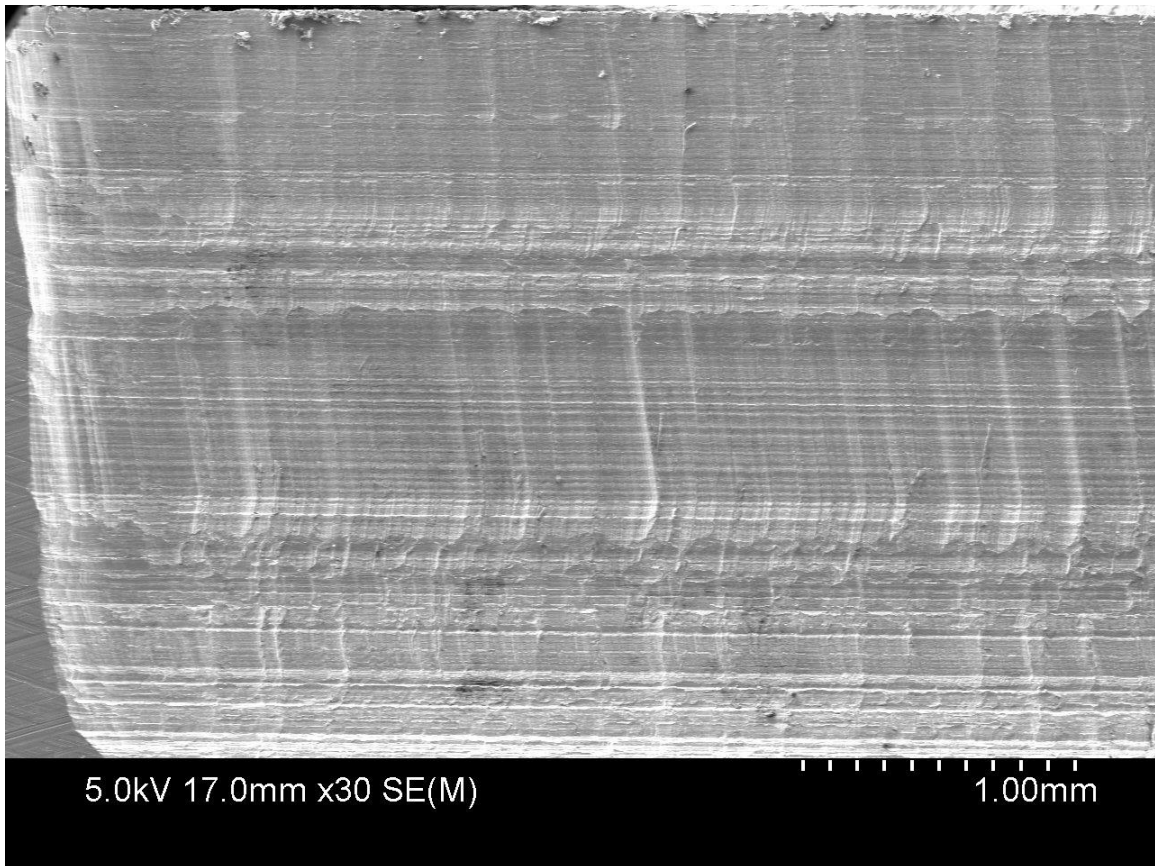


AR CoCrMo milled with Mill B.

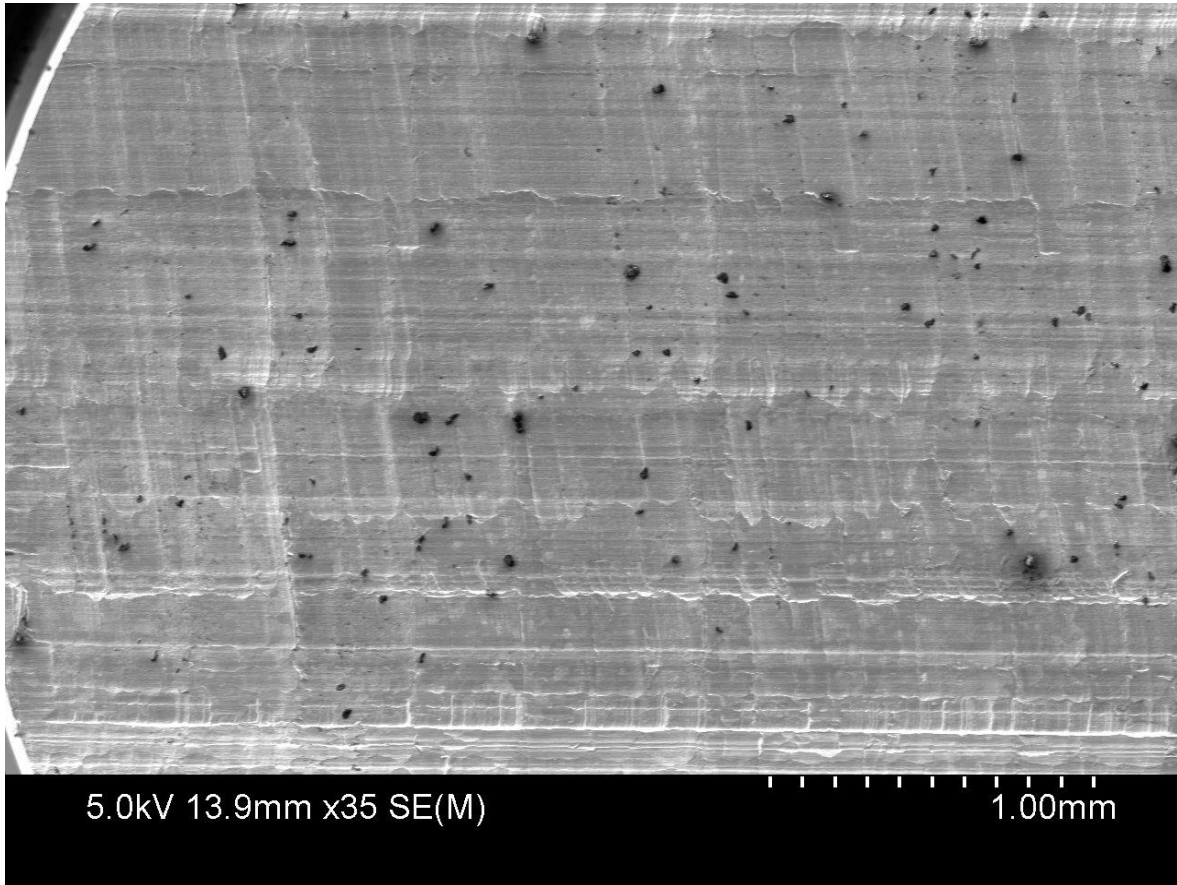


AR CoCrMo milled with Mill C.

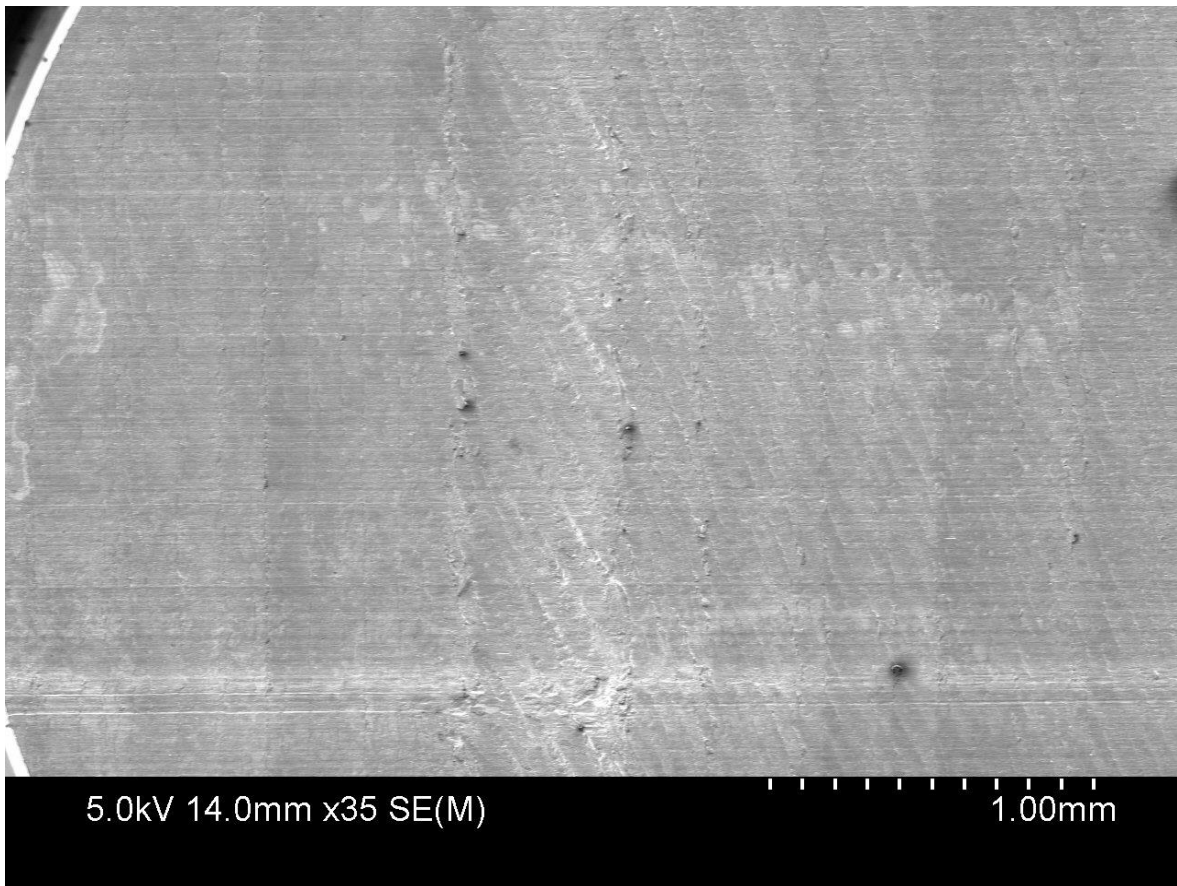
Appendices A6: SEM Images of surfaces milled at 35,000 RPM.



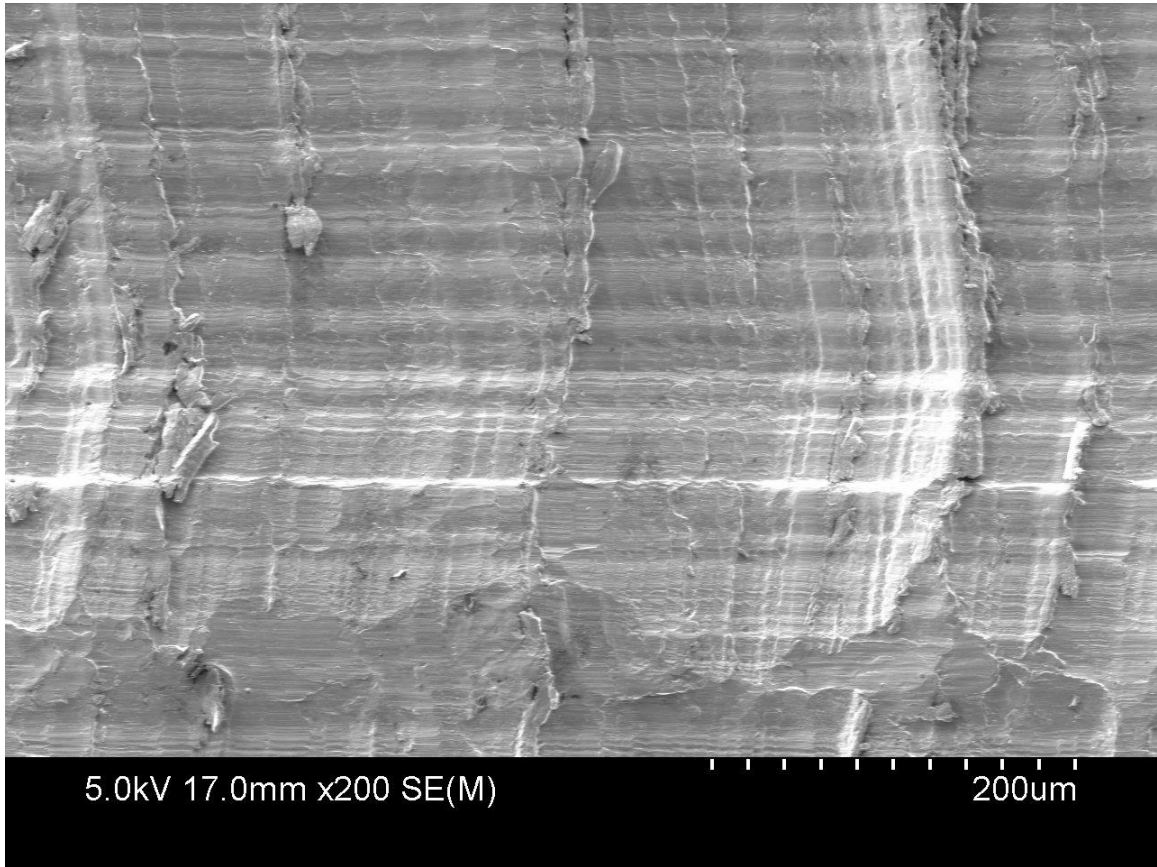
HT4H CoCrMo milled with Mill B.



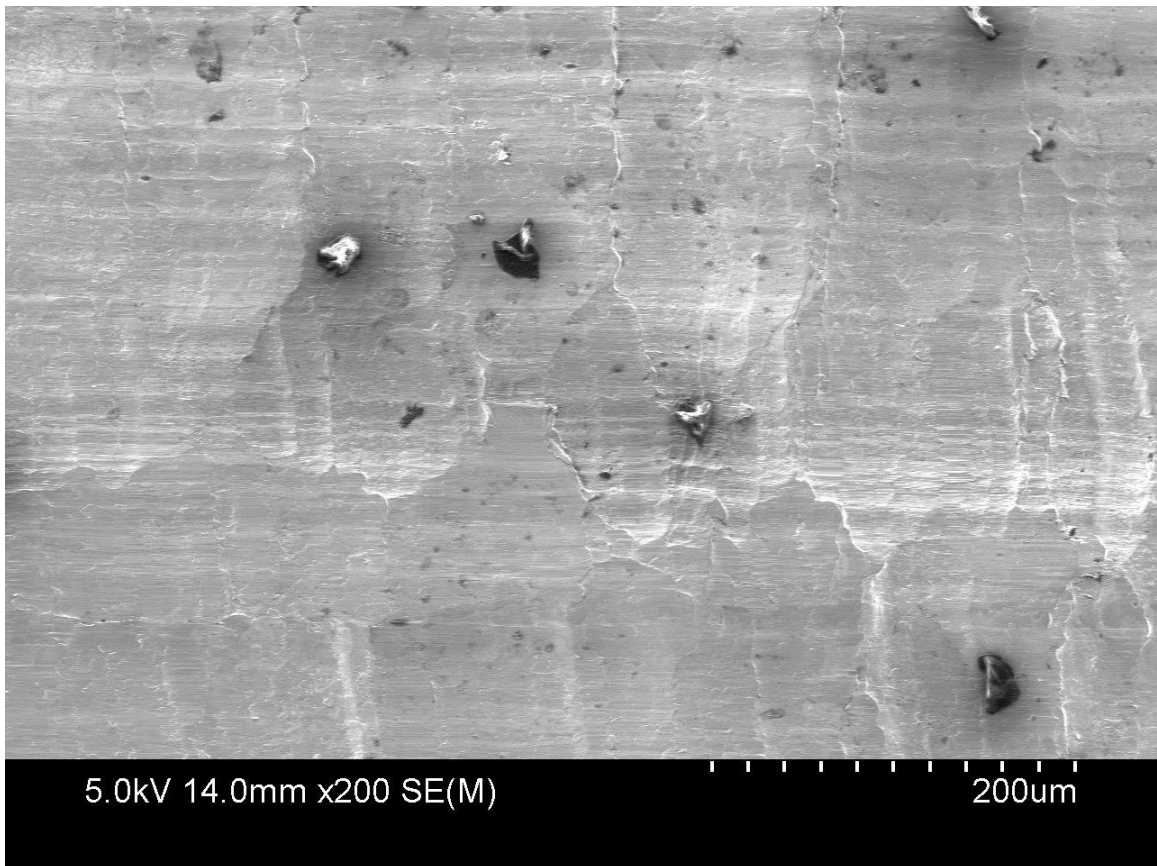
AR CoCrMo milled with Mill B.



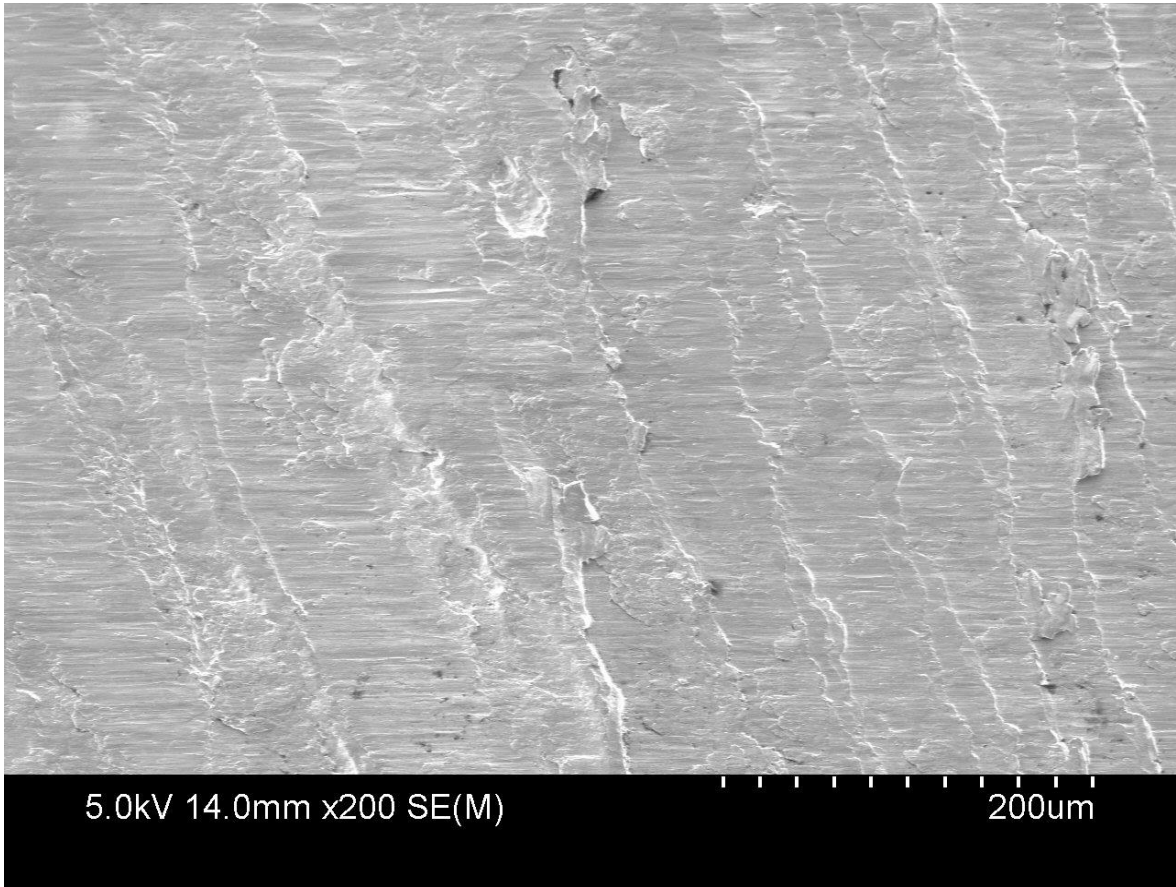
AR CoCrMo milled with Mill C.



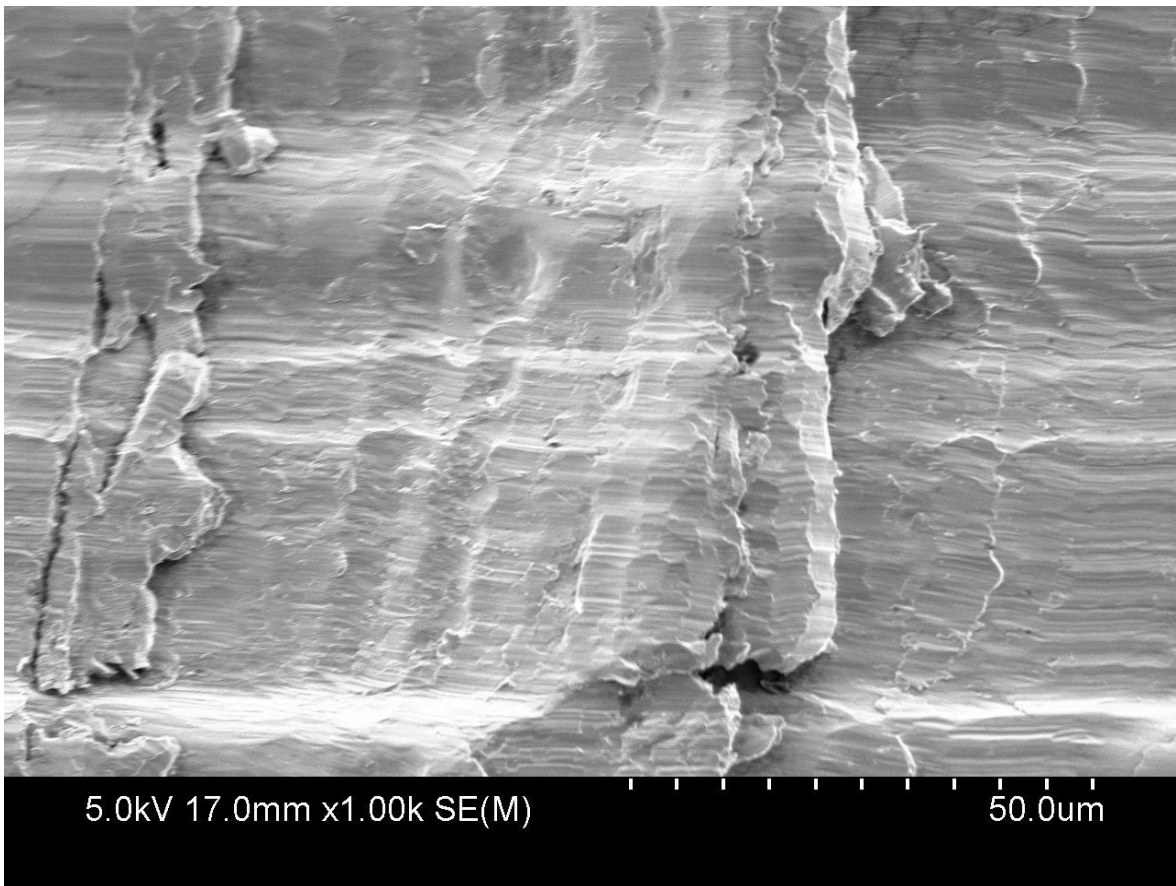
HT4H CoCrMo milled with Mill B.



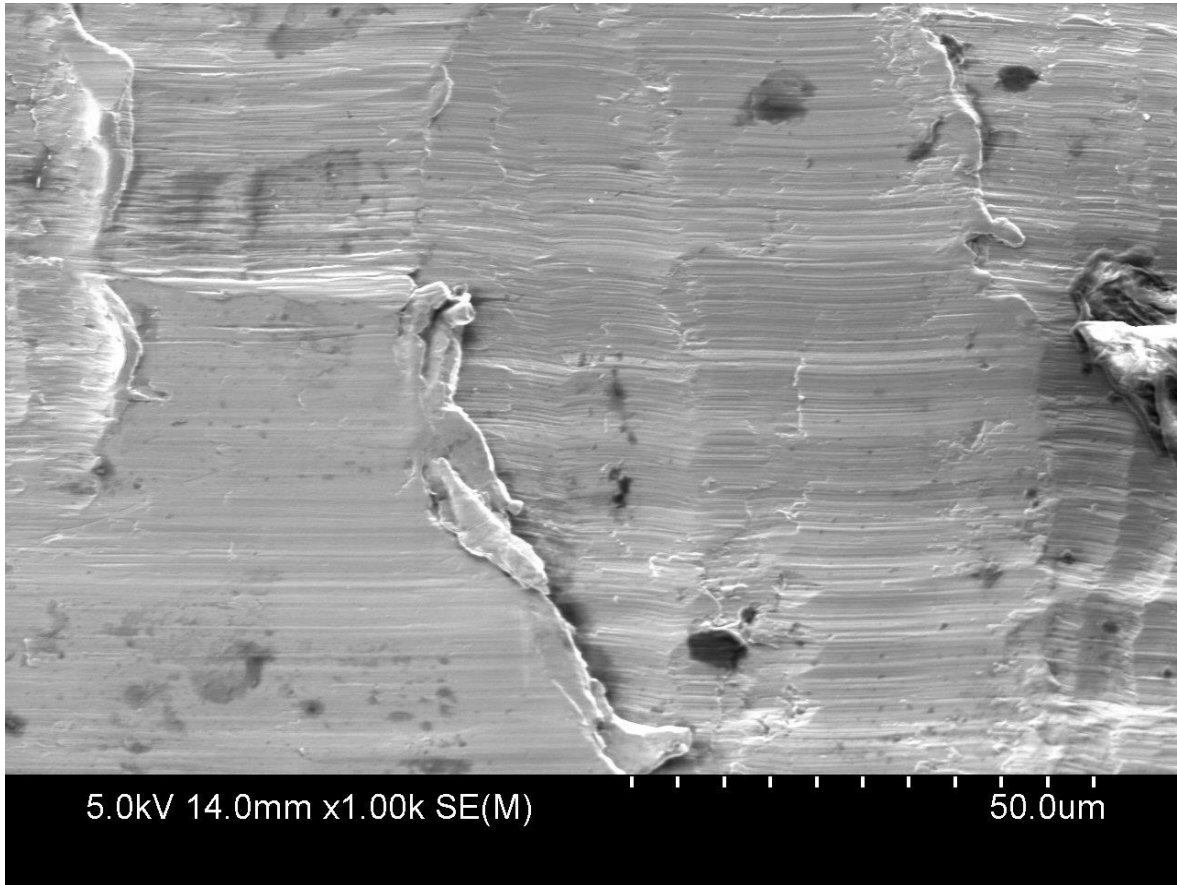
AR CoCrMo milled with Mill B.



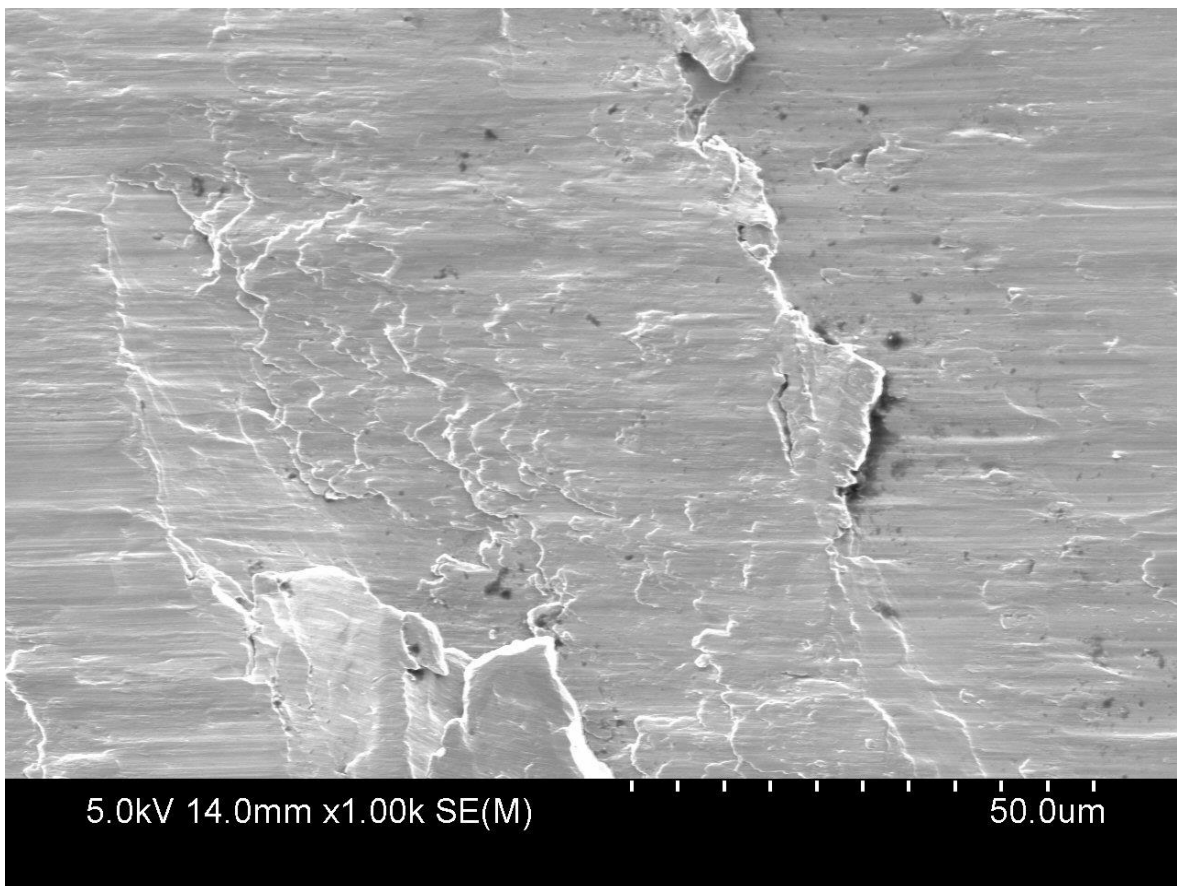
AR CoCrMo milled with Mill C.



HT4H CoCrMo milled with Mill B.



AR CoCrMo milled with Mill B.



AR CoCrMo milled with Mill C.